Investigation of mRNP export kinetics and gene expression regulation by the DEAD-box protein Dbp5p in *Saccharomyces cerevisiae*

by

Azra Lari

A thesis submitted in partial fulfillment of the requirements for the degree of

Doctor of Philosophy

Department of Cell Biology
University of Alberta

Abstract

The intricate architecture of the eukaryotic cell, which includes the partitioning of the cell into discrete membrane bound organelles, necessitates that various cargos must cross the nuclear envelope (NE). Nuclear pore complexes (NPCs) are large macromolecular assemblies embedded within the NE that function as selective transport channels to facilitate such transport events. As part of gene expression, the export of mRNA occurs through assembly of the mRNA into a ribonucleoprotein (RNP) complex, termed an mRNP. Consequently, nuclear mRNP export requires the complex regulation and activity of dozens of RNA binding proteins (RBPs) and ~30 NPC proteins (Nups) to be successful. Yet the spatial and temporal activities of these proteins and how they determine directionality of mRNP export from the nucleus remain largely undefined. Towards understanding this complex regulation, an *in vivo* single particle imaging approach was employed in yeast to visualize mRNP export events with high spatial precision and temporal resolution. The resulting data reveal that mRNP export is fast (~200 ms), and that upon arrival in the cytoplasm, mRNPs are frequently confined near the NE. Furthermore, a mutant of the principal mRNP export receptor (Mex67p) exhibits delayed cytoplasmic release from NPCs and retrograde transport of mRNPs. These results demonstrate an essential role for Mex67p in cytoplasmic mRNP release and directionality of transport, and validating the use of a live-cell yeast model to study mRNP export dynamics.

Specifically, it is the activity of an essential DEAD-box protein, Dbp5p, that is critical in driving the directional nuclear export of mRNPs. DEAD-box proteins (DBPs) are a family of RBPs found in all domains of life, often displaying RNA-stimulated ATPase activity, with diverse roles in RNA biology. Dbp5p is a dynamic shuttling protein, which accesses both the nuclear and cytoplasmic compartments. Consistent with this, activity of Dbp5p has also been

linked to processes beyond mRNP export, including transcription, translation, and non-coding RNA export, suggesting the presence of distinct functional pools of Dbp5p in the nucleus and cytoplasm. However, the mechanism(s) by which nucleocytoplasmic transport occurs and how Dbp5p specifically contributes to each of these processes remain unclear. Towards understanding the functions and mechanisms of transport of Dbp5p in yeast, an alanine scanning mutagenesis was employed to generate point mutants at all possible residues within a GFP-Dbp5p reporter. Characterization of these mutants led to the identification of an N-terminal Xpo1p-dependent nuclear export signal in Dbp5p, in addition to other separation-of-function alleles. Furthermore, through characterization of mutants that alter the sub-cellular localization of Dbp5p, these data provide evidence that efficient Dbp5p nuclear shuttling is not critical for mRNP export. Rather, disruptions in Dbp5p nucleocytoplasmic transport result in tRNA export and processing defects, including changes in tRNA shuttling dynamics during recovery from nutrient stress. These data point to distinct mechanisms through which Dbp5p activity is contributing to both coding and non-coding RNP export in eukaryotic cells.

Overall, my doctoral research has provided new knowledge describing mRNP export kinetics for the first time in *S. cerevisiae* and a novel role for Dbp5p in tRNA processing and export. These data also provide for more accurate models of mRNA export with respect to the functions of both Mex67p and Dbp5p, and a new understanding of how Dbp5p may be centrally positioned as a global regulator of eukaryotic gene expression.

Preface

Portions of Chapters I and V have been previously published as a review article in: **Heinrich S, Derrer CP, Lari A, Weis K, Montpetit B. 2017. Temporal and spatial regulation of mRNA export: Single particle RNA-imaging provides new tools and insights. *BioEssays* 39.doi:10.1002/bies.201600124.** Stephanie Heinrich, Carina Derrer, and myself were responsible for manuscript composition, figure generation and editing. Drs. Ben Montpetit and Karsten Weis (ETH Zurich) were the supervisory authors, and were involved with concept formation, manuscript composition, and editing. All authors performed editing of the final manuscript.

A version of Chapter III of this thesis has been previously published in: **Smith C, Lari A, Derrer CP, Ouwehand A, Rossouw A, Huisman M, Dange T, Hopman M, Joseph A, Zenklusen D, Weis K, Grunwald D, Montpetit B. 2015. In vivo single-particle imaging of nuclear mRNA export in budding yeast demonstrates an essential role for Mex67p. Journal of Cell Biology. 211:1121–1130.** I was responsible for data collection and analyses, and manuscript composition. Carlas Smith, Carina Derrer, and myself contributed equally to this work as co-first authors. I have indicated their data contributions in the corresponding figures. Drs Ben Montpetit, David Grunwald (University of Massachusetts Medical School), and Karsten Weis (ETH Zurich) were the supervisory authors, and were also involved with concept formation, manuscript composition, and data analysis. These six authors mentioned performed editing of the final manuscript. The remaining authors contributed to the development of data analysis pipelines.

Portions of Chapter IV of this thesis have been previously published as: **Lari A, Arul Nambi Rajan A, Sandhu R, Reiter T, Montpetit R, Young BP, Loewen CJR, and Montpetit B. 2019. A nuclear role for the DEAD-box protein Dbp5 in tRNA export. Elife. pii:e48410. doi:10.7554/eLife.48410.** I was responsible for concept formation, data collection and analyses, and original manuscript composition. Arvind Arul Nambi Rajan, Rima Sandhu, Taylor Reiter, Rachel Montpetit, and Barry Young assisted with data collection and analyses, which I have indicated in the corresponding figures. Dr. Ben Montpetit was the supervisory author, and was also involved with concept formation, original manuscript composition, and data analysis. Resources for the SGA screening were provided by our collaborator, Dr. Chris Loewen (University of British Columbia). All authors performed editing of the final manuscript.

I dedicate this thesis to three members of the small but inspiring Lari family:

To my mom, dad, and brother.

Acknowledgements

My time in graduate school has been a unique experience, spanning across two different countries, which has been both challenging and immensely rewarding. This thesis would not have been completed without support and guidance from the many individuals with whom I had the privilege to engage with throughout my studies. First and foremost, I must acknowledge the unwavering support, guidance, and knowledge provided to me over the years by my PhD mentor, Dr. Ben Montpetit. Ben, thank you for giving me the opportunity to join your research program, and continually challenging me to be a better scientist while providing me with the tools to achieve that. Your passion for science, attention to details, and determination has been truly inspiring and has forever shaped me as a student and scientist. I feel incredibly privileged to be the first student to graduate from your lab.

I would like to thank all current and past members of the Montpetit Lab, both at the University of Alberta and at the University of California, Davis. I had the unique experience of completing my studies in both these environments and had the opportunity to engage with a number of outstanding individuals. At UAlberta, I would especially like to thank Kelly Tedrick and Brenda Lam whose work has directly contributed to parts of my thesis presented here, and for this I am extremely grateful. I would also like to thank past lab member, Dr. Judit Vörös, for always providing compelling scientific discussion and input. Most importantly, thank you for your friendship and encouragement throughout the early years of my graduate studies, which was immensely missed after the lab re-located.

At UC Davis, I would especially like to acknowledge Arvind Arul Nambi Rajan, Dr. Rima Sandhu, Taylor Reiter, and Rachel Montpetit for their direct contributions to my thesis work presented here. Thank you for joining team Dbp5 and providing me with your valuable time, support, and scientific know-how over the years. I would also like to thank lab members Biplab Paul and Dr. Ryuta Asada. I am extremely thankful for all the enriching scientific discussions over the years surrounding this work. Again most importantly, thank you all for your friendship, encouragement, laughs, and time spent over coffee, which was indispensible to me for completing my graduate studies and will be so missed.

Part of the work presented here was also done in collaboration with Drs David Grunwald (University of Massachusetts Medical School), Karsten Weis (ETH Zurich), Chris Loewen (University of British Columbia), and members of their respective labs. Particularly, I would like to acknowledge Dr. Carlas Smith (UMass Med), Dr. Carina Derrer (ETH Zurich), Dr. Stephanie Heinrich (ETH Zurich), and Dr. Barry Young (UBC), who have all directly contributed to parts of the work presented here. I am extremely grateful for their expertise, support, and contributions to this work.

I would also like to thank the members of my graduate committee, Drs Richard Wozniak, Sarah Hughes, and Richard Rachubinski. Their guidance over the years has been enormously helpful through my graduate studies. Thank you for your willingness to provide support to me through my studies, which even extended to my time at UC Davis. I would also like to extend my gratitude to the staff, students, and faculty in the Department of Cell Biology at UAlberta to which I call “home”. Thank you for providing such an enriching research environment, and for the continued support over the years, both professionally and personally.

Finally, as with any endeavor in life, success requires immense support from those closest to you. Remarkably, I met four inspiring women over a decade ago that have since provided me with a once in a lifetime friendship. Naima, Lauren, Gillian, and Brielle, thank you for flying to California, laughing with me until we cry, and being the best cheering squad anyone could ask for – I am forever grateful to you all. To my brother, Adel, thank you for always just getting it. Lastly, I do not have enough words to express my gratitude to my parents for their unwavering love and support throughout my life. Dad, you are my scientific inspiration. Mom, you are the fuel behind all of my achievements. Your immense sacrifices have never gone unnoticed, and I am forever grateful to you.

Table of Contents

List of Tables

Appendix

List of Figures

List of Symbols, Abbreviations, and Nomenclature

ATP ……..... adenosine triphosphate
RGG……arginine-glycine-glycine
BR…… Balbiani Ring
bp……. base pair
ChIP……....chromatin immunoprecipitation
CLIP……..cross-linking immuoprecipitation
CTD…….. carboxyl-terminal domain
CRAC…….crosslinking and analysis of cDNA
CP……coat protein
CRLB…….Cramer-Rao lower bound
DBP…….dead-box protein
°C…….. degrees Celsius
DNA……deoxyribonucleic acid
dsRBD……..double stranded RNA binding domains
EM……..electron microscopy
FISH……..fluorescence *in situ* hybridization
g……..gram
x g……..gravitational force
GFP…….green fluorescent protein
GAP……..GTPase activating protein
GTP……guanosine triphosphate
HS……..heat shock
IgG……...immunoglobulin G
IP……...immunoprecipitation
IP_6…….inositol hexakisphosphate
j……joules
KH……..K homology
Kap……. karyopherin
kbp……...kilo base pairs
LRR……...leucine rich repeat
L……...liter
MLE……maximum likelihood estimate
mRNA……..messenger RNA
mRNP……messenger RNP
m……..meters
µl…….microliter
mg……...milligram
ml……..milliliter
mM……millimolar
ms…….millisecond
min……...minute
M……...molar
ng……nanogram
nm……. nanometer

ncRNA……non-coding RNA
NE……nuclear envelope
NES……..nuclear export sequence
NLS……..nuclear localization sequence
Nup……..nucleoporin
NPC……..nuclear pore complex
NA……numerical aperture
ORF……open reading frame
OD…….. optical density
PTC…….. peptdyl-transferase center
FG…….. phenylalanine-glycine
P-body……..…processing body
PCR…….polymerase chain reaction
PAGE……....poly-acrylamide gel electrophoresis
PEG……....polyethylene glycol
Poly(A)……poly-adenylated
PABP……..poly(A) binding proteins
RecA…….Recombinase A
REF……reference
RT……..reverse transcriptase
RNA……..ribonucleic acid
RNP……ribonucleoprotein
rRNA…….ribosomal RNA
RBD…….RNA binding domain
RBP…….. RNA binding protein
RNAP……..RNA polymerase
RRM……....RNA recognition motifs
s……second
SNR…….signal to noise ratio
smFISH……single molecule FISH
SMI……..single molecule imaging
snRNA…….small nuclear RNA
SDS……sodium dodecyl sulfate
SD……..standard deviation
SEM…… standard error of the mean
SF2……superfamily 2
SC…….synthetic complete
Ts……..temperature sensitive
TEC……transcription elongation complex
TREX……transcription export complex
TF…… transcription factor
tRNA…….transfer RNA
TEM……..transmission electron microscopy
UV…… ultra-violet
WT…….. wild-type
YPD…….yeast extract peptone and dextrose

Chapter I: *Introduction******

* A portion of this chapter has been reproduced from Heinrich, Derrer, Lari *et al., BioEssays,* 2017, 39: 1600124.

1.1 Eukaryotic RNA biogenesis and metabolism

The defining hallmark of eukaryotic cells - membrane bound organelles - has demanded increased complexity in eukaryotic RNA metabolism. The presence of the nuclear envelope (NE), composed of two concentric lipid bilayers encapsulating the nucleus, requires the regulated transport of RNA-protein complexes known as ribonucleoproteins (RNPs) to the cytoplasm for downstream processes. Transport of cargos occurs through specialized channels known as nuclear pore complexes (NPCs) embedded within the NE. Generally, coding RNAs or messenger RNAs (mRNAs) are transcribed from a genomic DNA template in the nucleus and undergo various processing stages, such as 5′ capping, 3′ poly-adenylation, and splicing to remove introns (reviewed in Moore, 2005). mRNPs are subsequently exported to the cytoplasm to participate in translation for protein synthesis, or they may be stored or decayed there. Non-coding RNA (ncRNA) species, such as ribosomal RNA (rRNA) or transfer RNA (tRNA) provide the critical structural elements required for protein synthesis machinery in the cytoplasm (Baßler and Hurt, 2019; Hopper, 2013). These ncRNAs also undergo extensive nuclear processing following transcription, which may include splicing, and nuclear export via pathways largely distinct from mRNAs. Various rRNA and tRNA processing or modification steps also occur within the cytoplasm.

Notably, RNAs do not transit the cell as free nucleic acids; rather both coding and non-coding RNAs are bound by dozens of RNA binding proteins (RBPs) at any given time to form RNPs. The protein composition of each RNP is both compartment specific (e.g. nucleus vs. cytoplasm) and highly specific to the processing stage of the RNP. In the budding yeast *Saccharomyces cerevisiae* (*S. cerevisiae*), over 500 different proteins have been predicted with the capacity to bind RNA with diverse affinities (Glisovic et al., 2008; Hogan et al., 2008). RBPs can interact with RNA substrates through various RNA binding domains (RBDs) such as RNA recognition motifs (RRMs), K homology (KH) domains, double-stranded RNA binding domains (dsRBD), zinc fingers, and arginine-glycine-glycine (RGG) boxes (Chen and Varani, 2005; Lunde et al., 2007). These domains often identify sequence specific motifs in the 5′ or 3′ untranslated regions of the RNA. RBPs may also interact with unique elements/modifications of the RNA. For example in mRNAs, this can include interactions with the 5′ cap or the 3′ polyadenylated (A) tail that is found in almost all coding transcripts (Calero et al., 2002; Kühn

and Wahle, 2004; Mazza et al., 2002). However, a large subset of RBPs interact with target RNA substrates in a sequence-independent manner through interactions with the negatively charged phosphate backbone of the RNA, and likely bind across the entire length of the RNA (Lunde et al., 2007). RBPs may stably bind RNA substrates or be dynamically exchanged at various processing stages. Ultimately, it is these RBPs that define the function of a specific RNP and/or drive the various processing steps within the life span of an RNP.

Put simply, the role of a RBP is to effectively function as an adaptor mediating interactions with machinery encountered at the various RNA processing stages. For example, this can include promoting interactions between an mRNA and nuclear export machinery or protein translation machinery in the cytoplasm to facilitate these processes. RBPs can stimulate positive interactions with this machinery allowing for activation of these processes, or conversely, RBPs may act as repressors by negatively affecting other protein-protein or protein-RNA interactions to inhibit these processes (reviewed in Moore, 2005). These highly coordinated positive and negative interactions of a diverse array of RBPs and their target RNAs allows for successful RNA processing. Importantly, these interactions can be finely modulated in response to changes in cellular conditions to ultimately drive changes in global gene expression.

1.2 Nuclear mRNP biogenesis and processing

The *S.cerevisiae* genome is predicted to be comprised of greater than 6000 protein-coding genes, which is about 70% of the genomic DNA in the cell (Lin et al., 2013). This renders coding RNAs, or mRNAs, as the largest class of RNAs encoded within the genome. Thus, a large component of the eukaryotic gene expression program is comprised of processes required for the accurate biogenesis and processing of mRNAs. Ultimately, mRNA processing is essential for generating functional transcripts that serve as templates for protein synthesis in the cytoplasm.

The biogenesis and first stages of mRNA processing occur within the nuclear compartment of the cell, and generally include three stages: (1)- transcription from a DNA template to generate a pre-mRNA, (2)- maturation of the pre-mRNA through end processing and splicing, and finally, (3)- generation of export competent mRNPs. Although these stages can be outlined as distinct stages, *in vivo* many of the processes occur simultaneously and are in fact intimately linked and

regulated (reviewed in Bentley, 2014). Largely, this coordination is achieved through co-transcriptional mRNP processing, which is achieved through two mechanisms: (1)- RNA maturation factors binding to the polymerase complex itself that can be transferred to the nascent transcript, and (2)- RNA maturation factors directly recruited to the nascent transcript during transcription (reviewed in Oeffinger and Zenklusen, 2012). This coordination allows for increased efficiency and fidelity by linking the first stages of mRNA biogenesis to the final formation of export competent mRNPs. This aids in ensuring only functionally mature and properly assembled mRNPs are released to the cytoplasm. Moreover, efficiency in coordination of these processes is paramount under cellular stress conditions in which the gene expression program is rapidly modulated to face the challenge presented to the cell. The following section will discuss these coupled processes of nuclear mRNA biogenesis and processing prior to formation of an export competent mRNP.

1.2.1 mRNA transcription and coupled end processing

The cellular fate of an RNA is determined as early as transcription through the RNA polymerase by which it is transcribed. In eukaryotic cells, there are three distinct RNA polymerases, RNA polymerase I, II, or III, which transcribe all RNAs in the cell. mRNAs are transcribed by RNA polymerase II (RNAPII), and RNAPII is distinct from other RNA polymerases as it is mechanistically equipped to support the coupling of transcription and pre-RNA processing. A key defining feature of RNAPII is the conserved carboxy-terminal domain (CTD) of the large subunit, which functions as the appendage to mechanistically couple transcription and pre-mRNA processing (Egloff et al., 2012; Hsin and Manley, 2012; Perales and Bentley, 2009). The CTD promotes mRNA maturation by recruiting various RNA processing factors, thus concentrating them at the transcription elongation complex (TEC) to promote these activities.

The first step in pre-mRNA processing is the addition of a 5′ 7-methylguanosine cap to the nascent transcript. Capping protects the pre-mRNA from enzymatic degradation and aids in ribosome binding for translation. The 5′ cap is bound by the cap-binding complex, Cbc1p/Cbc2p in yeast (or CBC20/80 in humans), which further protects the transcript from degradation and

promotes downstream mRNP export (Glover-Cutter et al., 2007; Listerman et al., 2006). Co-transcriptional capping is thought to be a universal modification to RNAPII transcripts. An additional common co-transcriptional modification to RNAPII transcripts is 3′ polyadenylation, which is required for transcription termination (Logan et al., 1987; Whitelaw and Proudfoot, 1986; Zaret and Sherman, 1982). Polyadenylation is the addition of a poly-adenosine (A) tail to the 3′ end of the transcript. This further functions to protect the mRNA from enzymatic degradation throughout all post-transcriptional processing, and provides binding sites for RBPs, often referred to as polyA-RNA binding proteins (PABPs), that aid in downstream processes such as splicing, mRNP export, and translation (Mangus et al., 2003).

1.3 Nuclear mRNP export

One of the defining hallmarks unique to eukaryotic RNA metabolism is the requirement of an active and regulated export process to translocate RNPs from the nucleus to the cytoplasm. Subsequent to mRNA biogenesis and pre-mRNA processing in the nucleus, mRNPs must be exported to the cytoplasm for downstream processes such as translation. Key RBPs or mRNP export factors bind the mature mRNA to facilitate competency for transport across the NE. Historically, genetic approaches employed in a yeast model have proved to be a powerful means in identifying host of factors essential for mRNP export. Both the entire non-essential yeast gene deletion collection and essential temperature-sensitive yeast mutant collections have been employed in fluorescent *in-situ* hybridization (FISH) experiments, using an olidgo-dT probe, to determine the poly(A)-RNA export status in these mutants (Amberg et al., 1992; Hieronymus et al., 2004; B. Paul and Montpetit, 2016; Thomsen et al., 2008). Accumulation of poly(A)-RNA in the nucleus of these mutants is the read-out for the requirement of the gene-product in mRNP export (Cole et al., 2002). Using this approach and various other biochemical means, over 80 factors have been identified to play a role in mRNP export in yeast (reviewed in Nino et al., 2013). These factors overlap in functions to include roles in upstream mRNA transcription processing, splicing, and decay, and also include several Nups, again exemplifying the coupled nature of these processes.

Factors required for mRNP export are loaded on as early as transcription, end processing and/or splicing (Perales and Bentley, 2009). Generally, an export competent mRNP includes a fully mature (i.e. processed) mRNA, factors to protect the mRNA from degradation, factors required for engagement and release from NPCs, and factors that promote translation initiation in the cytoplasm. There are both universal factors required for export that are present in all export competent mRNPs, and also unique factors based on the upstream processing of the transcript (e.g. spliced mRNAs). However, the exact stoichiometry and architecture of export competent mRNPs remains unknown.

The composition of exporting mRNPs is also altered in response to changing cellular conditions (e.g. stress), which may promote or prevent export of specific mRNAs and serves as another mode for altering the gene expression program (Saavedra et al., 1996; Zander et al., 2016). Subsequent to loading of nuclear mRNP export factors, export consists of three distinct steps to mediate interactions with NPCs sufficient for export: (1)- docking to NPCs, (2)- translocation through the channel, and (3)- release from cytoplasmic NPC components in the cytoplasm (reviewed in Heinrich et al., 2017; Oeffinger and Zenklusen, 2012). These interactions are mediated by RBPs and Nups. Unlike protein transport through NPCs, mRNP export is not achieved via a single export receptor, rather it requires the highly coordinated activity of a number of factors that are both stably and dynamically associated with the exporting mRNA. The following sections focus on the steps within mRNP export, including key RBPs that mediate this process, and the spatial and temporal regulation of these factors required for efficient export.

1.3.1 mRNP export coupled to transcription and end processing

Recruitment of nuclear mRNP export factors to mRNAs occurs as early as transcription and 3′ end processing (See Figure 1-1). For example, the essential mRNP export adaptor Yra1p (or Aly/REF in humans) is recruited to RNAPII during elongation through the 3′ end-processing factor Pcf11p, which is bound to the CTD of RNAPII (Johnson et al., 2011, 2009). Yra1p is competed off RNAPII by cleavage and polyadenylation factors once transcription termination occurs and is then free to bind directly bind the mRNA and Sub2p, which is required for both

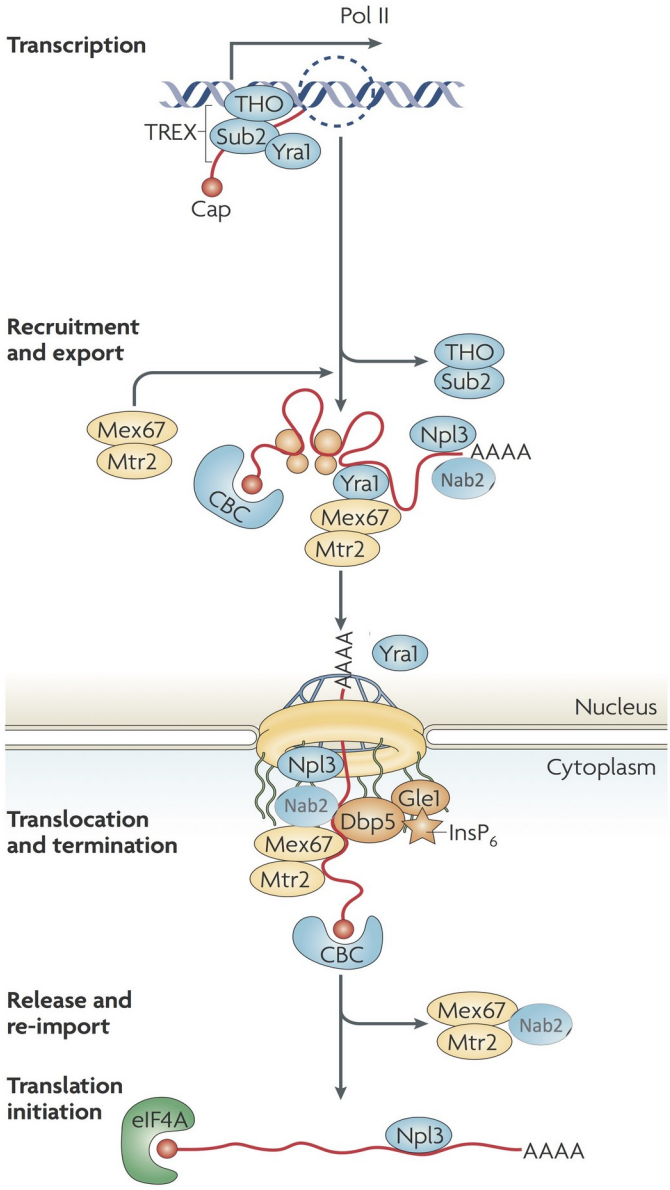

Figure 1-1. Coupled processes within mRNA metabolism. Schematic depicts transcription-coupled mRNP export in yeast. Coincident with nascent transcript generation by RNAPII, factors required for export competency are loaded on the transcript (e.g. Yra1p and Sub2p of the TREX and THO complexes). The major export factor required for mRNP export, the Mex67p-Mtr2p heterodimer, is then recruited to the mRNP via adaptor proteins, such as Yra1p, which enables translocation through NPCs. At the cytoplasmic face of NPCs mRNPs are remodeled through the ATPase activity of Dbp5p, regulated by factors such as Gle1p. This remodeling is thought to remove key RNP export factors such as Mex67p-Mtr2p and Nab2p to enforce directionality. Removal of these factors then enables the initiation of the pioneering round of translation. Figure reprinted by permission from Springer Nature: Nature. Nature Reviews Molecular Cell Biology (Exporting RNA from the nucleus to the cytoplasm, Kohler and Hurt). 2007.

splicing and mRNP export. Importantly, Yra1p is required for the recruitment of the major mRNP export receptor Mex67p (or TAP in humans), and loss of Yrap1 in yeast results in poly(A)-RNA accumulation in the nucleus (Sträßer and Hurt, 2000; Stutz et al., 2000; Zenklusen et al., 2001). Yra1p is removed from the mRNP prior to export and remains localized to the nucleus. Sub2p is a component of the TREX complex and is recruited to elongating transcripts via the THO (Tho2, Hpr1, Mft1, and Thp2) complex, which is required for efficient transcription elongation. Both *sub2* and *THO* mutants also exhibit poly(A)-RNA export defects, thus linking regulation of transcription elongation machinery and mRNP export (Rougemaille et al., 2008; Sträßer et al., 2002; Zenklusen et al., 2002).

Members of the serine/arginine (SR) family of proteins also link transcription, 3′ end processing, and mRNP export in yeast. This includes Npl3p, which participates in transcription elongation, splicing, and mRNP export. Npl3p can directly bind mRNAs through an RRM type RNA-binding motif (Bossie et al., 1992; Russell and Tollervey, 1995; Singleton et al., 1995). In yeast, Npl3p directly interacts with Mex67p and functions as an adaptor for Mex67p to promote export (reviewed in Nino et al., 2013). In yeast, the nuclear poly(A) binding protein Nab2p also functions as an adaptor to Mex67p and is required for mRNP export. Nab2p promotes export through binding of mRNA substrates via poly(A) tails, and also facilitates interactions with NPC proteins (Brockmann et al., 2012; Kelly et al., 2010). Nab2p forms a tripartite complex with both Yra1p and Mex67p (Iglesias et al., 2010). However, unlike Yra1p, Nab2p (and Npl3p) travel with the mRNP to the cytoplasm and is recycled to the nucleus after mRNP release from NPCs. Together, these export factors link nuclear mRNA biogenesis, processing, and mRNP export.

1.3.2 mRNP export receptor Mex67p

Nuclear mRNP export is distinct from other export pathways (e.g. protein export) given that it is not dependent on the importin/karyopherin superfamily of transport receptors that interact with the small GTPase Ran. Rather, mRNP export is dependent on the essential non-β karyopherin export receptor, Mex67p (NXF1 or TAP in humans) (Bear et al., 1999; Grüter et al., 1998; Kang and Cullen, 1999; Alexandra Segref et al., 1997; Zenklusen and Stutz, 2001). Mex67p is a member of the NXF family of proteins that is conserved from yeast to humans.

Although the yeast and human homologs of MEX67 share poor sequence similarity, overexpression of human TAP in a *mex67*Δ deletion strain in yeast will in fact allow for functional complementarity and rescue the lethal growth defect (Katahira et al., 1999). Mex67p forms a heterodimer with Mtr2p (NXT1 or p15 in humans) *in vivo* to function in mRNP export (Fribourg et al., 2001; Lévesque et al., 2001; Sträßer et al., 2000; Wiegand et al., 2002). In yeast, this heterodimerization with Mtr2 is required for mRNP export, however in humans, TAP can facilitate efficient export independent of p15.

Mex67p is a dynamic nuclear shuttling protein that can interact with phenylalanine-glycine Nups (FG Nups) that facilitate transport, and engages mRNPs through adaptor proteins, thus situating itself as a key factor in driving export. Mex67p is composed of four domains separated by flexible linkers. The N-terminal RRM and leucine rich repeat (LRR) domains promote interactions with mRNP adaptor proteins (e.g. Yra1p) and associated mRNAs (Kang and Cullen, 1999; Liker et al., 2000). The central NTF2-like domain within Mex67p allows for heterodimerization with Mtr2p (Katahira et al., 1999; Santos-Rosa et al., 1998). Mtr2p functions to promote interactions between FG Nups and the NTF2-like domain in Mex67p to promote export. The ubiquitin-associated domain (UBA) provides an overlapping binding site for FG Nups and other specifically ubiquitylated proteins (Katahira et al., 1999). Under steady-state conditions, Mex67p is predominantly localized to the nuclear envelope. This has led to the inference that the majority of the cellular pool of Mex67p is engaged in transport and is likely loaded onto the mRNP just prior to transport (Sträßer et al., 2000). However, evidence from chromatin immunoprecipitation (ChIP) experiments have identified Mex67p to be recruited to a subset of transcribing genes and then transferred to the nascent mRNAs (Dieppois and Stutz, 2010; Rougemaille et al., 2008). Given that Mex67p has a low intrinsic affinity for mRNA binding, adaptor proteins then likely promote interactions with the transcript in the nucleus.

1.3.3 Nuclear pore complexes and nucleocytoplasmic transport

NPCs are specialized transport channels embedded within the NE that facilitate nucleocytoplasmic transport in eukaryotes. Molecules that are less than nine nanometers in diameter can passively diffuse through NPCs, however the majority of macromolecule transport

substrates (e.g. proteins and RNPs) are larger than this and require active transport. Active transport through NPCs can be mediated by a family of structurally related soluble transport receptors, collectively known as karyopherins (Kaps). In yeast, 15 Kaps have been identified, while in vertebrates, 22 Kaps have been identified termed as Importins (Kaps mediating import) or Exportins (Kaps mediating export) (Fried and Kutay, 2003; Görlich and Kutay, 1999; Pemberton and Paschal, 2005; Ström and Weis, 2001; Wente and Rout, 2010; Wozniak et al., 1998). Kaps rely upon recognition of specific amino acid sequences in protein cargos known as nuclear export sequences (NESs) or nuclear localization sequences (NLSs). NPCs and Kaps provide the machinery required for nucleoctyoplasmic transport; however, it is the small shuttling GTPase protein, Ran that provides the directionality and energy required for this process. Although Kaps share minimal sequence homology, the amino-terminal Ran binding domain is highly conserved. Xpo1p (or CRM1 in humans) is the major Kap (exportin) that supports export of proteins and ncRNAs (through adaptor proteins) (Fornerod et al., 1997; Fukuda et al., 1997; Ossareh-Nazari et al., 1997; Stade et al., 1997). In the case of Xpo1p-mediated export, the substrate is recognized through a short, leucine rich NES in the nucleus. This occurs in a stepwise manner in which the Xpo1p-Ran-GTP binds the cargo substrate in the nucleus, which then shuttles to the cytoplasm through NPCs and is then dissociated in the cytoplasm through the action of the cytoplasmic Ran GTPase activating protein (Ran-GAP). Ran-GAP hydrolyzes GTP to form Ran-GDP and this dissociates the tripartite complex, leaving the cargo free in the cytoplasm. mRNP export requires transit through NPCs; however, as described in the previous section, this process relies on the major non-karyopherin receptor, Mex67p, for transport.

NPCs themselves are macromolecular assemblies of approximately 30 different proteins, or Nucleoporins (Nups), forming a structure with eight-fold rotational symmetry with each Nup present in copies of eight. NPC structure is evolutionarily conserved, and in yeast this amounts to a ~ 66 MDa complex and a ~ 125 MDa in vertebrates (Aitchison and Rout, 2012; Brohawn et al., 2009; Fahrenkrog and Aebi, 2003). In a simplified view, NPCs are composed of transmembrane, structural, and FG Nups. Transmembrane Nups anchor the NPC to the NE, while structural Nups provide a scaffold for other Nups. FG Nups, being the most critical for interaction with nuclear mRNP export factors, are composed of phenylalanine-glycine (FG) repeats that adopt a natively unfolded conformation and form unstructured, flexible filaments that fill the central NPC channel between the nucleus and the cytoplasm (See Figure 1-2)

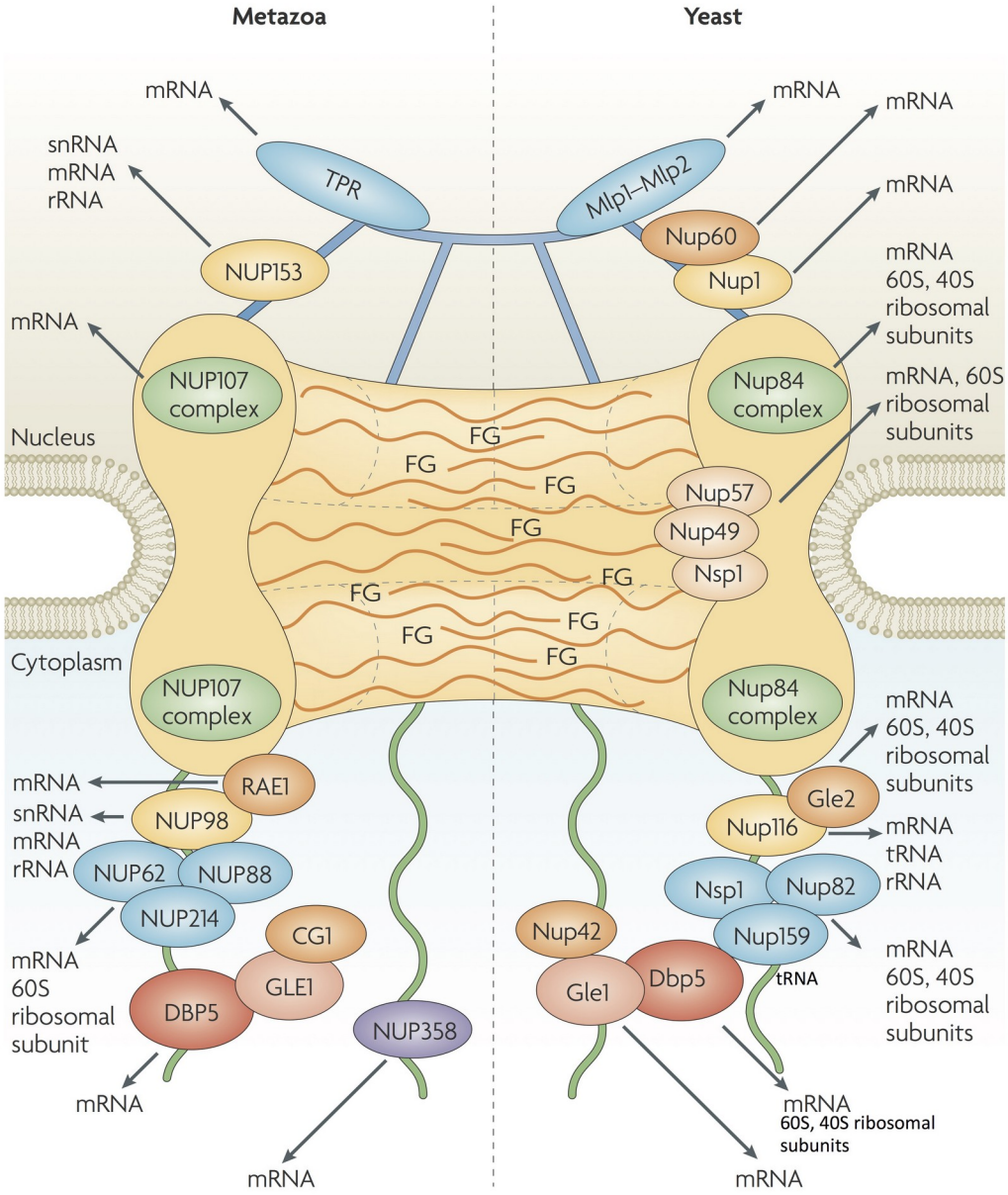

Figure 1-2. NPC organization and nucleoporins that facilitate RNP export. Schematic displays both metazoan and yeast NPC organization. The NPC core structure contains eight spokes surrounding a central channel. The nucleoplasm and cytoplasm are connected through this central channel, in which macromolecular exchange occurs, including RNP export. Peripheral FG filaments, which are sites for RNP remodeling are also displayed. These filaments are attached to the core and emanate into the nucleoplasm and cytoplasm, and fill the central channel. On the nuclear side, these filaments form a basket-like structure. Functional roles for Nups and NPC associated proteins, including in RNP export, are indicated. Figure reprinted by permission from Springer Nature: Nature. Nature Reviews Molecular Cell Biology (Exporting RNA from the nucleus to the cytoplasm, Kohler and Hurt). 2007.

(Aitchison and Rout, 2012; Wente and Rout, 2010). FG Nups provide both the permeability barrier and interact with transport receptors to facilitate nuclear transport. Among FG Nups, there are those that are symmetrical and are present on both sides of the NPC, lining the central channel; however, there are also those asymmetrically positioned FG Nups that are localized to either the cytoplasmic or nucleoplasmic regions of the NPC, also forming unstructured, flexible fibrils. The cytoplasmic FG fibrils, which extend out into the cytoplasm, also in eight-fold symmetry, are composed of Nup159p, Nup82p, and Nup49p in yeast. Alternatively extending into the nucleoplasm, these fibrils are composed of Nup60p, Nup2p, and Nup1 in yeast. The nucleoplasmic basket of the NPC is extended from this face and includes the myosin-like proteins, Mlp1p and Mlp2p, which play a role in recruiting mRNPs to NPCs (Galy et al., 2004; Green et al., 2003; Vinciguerra et al., 2005). Loading of key nuclear mRNP export factors is critical for facilitating interactions with FG Nups to allow directional export of these substrates. Importantly, mutations in many additional essential Nups results in mRNP export defects likely arising from indirect effects of non-functional transport channels (reviewed in Nino et al., 2013).

1.3.4 Nuclear mRNP-NPC interactions and mRNP quality control

Although a detailed composition of mRNPs arriving at NPCs prior to export remains elusive, there are some factors that are thought to bind the majority of mRNPs in the nucleus prior to export, such as Nab2p, Yra1p, and the Mex67p-Mtr2p heterodimer. mRNP passage through an NPC is enabled by the Mex67p-Mtr2p heterodimer, which is likely initially constituted through interactions with the nucleoplasmic FG Nups, Nup1p and Nup2p (Terry and Wente, 2007). The FG-repeats of Nup1p and Nup2p are proposed to be the first binding sites of the mRNP to the NPC. Docking to the NPC itself induces mRNP rearrangement and dissociation of specific factors, such as Yra1p, which does not translocate to the cytoplasm with the mRNP (Sträßer and Hurt, 2000; Stutz et al., 2000; Zenklusen et al., 2001). It has also been shown that deletion of the factor required to ubiquitinate Yra1p, which marks it for degradation at NPCs, leads to retention of poly(A) mRNA in the nucleus (Iglesias et al., 2010). Thus, removal of Yra1p is a key step in marking an mRNP competent for export.

Interestingly, an mRNP particle behavior termed scanning has been observed in both yeast and mammalian systems, in which an mRNP reaches the nuclear periphery, and prior to undergoing export, moves or "scans" along the nuclear periphery (Grünwald and Singer, 2010; Saroufim et al., 2015). This scanning process remains poorly understood and has so far only been reported for a few transcripts. However, it does raise questions as to why some mRNPs are exported immediately and others are not. This may involve differential Mex67p-Mtr2p binding and the acquisition of export competency. Scanning may also be indicative of other changes in mRNP composition that need to occur prior to NPC translocation and/or quality control events that have been linked to the nuclear periphery and NPCs.

In yeast, several proteins have been implicated in mRNP quality control at the site of docking at NPCs prior to export. This includes Mlp1p, Mlp2p, Nup60p, Pml39p, Swt1p, and Ulp1p (Galy et al., 2004; Lewis et al., 2007; Palancade et al., 2005; Skružný et al., 2009; Vinciguerra et al., 2005). These proteins function in identifying unspliced or improperly processed mRNPs, which may then be degraded or repaired. For example, loss of Mlp1p increases the "leakage" of unspliced and other aberrant mRNAs into the cytoplasm (Galy et al., 2004; Vinciguerra et al., 2005). Thus, the nucleoplasmic face of the NPC is spatially important for defining mRNP competency and serves as the final gatekeepers for improperly assembled mRNPs.

1.3.5 mRNP translocation through NPCs

Decades ago, mRNP translocation through NPCs was first observed using transmission electron microscopy (TEM) to follow the Balbiani ring (BR) mRNP, from the *Chironomus tentans* (*C. tentans*) insect (Mehlin et al., 1995). The BR mRNP is composed of a large 35-40 Kb RNA which folds into a globular 50 nm particle that is easily visible by TEM. In contrast, the average size of an mRNA in yeast is closer to 2 Kb and folds into an mRNP closer to 5-7 nm in size (Batisse et al., 2009). TEM images of the BR mRNP show docking to NPCs, rearrangements into a more rod-like shape as it translocates through the NPC, and emergence on the cytoplasmic face associating with ribosomes. Although the BR mRNP is uniquely distinct in size, there are several pieces of evidence to suggest that more average sized mRNPs may also exhibit this

rearrangement through the NPC channel. This includes data from experiments isolating mRNPs through Nab2p immunoprecipitations (IPs) from yeast cells that exhibit rod like shapes (20nm in length) (Batisse et al., 2009). Furthermore, fluorescent single molecule experiments in metazoan systems visualizing the dystrophin mRNP identified a more spherical mRNP structure prior to translocation through NPCs, a subsequent decrease in fluorescence during translocation suggestive of rearrangement, and a more open disorganized structure in the cytoplasm (Mor et al., 2010). However, analysis of NPC translocation times of the β-actin mRNA in mouse cells points to translocation through NPCs as not being the rate-limiting step (Grünwald and Singer, 2010). Rather, events close to the nucleo- and cytoplasmic faces of the NPC were observed to contribute to the overall export times. If this is in fact a general feature of mRNP export, extensive remodeling may not be occurring during translocation. Ultimately, the degree to which rearrangements occur during translocation for varying sizes of mRNPs remains to be tested.

mRNP translocation through the NPC channel is thought to be largely driven by sequential interactions between the Mex67p-Mtr2p heterodimer and specific FG Nups lining the central channel. Here, Mtr2p is key to promoting interactions between FG Nups and the NTF2-like domain in Mex67p. Although Mex67p harbors the capacity to bind all FG Nups, it likely interacts with a unique subset of FG Nups, distinct from those used by other Kaps (Terry and Wente, 2007). There are three existing models for how the barrier function of FG Nups is breached to allow for mRNP translocation through this selective channel (reviewed in Björk and Wieslander, 2014; Terry and Wente, 2007). The “selective phase partitioning model” proposes that the export receptor itself (Mex67p) disrupts the FG-repeat meshwork, the “oily spaghetti model” proposes that it is the successive binding and dissociation of export receptors to the FG-repeats that allows for translocation, and lastly the “virtual gating model” proposes that a stepwise binding of export receptors and FG-repeats overcomes the entropic barrier of the meshwork itself. Importantly, varying FG Nup requirements exist for translocation of proteins versus mRNPs versus the passive diffusion of small molecules.

1.3.6 Cytoplasmic mRNP-NPC interactions and remodeling

The NPC itself does not inherently provide directionality for translocating substrates, and in the case of mRNP export directionality is enforced through remodeling at the cytoplasmic face of the NPC. A mechanism for this remodeling hinges on the idea that translocating mRNPs are stripped of key export factors, preventing further interaction with NPCs. The essential DEAD-box protein, Dbp5p (DDX19 in humans), is critical in driving this mRNP remodeling, thus enforcing this directionality and allowing for release into the cytoplasm (Hodge et al., 1999; Lund and Guthrie, 2005; Schmitt et al., 1999; Snay−Hodge et al., 1998; Tran et al., 2007; Tseng et al., 1998). Dbp5p is a nuclear shuttling RNA-stimulated ATPase that is predominantly localized to the cytoplasmic face of the nuclear envelope where its ATPase activity is modulated by the cytoplasmic oriented NPC proteins, Nup42p, Nup159p, and Gle1p together with the endogenous small molecule inositol hexakisphosphate (IP_6) (Adams et al., 2017; Alcazar-Roman et al., 2006; Dossani et al., 2009; Hodge et al., 1999; Montpetit et al., 2011; Napetschnig et al., 2009; Noble et al., 2011; Schmitt et al., 1999; von Moeller et al., 2009; Weirich et al., 2006, 2004; Wong et al., 2018). Dbp5p stimulated activity is thought to induce mRNP remodeling resulting in the removal of export factors such as Nab2p and the Mex67p-Mtr2p heterodimer from the translocated mRNPs (See Figure 1-1) (Lund and Guthrie, 2005; Tran et al., 2007). *In vitro* experiments suggest that Dbp5p does not directly interact with Nab2p or Mex67p to initiate this remodeling, but rather it more likely utilizes ATP binding or hydrolysis to re-structure the mRNA, thus leaving export factors such as Nab2p or Mex67p incapable to bind. This could potentially occur through duplex unwinding since Dbp5p exhibits helicase activity *in vitro* (Tseng et al., 1998); however, the exact mechanism and which proteins are targeted for removal directly or indirectly by Dbp5p remains unclear *in vivo*. Although the mRNA binding preferences for Mex67p (across the entire length of the mRNA) or Nab2p (bias towards the 3′ end) are known, the exact stoichiometry of export factors in a given mRNP remains unclear (Tuck and Tollervey, 2013). Thus, it remains challenging to determine exactly to what extent the mRNP is remodeled at this interface.

1.3.7 Models of Dbp5p activity in mRNP export

Two prevailing models regarding how Dbp5p functions in mRNP export have been proposed (reviewed in Heinrich et al., 2017) (See Figure 1-3). In the Dbp5p "scaffold" model, nuclear shuttling would facilitate Dbp5p recruitment to the mRNA in the nucleus to generate a platform for other proteins to bind, which would persist as the mRNP travels to and through an NPC (von Moeller et al., 2009). On the cytoplasmic side of the NPC, due to the presence of regulators (e.g. Nup159p and Gle1p-IP_6), ATP hydrolysis and/or mRNA release would be promoted causing Dbp5p and other proteins to be displaced from the mRNA. This would lead to the removal of specific nuclear export factors from the mRNP, thereby terminating mRNP export.

Alternatively, an RNPase model has been proposed, in which Dbp5p waits at the cytoplasmic side of the NPC for a translocating mRNP and continuously remodels it through co-regulator-stimulated ATPase activity, thereby driving directional export. In the RNPase model, export factors are distributed along the transcript to allow step-wise remodeling by Dbp5p and prevents backsliding of the mRNA into the nucleus. This is supported by studies on global mRNP composition showing that export factors such as Mex67p bind across the length of an mRNA with no apparent sequence specificity (Baejen et al., 2014; Tuck and Tollervey, 2013). In addition, computational modeling of mRNP export emphasized that a symmetrical distribution of export factors along the transcript strongly correlates with successful transport (M. Azimi et al., 2014). This model also suggested that mRNP export is very sensitive to the number of export receptors on the mRNA, and that one export factor per mRNP might not be sufficient to facilitate transport. Of course, it is possible that Dbp5p functions in multiple ways to facilitate export that may include both a scaffold and RNPase type activity that may in part depend on the specific transcript being exported. (See **Section 1.8** for a detailed discussion of Dbp5p regulated activity in gene expression).

1.3.8 mRNP export kinetics and spatial and temporal regulation

In *S. cerevisiae,* it is estimated that approximately 60,000 mRNA molecules are present per cell at any given time, and given a median transcript half-life of 11-18 minutes, roughly 2,000-

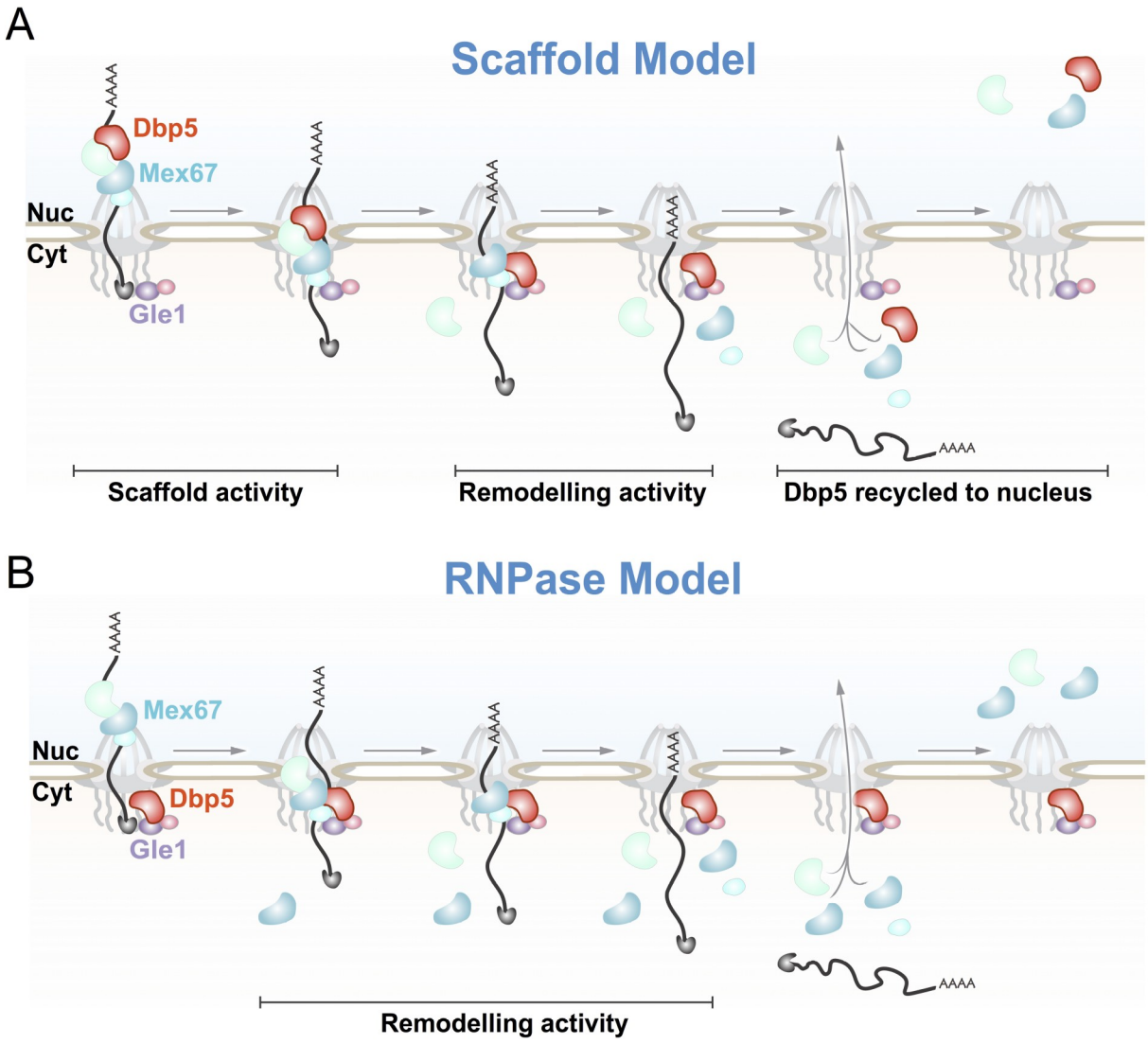

Figure 1-3. Models of Dbp5p-dependent directional mRNP export. A. Schematic of a "scaffold" model of Dbp5p-dependent export. Dbp5p is recruited to the mRNA in the nucleus and incorporated into the mRNP to generate a platform for other proteins to bind. Dbp5p travels through the pore with the mRNP and upon reaching the cytoplasmic side of the NPC remodels the mRNP though its ATPase activity due to the presence of regulators (e.g. Gle1p-IP_6 and Nup159p). Dbp5p is then recycled back to the nucleus. **B.** Schematic of a "RNPase" model of Dbp5p-dependent export. Dbp5p waits at the cytoplasmic side of the NPC for a translocating mRNP with regulators (e.g. Gle1p-IP_6 and Nup159p) and continuously remodels the mRNP through its ATPase activity. Figure reprinted by permission from John Wiley and Sons: Bioessays (Temporal and spatial regulation of mRNA export: Single particle RNA-imaging provides new tools and insights, Heinrich et al.,). 2017.

3,000 transcripts must be transported out of the nucleus per minute (Miller et al., 2011; Munchel et al., 2011; Zenklusen et al., 2008). Taking into account a density of 60–200 NPCs per yeast nucleus, this translates to around 10–50 mRNP export events per NPC every minute (Winey et al., 1997). Thus, mRNP export likely requires a high level of spatial and temporal regulation to maintain this level of transport in the face of protein transport and flux of ncRNAs through NPCs as well. By in large, studying export events has been challenging due to the lack of "sensitive" assays to monitor where and when export occurs, and to define where in the process a given export factor functions. As mentioned above, the commonly used oligo-dT FISH assay that allows for bulk poly(A)-RNA to be visualized in the cell has led to the identification of almost all known export factors. However, all these mutants exhibit very similar phenotypes, which is the accumulation of poly(A)-RNA in one or more compartments of the nucleus (Hieronymus et al., 2004; Paul and Montpetit, 2016). Consequently, this has provided little insight into how mRNP export factors are spatially and temporally regulated *in vivo* given the similarity in these phenotypes from bulk measurements.

To step away from such bulk measurements and begin to ascertain where mRNP export factors function in the process, single transcript analyses using single molecule FISH (smFISH) approaches have been more recently employed (Femino et al., 1998; Paul and Montpetit, 2016; Raj et al., 2006; Zenklusen et al., 2008). smFISH can reveal "snap-shot"-like information on transcript localization, transcript abundance, and cell-to-cell variability. However, *in vivo* dynamics, such as nuclear export kinetics or transport directionality, cannot be measured through this approach (See Figure 1-4). To overcome these limitations, recent advancements in RNA labeling and imaging technology have allowed various groups to address the dynamics of export *in vivo*. Importantly, this has provided an opportunity to spatially and temporally characterize nuclear biogenesis and export in live cells at the level of individual mRNPs (Grünwald and Singer, 2010; Mor et al., 2010; Siebrasse et al., 2012; Smith et al., 2015). Imaging of single RNPs in a living cell is made possible by the introduction of sequence tags into the transcript. A common strategy is based on the sequence-specific interaction of a fluorescently labeled bacteriophage coat protein (CP) with specific RNA binding sites (reviewed in Urbanek et al., 2014). This approach was initially established using protein and RNA components from the phage MS2 (Beach et al., 1999; Bertrand et al., 1998). An orthologous system has also been described from the phage PP7 (Chao et al., 2008; Larson et al., 2011). PP7 and MS2 CPs retain

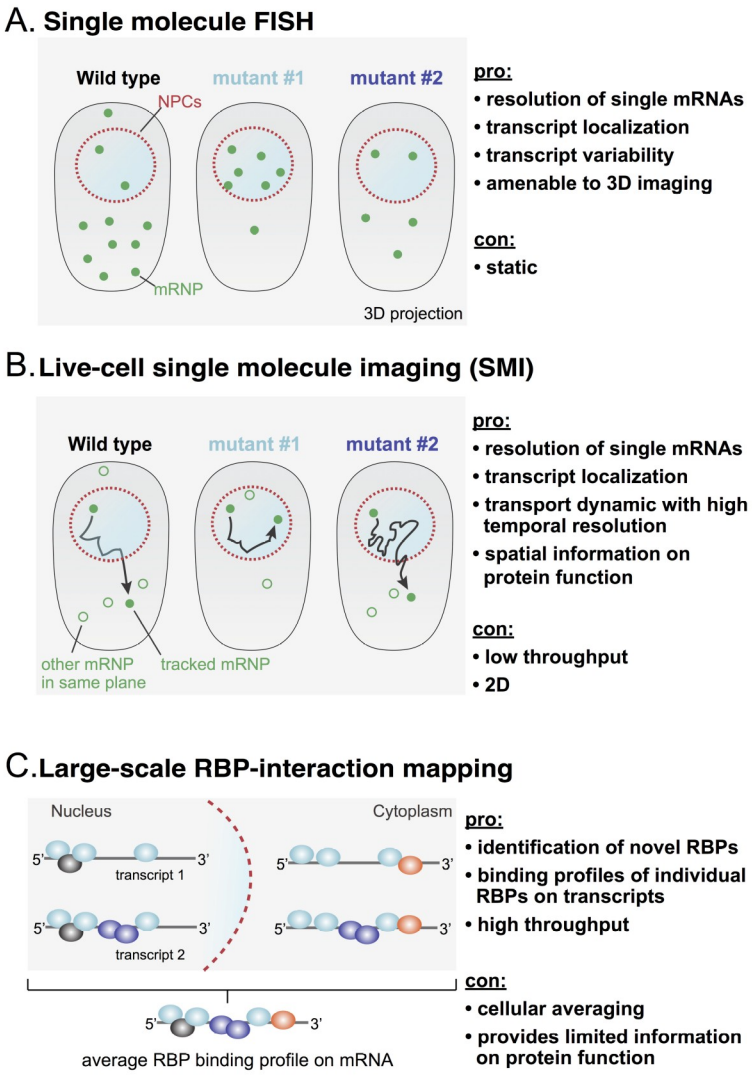

Figure 1-4. Single molecule techniques can overcome limitations in understanding cellular mRNP function obtained from ensemble composition data from large-scale sequencing and proteomic approaches. A. Single molecule fluorescence *in situ* hybridization (smFISH) can reveal localization, abundance, and cell-to-cell variability of individual mRNPs, but is a static method that does not allow visualization of *in vivo* dynamics, such as nuclear export kinetics or transport directionality of single transcripts. **B.** Single molecule imaging (SMI) enables a dynamic profiling of individual transcripts *in vivo* and provides spatial information on RBP function with high temporal resolution. **C**. Large-scale approaches analyzing RBP binding to mRNA transcripts are based on numerous data points that are compiled into an ensemble average, which may not be representative of individual mRNP composition *in vivo*. For example, the binding profile of an RBP may differ substantially across transcripts from different genes and/or transcripts residing in different cellular compartments. Figure reprinted by permission from John Wiley and Sons: Bioessays (Temporal and spatial regulation of mRNA export: Single particle RNA-imaging provides new tools and insights, Heinrich et al.,). 2017.

binding specificity when combined *in vivo*, allowing for double labeling of individual transcripts, which was recently employed to monitor translation *in vivo* (Halstead et al., 2015; Hocine et al., 2013).

To observe mRNP transport from the nucleus to the cytoplasm the MS2 or PP7 systems have been employed in yeast, *C. tentans*, mouse, and human cells (Grünwald and Singer, 2010; Ma et al., 2013; Mor et al., 2010; Saroufim et al., 2015; Siebrasse et al., 2012; Smith et al., 2015). Whereas some studies observe similar mRNP behaviors (e.g. mRNP retention close to NPCs), the reported NPC transit times (ranging from 11 ms to 0.5 s) vary by several orders of magnitude (See Table 1-1). Although these numbers are likely dependent on the transcript and organism characterized, differences in image acquisition strategies and data interpretation have also been pointed out as a source of discrepancy (Azimi et al., 2014; Musser and Grünwald, 2016). Further application of these imaging approaches is required to clarify these differences and to address unresolved questions about directional mRNP export.

To visualize discrete steps of mRNP remodeling within and around the NPC, (sub-) millisecond resolution and high signal to noise ratio (SNR) are critical, but the higher laser powers that are currently required for this can lead to photodamage and phototoxicity. Thus, current mRNA labeling approaches suffer from low SNR when used to follow dynamic processes due to the requirement of short exposure times (10–20ms) and photobleaching over an imaging series. Consequently, 6–24 repeats of the MS2 or PP7-specific RNA hairpins are commonly introduced into an mRNA to achieve the required SNR. Both MS2 and PP7 bind as dimers, therefore, up to 48 FP-CP can bind to an array of 24 RNA hairpins, adding significant protein mass to the labeled mRNP. This must be taken into consideration, in addition to the location of the hairpins in the transcript, to ensure that the mRNP retains its functionality. With proper characterization, transcripts have been identified that when tagged show no differences in abundance or functionality (Hocine et al., 2013; Smith et al., 2015). However, recent publications have reported that the presence of multiple MS2 hairpins can lead to the stabilization of MS2-containing decay fragments, which may act as false-positive signals in imaging experiments (Garcia and Parker, 2016, 2015; Haimovich et al., 2016; Heinrich et al., 2017). Thus, further advancements in *in vivo* RNA-tagging approaches and imaging technology is still required to address the many questions about the spatial and temporal regulation of mRNP export.

Table 1-1. Reported mRNP export dynamics in live cells

Cellular system	mRNA(s)	mRNA size	Labeling system	Average pore transit times	Spatial precision (nm)	Temporal precision (ms)	Reference
H. sapiens	Dystrophin[a]	4.8 kb	MS2-MCP	0.5s[b]	n.d.	1000	Mor et al. 2010
M. musculus	β-actin	1.9 kb	MS2-MCP	180ms	26	20	Grunwald and Singer, 2010
C. tentans	All hrp36-containing RNAs	various	hrp36	20s	10	20	Siebrasse et al., 2012
H. sapiens	β-actin Firefly luciferase	3.3 kb 3.3 kb	MS2-MCP	12ms 11ms	8	2	Ma et al., 2013
S. cerevisiae	*GFA1*	2.2 kb	PP7-PCP	188ms[c]	56	15	Smith et al., 2015
S. cerevisiae	*MDN1* *GLIT1* *CLB2*	14.7 kb 6.4 kb 1.5 kb	PP7-PCP	n.d.	n.d.	37	Saroufim et al. 2015

n.d., not determined

[a] truncated ½ - mini dystrophin construct

[b] estimate, limited by temporal resolution

[c] dwell time analysis; 215ms with maximum likelihood estimate

Table reprinted by permission from John Wiley and Sons: Bioessays (Temporal and spatial regulation of mRNA export: Single particle RNA-imaging provides new tools and insights, Heinrich et al.,). 2017.

1.3.9 Modulation of mRNP export during cellular stress

mRNP export serves as another point within the gene expression program that is rapidly modulated in response to altered cellular conditions. In yeast, various environmental stresses such as heat shock and osmotic stress induce the cellular heat shock response to promote the expression of heat shock proteins, which aids in the protection of the cellular proteome (reviewed in Verghese et al., 2012). Consequently, mRNP export is rapidly modulated during this response to prevent the export of "house keeping" mRNAs and promote the export and rapid expression of heat shock (HS) mRNAs required for survival. For example, it was shown many years ago that after a 42°C heat shock in yeast, bulk poly(A)-RNA is sequestered in the nucleus, while the *SSA4* mRNA, encoding a member of the heat shock 70 family of proteins, is rapidly expressed and exported to the cytoplasm (Saavedra et al., 1996). Early studies pointed to the notion that the same machinery (mRNP export factors and NPC proteins) is required for both HS and non-HS mRNPs for export. However, more recent studies have provided insight into how this differential modulation of mRNP export is mechanistically achieved in response to heat shock. Using RNA co-IP experiments, it was found that HS specific mRNAs lack Mex67p adaptor proteins such as Nab2p and Npl3p (Zander et al., 2016). This paired down mRNP composition is thought to promote rapid expression of these mRNAs in two ways: speeding up export competent mRNP formation, and allowing escape of these HS mRNPs from nuclear quality control machinery due to the absence of these adaptor proteins that play a role in nuclear surveillance (Zander and Krebber, 2017). Furthermore, it was identified that Mex67p directly binds HS mRNAs as opposed to interactions through adaptor proteins. This exemplifies the role of Mex67p as a key export receptor sufficient to drive nuclear export of mRNP substrates.

1.4 Cytoplasmic mRNP metabolism coupled to mRNP export

Not surprisingly, mRNP export factors loaded within the nucleus also support translation initiation in the cytoplasm, linking these processes (reviewed in Moore, 2005). The cap binding complex (CBC20/80), which binds the 5′ cap of mRNAs in the nucleus, provides a non-essential role in mRNP export and subsequently supports translation initiation in the cytoplasm. Generally,

CBC20/80 engages with the translation initiation factor 4G (eIF4G), which will recruit the small ribosomal subunit and scan for the translation start site on the mRNA (reviewed in Lejeune et al., 2004; Maquat, 2004). Once the start site is identified, the large ribosomal subunit will be recruited to form the 80S complex required for protein synthesis. Translation requires four distinct stages: (1) initiation, (2) elongation, (3) termination, and (4) recycling to begin initiation again. The first or "pioneering" round of translation results in mRNP remodeling in which the majority of the mRNP export factors loaded on the open reading frame of the mRNA (ORF), within the nucleus, are removed. CBC proteins and other poly(A) binding proteins are also removed following this, being replaced by eIF4E and alternative poly(A) binding proteins. Alterations in mRNP composition continue through the stages of translation. Finally, translation termination occurs following recognition of the stop codon and is facilitated by two essential proteins, eukaryotic release factor 1 and 3 (eRF1 and eRF3) (reviewed in Dever and Green, 2012). eRF1 (or Sup45p in yeast) supports the recognition of the stop codon and promotes hydrolysis of the peptidyl-tRNA in the ribosomal peptidyl-transferase center (PTD). eRF3 (or Sup35p in yeast) enhances this activity to terminate translation through its GTPase activity. Improper termination will lead to recruitment of cytoplasmic mRNA decay machinery (reviewed in Parker and Sheth, 2007).

Notably, where and when the first round of translation occurs in relation to NPCs and the completion of export is not well understood. Towards addressing these questions, an RNA biosensor was recently developed that could visualize the pioneer round of translation in live *Drosophila* oocytes, showing that the translation event first occurs within minutes of export for the transcript tested (Halstead et al., 2015). Moreover, a subpopulation of their reporter construct diffused several micrometers away from the nucleus before being translated, indicating that, at least in *Drosophila* oocytes and for this transcript, the first round of translation does not need to be spatially confined to NPCs or the immediate vicinity. However, EM images have shown that BR mRNPs in the process of export are often oriented to export 5′ cap first and the cytoplasmic portion of the exporting mRNP can be bound by ribosomes, which suggests that the mRNAs can associate with translation machinery coupled to the export process (Mehlin et al., 1995; Visa et al., 1996). Whether translation plays a role in export and mRNP remodeling of this extremely large mRNP or whether it is a result of slow transport times remains unclear. In yeast, export factors are not asymmetrically distributed over mRNA transcripts in a manner that would provide

a mechanism for asymmetric export to promote a pioneering round of translation for example (Baejen et al., 2014; Tuck and Tollervey, 2013). Furthermore, during the pioneer round of translation, mRNAs are subject to quality control to ensure upstream biogenesis events have successfully been completed (Maquat et al., 2010). Key to the surveillance process is the presence of factors in the mRNP that were loaded in the nucleus (e.g. exon-junction complex), which interact with cytoplasmic components to provide an opportunity for crosstalk between nuclear and cytoplasmic processes for the purposes of quality control. Whether certain aspects of quality control are linked to NPCs and export remains an open question.

1.5 rRNA biogenesis and export

rRNAs are the most abundant ncRNAs in the cell and are critical for protein translation. In eukaryotes, four rRNAs and about 80 other proteins form the large and small subunit of the ribosome generating the machinery required for translation (Tschochner and Hurt, 2003). Unlike mRNP processing, rRNP processing begins with biogenesis in the nucleolus, further maturation in the nucleus, export to the cytoplasm, and lastly cytoplasmic maturation to become competent for a role in translation (reviewed in Fromont-Racine et al., 2003; Granneman and Baserga, 2004; Johnson et al., 2002; Kressler and Linder, 1999; Nazar, 2004; Tschochner and Hurt, 2003; Venema and Tollervey, 1999). The nucleolus is a non-membrane bound compartment within the nucleus that serves as the site of ribosome biogenesis. Here, rRNAs are transcribed from rDNA tandem repeats by RNA polymerase I (RNAPI) and RNA polymerase III (RNAPIII). In yeast, RNAPIII synthesizes the 5S transcript, while RNAPI synthesizes a long pre-rRNA transcript containing the mature 18S, 5.8S, and 25S rRNAs, which are separated by spacer sequences. These pre-rRNA transcripts are bound by various RBPs required for further maturation and processing that ultimately results in the formation of the 90S pre-ribosome subunit. Through various nucleotlytic and cleavage events, the 18S is cleaved to form the pre-40S ribosomal subunit and the 5.8S and 25S together form pre-60S ribosomal subunits with the 5S rRNA. Subsequent nuclear maturation and export for each subunit occurs separately.

In contrast to mRNP export, pre-ribosomal subunit export occurs through multiple redundant pathways (reviewed in Zemp and Kutay, 2007). This is likely due to the large number

of pre-ribosomal subunits that are produced and need to be exported to the cytoplasm to maintain cellular survival. There are various NPC components that are critical for the export of pre-ribosomal subunits, however export itself is thought to be dependent on the small shuttling GTPase, Ran, which supports the nucleocytoplasmic transport of a majority of cellular substrates through NPCs (Gleizes et al., 2001; Hurt et al., 1999; Stage-Zimmermann et al., 2000). The pre-60S ribosomal subunit that is exported is composed of the mature 25S, 5.8S, and 5S rRNAs, and its export is largely dependent on Xpo1p activity mediated through the adaptor protein Nmd3p, which contains a C-terminal NES. More recently in yeast, there have been two additional non Xpo1p-dependent pathways that have been attributed to pre-60S ribosomal subunit export. This includes the major mRNP export receptor heterodimer Mex67p-Mtr2p and the pre-60S subunit biogenesis factor Arx1p (Bradatsch et al., 2007; Hung et al., 2008; Wei Yao et al., 2007). Similarly, nuclear export of pre-40S ribosomal subunits is largely dependent on Xpo1p mediated export, and more recently a role for the Mex67p-Mtr2p heterodimer has also linked to pre-40S subunit export (Faza et al., 2012). This study also identified a role for Slx9p in pre-40S subunit export. Slx9p was initially identified to play a role in pre-rRNA processing, however a *slx9Δ* mutant was determined to show pre-40S subunit export defects. Interestingly, Slx9p does not contain an NES or interact with Xpo1p *in vitro*, suggesting it does not serve as an adaptor for Xpo1p. However, Mex67p-Mtr2p binding to the pre-40S subunit is required for Slx9p binding to the pre-40S subunit, suggesting some kind of interplay between these factors.

1.6 tRNA biogenesis and processing

tRNAs represent another subset of structured ncRNAs in the cell that undergo complicated and intricate processes to direct biogenesis and subsequent post-transcriptional alterations required for translation. The requirement of these processing stages, that occur both in the nuclear and cytoplasmic compartments, also necessitates regulated tRNA subcellular trafficking (See Figure 1-5). The essential role of tRNAs is to deliver amino acids to the protein synthesis machinery in the cytoplasm to be incorporated into the nascent polypeptide. There are 42 different families of tRNAs encoded by 274 genes in yeast, which are transcribed in the nucleus by RNAPIII to generate a pre-tRNA transcript (Chan and Lowe, 2008). This pre-tRNA,

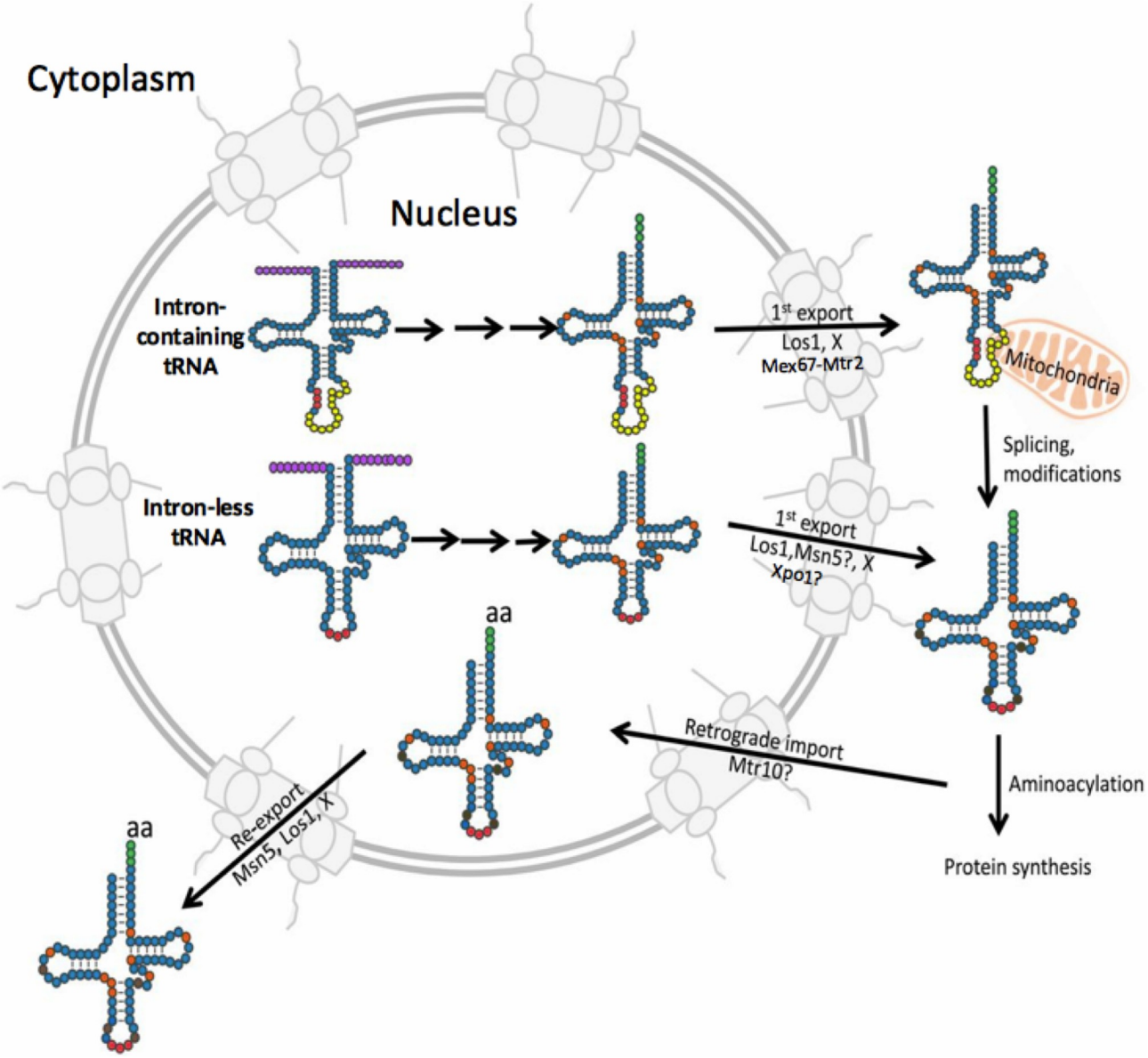

Figure 1-5. tRNA processing and subcellular dynamics. Schematic depicts intron-containing and intron-less pre-tRNAs in the nucleus, which both undergo processing to remove 5′ leader and 3′ trailer sequences (purple), followed by CCA addition (green). Intron-containing tRNAs are exported by Los1p or the Mex67p-Mtr2p heterodimer, and intron-less tRNAs are thought to be exported by Los1p or Msn5p, and Xpo1p may also function here. Splicing of intron-containing tRNAs (intron=yellow), and additional tRNA modifications occur in the cytoplasm. Mature tRNAs can also be imported back into the nucleus which requires Mtr10p, however this may be an indirect function. Mature tRNAs are re-exported by Los1p or Msn5p. X represents the possibility of another unknown exportin/importin functioning here. Figure reprinted by permission from Genetics Society of America: Genetics (Transfer RNA Post- Transcriptional Processing, Turnover, and Subcellular Dynamics in the Yeast Saccharomyces cerevisiae, Anita K. Hopper). 2013.

subsequently serves as a substrate for the various post-transcriptional processing required for functionality in protein synthesis. A majority of pre-tRNAs require a 12 nucleotide leader and trailer sequence to be removed from the 5′ and 3′ ends respectively, and nucleotide addition to the 3′ end (reviewed in Hopper and Phizicky, 2003; O'Connor and Peebles, 1991). In some cases, nucleotide addition to the 5′ end is required, and splicing is required for the subset of tRNAs that contain an intron. Furthermore, tRNA nucleoside modifications include 25 different base or sugar modifications, base deaminations, base isomerizations, and other moiety additions (reviewed in Phizicky and Alfonzo, 2010; Phizicky and Hopper, 2010). Functional tRNAs have a cloverleaf secondary structure and an L-shaped tertiary structure. This includes structural elements such as the 3′ CCA tail that is required for amino acid loading, an acceptor stem (7-9 base pairs) that base pairs the 5′ and 3′ ends of the tRNA and contains the CCA tail, and an anticodon stem loop (5 base pairs) required to read the mRNA matched codon.

For most pre-tRNAs the 5′ end is removed first, through the activity of the endonuclease, RNase P in the nucleus. Removal of the 3′ end is more complex in both bacteria and yeast, requiring the activity of both endo- and exonucleases (Li and Deutscher, 1996; Phizicky and Hopper, 2010). Rex1p functions as the 3′ to 5′ exonuclease in this process, while RNase Z, serves as the endonuclease required for 3′ processing. Following 3′ end removal in yeast and vertebrates, a CCA sequence must be added to the 3′ termini of the pre-tRNA for aminoacylation. This is catalyzed by a tRNA nucleotidyl transferase, CCA1 (Aebi et al., 1990).

Greater than 20% of yeast tRNAs (10 tRNA families) contain an intron and are required to be spliced to be functional and contribute to a complete set of tRNAs for protein synthesis (Chan and Lowe, 2008). Unlike splicing in vertebrates, yeast tRNA splicing enzymes are predominantly localized to the surface of the mitochondria (e.g. tRNA splicing endonuclease) or in the cytoplasm (tRNA ligase), and thus splicing occurs outside of the nuclear compartment in yeast (Huh et al., 2003; Mori et al., 2010; Yoshihisa et al., 2003). Although splicing is confined outside of the nuclear compartment in yeast, work has shown that nuclear splicing is not detrimental to yeast survival (Dhungel and Hopper, 2012). However several splicing enzymes localized to regions outside the nucleus are in fact essential, suggesting essential functions for these factors in the cytoplasm (Dhungel and Hopper, 2012). Thus, intron-containing tRNAs must be exported to the cytoplasm for splicing, and like other tRNAs export is also required for downstream cytoplasmic processing and ultimately a role in protein synthesis. The following sections will

focus on mechanisms of tRNA subcellular trafficking under steady state conditions and during stress.

1.6.1 tRNA export

Similar to pre-ribosomal subunit export through NPCs, tRNA export is largely dependent on the activity of Ran GTPase dependent karyopherins. Although tRNAs are smaller (76-90 nucleotides) than the 40kDa cutoff for passive diffusion through NPCs, export of these substrates nonetheless requires an energy dependent, regulated process. The major export receptor required for tRNA export is the conserved β-karyopherin family member, Los1p (or Exportin-t in humans) (Hellmuth et al., 1998; Hopper et al., 1980; Sarkar and Hopper, 1998). *In vitro* experiments in vertebrates and fission yeast (*S. pombe*) have shown that Exportin-t/Los1p interacts with the structured tRNA backbone and mature 5′ and 3′ ends of tRNAs, not the anticodon stem-loop or introns. As such, it engages with both intron containing pre-tRNAs and spliced tRNAs with equal affinity (Arts et al., 1998; Cook et al., 2009; Lee et al., 2011; Lipowsky et al., 1999). Work in yeast has shown that a *los1Δ* mutant exhibits accumulation of end-processed intron containing tRNAs in the nucleus due to an export block of these substrates, with export being required for splicing to occur in the cytoplasm (Sarkar and Hopper, 1998; Yoshihisa et al., 2003). Los1p mediated export also serves as a key quality control point within tRNA processing given that it binds only end processed tRNAs with an aminoacyl stem. This prevents the premature export of tRNAs that have not been properly matured in the nucleus. Work in vertebrates has shown that Exportin-t binds different tRNAs with varying affinities, and complementary to this work in yeast, it has been shown that the export of various intron-containing tRNAs is affected to varying degrees in a *los1Δ* mutant (Sarkar and Hopper, 1998). Thus, specific tRNAs may have varying affinities for tRNA export receptors requiring multiple redundant pathways (See Figure 1-5).

Surprisingly, Los1p is not essential, thus providing evidence that other parallel pathways for tRNA export must exist. More recent work has identified the major non-karyopherin mRNP export receptor, the Mex67p-Mtr2p heterodimer, to function in tRNA export (Chatterjee et al., 2017; Wu et al., 2015). Accumulation of end-processed, intron containing tRNAs were observed in conditional alleles of *mex67* and *mtr2,* with increased nuclear pools of tRNAs suggesting an

export block shown by FISH. Furthermore, over expression of the Mex67p-Mtr2p heterodimer overcomes tRNA export defects in a *los1Δ* mutant. A direct role for the Mex67p-Mtr2p heterodimer was further established through *in vivo* cross-linking RNA-IP experiments showing that Mex67p binds intron-containing tRNAs. It remains unclear how Mex67p establishes an interaction with tRNAs and if this requires adaptor proteins such as those required for interactions with mRNPs, or if it is more similar to its interaction with rRNAs through a positively charged loop sequence (Yao et al., 2007). Similarly to *los1Δ* cells, mutants of *mex67* and *mtr2* affect the export of various tRNA species to varying degrees with overlap with *los1Δ*, suggesting that there are further unknown components directing tRNA export. This is further supported by the finding that a *mex67/los1* double mutant do not exhibit a more severe growth defect than the single mutants alone. Xpo1p itself may serve as an additional export receptor for tRNAs, as the *xpo1-1* conditional allele exhibits tRNA processing and export defects (Wu et al., 2015). To date, Xpo1p has not been shown to directly interact with tRNAs, thus this may in fact be an indirect effect of general defects in nucleocytoplasmic transport.

The final, most well characterized tRNA export receptor in yeast is another conserved β-karyopherin family member, Msn5p (Exportin-5 in humans). Early work identified Msn5p to be involved in the nuclear export of phosphorylated transcription factors (Kaffman et al., 1998). However, the *msn5Δ* mutant was discovered to exhibit tRNA accumulation in the nucleus, leading to a role for Msn5p in tRNA export (Murthi et al., 2010; Takano et al., 2005). As with *MEX67*, an *msn5Δ/los1Δ* double mutant does not exhibit further growth defect as compared to single mutants, but it does exhibit increased cellular pools of tRNAs. Interestingly, in contrast to a *los1Δ* mutant, an *msn5Δ* mutant does not accumulate intron-containing tRNAs, only spliced tRNAs (Murthi et al., 2010), leading to the hypothesis that Msn5p supports the export of intronless tRNAs only. However, further work has supported that notion that Msn5p in fact supports the re-export of mature tRNAs that have undergone retrograde transport into the nucleus (See Figure 1-5).

1.6.2 Retrograde tRNA import and modulation of tRNA shuttling dynamics during stress

tRNA export was initially thought to occur in an unidirectional manner similar to the export of various other coding and ncRNAs. However, phenotypic characterization of various tRNA processing mutants provided observations that spliced tRNAs can accumulate in the nucleus**.** Given that in yeast, tRNAs are spliced on the surface of mitochondria, these observations were inconsistent with a unidirectional model for tRNA export. Ultimately these observations led to the discovery that tRNAs can undergo retrograde import into the nucleus after an initial export event (Yoshihisa et al., 2007, 2003). Furthermore, evidence for retrograde import has also been found in vertebrates (Barhoom et al., 2011; Miyagawa et al., 2012; Shaheen et al., 2007).

There are several key pieces of evidence that support retrograde import of tRNAs into the nucleus (reviewed in Hopper, 2013). This includes heterokaryon assays in which foreign tRNA encoded in one nucleus accumulates in the other, the observation that mature tRNAs accumulate in the nucleus following nutrient stress in the absence of RNAPIII transcription, and a mutant of the β-karyopherin family (*mtr10 Δ*) prevents the accumulation of spliced tRNAs in the nucleus (Murthi et al., 2010; Senger et al., 1998; Shaheen and Hopper, 2005; Takano et al., 2005; Whitney et al., 2007). There are two reported pathways that contribute to tRNA import, which includes Mtr10p and Ssa2p (Murthi et al., 2010; Senger et al., 1998; Shaheen and Hopper, 2005; Takano et al., 2015). A physical interaction between Mtr10p and spliced tRNAs has not been identified, therefore Mtr10p dependent import may occur indirectly via an additional adaptor protein. Ssa2p is a cytoplasmic heat shock protein that shuttles into the nucleus and can bind tRNAs (Takano et al., 2015). An *ssa2Δ* mutant affects the import of mature tRNAs in response to nutrient starvation.

The complete functional relevance of tRNA import remains unclear; however, there are several hypotheses and evidence to support why this occurs (reviewed in Hopper, 2013). tRNA import may be critical for nuclear tRNA modifications that can only occur after splicing occurs. For example, the yW modification, which only occurs on the $tRNA^{Phe}$, requires the activity of five proteins one of which is nuclear (Trm5p). Trm5p can only function after $tRNA^{Phe}$ has been spliced in the cytoplasm, therefore $tRNA^{Phe}$ must be imported (Ohira and Suzuki, 2011). Additionally, tRNA import may provide a mechanism to modulate global protein synthesis

and/or contribute to tRNA quality control. A mechanism to down-regulate translation in the cytoplasm may include sequestering tRNAs in the nucleus, which is observed upon nutrient starvation (Whitney et al., 2007). Similarly, given the high number of intricate modifications required to generate a mature tRNA, which can be unique to a specific tRNA, and the cellular distribution of tRNA modifying enzymes in both nuclear and cytoplasmic compartments, tRNA import may serve as a mechanism to correct improper processing. For example, pre-tRNAs that have been exported and spliced before appropriate nuclear maturation events have occurred could be imported into the nucleus to correct for this.

tRNAs that experience retrograde transport must then be re-exported to finally function in protein synthesis in the cytoplasm. The observation that only mature tRNAs that have been spliced accumulate in a *msn5Δ* mutant, suggests that Msn5p is required for the re-export of these tRNAs (Murthi et al., 2010). There is no evidence to suggest that Los1p is not also contributing to both the initial export and re-export of tRNAs that are genome encoded with introns. Similarly, both Los1p and Msn5p may contribute to the initial and re-export of tRNAs that are encoded without introns. Furthermore, another mechanism to drive changes in tRNA trafficking may occur through alteration in Los1p localization. When grown in the presence of a non-fermentable carbon source, Los1p localization is altered from being nucleoplasmic to being largely cytoplasmic, and thus unable to function in tRNA nuclear export, leading to a nuclear accumulation of mature tRNAs (Karkusiewicz et al., 2011; Quan et al., 2007). An alternative stress such as DNA damage, induced by methylmethanesulfonate (MMS), also alters Los1p localization in a similar manner resulting in a cellular G1 checkpoint arrest (Ghavidel et al., 2007). Therefore, alteration of tRNA shuttling dynamics mediated though changes in Los1p localization may serve as a mode to modulate/contribute to these cellular stress responses.

1.7 DEAD-box family of ATPases in RNA metabolism

DEAD-box proteins (DBPs) are a family of RBPs found in all domains of life, often displaying RNA-stimulated ATPase activity, with diverse roles in RNA biology (reviewed in Linder and Jankowsky, 2011). DBPs are ubiquitous across RNA metabolism and contribute to almost every RNA-mediated process within the eukaryotic gene expression program. In yeast,

there are 27 DBPs, while in humans this is expanded to 38 (reviewed in Linder, 2006). Extensive biochemical analyses of DBPs have led to the discovery that these proteins can exhibit RNA-stimulated ATPase activity and ATP-dependent RNA helicase activity. These activities are thought to promote RNA folding and RNP arrangements that are critical for driving RNA metabolism. DBPs display highly conserved protein architecture with various critical conserved sequence motifs required for ATP-binding and hydrolysis, and RNA binding. Generally, DBPs are thought to function in three different capacities in RNA metabolism (reviwed in Linder, 2006). First, DBPs can function as helicases, which promotes duplex unwinding of double stranded RNA in an ATP-dependent manner, which can be found in structured RNAs such as rRNAs, or during processes such as pre-mRNA splicing when short RNA-RNA interactions are formed. Second, DBPs can function as RNPases, which alter the RNA structure in an ATP-dependent manner to promote changes in RNA-protein interactions leading to remodeling of the RNP. Third, DBPs can function as scaffolds by stably binding to RNA substrates, which promotes the binding and assembly of various other RBPs to generate a functional RNP. DBPs can exhibit one or all three of the activities; however, the most common defining feature among DBPs is the ability to bind and hydrolyze ATP in a single-stranded or double-stranded RNA-dependent manner. In a rare case, a DBP has also been shown to be stimulated by only DNA, not RNA (Kikuma et al., 2004). It is the progression through the ATPase cycle, which alters the DBPs affinity for RNA and promotes these various activities. The following section will discuss the conserved architecture of DBPs required to facilitate ATPase activity.

1.7.1 Conserved architecture of DEAD-box proteins

DBPs are the largest family within the superfamily 2 (SF2) helicases (Gorbalenya and Koonin, 1993). Like other members in this family, DBPs are composed of two almost identical core domains, which resemble the bacterial recombination protein, recombinase A (RecA) (Caruthers and McKay, 2002; Fairman-Williams et al., 2010; Singleton et al., 2007). These RecA-like domains are connected through a flexible linker region, with conserved sequence motifs found within both domains (See Figure 1-6). Upon binding RNA and nucleotide, the RecA-like domains come together forming a nucleotide binding pocket and an RNA interaction surface. Structural information from various DBPs has provided insight into how conserved

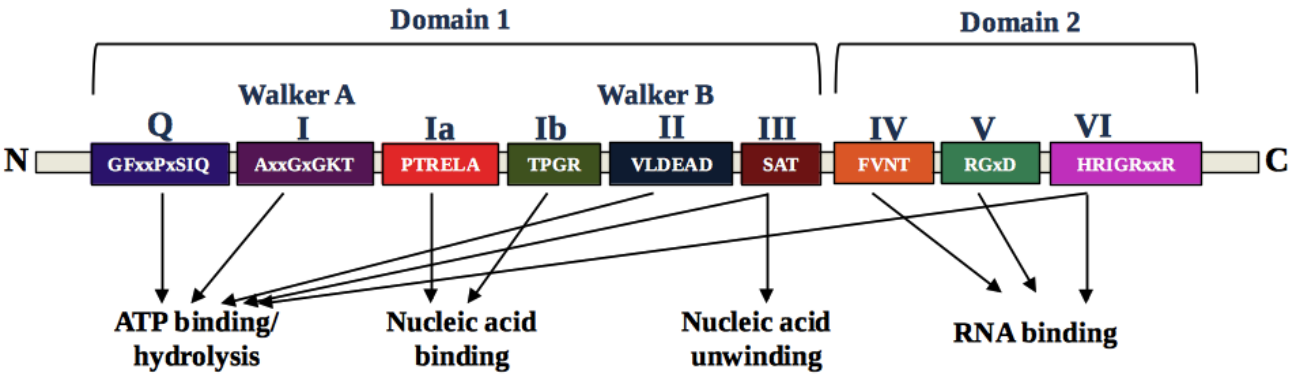

Figure 1-6. Conserved architecture and sequence motifs of DEAD-box proteins. Schematic of DEAD-box protein architecture denoting the two conserved RecA-like domains and various conserved sequence motifs with consensus sequences shown. Arrows indicate evidence for roles for conserved sequence motifs in ATP-binding/hydrolysis, nucleic acid binding or unwinding and specifically RNA binding**.**

sequence motifs contribute to RNA and ATP-binding and hydrolysis. When in complex with RNA and ATP, all nine motifs within the enzymatic core interface between the two domains to form binding sites for RNA and ATP (reviewed in Jarmoskaite and Russell, 2011). Motif II (or the Walker B motif) contains the namesake amino acid sequence D-E-A-D, which along with Motif I (or the Walker A motif), the Q-Motif, and Motif VI is required for ATP recognition, binding, and hydrolysis. ATP binding is achieved through interaction with the ribose moiety and tight binding to the γ-phosphoryl group. Mutations in these motifs weaken or abolish ATPase activity of DBPs. Motifs Ia, Ib, III, IV, and V are required for interaction with RNA and other intramolecular arrangements required for activity. Unlike some other RBPs, the DBP core does not inherently bind RNA with any sequence specificity. The conserved core makes contacts with the negatively changed sugar-phosphate backbone of the RNA. This includes interactions with 2′-OH groups of the RNA, which provides specificity to distinguish between RNA and DNA (Sengoku et al., 2006). Also unique to DBPs, and unlike other SF2 and SF1 helicase families, the DBP core does not make contacts with nucleotide bases, precluding processive translocation along nucleic acids, rendering some DBPs as inefficient helicases in this regard (Pyle, 2008; Singleton et al., 2007). Rather, it is the presence of RNA binding domains in the N- and C-terminal extensions of some DBPs that may provide these interactions to allow for processive helicase activity (reviewed in Jarmoskaite and Russell, 2011).

DBP affinity for RNA is altered dramatically through its ATPase cycle given that the closed conformation (i.e. both domains together) is favored by both nucleotide and RNA binding, with binding of one likely increasing the affinity for binding the other, leading to cooperativity in binding. *In vitro* experiments have demonstrated that for many DBPs, energetic coupling for RNA is strongest after ATP hydrolysis in which the DBP is in an ADP and P_i bound state (Henn et al., 2008). Once P_i is released, the affinity for RNA decreases, leading to a release in RNA binding and the ability for the DBP to repeat the cycle.

DBP functional specificity is largely determined by unique, non-conserved, sequence extensions within the protein, and/or through the spatially constrained regulation of key co-regulators/adaptors for DBPs in the cell. Although the core domains and sequence motifs within DBPs remain highly conserved, DBPs often contain unique amino or carboxyl terminal extensions that provide specificity. These extensions can include features such as RNA binding motifs or other protein interaction sites. Importantly unique co-regulators for DBPs can, for

example, stabilize specific nucleotide bound or nucleotide free enzymatic states, which can spatially regulate activity and function of these enzymes.

1.8 Role of DEAD-box Protein 5 (Dbp5) in gene expression

The essential DBP required for driving the directional process of nuclear mRNP export is Dbp5p (See **section 1.3.6-1.3.7** and Figure 1-3). Several additional roles for Dbpp5 in gene expression have been proposed that point to functional pools of Dbp5p in the nuclear and cytoplasmic compartments. For example, studies have shown both physical and genetic interactions between Dbp5p and transcription initiation and translation termination machinery (Alcazar-Roman et al., 2010; Beißel et al., 2019; Estruch et al., 2012; Estruch and Cole, 2003; Gross et al., 2007). Additionally, a role for Dbp5p in the nuclear export of pre-ribosomal subunits has been identified (Neumann et al., 2016). Most recently, the mammalian and *Xenopus* homologs of Dbp5p, DDX19B, have been shown to stabilize ribosomal elongation and termination complexes *in vitro* and contribute to nuclear R-loop clearance upon replication or DNA damage stress (Hodroj et al., 2017; Mikhailova et al., 2016). These data suggest a much broader role for Dbp5p in RNA metabolism and gene expression, but the mechanisms by which Dbp5p contributes to these various cellular processes remains largely undefined. The following sections will discuss the spatial regulation of Dbp5p ATPase activity and its role in the eukaryotic gene expression program.

1.8.1 Dbp5p activity in mRNP export

Over two decades ago, a screen of temperature sensitive mutants affecting poly(A)-RNA export first identified RAT8 to be required for mRNP export (Amberg et al., 1992). Subsequent work identified RAT8 to be DBP5, which had been identified earlier in yeast as a putative DEAD-box protein of unknown function, and further characterized a role for Dbp5p in mRNP export (Chang et al., 1990; Snay−Hodge et al., 1998; Tseng et al., 1998). Given the spatial constraints of Dbp5p activation through co-regulators (Gle1p-IP_6 and Nup159p) at the

cytoplasmic face of NPCs, it is here that Dbp5p is thought to play an essential role in mRNP export. In fact, under steady state conditions GFP-Dbp5p is observed to be predominantly localized to the nuclear envelope (Snay−Hodge et al., 1998; Tseng et al., 1998). Mutants of Dbp5p in which RNA binding is abolished, still localize to NPCs, suggesting that this localization is not dependent on RNA binding (Hodge et al., 2011). However, mutations that affect Dbp5p binding to Nup159p change Dbp5p localization to cytoplasmic, supporting the importance of this interaction for steady-state localization at NPCs (Napetschnig et al., 2009; Noble et al., 2011; Schmitt et al., 1999; Weirich et al., 2004). There is no direct evidence to point to exactly what role Dbp5p has in mRNP export. Furthermore, RNA binding preferences for Dbp5p are not known, therefore it remains unclear what subset of RNAs Dbp5 is working on in the cell. However, biochemical and *in vitro* experiments have pointed to an RNPase role for Dbp5p at the cytoplasmic face of NPCs. For example, RNA-IP experiments from a cold sensitive mutant allele of DBP5, *rat8-7*, identified an increased level of Mex67p bound to mRNAs (Lund and Guthrie, 2005). This led to the hypothesis that Dbp5p remodels mRNPs, which removes Mex67p from exporting mRNPs leading to release into the cytoplasm. Similarly, *in vitro* assays revealed that Dbp5p activity can remove Nab2p bound to single-stranded RNA, which is further stimulated by the addition of Gle1-IP_6 (Tran et al., 2007). However confusingly, this activity is reported to occur when Dbp5p is bound to ADP, which has poor affinity for RNA. As such, how remodeling is mechanistically achieved remains unclear.

1.8.2 Spatial regulation of Dbp5p activity

Biochemical and structural insights into Dbp5p have provided extensive information into the regulation of Dbp5p, which includes mechanisms conserved with other DBPs. However, Dbp5p activity also includes several unique features separate from other DBPs. Primarily, Dbp5p binds RNA and ATP in a conserved manner similar to other DBPs (Collins et al., 2009; Dossani et al., 2009; Fan et al., 2009; Montpetit et al., 2011; Napetschnig et al., 2009; von Moeller et al., 2009). Both domains form a clamp around ATP, which then generates an RNA interaction surface across both domains to interact with the phosphate backbone of single stranded RNA with the highest affinity (See Figure 1-7). The N-terminal domain of Dbp5p interacts with the 3′

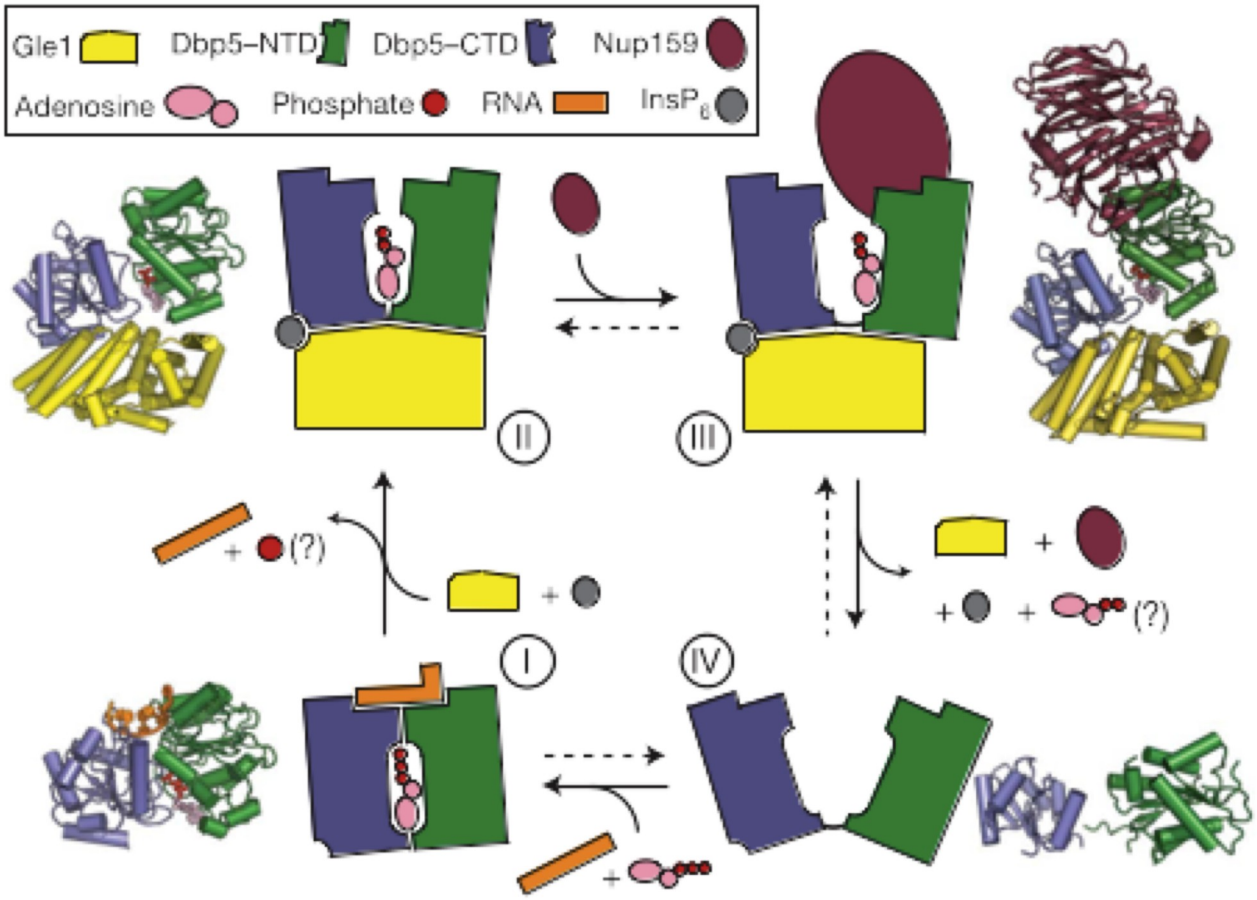

Figure 1-7. Mechanochemical ATPase cycle and structural models of Dbp5p. Dbp5p binds RNA, in the presence of ATP, which remodels duplexed RNA or RNPs (state I). ATP hydrolysis then allows the activator (Gle1p) to bind both the C-terminal and N-terminal RecA-like domains, separating the two domains and promoting RNA release (state II). Subsequent release of the bound RNA allows Nup159p to bind Dbp5p causing the two RecA domains to further separate (state III). The formation of this state then weakens the interaction between Dbp5p-ADP and Gle1p, preventing the rebinding of the RNA, and aids in enzyme recycling (state IV). Crystal structure models taken from PDB 3RRM and 3PEY (Fan et al., 2009; Montpetit et al., 2011). Figure reprinted from Montpetit et al., 2011. Figure reprinted by permission from Springer Nature: Nature (A conserved mechanism of DEAD-box ATPase activation by nucleoporins and InsP6 in mRNA export, Montpetit et al.,). 2011.

end of single stranded RNA, while the 5′ end interacts with the C-terminal domain. *In vitro* RNA binding assays have established that ATP binding is critical for Dbp5p to bind RNA tightly (Hodge et al., 2011; Montpetit et al., 2011; Tran et al., 2007). RNA binding is abolished in the absence of nucleotide, therefore it is likely that ATP binding occurs before RNA binding.

In vitro experiments have also shown that recombinant Dbp5p from yeast has poor intrinsic ATPase activity (Montpetit et al., 2011; Tseng et al., 1998). Furthermore, early experiments showed that Dbp5p ATPase activity is stimulated by the addition of Gle1p, which is further stimulated by the addition of IP_6 (Alcazar-Roman et al., 2006; Dossani et al., 2009; Montpetit et al., 2011; Weirich et al., 2006). IP_6 addition on its own is not stimulatory for Dbp5p. GLE1, IPK1 and IPK2 (required for the generation of IP_6) were identified in early screens probing for factors critical for bulk poly(A)-RNA export (Miller et al., 2004; York et al., 1999). In fact, subsequent X-ray crystal structures of Dbp5p in complex with Glep1 have shown that IP_6 binds in a positively charged pocket between Dbp5p and Gle1p, likely promoting these interactions leading to ATPase stimulation (Montpetit et al., 2011).

Additional unique features of Dbp5p ATPase regulation when compared to other DBPs is the non-essential auto-inhibitory function of the N-terminal domain, and the action of Nup159p in the ATPase cycle. An inhibitory function of the N-terminal domain (amino acids 1-90) of Dbp5p was first identified through X-ray crystallography experiments of the human homolog of Dbp5p, DDX19B, in which an alpha-helix was found to localize between the two RecA-like domains, stabilized in a Dbp5p-ADP and RNA-free conformation, disrupting the binding of ATP (Collins et al., 2009). Truncation of this N-terminal region in both human and yeast Dbp5p leads to increased stimulation of ATPase activity, however this is not further affected by the presence of RNA in yeast (Montpetit et al., 2011). These results suggest that in yeast, this N-terminal extension plays some role in auto-regulating Dbp5p ATPase activity, which is modulated by the presence of RNA. In the case of Nup159p (or NUP214 in humans), the C-terminal β-propeller of Nup159p interacts with the N-terminal domain of Dbp5p (Montpetit et al., 2011; Noble et al., 2011; Weirich et al., 2004). This interaction surface overlaps with the RNA binding interface of Dbp5p, which suggests RNA binding and Nup159p is mutually exclusive for Dbp5p (Montpetit et al., 2011; von Moeller et al., 2009). Early biochemical analyses predicted that Nup159p likely functions as an ADP release factor for Dbp5p, thus also promoting recycling of the enzyme (Noble et al., 2011). This was thought to be achieved through binding of Nup159p to Dbp5pp-

ADP in complex with Gle1-IP_6, promoting separation of the domains leading to release of ADP. However, more recent solution based *in vitro* approaches have determined that Nup159p does not accelerate ADP release in the mechanochemical cycle of Dbp5p (See Figure 1-7) (Wong et al., 2018). Rather, Nup159p weakens the interaction between Dbp5p-ADP and Gle1p, positing this to be the mode for enzyme turnover, and subsequent rounds of ATP hydrolysis and ADP release to not be a rate-limiting step for Dbp5p.

1.8.3 Dynamics of Dbp5p shuttling

To further complicate models of Dbp5p function, Dbp5p is a highly dynamic protein that rapidly shuttles between the nuclear and cytoplasmic compartments. Early electron microscopy experiments in *C. tentans* with immuno-gold labeled Dbp5 showed Dbp5 in the nucleus (Zhao et al., 2002). Dbp5p localization at 37°C in a temperature sensitive allele of MEX67 (*mex67-5*), in which mRNP export is blocked, is nucleoplasmic (Hodge et al., 1999). These results suggest that there is a nuclear pool of Dbp5p that is associated with nuclear RNPs, which then accumulates in the nucleus when export is disrupted. Similarly, Dbp5p localization is altered to become nucleoplasmic in an *xpo1-1* temperature sensitive mutant, suggesting that the nuclear export of a pool of Dbp5p is dependent on the exportin activity of Xpo1p, providing a potential mechanism for Dbp5p shuttling (Hodge et al., 1999). Like heat stress, ethanol stress also results in the accumulation of poly(A)-RNA. Interestingly only in response to ethanol stress, Dbp5p localization is altered to become nucleoplasmic (Takemura et al., 2004), which may be due to Dbp5p bound mRNPs accumulating in the nucleus. However, ethanol stress has also been shown to breakdown Xpo1p dependent nuclear export, which may inhibit Dbp5p export and also lead to the accumulation of Dbp5p in the nucleus. It remains to be determined what the functional role of nuclear Dbp5p is, and if it is distinct or integrated with the NPC associated pool of Dbp5p thought to be required for mRNP export.

1.8.4 Non-canonical roles for Dbp5p in gene expression

Providing further support for distinct functional pools of Dbp5p in the cell is work identifying genetic and physical interactions between Dbp5p and transcription initiation machinery. Estruch and Cole (2003) carried out multiple genetic screens to identify high-copy suppressors of the DBP5 temperature sensitive (Ts) allele, *rat8-6*, and synthetic lethal interactions with another Ts allele, *rat8-2*. These screens identified a mutant, which results in the N-terminal truncation of Ssl1p to suppress the growth defect of *rat8-6* and *rat8-2*. Ssl1p is a component of transcription factor IIH (TFIIH), which is essential for RNAPII transcription initiation and promoter clearance, and Ssl1p has also been linked to a role nucleotide excision repair (Feaver et al., 1993; Wang et al., 1995). Complementary to this, Dbp5p was determined to physically interact with Rad3p, Tfb1p, and Tfb2p, which are subunits of TFIIH. Furthermore, a synthetic lethal interaction between *rat8-2* and *bur6-ts* was identified. Bur6p is a component of a transcription regulator complex that can bind the TATA-box binding protein to activate RNAPII transcription at some promoters (Geisberg et al., 2001; Prelich, 1997).

More recently, studies of the mammalian homologs of Dbp5p have suggested a role for Dbp5 in the DNA-damage response (Hodroj et al., 2017). In response to DNA-damage inducing agents such as ultra-violet (UV) light, camptothecin, or MMS, Ddx19 re-localizes to the nuclear compartment. This re-localization is dependent on the activity of the ATR and Chk2 protein kinases that have been implicated in signaling pathways required to mitigate DNA-damage (Matsuoka et al., 2007). Furthermore, deletion of DDX19b results in the accumulation of aberrant RNA::DNA hybrids in the nucleus known as R-loops. These results are in line with Ddx19 playing a role in R-loop clearance upon DNA-damage stress. Together, these data suggest a role for Dbp5p in RNAPII transcription and the DNA-damage response, however further work is required to determine if and how Dbp5p activity is directly contributing to these processes.

Conversely, in the cytoplasm Dbp5p has also been linked to roles in translation termination (Beißel et al., 2019; Gross et al., 2007). First, sucrose density fractionation experiments in yeast identified Dbp5p to be localized to polysome-containing fractions. DBP5 Ts mutants, *rat8-2* and *rat8-3* were determined to have synthetic lethal interactions with eukaryotic translation release factors eRF1 (SUP45) and eRF3 (SUP35), which are required for polypeptide and tRNA release at the stop codon. Using luciferase reporter assays, these mutants were also shown to exhibit

increased translation termination read-through defects. To further support a direct role for Dbp5p in this process, a physical interaction between eRF1 and Dbp5p was identified. More recent work, through *in vitro* and *in vivo* approaches, has supported a model in which Dbp5p delivers eRF1 to the stop codon, likely preventing eRF3 from prematurely binding (Beißel et al., 2019). Dbp5p binding to eRF1 and eRF3 binding to eRF1 was found to be mutually exclusive supporting this model.

A screen identifying genome-wide synthetic lethal interactions with the *rat8-2* mutant allele of DBP5 has supported roles for Dbp5p in these pathways (Scarcelli et al., 2008). This screen expectedly identified mRNP export factors and non-essential components of NPCs. Interestingly, this screen revealed genetic interactions between *rat8-2* and mutants of transcription and translation machinery, chromatin remodelers, and also processing body (P-body) components. A direct role for Dbp5p in P-bodies has not be established, rather it was hypothesized that disruption of upstream processes such as mRNP export and translation termination may lead to an increased demand on cytoplasmic mRNA decay machinery, leading to these genetic interactions.

Finally, outside of mRNA metabolism, Dbp5p has been found to contribute to pre-ribosomal subunit and telomerase RNA export. Through FISH experiments probing for rRNAs, pre-40S and pre-60S ribosomal subunit export was found to be disrupted in *dbp5* Ts mutants under conditions in which mRNP export was largely unaffected (Neumann et al., 2016). Interestingly, an ATPase deficient *dbp5* mutant and mutants of *gle1,* which have robust mRNP export defects, do not show pre-ribosomal subunit export defects. Thus, suggesting the requirement for efficient Dbp5p ATPase activity in pre-ribosomal subunit export is less critical when compared to mRNP export. Similarly, the export of the telomerase RNA *TLC1* was found to be disrupted in a *dbp5* Ts mutant (Wu et al., 2014). However, mutants of other essential mRNP export machinery such as NUP159 and MEX67 also showed this phenotype. Both Mex67p and Dbp5p were also shown to physically interact with *TLC1*, further suggesting a role for mRNP export machinery in the export of *TLC1*.

1.9 Thesis Focus

This thesis focuses on understanding the spatial and temporal regulation of mRNP export in yeast, and further explores the broader role of an essential mRNP export factor, Dbp5p, in the eukaryotic gene expression program. As will be described in chapter III, this has involved the development of an *in vivo* single particle imaging approach in yeast to visualize mRNP export events with high spatial precision and temporal resolution. Through use of this system it was determined that mRNP export is fast, occurring on the order of hundreds of milliseconds in yeast, and that mRNPs are frequently confined near the NE following export to the cytoplasm. It was also demonstrated that mutation of the major mRNP export factor, Mex67p caused delay in cytoplasmic release of mRNPs and resulted in mRNPs undergoing retrograde transport into the nucleus. Thus providing evidence for the requirement of functional Mex67p in mRNPs for cytoplasmic release and directionality across NPCs.

With the goal of understanding the cellular functions of Dbp5p, studies presented in chapter IV employ a comprehensive alanine scanning mutagenesis approach to generate mutants encompassing residues 2-482 of Dbp5p. Combined with published Dbp5p structures, these resulting data provide a functional map of Dbp5p at a single amino acid resolution and mutant alleles that can be employed to detail mechanisms by which Dbp5p contributes to eukaryotic gene expression. This is exemplified by the identification of and characterization of key mutants that impact Dbp5p nuclear transport without perturbation of mRNP export. Rather, a novel role for nuclear Dbp5p in nuclear tRNA export was discovered. Overall, this new knowledge, combined with previous work, identifies Dbp5p as a critical mediator of global gene expression functioning to support the biogenesis and export of mRNAs, rRNAs, and tRNAs.

Chapter II: *Experimental Procedures*

2.1 Yeast strains and media

Yeast strains and plasmids used in this work are listed in Tables 2.1 and 2.2. Yeast strains were grown in YPD (1% yeast extract, 1% peptone, 2% glucose), or in selective drop out media referred to as synthetic complete (SC) media supplemented with 2% glucose if harboring plasmids with prototrophic markers (Sherman et al., 2003). SC media lacking amino acids for selection is specified for each experiment. Yeast transformations to introduce autonomously replicating plasmids (CEN) or PCR/plasmid-derived linear DNA fragments for targeted genome integration were performed using a previously described lithium acetate (LiAc)/polyethylene glycol (PEG) method with some alterations (Gietz and Woods, 2002). Briefly, 5ml of cell culture was grown overnight to mid-log phase (~$O.D_{600}$=0.5-1.0) and harvested by centrifugation (3000xg for 5 min), washed once with water, and then washed with 0.1M LiAc. Cells were then re-suspended in 336µl of transformation mix containing 240µl polyethylene glycol (PEG), 36µl LiAc, and 10µl of 10mg/ml salmon sperm DNA. For plasmid transformations, 1µl of plasmid DNA (~100ng/µl) and 49µl of water was added to the transformation mix. For transformations with linear DNA fragments, 50ul of the generated PCR product or 50ul of the digested plasmid (1µg) was added to the transformation mix. Next, the samples were vortexed and incubated at 30°C for 30 min and then at 42°C for 20 min. Cells were harvested by centrifugation and plated on SC media lacking the appropriate amino acid if prototrophic selection was required. When cassettes containing resistant markers were used (e.g. *KanMX* and *NatMX*), cells were plated on YPD media supplemented with the appropriate drug (e.g. G418 or nourseothricin).

To transform haploid yeast strains with DNA cassettes for endogenous genomic integration or tagging, a PCR based homologous recombination method was used as described previously (Longtine et al., 1998). DNA fragments used for this PCR based approach were generated using the high fidelity Q5 Polymerase (New England Biolabs) and used either plasmid or chromosomal DNA as a template. For endogenous tagging (tdTomato, MYC_{13}) at the carboxy-terminal end of the gene of interest, oligonucleotides were designed with 40 bps of homology to regions just upstream and downstream of the stop codon. For endogenous integration of DBP5 alleles, a DNA fragment with the mutation of interest, a selectable marker within a region of ~700 base pairs of sequence upstream of the start codon, and ~500 base pairs of sequence downstream of the stop codon was generated by digestion and transformed into BMY15. All

targeted genomic integrations were confirmed by PCR, sequencing, and/or fluorescence microscopy to confirm expression when appropriate.

2.1.1 Strain construction for single-particle imaging

To generate imaging strains, a set of *24xPP7* stem loops with a KanMX selectable marker flanked by loxP sites was integrated into the 3′ UTR of the *GFA1* gene using pDZ417 (Hocine et al., 2013) in the diploid yeast strain BY4743 (BMY008). Cre recombinase was expressed from pSH47 (Güldener et al., 1996) to remove the selectable marker and restore the 3′ UTR with the exception of the PP7 loops and a single loxP site. NDC1 was C-terminal tagged in the *GFA1-PP7* heterozygous diploid with tdTomato (Sheff and Thorn, 2004), followed by sporulation and tetrad dissection to isolate a haploid of each mating type that carried *GFA1-PP7* and the Ndc1-tdTomato fusion. The *mex67-5* allele was subsequently integrated into the genome of each haploid using a PCR-based homologous recombination approach, which was confirmed by PCR, temperature sensitivity, and an mRNA export phenotype. Haploids were then mated to form diploids homozygous for the PP7 loops and NDC1 fusion with and without the *mex67-5* allele. Finally, to allow for the visualization of the PP7 containing *GFA1* transcripts, a pRS313-P_{Met25}PP7-CP-3xYFP plasmid (pBM242) was introduced into the diploid strain to generate the *REF* (BMY083) and *mex67-5* (BMY135) strains. To assess growth after PP7 stem loop addition, growth rates were measured for a control strain with no PP7 loops (BMY642) and the *REF* strain (BMY83). Strains were grown overnight in a 24-well plate format with shaking at 26°C, and OD_{600} measurements were performed using the CLARIOstar plate reader (BMG Labtech). The *mex67-5* strain (BMY135) was also assessed for growth defects in comparison with a control strain (BMY129).

Table 2-1. Yeast strains

Name	Genotype	Reference
BMY008	BY4743 (MATa/Matα *his3Δ1/his3Δ1 leu2Δ0/leu2Δ0 LYS2/lys2Δ0 met15Δ0/MET15 ura3Δ0/ura3Δ0*)	(Brachmann et al., 1998)

BMY083	BY4743 (MATa/Matα *his3Δ1/his3Δ1 leu2Δ0/leu2Δ0 LYS2/lys2Δ0 met15Δ0/MET15 ura3Δ0/ura3Δ0) GFA1-24xPP7/ GFA1-24xPP7 NDC1-tdTomato::KanMX/NDC1-tdTomato::KanMX* + [pBM242])	This study
BMY129	BY4743 (MATa/Matα *his3Δ1/his3Δ1 leu2Δ0/leu2Δ0 LYS2/lys2Δ0 met15Δ0/MET15 ura3Δ0/ura3Δ0) NAT MX::DBP5/NAT MX::DBP5 GFA1-24xPP7/GFA1-24xPP7 NDC1-tdTomato::KanMX/NDC1-tdTomato::KanMX* + [pBM242])	This study
BMY135	BY4743 (MATa/Matα *his3Δ1/his3Δ1 leu2Δ0/leu2Δ0 LYS2/lys2Δ0 met15Δ0/MET15 ura3Δ0/ura3Δ0) mex67-5::NAT MX/mex67-5::NAT MX GFA1-24xPP7/GFA1-24xPP7 NDC1-tdTomato::KanMX/NDC1-tdTomato::KanMX* + [pBM242])	This study
BMY642	BY4743 (MATa/Matα *his3Δ1/his3Δ1 leu2Δ0/leu2Δ0 LYS2/lys2Δ0 met15Δ0/MET15 ura3Δ0/ura3Δ0) NDC1-tdTomato::KanMX/NDC1-tdTomato::KanMX* + [pBM242])	This study
KWY5566	BY4741 (MATa *his3Δ1 leu2Δ0 met15Δ0 ura3Δ0) MEX67-EGFP::HIS3MX GFA1-24xPP7 NDC1-tdTomato::KanMX*)	This study
KWY5567	BY4741 (MATa *his3Δ1 leu2Δ0 met15Δ0 ura3Δ0) mex67-5EGFP::HIS3MX GFA1-24xPP7 NDC1-tdTomato::KanMX*)	This study
BMY015	YPH500 (MATa *ura3-52 lys2-801 ade2-101 trp1-Δ1 his3-Δ200 leu2-Δ1 dbp5Δ*::HIS3 + [pCA5005])	(Tseng et al., 1998)
BMY830	YPH500 (MATa *ura3-52 lys2-801 ade2-101 trp1-Δ1 his3-Δ200 leu2-Δ1dbp5Δ*::HIS3 + [pBM464])	This study
BMY1000	W303 (MATa *leu2-3,112 trp1-1 can1-100 ura3-1 ade2-1 his3-15* GFP-DBP5::URA3 + [pBM497])	This study
BMY1001	W303 (MATa *leu2-3,112 trp1-1 can1-100 ura3-1 ade2-1 his3-15* GFP-*dbp5-L12A::*URA3 + [pBM497])	This study
BMY948	W303 (MATa *leu2-3,112 trp1-1 can1-100 ura3-1 ade2-1 his3-15* DBP5*::*URA3)	This study
BMY950	W303 (MATa *leu2-3,112 trp1-1 can1-100 ura3-1 ade2-1 his3-15 dbp5-L12A::*URA3)	This study
BMY1092	W303 (MATa *leu2-3,112 trp1-1 can1-100 ura3-1 ade2-1 his3-15 dbp5-R423A::*URA3)	This study
BMY1742	W303 (MATa *leu2-3,112 trp1-1 can1-100 ura3-1 ade2-1 his3-15 dbp5-L12A-R423A::*URA3)	This study
BMY1650	BY4743 (MATa *his3Δ1 leu2Δ0 lys2Δ0 met15Δ0 ura3Δ0* + [pBM394])	This study
BMY1652	BY4743 (MATa *his3Δ1 leu2Δ0 lys2Δ0 met15Δ0 ura3Δ0* + [pBM541])	This study
BMY1651	BY4743 (MATa *his3Δ1 leu2Δ0 lys2Δ0 met15Δ0 ura3Δ0* + [pBM504])	This study
BMY1653	BY4743 (MATa *his3Δ1 leu2Δ0 lys2Δ0 met15Δ0 ura3Δ0* + [pBM542])	This study
BMY624	W303 (MATa *leu2-3,112 trp1-1 can1-100 ura3-1 ade2-1 his3-15 xpo1Δ::LEU2* +[pKW711])	(Scott et al., 2009)

BMY1654	W303 (MATa *leu2-3,112 trp1-1 can1-100 ura3-1 ade2-1 his3-15 xpo1Δ::LEU2* +[pKW711] +[pBM394])	This study
BMY1656	W303 (MATa *leu2-3,112 trp1-1 can1-100 ura3-1 ade2-1 his3-15 xpo1Δ::LEU2* +[pKW711] +[pBM541])	This study
BMY1655	W303 (MATa *leu2-3,112 trp1-1 can1-100 ura3-1 ade2-1 his3-15 xpo1Δ::LEU2* +[pKW711] +[pBM504])	This study
BMY1657	W303 (MATa *leu2-3,112 trp1-1 can1-100 ura3-1 ade2-1 his3-15 xpo1Δ::LEU2* +[pKW711] +[pBM542])	This study
BMY647	W303 (MATα t*or1-1 fpr1*::NAT *ade2-1 trp1-1 can1-100 leu2-3,112 his3-11,15 ura3* GAL psi+)	(Haruki et al., 2008a)
BMY677	W303 (MATα t*or1-1 fpr1*::NAT *ade2-1 trp1-1 can1-100 leu2-3,112 his3-11,15 ura3* GAL psi+ GFP-FRB-DBP5::URA3 HTB2-2x-FKBP12::HIS3)	This study
BMY1392	W303 (MATα t*or1-1 fpr1*::NAT *ade2-1 trp1-1 can1-100 leu2-3,112 his3-11,15 ura3* GAL psi+ GFP-FRB-*dbp5-R423A*::URA3 HTB2-2x-FKBP12::HIS3)	This study
BMY676	W303 (MATα t*or1-1 fpr1*::NAT *ade2-1 trp1-1 can1-100 leu2-3,112 his3-11,15 ura3* GAL psi+ GFP-FRB-DBP5::URA3 PEX25-2x-FKBP12::HIS3)	This study
BMY1099	W303 (MATα t*or1-1 fpr1*::NAT *ade2-1 trp1-1 can1-100 leu2-3,112 his3-11,15 ura3* GAL psi+ GFP-FRB-*dbp5ΔNES*::URA3 PEX25-2x-FKBP12::HIS3	This study
BMY1357	W303 (MATα t*or1-1 fpr1*::NAT *ade2-1 trp1-1 can1-100 leu2-3,112 his3-11,15 ura3* GAL psi+ GFP-FRB-DBP5::URA3 PEX25-2x-FKBP12::HIS3 *xpo1-T539C*::KANMX)	This study
BMY836	W303(MATα *leu2-3,112 trp1-1 can1-100 ura3-1 ade2-1 his3-15* SUP45-13Myc*::*HIS3)	This study
BMY894	W303(MATα *leu2-3,112 trp1-1 can1-100 ura3-1 ade2-1 his3-15* SUP45-13Myc*::*HIS3 +pBM464)	This study
BMY900	W303(MATα *leu2-3,112 trp1-1 can1-100 ura3-1 ade2-1 his3-15* SUP45-13Myc*::*HIS3 +pBM720)	This study
BMY1940	W303 (MATa *leu2-3,112 trp1-1 can1-100 ura3-1 ade2-1 his3-15* DBP5*::*URA + [pBM729])	This study
BMY1941	W303 (MATa *leu2-3,112 trp1-1 can1-100 ura3-1 ade2-1 his3-15 dbp5-R423A::*URA3 + [pBM729])	This study
BMY1942	BY4742 (MATα *his3Δ1 leu2Δ0 lys2Δ0 ura3Δ0 rad54Δ::KANMX)*	(Brachmann et al., 1998)
BMY1328	W303 (MATa *leu2-3,112 trp1-1 can1-100 ura3-1 ade2-1* DBP5*::*URA3)	This study
BMY1330	W303 (MATa *leu2-3,112 trp1-1 can1-100 ura3-1 ade2-1 dbp5-L12A::*URA3)	This study
BMY1332	W303 (MATa *leu2-3,112 trp1-1 can1-100 ura3-1 ade2-1 dbp5-R423A::*URA3)	This study
BMY217 / (Y7092)	BY4742 (MATα can1*Δ::STE2pr-Sp_his5 lyp1Δ his3Δ1 leu2Δ0 ura3Δ0 met15Δ0)*	(Tong and Boone, 2007)
BMY794	BY4742 (MATα can1*Δ::STE2pr-Sp_his5 lyp1Δ his3Δ1 leu2Δ0*	This study

	ura3Δ0 met15Δ0 dbp5-L12A::URA3)	
BMY1308	BY4742 (MATα can1*Δ::STE2pr-Sp_his5 lyp1Δ his3Δ1 leu2Δ0 ura3Δ0 met15Δ0 dbp5-R423A::URA3)*	This study
BMY1051	BY4741 (MATα *his3Δ1 leu2Δ0 ura3Δ0 met15Δ0 ura10Δ::KANMX)*	(Li et al., 2011)
BMY320	BY4741 (MATα *his3Δ1 leu2Δ0 ura3Δ0 met15Δ0 mex67-5::KANMX)*	(Li et al. 2011)
BMY333	BY4741 (MATα *his3Δ1 leu2Δ0 ura3Δ0 met15Δ0 dbp5-1::KANMX)*	(Li et al. 2011)
BMY344	BY4741 (MATα *his3Δ1 leu2Δ0 ura3Δ0 met15Δ0 nup159-1::KANMX)*	(Li et al. 2011)
BMY338	BY4741 (MATα *his3Δ1 leu2Δ0 ura3Δ0 met15Δ0 gle1-4::KANMX)*	(Li et al. 2011)
BMY009	BY4743 (MATa his3Δ1 leu2Δ0 lys2Δ0 met15Δ0 ura3Δ0)	(Brachmann et al. 1998)
BMY1943	BY4743 (MATa his3Δ1 leu2Δ0 lys2Δ0 met15Δ0 ura3Δ0 *dbp5-V73A*::NATMX)	This study
BMY1335	BY4743 *(MATa his3Δ1 leu2Δ0 lys2Δ0 met15Δ0 ura3Δ0 pProtA-TEV-His6-DBP5::NATMX)*	This study
BMY1341	BY4743 *(MATa his3Δ1 leu2Δ0 lys2Δ0 met15Δ0 ura3Δ0 pProtA-TEV-His6-dbp5-R423A::NATMX)*	This study
BMY1903	BY4741 (MATα *his3Δ1 leu2Δ0 ura3Δ0 met15Δ0 ura10Δ::KANMX* + [pBM718]*)*	This study
BMY1904	BY4741 (MATα *his3Δ1 leu2Δ0 ura3Δ0 met15Δ0 mex67-5::KANMX* + [pBM718])	This study
BMY1906	BY4741 (MATα *his3Δ1 leu2Δ0 ura3Δ0 met15Δ0 nup159-1::KANMX)* + [pBM718])	This study
BMY1907	BY4741 (MATα *his3Δ1 leu2Δ0 ura3Δ0 met15Δ0 gle1-4::KANMX* +pBM718*)*	This study
BMY1939	YPH500 (MATa *ura3-52 lys2-801 ade2-101 trp1-Δ1 his3-Δ200 leu2-Δ1dbp5Δ*::HIS3 + [pBM939]	This study

2.2 Plasmids

Table 2-2. Plasmids

Name	Description	Reference
pKT178	pFA6a–link–tdimer2–KanMX (integrative plasmid, SP6 promoter for C-terminal tdimer2 protein fusion with KanMX-based selection)	(Sheff and Thorn, 2004)
pBM242	pRS313-PME TPP7-CP-3xYFP (HIS3 CEN plasmid, MET17 promoter for PP7-CP-3xYFP expression)	This study
pDZ417	pDZ417-24xPP7-loxP-KanMX-loxP (integrative plasmid, T7	(Hocine et al.,

	promoter for 24xPP7-loxP-KanMX-loxP cassette integration)	2013)
pYM28	pFA6-yEGFP-HIS3MX (integrative plasmid, SP6 promoter for C-terminal yEFG protein fusion with HIS3MX-based selection)	(Janke et al., 2004)
pSH47	pRS416-GAL1-Cre (URA3 CEN plasmid, GAL1 promoter for Cre recombinase expression)	(Güldener et al., 1996)
pCA5005	pRS316-DBP5::URA3 (CEN plasmid)	(Tseng et al., 1998)
pBM464	pRS315-GFP-DBP5::LEU2 (CEN plasmid)	This study
pBM497	pRS315-NOP1-RFP-LEU2 (CEN plasmid)	(Lapetina et al., 2017)
pBM394	pRS316-NLS^{sv40}-NES$^{PKI\text{-}inactive}$-2xGFP::URA3 (CEN plasmid)	This study
pBM541	pRS316-NLS^{sv40}-NES^{PKI}-2xGFP::URA3 (CEN plasmid)	This study
pBM504	pRS316-NLS^{sv40}-NES$^{PKI\text{-}inactive}$-NES^{DBP5}-2xGFP::URA3 (CEN plasmid)	This study
pBM542	pRS316-NLS^{sv40}-NES$^{PKI\text{-}inactive}$-NES$^{dbp5\text{-}L12A}$-2xGFP::URA3 (CEN plasmid)	This study
pKW711	pRS313-*xpo1-T539C*::HIS3 (CEN plasmid)	(Scott et al., 2009)
pBM720	pRS315-GFP-*dbp5-V73A*::LEU2 (CEN plasmid)	This study
pBM729	pRS413-RAD52-YFP::HIS3 (Replicative plasmid)	(Feng et al., 2007)
pBM718	pRS315-GFP-*dbp5-L12A*::LEU2 (CEN plasmid)	This study
pBM939	pRS315-GFP-*dbp5-L12A-R423A*::LEU2 (CEN plasmid)	This study

2.3 Oligos

Table 2-3. Oligos

Name	Description	Sequence	Reference
Probe 1	tRNAIleUAU exon and intron, employed for Northern analyses	GGCACAGAAACTTCGGAAAC CGAATGTTGCTATAAGCACGA AGCTCTAACCACTGAGCTACA CGAGC	(Wu et al., 2015)
KC031	tRNATyr complementary to and exons and intron, employed for Northern analyses	CCCGATCTCAAGATTTCGTAG TGATAAATTACAGTCTTGCGC CTTAAACC	(Wu et al., 2015)
SRIM04	tRNA$^{Ile}_{UAU}$ mature sequence; employed for FISH	GTGGGGATTGAACCCACGACG GTCGCGTTATAAGCACGAAGC TCTAACCACTGAGCTACA3	(Wu et al., 2015)
SRIM15	tRNA^{Tyr} mature sequence;	GCGAGTCGAACGCCCGATCTC AAGATTTACAGTCTTGCGCCT	(Wu et al.,

	employed for FISH	TAAACCAACTTGGCTACC	2015)
BMO861	$tRNA^{Ile}_{UAU}$ forward qPCR primer	GCTCGTGTAGCTCAGTGGTTAG	(Chatterjee et al., 2017)
BMO862	Un-spliced tRNAIleUAU reverse qPCR primer	CTTTTAAAGGCCTGTTTGAAAG	(Chatterjee et al., 2017)
BMO863	Spliced $tRNA^{Ile}_{UAU}$ reverse qPCR primer	ACGGTCGCGTTATAAGCACGA	(Chatterjee et al., 2017)

2.4 Antibodies and buffers

Table 2-4. Antibodies

Antigen	Antibody ID	Raised in	Dilution	Reference
GFP	□-GFP	Mouse	1:10000 in PBS-T	Roche
GAPDH	□-GAPDH	Mouse	1:10000 in PBS-T	Pierce
Dbp5	10F10	Mouse	1:2500 in PBS-T	Montpetit Lab, unpublished
Myc	9E10	Rabbit	1:10000 in PBS-T	Thermo Fisher
Mouse IgG	Anti-mouse IgG, DyLight 650 conjugated	Goat	1:10000 in PBS-T	Thermo Fisher
Rabbit IgG	Anti-rabbit IgG, DyLight 550 conjugated	Goat	1:10000 in PBS-T	Thermo Fisher

Table 2-5. Common buffers and solutions

Buffer	Composition
1X Phosphate buffered saline (PBS)	137mM NaCl, 2.7mM KCl, 4.3mM, Na_2HPO_4, 1.4mM KH_2O_4 pH 7.5
PBS-Tween (PBS-T)	137mM NaCl, 2.7mM KCl, 4.3mM, Na_2HPO_4, 1.4mM KH_2O_4 pH 7.5, 0.05% Tween-20
Milk blocking buffer (western)	137mM NaCl, 2.7mM KCl, 4.3mM Na_2HPO_4, 1.4mM KH_2O_4 pH 7.5, 0.05% Tween-20, 2.5% skim milk
5x SDS-PAGE running buffer	0.25M Tris-HCl, pH 8.8, 2M glycine, 0.5% SDS
1x SDS-PAGE transfer buffer	20% glycerol, 167mM Tris-HCl pH 6.8, 2% SDS, 0.05% bromophenol blue
SDS-PAGE sample buffer	20% glycerol, 167mM Tris-HCl, pH6.8, 2% SDS, 0.05%

	bromophenol blue
DNA-loading buffer (agarose gel)	0.30% bromophenol blue, 0.30% xylene cyanol, 45% glycerol
1X Tris buffered EDTA (TBE)	0.89M Tris-base, 0.89M boric acid, 0.02M EDTA
Blocking solution (northern)	10% Roche blocking reagent, 0.1M Maleic acid, 0.15 NaCl, pH 7.5
Washing buffer (northern)	0.1M Maleic acid, 0.15 NaCl, pH 7.5, 0.3% Tween-20
Detection buffer (northern)	0.1M Tris-HCl, 0.1M NaCl, pH 9.5

2.5 Live-cell single particle imaging

The overall system design and methodology for imaging was as previously described with the exceptions noted below (Grünwald and Singer, 2010). In brief, imaging was performed on a custom dual channel setup using a 60× 1.3 NA silicone oil immersion objective (refractive index 1.405; Olympus) combined with 500-mm focal length tube lenses, resulting in an effective 167× magnification and 95.8-nm-sized pixel with the emission split in the primary beam path onto two electron-multiplying charge-coupled devices (DU897 BI; iXon; Andor Technology). For excitation of fluorescent proteins, solid-state 514- and 561-nm laser lines (SE; Cobolt) were used, and intensity and on/off were controlled by an acousto-optic tunable filter (AA Opto-Electronics). Simultaneous imaging of NPCs and mRNPs was performed using subframes (approximately two fifths of each chip, 200 × 200 pixel) on both cameras at a frame rate of 67 Hz, equaling a time resolution of 15 ms.

Before imaging, cells were grown overnight at 26°C in SC/-HIS/-MET at 150 mg/liter, diluted to an OD_{600} of 0.1 the next morning, and grown at 26°C to allow at least three doublings. To remove the cell wall, ~2 ODs of cells were collected by centrifugation, washed with water, and resuspended in 50-mM Tris, pH 9.5, and 10-mM DTT solution at room temperature for 15 min. Cells were then collected and resuspended in a 0.3-ml spheroplast buffer (150-mM KPO_4, pH 7.5, 1-mM $MgCl_2$, and 250 µg/ml Zymolyase) and incubated at 26°C for 45 min. Cells were then placed in 35-mm glass-bottom dishes (MatTek Corporation), coated with concanavalin A (Sigma-Aldrich), and centrifuged at 500x*g* for 3 min to adhere cells. Unadhered cells were removed by washing with media containing 1.2-M sorbitol and left to recover in 2 ml of fresh

media for 30 min at 26°C before imaging. For each cell, four datasets, two in each color, were acquired. First, a registration image was recorded for 375 ms, automatically saved, and 500 ms later, the tracking dataset was recorded for 7.5 s (500 frames) in parallel for both channels.

All image processing for visual analysis was done using Fiji (Schindelin et al., 2012). First, each dataset was tested for drift during acquisition by creating 10 mean projections of 50 frames of the NPC channel video that were normalized and fused into a color-coded hyperstack. Color separation in the resulting stack indicated drift, and these datasets were discarded. Second, in the registration images, the tdTomato signal of Ndc1 was made visible in both channels using "cross-talk on demand" by using 10× more excitation power from the 561-nm laser than for the tracking videos. Using the sensitivity of our electron-multiplying charge-coupled device cameras and the surface reflection of the dichroic, the NPC signal was visible in both the mRNA (one image taken for 375 ms) and the NPC channel (25 images in 375 ms, the mean time projected for analysis). The mRNA and NPC signals were fine-registered postexperimentally by shifting the NPC channel registration image onto the mRNA channel registration image to calculate the parameters to be used for registration of the tracking videos (Preibisch et al., 2009). To make this alignment more robust, the mRNA channel registration image was filtered with a Gaussian kernel (1.5 pixel width) before registration. RGB images of the two registration images before and after registration were saved and visually compared if the correlation factor of the linear shift was better than 0.95. Registration failed at a frequency of ~50%, which we attribute to aberrations caused by heterogeneity in spheroplasting and, at later times, because of rebuilding of the cell wall. The resulting registration precision was determined to be 0.14 pixel, corresponding to 14 ± 17 nm. After these initial quality checks, we created two copies of each tracking video (NPC and mRNA channel), one being the raw data for quantitative image analysis and the other being enhanced for visual inspection. Raw data images were always displayed next to the enhanced images during subsequent visual analysis, and all traces of interest were double checked in the raw dataset to prevent a false positive event identification as a result of image processing. Tracking was done as described previously (Grünwald and Singer, 2010) using a supported fit routine where signals were identified visually in either the filtered or raw image, and the routine would execute a center of mass within 5 pixels around the click position to identify the coordinate for a 2D Gaussian fit. All fits were done in raw data and all fit parameters and initiation parameters reported to the user. For enhancement of images for visual inspection, we

used running mean and a subtraction of a Laplacian filter for the NPC channel and a Laplacian filter for the RNA channel. The kernel size was set relative to the theoretical width of the emission point spread function, and contrast was adjusted in the final RGB videos after processing. After filtering, the transition matrix was applied to the NPC channel video to overlay it onto the mRNA channel video. The following sections describe in more detail the imaging setup used here and the subsequent statistical analyses carried out.

2.5.1 Calculation of signal improvements

We quantify an increase or decrease in signal improvement as a change in the mean estimated localization precision. The smallest localization precision possible can be calculated using the Cramer-Rao lower bound (CRLB) and is attained using a maxium likelihood estimate (MLE) (Smith et al., 2010). The CRLB depends on the width of the point spread function, the intensity of the single molecule, and the background fluorescence. To quantify the signal improvement, we estimated these parameters in addition to assessing the location of each mRNP and calculated the corresponding CRLB (Smith et al., 2010). These calculations were performed based on mRNP signals from cells with (n = 86) and without (n = 156) a cell wall, and the localization precision was determined to be 64 ± 13 versus 52 ± 11 nm before and after cell wall removal. Note that total improvement in localization precision was 23% and the shape of the localization distributions significantly changed

2.5.2 Registration and co-localization precision

The registration precision between channels of 14 nm was determined by calculating the remaining offset between the registration data after linear translation. We chose the rather conservative linear registration model, as the quality of the registration data does not reach the level of individual pores (Grünwald and Singer, 2010). The standard deviation (SD) using this method is in the order of the mean. As a result, we do not report spatial binding site distributions, arguing that our total measurement precision is similar to the width of the expected binding site

distributions. For kinetic analysis, we use five classification states, but it is important to note that a four-state model also strongly supports our findings. Colocalization precision is given by the square root of the sum of the squared localization (54 nm) and registration precision (14 nm) values and is 56 nm. From binding profiles of β-actin mRNA at the NPC, we know the peak binding sites on the cytoplasmic and nucleoplasmic surface for mRNA transporting within ~200 ms to be 275 nm apart (Grünwald and Singer, 2010).

2.5.3 Definition of transport states and data analysis

Data analysis was performed using a manual-tracking interface in which the filtered and raw data were presented simultaneously and a particle of interest was tracked by consecutively clicking through image frames. The maximal displacement from frame to frame was displayed in the tracking channel to identify situations where two particles could be interchanged. In such cases, tracking was ended and the track dismissed. During manual tracking, a descriptive state was assigned to the particle in each frame based on the distance from the NE using the following guidelines: nuclear/cytoplasmic diffusion if the distance was >250 nm, nuclear/cytoplasmic docked if the distance was between 250 and 100 nm, and transition if the distance was <100 nm. The dynamic behavior of the particle (i.e., the direction and distance the particle moved with respect to the NE) in prior and subsequent frames was also used to inform state decisions. Using these descriptors, an analysis was performed in MatLab (MathWorks) using routines to search for specific events (e.g., export or scanning) based on these five states. We can make this classification because the localization precision of single molecules follows a Gaussian distribution described by $\theta-\hat{\theta}\sim N(0, C(\theta))$, where $\theta=(x,y,I,bg)$, $\hat{\theta}$ is the corresponding MLE, and $C(\theta)$ is CRLB (Kay, 1993). Using our current techniques, we have a total colocalization precision of 56 nm. C_{do} and N_{do} are 275 nm apart, and therefore we can calculate the false classification probability of a C_{do} being an N_{do} event (and the other way around) as $P(C_{do} | N_{do}) = 1-normcdf(x=135,\mu=0,\sigma=56)$ that defines the false classification rate as 0.01, or a 0.5% error to each side. When using $P(T|N_{do}, C_{do})$, this increases to 0.23 or an 11.5% error to each side ($2(1-normcdf(135/2,0,56))$). For a distance of 200 nm between the peak positions $P(C_{do}, N_{do}|T)$, this becomes 37% compared with 7% for $P(C_{do}|N_{do})$. In other words, we are able to describe a

two-state (C_{do}-N_{do}) model at the NPC (four states in total, with the diffusive nuclear and cytoplasmic states) with very high confidence (<0.5% error), whereas for a three-state model (C_{do}-T-N_{do}) at the NPC (five states in total), the classification of the transition state has an error probability between 10 and 17% on each side based on our obtained localization precision. As the transition state T is a shift in between docking states, its identification is partially based on our knowledge about the past and future of the particle within the trace. Therefore, we have included the transition state description, but note the related error, which does not impact the major findings of this work related to cytoplasmic docking differences in *mex67-5*.

2.5.4 Dwell time estimation

Because of the limited number of observations, we estimated dwell times using two methods, the dwell time fit based on the histogram (exponential distribution) and an MLE based on the assumption that the data follow an exponential distribution (Colquhoun et al., 1982; Kubitscheck et al., 2005). In the first method, (a) a histogram is constructed from all the observed dwell times, (b) the histogram is smoothed using a uniform filter having a width of 10 frames, (c) inverted cumulative distribution is constructed (Kubitscheck et al., 2005), and (d) a least squares fit is performed on the histogram. The second approach is an MLE (Kay, 1993). The transport times per condition are assumed to be an independently identical set of random variables having an exponential distribution. The probability density function of observing a dwell time x_j is given by:

$$f(x_j;\lambda)=\{\lambda e^{-\lambda x_j} 0 x_j \geq 0 x_j < 0,$$

where the mean dwell time is equal to λ^{-1}. The likelihood of a sequence of observed dwell times is given by:

$$L(\lambda)=\prod_{j=1}^{n} \lambda e^{-\lambda x_j},$$

and the value for $\lambda\hat{}$ that maximizes the likelihood is given by:

$$\lambda\hat{}=n\sum_{nj=1} x_j \ .$$

In both cases, based on the data having an exponential distribution, SD is equal to the mean.

2.5.5 Statistical analyses

Reported p-values were calculated using either *t* tests or Wilcoxon rank-sum tests. The latter can be used in place of *t* tests when it cannot be assumed that the population is distributed normally (Gibbons and Chakraborti, 2011). For all results, the test used is stated in the text. In analyzing transition times across the NE, the shape of the distribution determines the interpretation of the SD or SEM reported. Although often associated with the symmetric interval of errors around normal distributed data, the SD or SEM can also be used to report on nonnormal distributed data. In this case, the interpretation is based on Chebyshev's theorem specifying that no more than $1/k^2$ fraction of values can be more than k SDs away from the mean. In case of an exponential distribution, this translates into the SD being equal to the mean. In our case, the cumulative distribution of translocation times is equal to the cumulative distribution function of an exponential distribution, as expected (Colquhoun et al., 1982; Kubitscheck et al., 2005) or arrival time distributions in general. Because of the limited number of observations, we estimate the dwell time using two methods, the dwell time fit based on the histogram (exponential distribution) and an MLE based on the assumption of the data after an exponential distribution. For exponential distributions, the SD is expected to be equal to the mean. Note that a limited amount of data underlies some of the values in Table 3-1 and that the error reported in Table 3-1 is the standard error of the measurement.

2.6 Scanning mutagenesis

A plasmid (pBM464) containing DBP5 +/- 500 base pairs of flanking sequence was generated with an N-terminal GFP sequence fused to the DBP5 coding region as a template for mutagenesis. Primers for alanine scanning mutagenesis were designed using the AAscan program against all residues (Sun et al., 2013). PCR was carried out using Q5 high fidelity enzyme (New England Biolabs) in 12.5µl reactions, followed by DpnI (New England Biolabs) digestion for 2 hours. Digested PCR product (5µl) was transformed into DH5α competent *Escherichia coli (E. coli)* cells and plated onto LB ampicillin in a 12 well plate format. Mini preps were performed in

a 96 well format (BioBasic Inc.) on selected single colonies to purify mutagenized plasmids. The presence of each mutation was verified by sequencing (Genome Quebec).

2.7 Yeast mutant library generation

Sequence verified plasmids were transformed into yeast in a 96-well plate format using a *dbp5Δ* strain carrying DBP5 on a URA3 marked CEN plasmid (BMY015). BMY015 cells were grown to an $O.D_{600}$ of 1.0 in 1.5 L of selective media, centrifuged at 3000xg for 5min, washed once in water, and then in 50 ml of 100mM lithium acetate (LiAc). The culture was re-suspended in 30 ml of 100mM LiAc and 50 µl of culture was aliquoted into each well of a 96-well plate. Plates were centrifuged at 3000xg for 5min and supernatant was removed. Cells were re-suspended in a transformation mix (80 µl of 50% PEG, 12 µl of 1.0 M LiAc, 3.3 µl of 10 mg/ml salmon sperm single stranded DNA, and 22.5 µl of water). Mutated plasmid DNA (250 ng) was added to each well and mixed. Plates were incubated at 30°C for 45 min and then at 42°C for 30 min. Plates were centrifuged again and the supernatant was removed and 150µl of synthetic complete (SC)-LEU/-URA media was added. Cultures were grown for 3 days at 25°C and then 5µl of culture was diluted into 200µl of fresh media and grown for another 2 days. Transformants were then pinned for two rounds onto SC/-LEU/-URA selective agar plates and grown at 25°C. To remove the wild-type plasmid, strains were also pinned on to 5-FOA for two rounds of selection before finally pinning onto SC/-LEU plates. Strains that did not grow following plating on 5-FOA were considered to contain lethal mutations. To determine which mutant strains were temperature sensitive, the mutant array was plated on SC –LEU plate, grown at 37°C for 3 days, and then repined on SC –LEU and grown at 37°C for 3 days. Strains that did not grow when compared to a 25°C control plate were noted to be temperature sensitive and were subsequently verified by additional spot plating assays at 37°C.

2.8 Fluorescence microscopy and image analysis

Live cell imaging was mostly performed either using a widefield or confocal configuration on an Andor Dragonfly microscope equipped with an EMCCD camera driven by Fusion software (Andor) with a 60x oil immersion objective (Olympus, numerical aperture [NA] 1.4). Otherwise imaging was performed (as specified) on a DeltaVision Elite (GE Healthcare) microscrope equipped with a front-illuminated scientific complementary metal-oxide (sCMOS) camera driven by softWoRx 6 (GE Healthcare) at 23°C using a 60× 1.4 NA oil objective (Olympus) or an inverted epifluorescence microscope (Ti; Nikon) equipped with a Spectra X LED light source and an sCMOS camera (Flash 4.0; Hamamatsu Photonics) using a 100× Plan-Apo 1.4 NA objective and the NIS Elements software (Nikon). The following sections outline methods for experiments using fluorescence microscopy.

2.8.1 *GFA1* transcript counting

To determine *GFA1* mRNP subcellular localization with respect to the NE, *REF* and *mex67-5* strains were fixed in 2% paraformaldehyde for 15 min, washed with media, spheroplasted, and smFISH was performed (see section 2.12.1). The *GFA1* transcript number was determined by manually counting *GFA1* foci, and the frequency of NE-associated mRNPs was determined by scoring colocalization between the mRNP (YFP) and NPC (tdTomato) signals, followed by imaging on the DeltaVision Elite (GE Healthcare). Before analysis, images were deconvolved in softWoRx 6 and processed in ImageJ (National Institutes of Health). Specifically, images were adjusted for brightness and contrast, background subtraction was performed, and a Gaussian blur 3D filter was applied.

2.8.2 Mex67p localization

To localize Mex67p, haploid strains were generated (KWY5566 and KWY5567) expressing Ndc1p-tdTomato, *GFA1-PP7*, and GFP-tagged MEX67. To avoid cross talk from the

PP7-CP tagged with YFP, we used strains that did not express the coat protein. Cells were grown in a synthetic complete medium at 26°C and then imaged in a 384-well plate coated with concanavalin A at 26°C using an inverted epifluorescence microscope (Ti; Nikon). All image processing was done using Fiji (Schindelin et al., 2012).

2.8.3 Imaging *dbp5* mutant collection

For imaging of the mutant collection, strains were grown overnight in 96 well plates at 25°C to mid-log phase in SC media and then placed in 384-well glass bottom plates (VWR) treated with Concanavalin A. To determine changes in localization as a result of ethanol stress, media containing 24% ethanol was added to each plate well to achieve a final concentration of 12% ethanol, followed by imaging 15 min after ethanol addition. Image analyses were performed in FIJI, including maximum z-projections, image cropping, and brightness/contrast adjustments (Schindelin et al., 2012).

2.8.4 Anchor away and 2xGFP-NLS/NES reporter experiments

Anchor away or GFP-NLS/NES reporter experiments were similarly performed in glass bottom plates. For anchor away experiments, strains were treated with 1μg/ml rapamycin, pre-treated with or without 100ng/ml leptomycin B, followed by imaging for 20 min at 1 min intervals. To quantify the nuclear/cytoplasmic fluorescence intensity of GFP anchor away signals or GFP reporters, the mean integrated fluorescence intensity was measured for a 0.5 μm x 0.5 μm region in the nucleus or cytoplasm. Signal intensity was normalized to a background fluorescent intensity value adjacent to each cell and used to calculate the nuclear/cytoplasmic ratios. For each condition, measurements for 24-100 cells were obtained and the average ratios were plotted in a bar graph with the variability between cells expressed as standard deviation. Image analyses were performed in FIJI, including maximum z-projections, image cropping, and brightness/contrast adjustments (Schindelin et al., 2012).

2.8.5 Rad52p-YFP foci counting

For Rad52p-YFP foci imaging, strains were grown to early log-phase (~$O.D._{600}$=0.2) in SC media and imaged before and after treatment with 0.5% MMS for 20 min. Cells were then washed with fresh SC media and imaged again after 20 min. Number of Rad52p-YFP foci were quantified by counting the number of bright YFP foci within the cell (n≥100). Image analyses were performed in FIJI, including maximum z-projections, image cropping, and brightness/contrast adjustments (Schindelin et al., 2012).

2.9 Immunoblotting

Yeast cell lysate was prepared using glass bead lysis in 2x sodium dodecyl sulfate (SDS) loading buffer. Total protein lysate samples were loaded and run on 10% SDS-polyacrylamide gels, transferred to a nitrocellulose membrane, and then blocked in 2.5% skim milk powder and 1x Phosphate Buffered Saline (PBS) for 30 min. The membrane was probed with a mouse monoclonal anti-GFP primary antibody (Roche) and mouse anti-GAPDH antibody (Pierce®) primary antibody. Goat anti-mouse DyLight 650 (Thermo Fisher) was used as a secondary antibody. Protein detection and quantification was measured using a gel-doc imaging system (BioRad).

2.10 Silver staining

SDS-PAGE was carried out as described above. Gels were fixed with 50% ethanol 2x for 15 min followed by 20 min incubation in DTT (5ug/ml) and 20min incubation in 0.1% Silver nitrate $AgNO_3$. Finally, the gel was developed in developing solution (3% Na_2CO_3 (w/v), 2% formaldehyde) and stopped by incubation in 1% Acetic Acid.

2.11 Phenotypic screening of mutant collection

dbp5 mutant collection strains were grown overnight to saturation in 200µl of YPD in a 96-well plate format. Strains were pinned onto YPD agar or YPD + drug using a 96-well manual pipetting system (Liquidator, Mettler Toledo). The following drug conditions were used for Hygromycin B: 10µg/ml, 20µg/ml, 40µg/ml. For UV induced DNA-damage screening, strains were plated on YPD and then exposed to 40 J/m^2, 80 J/m^2, 120J/m^2 of UV light (UV Crosslinker, VWR). Strains were grown at room temperature for five days and imaged twice per day using a gel-doc imaging system (BioRad). Growth of the colonies was then quantified using Balony software (Loewen Lab-UBC).

2.12 Imaging of fluorescence *in situ* hybridization (FISH) experiments

Live cell imaging was performed either using a widefield or confocal configuration on an Andor Dragonfly microscope equipped with an EMCCD camera driven by Fusion software (Andor) with a 60x oil immersion objective (Olympus, numerical aperture [NA] 1.4) or on a DeltaVision Elite (GE Healthcare) microscrope equipped with a front-illuminated scientific complementary metal-oxide (sCMOS) camera driven by softWoRx 6 (GE Healthcare) at 23°C using a 60× 1.4 NA oil objective (Olympus). The following sections describe single molecule (SM), poly(A)-RNA, and tRNA FISH protocols.

2.12.1 *GFA1* transcript counting using SM FISH

Yeast were grown overnight at 26°C, diluted to an OD_{600} of ~0.1 the next morning, and grown at 26°C to allow at least three doublings. For transcript counting using single-molecule FISH, cells were fixed and GFA1 mRNAs were detected using 48 probes (20mers) directed against GFA1 (BioSearch Technologies) in strains with (BMY83) and without PP7 stem loops (BMY642), as previously described with the noted changes (Hocine et al., 2013). In brief, cells were fixed by the addition of 37% formaldehyde to the cultures (3.7% final concentration) for 30

min at 26°C. Yeast cell walls were digested with Zymolyase (Cedarlane), and spheroplasted cells were applied to 8-well slides coated with poly-l-lysine. Cells were permeabilized using ice-cold methanol for 6 min followed by ice-cold acetone for 30 s. After rehydration and incubation with a hybridization buffer for 1 h at 37°C, 30 µl of a hybridization buffer containing 20 ng of the GFA1 probes was added to each well and incubated overnight at 37°C. Wells were then washed, and mounting media containing DAPI was added followed by imaging on a microscope (DeltaVision Elite; GE Healthcare).

2.12.2 poly(A)-RNA FISH

FISH was carried out as described with modifications (Chen et al., 2018). Briefly, strains were grown overnight to mid-log phase at 25°C and in some cases shifted to 37°C for indicated time points. Samples were fixed with formaldehyde overnight at a final concentration of 3.7%. Samples were then washed three times with ice cold Buffer B (1.2M Sorbitol, 0.1M Potassium Phosphate, 0.5mM $MgCl_2$). To remove yeast cell walls, 2.5µL 20mg/mL zymolyase T20 and 5µL of 200mM vanadyl ribonucleoside complex (VRC) were added to cells re-suspended in 425µL of Buffer B for 30 minutes at 30°C. Samples were washed once with Buffer B and then re-suspended in 70% ethanol and incubated for 4 hours at room temperature. After washing samples with Buffer B, hybridization was carried out in 50ul of buffer containing 1X saline sodium citrate (SSC), 0.34mg/ml E.coli tRNA, 20% formamide, 0.2mg/ml BSA, 11% dextran sulphate, 4mM VRC, and oligo-dT or gene specific probes as indicated at 37°C for 16 hours. A final concentration of 0.4mM was used for the fluorescein isothiocyanate (FITC) labeled oligo dT probe (Qiagen). Samples were washed two times with 1X SSC and 15% formamide followed by application onto 8-well slides (Fisher Scientific) treated with Poly-L-Lysine (SIGMA). After washing twice with 1x PBS, mounting medium with DAPI was applied to each sample and a coverslip was affixed. Imaging was performed using a microscope (Dragonfly; Andor) equipped with an EMCCD camera driven by Fusion (Andor) using a 60x x 1.4NA oil objective (Olympus). Image analysis was performed in FIJI, including maximum z-projections, image cropping, and brightness/contrast adjustments (Schindelin et al., 2012).

2.12.3 tRNA FISH

tRNA specific FISH was carried out as previously described (Chatterjee et al., 2017) with some modifications. Briefly, samples were grown to early log phase (~$O.D._{600}$=0.3) in YPD at 25°C (or in some cases in YPD at 37°C or in SC media lacking leucine, histidine, uracil, methionine and tryptophan) followed by formaldehyde fixation at a final concentration of 3.7% for 15 minutes. Samples were then re-suspended in 5ml of fresh Buffer A (2% paraformaldehyde, 0.1M Potassium Phosphate, 0.5mM $MgCl_2$) for 3 hours at room temperature. Cells were then washed two times with Buffer B. To spheroplast cells, 8µL of 20mg/mL zymolyase T20 and 1µL of β-mercaptoethanol was added to cells re-suspended in 500µL of Buffer B for 30 minutes at 37°C. Cells were then washed one time with Buffer B and adhered to 8 well slides coated with Poly-L-lysine. Slides were treated with 70%, 90%, and 100% ethanol for 5 minutes. Cells were then incubated in a pre-hybridization buffer (10% dextran sulfate, 0.2% BSA (acetylated), 2× SSC (1× SSC is 0.15 M NaCl and 0.015 M Na-citrate), 1X Denhardt's solution, 250 µg *Escherichia coli* tRNA/ml) for 2 hours at 37°C. For hybridization, 1pmol/ul of Cy3-dUTP end labeled tRNA probes were added to fresh hybridization buffer and incubated overnight at 37°C. All tRNA FISH probes were 3'end labeled using an oligonucleotide end labeling kit (Roche) and Cy3-dUTP (Enzo Life Sciences). Cells were washed one time in 2xSSC at 50°C, followed by two washes for 10 minutes at room temperature each in 1X SSC, 4X SSC, 4X SSC + 1% Triton X-100. Slides were then washed in 4X SSC again briefly, and once in 1X PBS and then mounted with DAPI and sealed. Imaging was performed using a microscope (Dragonfly; Andor) equipped with an EMCCD camera driven by Fusion (Andor) using a 60x x 1.4NA oil objective (Olympus). Image analysis was performed in FIJI, including maximum z-projections, image cropping, and brightness/contrast adjustments (Schindelin et al., 2012).

2.13 Immunofluorescence (IF)

Strains were grown overnight to mid-log phase at 25°C and were fixed with formaldehyde at a final concentration of 3.7% for 15 minutes. Samples were then washed two times with Buffer A (10.1M Potassium Phosphate, 0.5mM $MgCl_2$) and re-suspended in 1ml of Buffer B (1.2M

Sorbitol, 0.1M Potassium Phosphate, 0.5mM $MgCl_2$). To spheroplast cells, 2.5µL 20mg/mL zymolyase T20 and 1µL of β-mercaptoethanol were added to cells for 30 minutes at 37°C. Samples were washed once with Buffer B and then adhered to 8 well slides coated with Poly-L-lysine. Slides were treated with ice-cold methanol for 6 minutes and then acetone for 30 seconds. Samples were blocked with 1X PBS containing 5mg/ml bovine serum albumin (PBS-BSA) for 1 hour at room temperature. Samples were incubated with a mouse monoclonal anti-DBP5 primary antibody overnight at room temperature in PBS-BSA with 0.05% Tween-20. Slides were then washed 5 times with PBS-BSA-Tween for 5 minutes each and then incubated with a Goat anti-mouse DyLight 650 (Thermo Fisher) secondary antibody in PBS-BSA-Tween. Slides were then washed 5 times with PBS-BSA-Tween for 5 minutes each, and twice in 1X PBS and then mounted with DAPI and sealed. Imaging was performed using a microscope (Dragonfly; Andor) equipped with an EMCCD camera driven by Fusion (Andor) using a 60x 1.4NA oil objective (Olympus). Image analysis was performed in FIJI, including maximum z-projections, image cropping, and brightness/contrast adjustments (Schindelin et al., 2012).

2.14 Sup45p-13myc co-immunoprecipitation

Strains were grown overnight to mid-log phase and 30 O.Ds of cells were harvested at room temperature. Samples were washed one time in water and re-suspended into a PBS-MKT lysis buffer (50mM Tris-HCL pH 7.5, 100mM NaCl, 5mM EDTA, 10% glycerol, 0.1% Triton X-100, protease inhibitor cocktail). Cells were lysed using glass beads and vortexing and then centrifuged at 10 000xg for 10 min at 4°C. Samples of cleared lysates were acquired for pre-IP sample controls. 0.8mg of magnetic Dyna Beads (Life Technologies) conjugated to GFP were added to the lysate for 2 hours at 4°C while rotating. Samples were placed on a magnet, and samples for post-IP controls were obtained. Beads were washed with 1mL lysis buffer 2 times. Proteins were eluted from the beads in 1x SDS buffer and incubated at 70°C for 10minutes. Protein samples were used for SDS-PAGE and immunoblotting as described above with a rabbit anti-myc antibody and Dylight 650 secondary antibody (Thermo Fisher).

2.15 3′-TAG RNA-Seq

Strains were grown overnight to early log phase in SC -URA media and treated with 0.5% methyl methanesulfonate (MMS) for 30 minutes to induce DNA damage. 5.0 ODs of cells were harvested and snap frozen in liquid nitrogen. RNA was extracted using the Quick-RNA Fungal/Bacterial prep kit (Zymo Research). Samples were treated with DNAase I (Zymo Research) on the RNA extraction column. RNA integrity was assessed by 2% agarose gel electrophoresis. Library preparation was carried out by UC Davis Genome Center following the 3' Tag Sequencing method. The adapters, polyA tails, and the first 12 basepairs of each read were trimmed according to manufacturer instructions (https://www.lexogen.com/quantseq-data-analysis/). Gene expression was quantified with *salmon* using the *S. cerevisiae* R64 GCA_000146045.2_R64_rna_from_genomic file (Patro et al., 2017). Differential expression was performed using *edgeR* using the glmQLFit function (Robinson et al., 2010). Significance cutoff was at FDR < .05. All code used to complete differential expression analysis is available at https://github.com/montpetitlab/Lari2019.git.

2.16 Synthetic gene array screen (SGA)

SGA screening was carried out as previously described (Young et al., 2010). Query strains were mated to the yeast deletion mutant array (DMA) at a density of 1536 spots per plate using a Singer RoToR HDA pinning robot. Following selection, diploids were sporulated and then germinated on SD-HIS/ARG/LYS media supplemented with 100 mg/L canavanine, 100 mg/L thialysine, 200 mg/L G418 sulphate (HRK media) to select for MATa haploid cells. Control data sets were generated by pinning the array to HRK media + 1 g/L 5-FOA, followed by a further pinning to HRK media. The experimental data sets were generated by two rounds of pinning to HRK media without uracil to select for strains carrying *dbp5* alleles. Images of plates were captured on a flatbed scanner and analyzed using *Balony* software (Young and Loewen, 2013).

2.17 Protein purification and ATPase assay

Protein purification and in vitro ATPase assays were carried out as previously described using full-length Dbp5p or Dbp5p-R423A (Montpetit et al., 2011).

2.18 RNA extraction

Total RNA, enriched for small RNAs, was extracted from yeast cultures as described previously (Hopper et al., 1980). Briefly, strains were grown overnight to early log phase and harvested. Cell pellets were re-suspended in equal volumes of ice-cold TSE buffer (0.01M Tris pH7.5, 0.01M EDTA, 0.1M sodium chloride) and TSE saturated phenol. The mixture was incubated for 20 minutes at 55°C and vortexed every 3 minutes. Phases were separated by centrifugation at 20 000g for 10 minutes and re-extracted with phenol. RNA was precipitated overnight in ethanol at -80°C.

2.19 Northern blotting

Northern blotting was carried out as previously described by (Chatterjee et al., 2017). 2.5 micrograms of total RNA was separated by electrophoresis in 10% TBE-Urea gels and transferred onto a Hybond N^+ membrane (Amersham). Membranes were cross-linked at 2400 J/ m^2 (UV Crosslinker, VWR). tRNAs were detected using digoxigenin-labeled (DIG) probes as described previously (Wu et al., 2015). Gels were stained with 1µg/ml ethidium bromide to detect 5.8S and 5S rRNAs as loading controls. Mean integrated intensities of the bands detected were measured using FIJI, and normalized to a background signal for each lane (Schindelin et al., 2012). These values were then used to calculate the ratio between the intron containing tRNA species and the precursor tRNA species and normalized to the value calculated for the wild-type control sample.

2.20 RNA-immunoprecipitation (RNA-IP)

RIP experiments were performed with Protein-A tagged Dbp5 strains, in parallel with an untagged control strain to assess background binding of non-specific RNAs following IP. Strains were grown overnight to mid-log phase at 25°, formaldehyde was added to a final concentration of 0.3%, and incubated for 30 min. Cross-linking was quenched by addition of glycine to a final concentration of 60 mM and incubated for 10 min. Cells were harvested and flash frozen in liquid nitrogen. Pellets were re-suspended in 1.5 ml TN150 lysis buffer (50 mM Tris-HCl pH 7.8, 150 mM NaCl, 0.1% IGEPAL, 5 mM beta-mercaptoethanol), Protease Inhibitor Cocktail was added to 1X concentration and lysis was performed by vortexing with 1 ml Zirkonia beads (0.5 mm) 5 times for 1 min with 1 min incubation on ice between each cycle. 5 ml TN150 was added and lysate was cleared by centrifugation (20 min at 4000xg; then 20 min at 20000xg; 4°C). Lysates were diluted to 10 ml with TN150 and incubated with IgG-conjugated magnetic dynabeads at 4°C 1 hr with rotation. Immuno-precipitate was washed once for 5 min with 1 ml TN150, followed by 5 min 1 ml TN1000 (50 mM Tris-HCL pH7.8, 1M NaCl, 0.1% IGEPAL, 5 mM beta-mercaptoethanol), and once more with 1 ml TN150 for 5 min at 4°C with rotating. Immuno-precipitate was re-suspended in 100 µl TurboDNase reaction (1X TurboDNase Buffer, 2U Turbo DNase) and incubated on a thermomixer at 37°C for 30 min at 1200 RPM. Magnetic beads were washed 3 times with 1 ml TN150 and 50 µl of beads were retained for western blot analysis. Remaining beads were aspirated of TN150 and re-suspended in 400 µl Proteinase K elution mix spiked with exogenous Luciferase RNA (50 mM Tris HCL pH7.8, 50 mM NaCl, 1 mM EDTA, 0.5% SDS, 1 ng Promega Luciferase Spike-In RNA, 100 µg proteinase K). Elution was carried out at 50°C 1200 rpm for 2 hr on thermomixer. Magnetic beads were incubated at 65°C for 1 hr to allow cross-link reversal by heat. RNA was extracted from IP with 400 µl Sigma 5:1 phenol:chloroform pH 4.3–4.7 followed by back extraction with chloroform:isoamylalcohol and ethanol precipitation for 1 hr at −80°C using linear acrylamide as a carrier. Half volume of RIP RNA was reverse transcribed with Superscript III using random priming, while the other half was retained for -RT reaction to assess genomic contamination. Reverse transcription was carried out as per manufacturer's instructions. Resulting cDNA from RIPs was used in standard PCR followed by 2% gel electrophoresis in addition to being used as template in qPCR to quantify fold enrichment of target RNAs in RIP.

2.21 RT-qPCR analyses of RIPs

RT-qPCR experiments were carried out using Power SYBR (Applied Biosystems) on an Applied Biosystems instrument. Target RNA abundance in each RIP was normalized to the abundance of an exogenous spike-in Luciferase RNA control to correct for differences in sample preparation (dCt). ddCt values were then calculated as the difference in relative abundance of the target RNA isolated via immunoprecipitation using a Protein-A tagged Dbp5 strain vs. an untagged strain (non-specific binding control). Relative fold-enrichment above the untagged background control was calculated using the Livak Method (Livak and Schmittgen, 2001). Standard curves were generated to test PCR efficiencies of all primer sets used in this study. Averages, SD, and p-values were calculated on dCt values across three independent RIP experiments.

Chapter III: *In vivo single particle imaging of nuclear mRNP export**

* A version of this chapter has been published as Smith, Lari, Derrer *et al.,* 2015. Journal of Cell Biology, 211(6), pp1121-1130.

3.1 Overview

In eukaryotes, the physical separation of transcription and translation by the NE allows for additional modes of quality control and regulation to be imposed on the gene expression program and necessitates transport of mRNA from the nucleus to the cytoplasm. Passage across the NE is predominantly mediated by the NPC, which is composed of ~30 Nups that together form a channel connecting the nucleoplasm and cytoplasm (Floch et al., 2014; Wente and Rout, 2010). To access this channel, each mRNA must be assembled into an RNP complex with export factors (e.g., Mex67p) to allow a mRNP to dock to an NPC, translocate across the NE through the transport channel, and reach the cytoplasm (Niño et al., 2013). During export, mRNPs undergo temporally and spatially ordered remodeling in which certain proteins are removed before export (e.g., Yra1p), whereas others are removed upon arrival in the cytoplasm (e.g., Mex67p and Nab2p). This provides a mechanism to regulate and impose directionality on the transport process (Iglesias et al., 2010; Köhler and Hurt, 2007; Lund and Guthrie, 2005; Oeffinger and Zenklusen, 2012; Tran et al., 2007). Overall, many proteins have been identified that, as part of an mRNP, are required for nuclear maturation, export, and cytoplasmic release (Bonnet and Palancade, 2014; Müller-McNicoll and Neugebauer, 2013; Niño et al., 2013; Oeffinger and Montpetit, 2015). However, numerous questions remain regarding the assembly and composition of the mRNP and how each protein factor contributes to the export event.

Recent advances in imaging technology (e.g., camera sensitivity and microscope design) and methodology (e.g., RNA-tagging strategies) allow individual mRNAs to be visualized *in vivo*. The ability to image individual mRNPs in living cells has provided important insight into various aspects of mRNP export, including the first measurements of export kinetics (Grünwald and Singer, 2010; Ma et al., 2013; Mor et al., 2010; Siebrasse et al., 2012). As presented in this chapter, these methods have been applied to single-particle imaging of mRNP export in the budding yeast *S. cerevisiae*. The availability of mutants that disrupt yeast mRNP export and NPC function allows for the investigation of the kinetics and regulation of mRNP export at the level of a single RNA molecule. Using this approach, hundreds of mRNPs were tracked in living cells, kinetics of mRNA export events were analyzed, and the role of the essential mRNA export factor Mex67p was characterized. These results show that mRNP transport across the NE inside the living cell is fast (~200 ms), well in agreement with prior findings (Grünwald and Singer, 2010;

Mor et al., 2010; Siebrasse et al., 2012), and demonstrate a critical role for Mex67p in cytoplasmic mRNP release and directional NPC transport.

3.2 Results

3.2.1 *GFA1-24xPP7* Ndc1p-tdTomato reference (*REF*) imaging strain

To observe the mRNP export process in living cells, a bacteriophage PP7 RNA-labeling system was used (Chao et al., 2008; Hocine et al., 2013). This involved insertion of 24 copies of the PP7 operator sequence into the 3′ UTR of the GFA1 gene (*GFA1-PP7*), which can be fluorescently labeled when bound by the PP7 coat protein (PP7-CP) fused to YFP (Figure 3-1A-B). GFA1 is an essential gene involved in chitin synthesis (Watzele and Tanner, 1989) and was selected because its relatively low expression level was suitable for single-particle tracking (Lipson et al., 2009). Like most yeast genes, *GFA1* lacks introns (Rodriguez-Medina and Rymond, 1994; Spingola et al., 1999), and the *GFA1* mRNA is near the mean mRNA length in yeast (2,154 nt vs. ~1,400 nt; Hurowitz and Brown, 2003). Ndc1p fused to tdTomato was also co-expressed with *GFA1-PP7* and PP7-CP-3xYFP, resulting in the reference (*REF*) strain, in which the position of a *GFA1* mRNP (PP7-CP-3xYFP multiplexed on the PP7 operator) could be determined relative to NPCs (Ndc1p-tdTomato) to track mRNP export (Figure 3-1A).

Previous studies using PP7 and the related MS2 RNA-labeling approach in yeast and metazoan systems have demonstrated that the presence of stem loops in the 3′ UTR of a transcript does not alter transcript levels, localization, or RNP assembly (Bertrand et al., 1998; Haim et al., 2007; Hocine et al., 2013; Park et al., 2014; Song et al., 2015). Importantly, the additional sequence in the *GFA1* 3′ UTR and fusion of tdTomato to Ndc1p, both essential genes, did not impact growth of the *REF* strain (Figure 3-1C), suggesting that the presence of the operator stem loops, the binding of PP7-CP-3xYFP to the *GFA1-PP7* mRNA, and the tagging of Ndc1p do not significantly affect *GFA1* mRNP biogenesis or overall cellular fitness. The possibility that the addition of PP7 stem loops might subtly affect the *GFA1* mRNA cannot be ruled out, as it was recently shown that the presence of MS2 stem loops can interfere with the cytoplasmic degradation of an mRNA by Xrn1p (Garcia and Parker, 2015). However, by focusing on nuclear

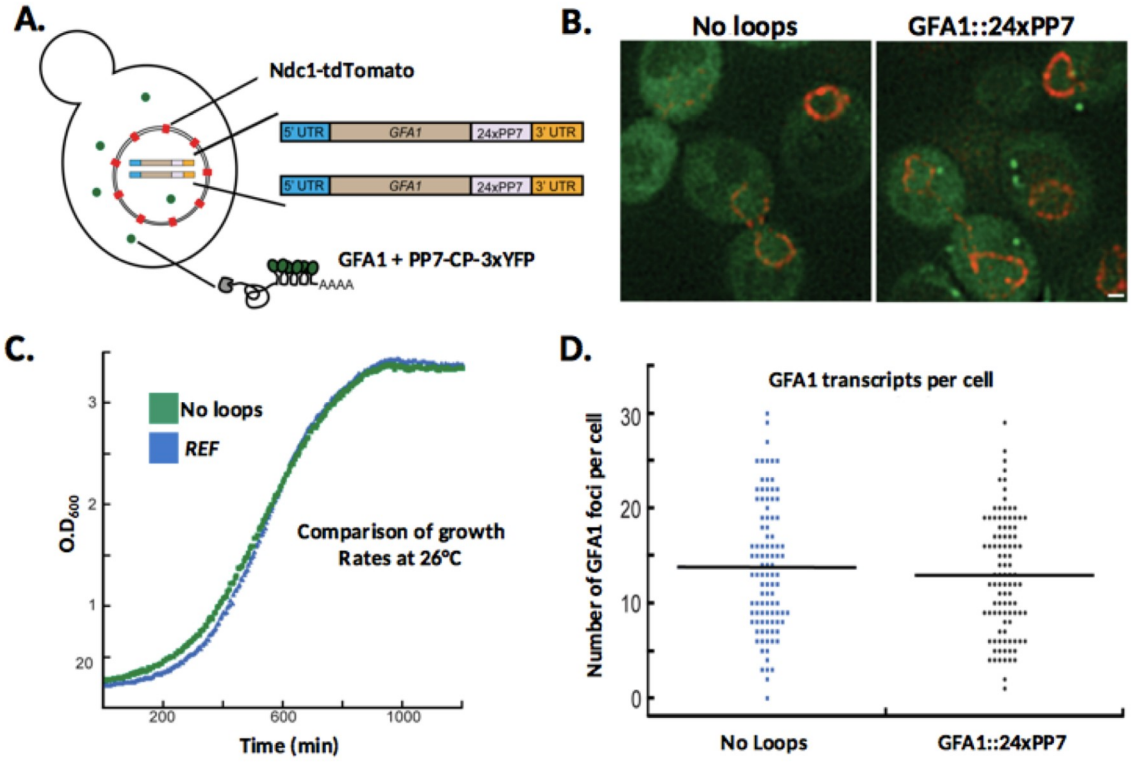

Figure 3-1. *REF* strain design and characterization. A. Schematic displaying features of the yeast strains used to monitor mRNP export. Upon transcription, the *GFA1* mRNA that carries 24xPP7 loops in the 3′ UTR is bound by the PP7-CP-3xYFP appearing as particles that can be tracked in relation to NPCs that are marked by Ndc1-tdTomato. **B.** Comparison of PP7-CP-3xYFP localization in a strain with no PP7 stem loops (BMY642) and the REF strain with GFA1-24xPP7. Bar, 1 µm. **C.** Growth curves of a control strain with no PP7 stem loops (BMY642) and the REF strain with GFA1-24xPP7 at 26°C. The data shown are from a single representative experiment out of three repeats. **D.** Dot plot shows the number of GFA1 mRNAs per cell observed using single-molecule FISH probes against GFA1 in a strain with no PP7 stem loops (BMY642) and the REF strain at 26°C, with the mean denoted by a black line (n = 100 cells).

mRNA export events, analyses here selected for functional mRNPs that were transported across an NPC and were not recognized by nuclear surveillance machinery. To further verify that the PP7 stem loops did not alter steady-state *GFA1* transcript levels, the number of transcripts per cell was determined using single-molecule FISH to be 14 ± 7 in the parental strain (no PP7 stem loops) and 13 ± 6 in the *REF* strain. This indicates that the presence of the PP7 stem loops in the 3′ UTR of GFA1 does not significantly alter steady-state mRNA expression levels (P = 0.37; two-tailed *t* test; *n* = 100 cells; Figure 3-1D).

In the *REF* strain, PP7-CP-YFP–positive particles were predominantly observed in the cytoplasm, as would be expected at steady state, and this is consistent with the *GFA1* single-molecule FISH data. The ability to observe particles was dependent on the presence of PP7 operator loops within the *GFA1* 3′ UTR (Figure 3-1B), and most particles were relatively uniform in size and brightness, but some cytoplasmic particles appeared brighter and larger. On occasion, these large particles within the cytoplasm merged and split, suggesting that they may contain multiple mRNAs (Figure 3-2). This may represent the accumulation of decay intermediates in P-bodies (Garcia and Parker, 2015) or other assemblies containing multiple mRNAs, which have recently been reported in live cultured neurons and *S. cerevisiae* (Park et al., 2014; Simpson et al., 2014). Large assemblies were rarely observed in the nucleus of *REF* cells and were not observed to undergo mRNP export.

3.2.2 Dwell time analysis of mean mRNP export time in budding yeast

Measurements of mRNP export kinetics have shown that mRNP export occurs within a few hundred milliseconds and involves discrete steps that include NPC docking, translocation, and cytoplasmic release (Grünwald and Singer, 2010; Siebrasse et al., 2012). Imaging the rapid dynamics of cellular processes, including mRNA export, at the single particle level presents a major challenge (Liu et al., 2015). For instance, information from multiple channels (i.e., mRNP and NPC signals) must be collected concurrently at high frame rates in a manner that maximizes signal to noise ratios (SNRs) and localization precision. To address this challenge, an imaging setup capable of simultaneously capturing two-channel imaging data at high frame rates with precise image registration was used (see section 2.5 for live cell imaging of mRNP export and

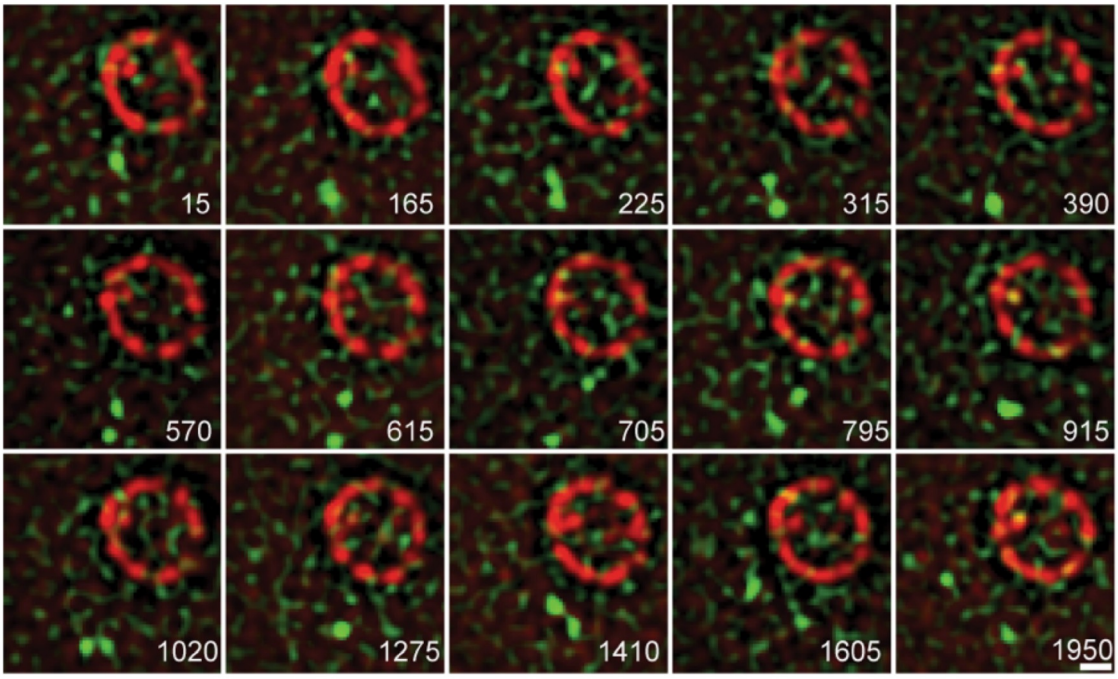

Figure 3-2. Merging and splitting of *GFA1-PP7* mRNPs. Selected nonconsecutive frames showing the splitting and merging of cytoplasmic particles in a *REF* cell with the time from the start of the event given in the bottom right of each image in milliseconds. Bar, 1 μm.

image processing; Grünwald and Singer, 2010). Importantly, complications introduced by system drift or cellular movement (e.g., NPC mobility) are negated by this imaging setup that allows for monitoring the position of both the mRNP and Ndc1p channels in every frame at the same instance in time.

Still, imaging at the rate required to measure export kinetics (67 Hz in this study) limited photon collection, which, combined with cellular background and light scatter introduced by the yeast cell wall, diminished SNR. To overcome this issue, the yeast cell wall was removed, and cells were imaged in medium containing sorbitol for osmotic support (Figure 3-3A), which substantially increased the SNR (see see section 2.5.1 for calculation of signal improvements). This resulted in reduced widths (σ) of single-particle signals ($P < 0.01$; Wilcoxon rank-sum test) and a 23% increase in localization precision (Figure 3-3B). Cell wall removal also had the effect of inducing *GFA1* expression for the purpose of cell wall synthesis; consequently, cells with labeled *GFA1* mRNPs became apparent within 15 min after reintroducing growth media, and data was collected for ~90 min before the newly forming cell wall increased the background as a result of light scatter.

Using this approach, two-channel imaging data for 500 frames at 67 Hz from *REF* cells were collected with a measured co-localization precision of 56 ± 20 nm between the two channels (see section 2.5.2 for registration and co-localization precision). Because of the small size of yeast, the use of a 1.3 NA objective allowed ~60% of the nuclear volume to be imaged in a single focal plane; thus, mRNP particles could be tracked for significantly more frames than in mammalian cells (Grünwald and Singer, 2010).

In the dataset collected from ~450 *REF* cells, 43 successful mRNP export events were identified. Each event contained a tracked particle, which docked to the nuclear side of the NE and moved in successive frames from the interior of the nucleus to the cytoplasm, where it was released (Figure 3-4A). mRNPs were classified within every frame as being in one of the following states: nucleoplasmic, nuclear docked, transition between docked states, cytoplasmic docked, or cytoplasmic. Each state was assigned based on the distance between an mRNP and the NE, plus the dynamic behavior (i.e., the direction and distance the particle moved with respect to the NE) of the particle in the preceding and subsequent frames (see section 2.5.3 for definition of transport states and data analysis). Using these state values, the duration of an export event was calculated from the time of nuclear docking until mRNP release into the cytoplasm, as previously

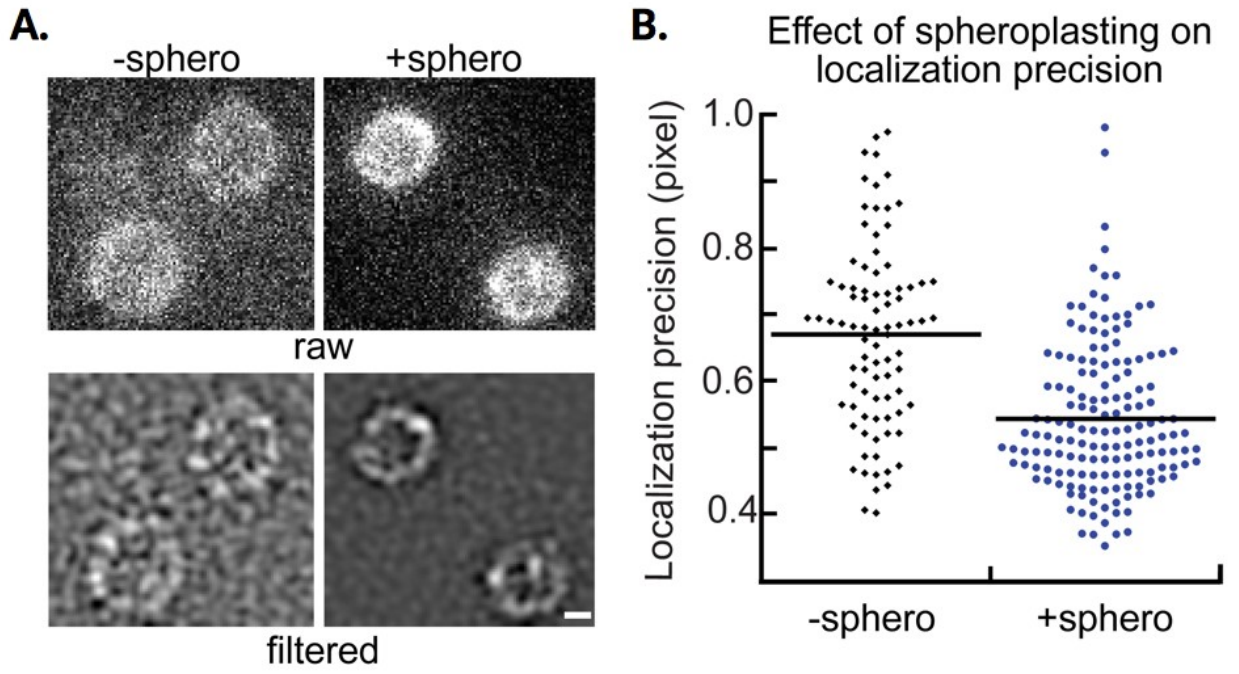

Figure 3-3. Effect of spheroplasting on localization precision in *REF* strain. A. Fluorescent images of the Ndc1-tdTomato signal in *REF* cells using identical image acquisition settings showing the improvement in image quality after removal of the yeast cell wall. Examples of both raw and Laplacian filtered images are shown. Bar, 1 μm. **B.** Dot plot displaying the localization precision (pixel = 96 nm) obtained when tracking mRNP particles in cells with (−sphero; n = 86) and without a cell wall (+sphero; n = 156), with the mean denoted by a black line for each. Localization precision analyses by Carlas Smith.

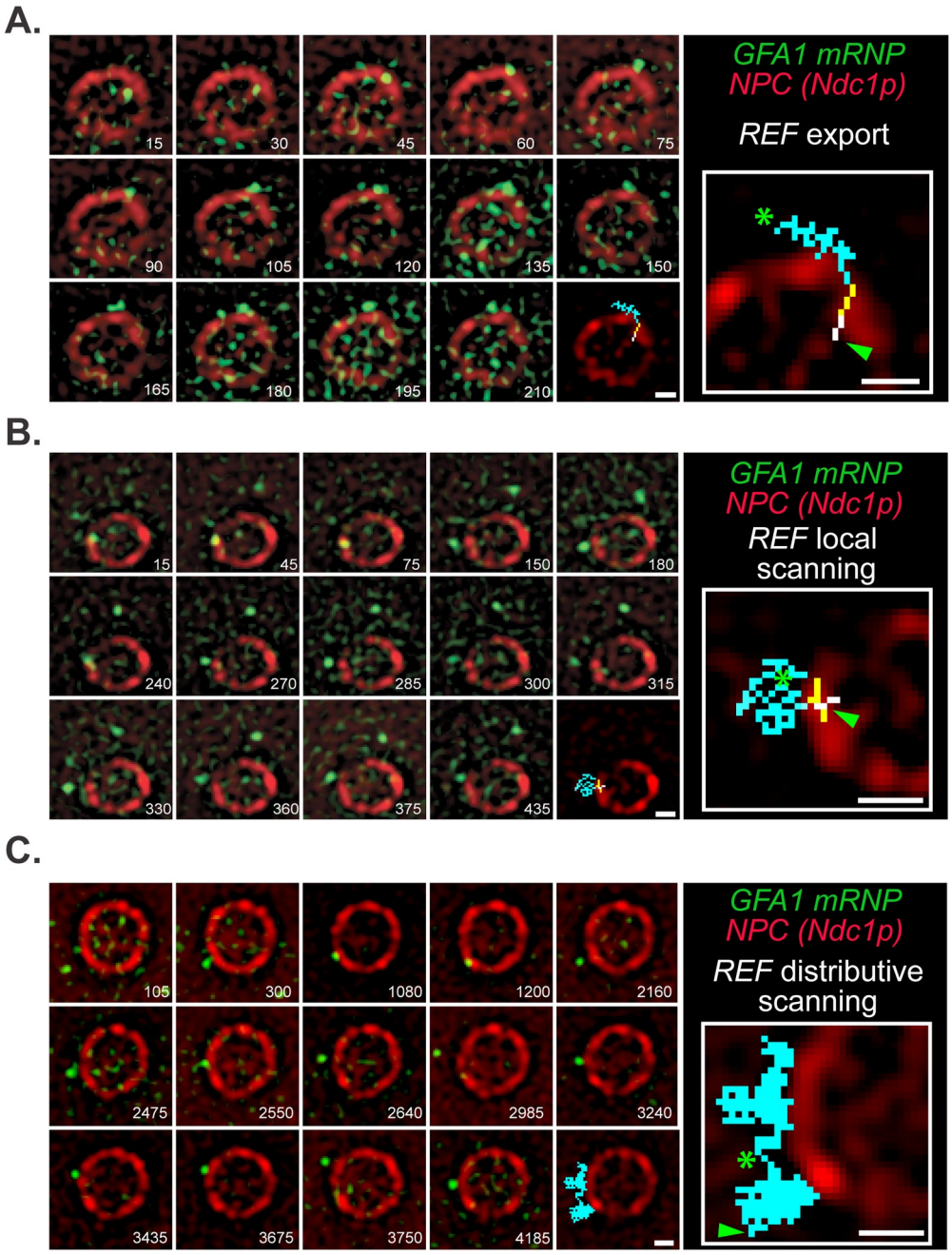

Figure 3-4. *GFA1-PP7* mRNP export and NE scanning in *REF* strain. A. Merged and registered images show consecutive frames of a successful export event based upon tracking of the tagged *GFA1* mRNP across the NE in the *REF*. **B and C.** Selected nonconsecutive frames show local (B) and distributive (C) NE scanning interactions between an mRNP and the NE. For all panels, cells were imaged at 26°C and 67 Hz with the time from the start of the event given in the bottom right of each image in milliseconds. The last image and inset show an overlay of the mRNP path that is color-coded based on position (white, nuclear docked; yellow, transition; blue, cytoplasmic docked/cytoplasm). Each green arrowhead and star denotes mRNP positions at the beginning and end of the track, respectively. Bars, 1 μm.

described (Kubitscheck et al., 2005; Dange et al., 2008; Grünwald and Singer, 2010). Using these data, both dwell time analysis (Kubitscheck et al., 2005) and maximum likelihood estimate (MLE; Kay, 1993) yielded total mean export times of 188 and 215 ms, respectively (Table 3-1; see section 2.5.4 for dwell time estimation).

3.2.3 mRNPs frequently exhibit cytoplasmic scanning behavior in *REF* strain

During analysis of the *REF* dataset, it was noted that mobile GFA1 mRNPs would remain in close proximity to the NE and repeatedly enter a docked state, which was observed as confinement of mRNPs near the NE. To quantify this behavior, the states defined in the tracking data were used and particles that docked at the NE multiple times were counted, each separated by a state of nucleoplasmic or cytoplasmic diffusion for less than seven frames (105 ms). This behavior was termed "scanning." NE scanning was predominantly observed in the cytoplasm (n = 102), but also occurred infrequently in the nucleus (n = 4). NE scanning has also been observed for *MDN1*, *GLT1*, and *CLB2* mRNAs and was shown to be dependent on the nuclear basket components Mlp1p and Mlp2p (Saroufim et al., 2015). The low frequency of nuclear scanning suggests that docking of the *GFA1* mRNP to the NE often results in a productive NPC interaction and export. Indeed, it was found that ~90% of the mRNPs observed to dock at the NE were successfully exported (Table 3-1). The functional significance of nuclear scanning remains unclear, but given the low frequency observed here, this may relate to mRNP quality control mechanisms occurring at NPCs, to limited access of an mRNP to a channel engaged with other cargoes, or to differences in cellular status (Tutucci and Stutz, 2011; Bonnet and Palancade, 2014). In addition, ~35% of successfully exported mRNPs underwent cytoplasmic scanning directly after export. The observed NE scanning frequency after export is likely an underestimate because many tracked particles moved out of focus after arrival in the cytoplasm.

Two types of cytoplasmic scanning behaviors that confined the mRNP in close proximity to the NE could be further distinguished. Particles were observed that interacted with the same area of the NE (local scanning; Figure 3-4B) or particles that made contacts over a large area of the NE (distributive scanning; Figure 3-4C). Local NE scanning may reflect an mRNP remaining

Table 3-1. Summary of *GFA1-PP7* mRNP imaging data

	REF	***mex67-5***
Particles tracked	291	203
Nuclear docking events	47	23
Export events	43	9
Retrograde export events	0	7
Mean export time – dwell time analysis (ms)	188[a]	n.d.
Mean export time – MLE (ms)	215[a]	n.d.
Mean nuclear docking time during export – dwell time analysis (ms)	32[a]	362[a]
Mean nuclear docking time during export – MLE (ms)	39[a]	202[a]
Mean transition time during export – dwell time analysis (ms)	87[a]	406[a]
Mean transition time during export – MLE (ms)	99[a]	383a
Mean cytoplasmic docking time during export – dwell time analysis (ms)	62[a]	1258a
Mean cytoplasmic docking time during export – MLE (ms)	77[a]	943[a]
NE associated mRNPs per cell	0.2±0.4[b]	0.5±0.7[b]
Nuclear scanning events	4	2
Cytoplasmic scanning events	102	16

n.d., not determined

[a] Export data underlying dwell time analysis may not have a normal distribution; consequently, an MLE analysis was performed (Kay, 1993). The differences between dwell times in REF and mex67-5 strains were tested using the distribution independent Wilcoxon rank-sum test and were found to be significant at $P < 0.05$ for the transition and cytoplasmic docking states. For more details and a discussion of error measurements, see Chapter II materials and methods section - statistical analyses.

[b] Standard deviation.

engaged with cytoplasmic Nups within the same NPC that facilitated transport. In this case, the apparent distance that the particle is able to travel into the cytoplasm and along the NE would be determined by the ~50 nm distance that NPC fibrils extend into the cytoplasm and the flexibility of an mRNA molecule (Fahrenkrog et al., 1998; Alber et al., 2007). In contrast, distributive NE scanning involves distances far beyond 50 nm, suggesting that an mRNP could make repeated contacts with the NE involving multiple NPCs (Figure 3-4C).

3.2.4 Generation and characterization of *GFA1-24xPP7* Ndc1p-tdTomato in the background of *mex67-5* mutant allele

Having established an imaging approach in yeast to measure mRNP export kinetics, the impact of a mutant Mex67p protein on nuclear export dynamics of *GFA1* mRNPs was examined. Mex67p (NXF1/TAP in metazoans) is an essential export factor that, as part of the mRNP, interacts with components of the NPC to facilitate export (Segref et al., 1997; Grüter et al., 1998; Santos-Rosa et al., 1998; Katahira et al., 1999; Bachi et al., 2000; Hurt et al., 2000; Strässer et al., 2000; Stutz et al., 2000; Rodrigues et al., 2001; Lund and Guthrie, 2005; Tuck and Tollervey, 2013; Baejen et al., 2014). Together, these works support a model of export where (a) multiple Mex67p molecules bind along the length of mRNA during nuclear maturation, (b) Mex67p promotes mRNP transport through the NPC by binding FG Nups, and (c) Mex67p dissociates from the mRNP on the cytoplasmic face of the NPC, preventing further interactions with the NPC. Displacement of Mex67p would therefore impart directionality on nuclear mRNA export (Stewart, 2007).

Cells carrying the temperature-sensitive *mex67-5* allele were initially imaged at the non-permissive temperature of 37°C (Segref et al., 1997), but mRNPs became static and reduced in number, precluding analysis of export. Consequently, imaging was performed at 26°C, which was also used to collect the *REF* dataset. At 26°C, the *mex67-5* strain did not have observable growth defects or mRNA export defects, as measured using an oligo-dT FISH assay to determine steady-state mRNA localization (Figure 3-5A and 3-5B). Using GFP-tagged versions of Mex67p and Mex67-5p, an increased nuclear pool of Mex67-5p was observed at 26°C, but the majority remained at the NE similar to Mex67p. This is in contrast to Mex67-5p localization at 37°C,

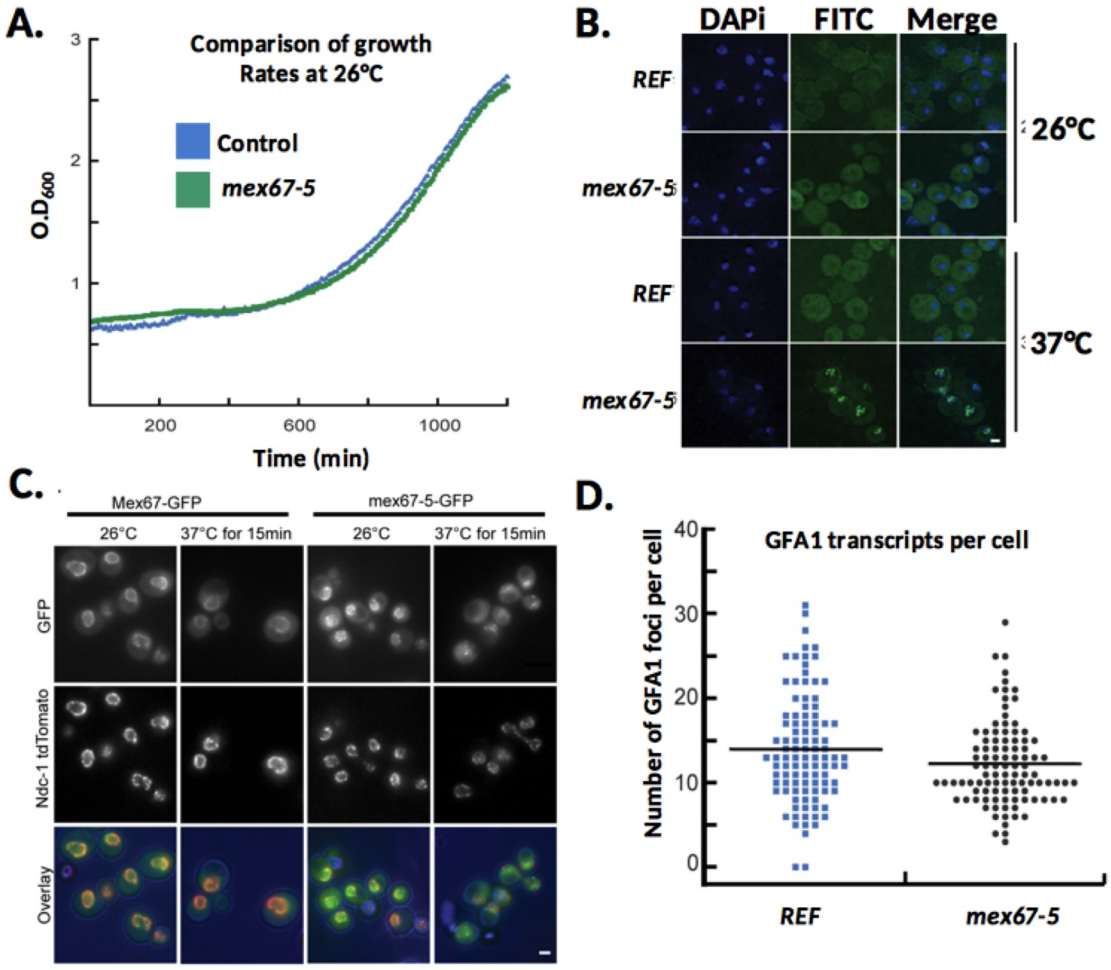

Figure 3-5. *mex67-5* strain characterization. **A.** Growth curves of control (BMY129) and *mex67-5* (BMY135) strains at 26°C. The data shown are from a single representative experiment out of three repeats. **B.** Representative images showing poly(A)-RNA localization in the *REF* and *mex67-5* strains at 26°C and 37°C. FISH was performed using a FITC-labeled oligo-(dT) probe, and DNA was stained with DAPI. **C.** GFP-tagged Mex67 localization in control (KWY5566) and *mex67-5* (KWY5567) strains at 26°C and 37°C as compared with Ndc1-tdTomato. Overlay displays the green and red channels as well as the bright eld image. **D.** Dot plot shows the number of *GFA1* mRNAs per cell in logarithmically growing *REF* (14 ± 6) and *mex67-5* (12 ± 5) strains at 26°C determined by single-molecule FISH with the mean denoted by a black line (n = 100 cells). Bars, 1 µm. Mex67p localization and *mex67-5* FISH experiments performed by Carina Derrer.

where foci within both the nucleus and cytoplasm formed (Figure 3-5C). The mean number of *GFA1* mRNAs observed in the *mex67-5* strain (12 ± 5) by single-molecule FISH was significantly different ($P < 0.05$; two-tailed *t* test; $n = 100$ cells) than the *REF* strain (14 ± 6; Figure 3-5D). The *mex67-5* mutation, therefore, impacts Mex67p localization and GFA1 mRNA levels, indicating that Mex67-5p has a partial loss of function at 26°C, but this does not result in significant changes in mRNA distributions at steady state.

3.2.5 Mex67p is critical for release of mRNPs from NPCs and required to maintain directionality of mRNP export through NPCs

By using single-particle imaging, the *GFA1* mRNPs in the *mex67-5* mutant that were observed at 26°C were threefold more frequently associated with the NE (Table 3-1). Data from all tracked mRNPs (i.e., independent of being part of a successful export event) were further used to estimate the length of time a particle spent in a single state (e.g., cytoplasmic docked) before transitioning to the next state (e.g., cytoplasmic). It was determined that mRNPs in the *mex67-5* strain persisted significantly longer in each of the states ($P < 0.01$; Wilcoxon rank-sum test; (Figure 3-6A). The number of cytoplasmic scanning events was also decreased in the *mex67-5* strain (Table 3-1), and mRNPs in the cytoplasmic docked state were observed for the entire duration of imaging (Figure 3-6B). These data demonstrate that Mex67-5p alters the dynamics of mRNP–NPC binding interactions at 26°C, which can be quantified using this single-particle imaging approach.

In the dataset collected from ~250 *mex67-5* cells, only nine successful mRNP export events were identified (Figure 3-7A and 3-7B). These ranged in length from 210 to 4,080 ms, and a comparison of successful export times from *REF* and *mex67-5* cells showed a clear bias ($P < 0.01$; Wilcoxon rank-sum test) toward long events in *mex67-5* cells (Figure 3-7B). However, the low number of successful events precluded an accurate calculation of a mean export time. Dwell time analysis of the states occupied by successfully exported mRNPs showed that in *mex67-5* cells, the lengthening of export times was the result of an ~6-fold increase in nuclear docking times, an ~4-fold increase in transition times, and an ~20-fold increase in cytoplasmic docking times when compared with the duration of these states in *REF* export events (Table 3-1 and Figure 3-1). The differences between *REF* and *mex67-5* strains for transition times

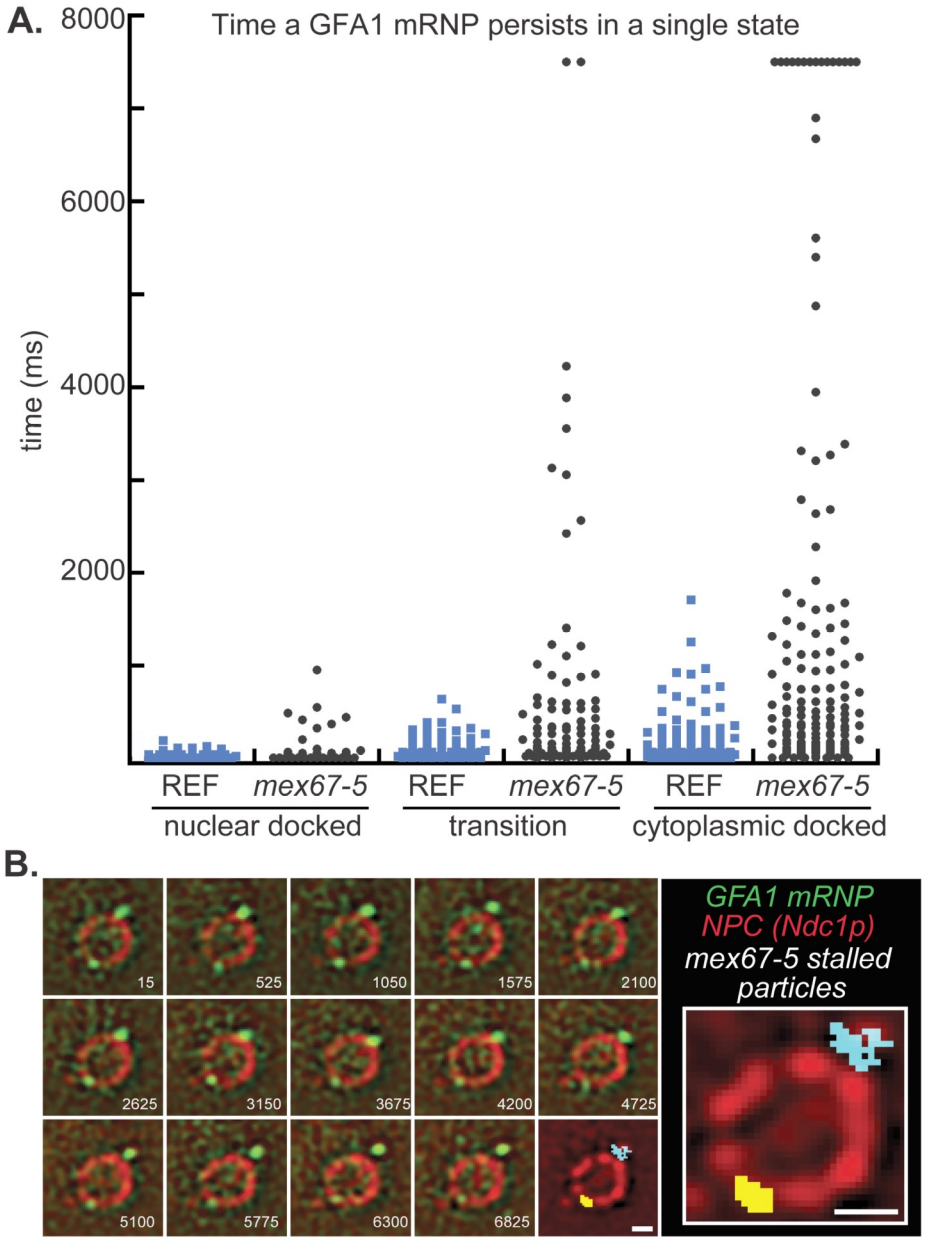

Figure 3-6. Prolonged *GFA1-PP7* mRNP interactions with the NE in *mex67-5*. A. Dot plot displaying the length of time a *GFA1* mRNP persists in a single state (nuclear docked, transition, or cytoplasmic docked) in *REF* (n = 49, 82, and 108) and *mex67-5* (n = 34, 94, and 151) strains. Note that the data presented here use all trace data where a particle interacted with the NE independent of the trace resulting in mRNP export. **B.** Selected non-consecutive frames show the persistent interaction of *GFA1* mRNPs with the NE in *mex67-5* cells. Cells were imaged at 26°C and 67 Hz with the time from the start of the event given in the bottom right of each image in milliseconds. The last image and inset show an overlay of the mRNP path that is color-coded based on position (gray, nuclear docked; yellow, transition; blue, cytoplasmic docked/cytoplasm). Bars, 1 µm.

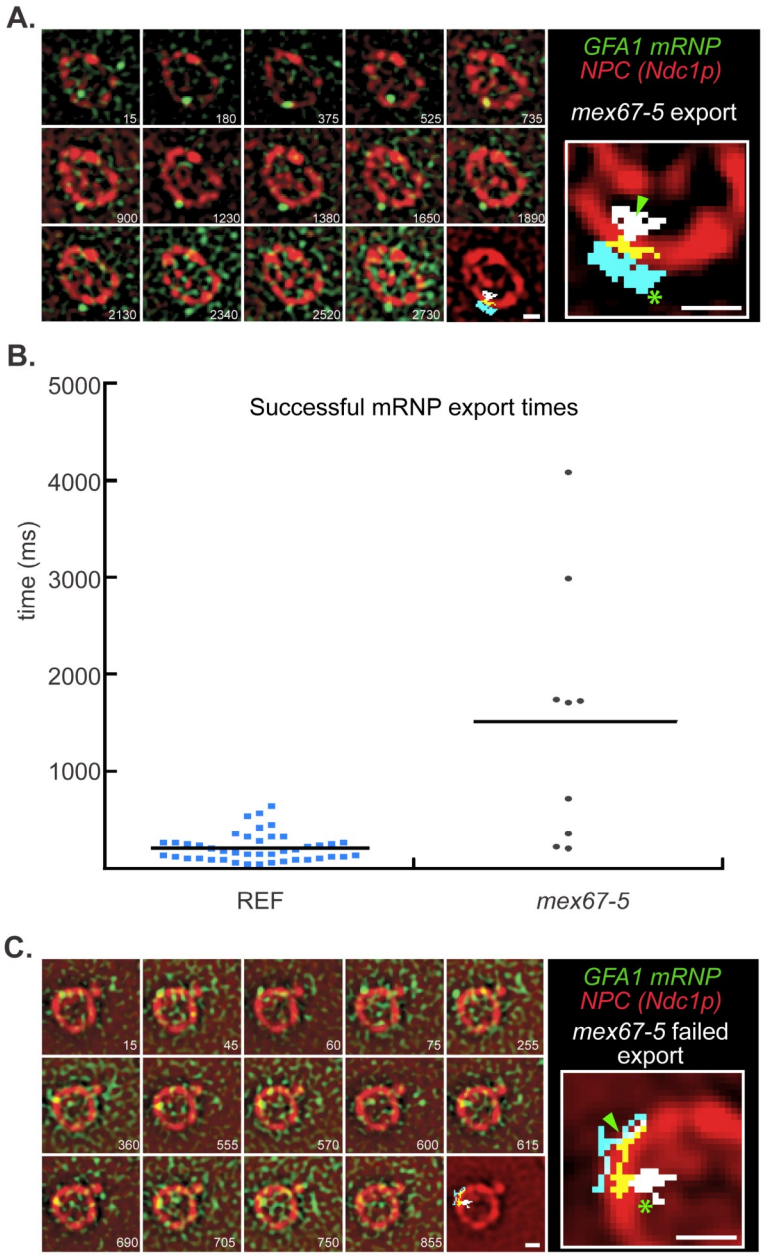

Figure 3-7. mRNP export kinetics and retrograde transport in *mex67-5*. A. Merged and registered images show select frames of a successful export event in a *mex67-5* cell. **B.** Dot plot showing the distribution of *GFA1* mRNP export times in *REF* ($n = 43$) and *mex67-5* ($n = 9$) cells, with the mean denoted by a black line. **C.** Selected nonconsecutive frames show a retrograde transport event in which an mRNP on the cytoplasmic side of the NE returns to the nucleus. For A and C, cells were imaged at 26°C and 67 Hz with the time from the start of the event given in the bottom right of each image in milliseconds. The last image and inset show an overlay of the mRNP path that is color coded based on position (white, nuclear docked; yellow, transition; blue, cytoplasmic docked/cytoplasm). Each green arrowhead and star denotes mRNP positions at the beginning and end of the track, respectively. Bars, 1 µm.

($P < 0.01$; Wilcoxon rank-sum test) and cytoplasmic docking times ($P < 0.01$; Wilcoxon rank-sum test) were statistically significant, whereas the 6× increase in nuclear docking times was not ($P > 0.05$; Wilcoxon rank-sum test). These data fit well with the observed increase in NE-associated mRNPs (Table 3-1), the low number of observed successful export events, and the extended interactions of tracked mRNPs with the NE in *mex67-5* cells (Figure 3-6). Of the nuclear mRNPs that docked with the NE in *mex67-5*, only 32% (9 of 23) were ultimately exported, which contrasted with the *REF* strain, where 90% of nuclear docking events led to export (Table 3-1). Interestingly, from the 14 particles that did not export, seven retrograde transport events were identified in which mRNPs traverse the NE and achieve a state of cytoplasmic docking before ultimately returning to the nucleoplasm (Figure 3-7C). Retrograde mRNP transport was never observed in *REF* cells. Collectively, the seven re-import events and the ~20-fold increase in cytoplasmic dwell times (Table 3-1 and Figure 3-1) during successful export events strongly argue that the *mex67-5* mutant perturbs directional mRNP export and cytoplasmic release.

3.3 Discussion

Overall, this work has measured mRNP export kinetics for the first time in *S. cerevisiae* by taking advantage of two powerful experimental systems: single-particle RNA localization microscopy and yeast genetics. Importantly, this approach provides a platform upon which to address fundamental questions related to nuclear mRNA export, including kinetics, regulation, and the mechanisms of transport through NPCs. mRNP export times estimated here are similar to those reported for transcripts modified with the MS2 RNA-tagging system in mouse cells and for unmodified transcripts labeled by fluorescently tagged mRNP proteins injected into insect salivary gland cells (Grünwald and Singer, 2010; Mor et al., 2010; Siebrasse et al., 2012), but are slower than times reported using single-point edge-excitation sub-diffraction microscopy (Ma et al., 2013). These findings, therefore, indicate that export in yeast and mammals occur on a similar time scale, consistent with a conservation of the NPC transport mechanism between these species.

The observation that mRNPs are frequently confined near the NE after arrival in the cytoplasm may suggest that mRNPs visit multiple NPCs for the purpose of mRNP remodeling after export. However, given that the detailed composition of mRNPs, which includes the number and spacing of every mRNP export factor across an exporting transcript, remains unclear; the extent to which mRNPs require remodeling following export also remains unclear. Large-scale proteomic and sequencing approaches to study mRNP composition have determined that several mRNP export factors bind across the entire length of transcripts without sequence specificity (Tuck and Tollervey, 2013). These ensemble measurements may suggest that many copies of a single mRNP export factor binds a single transcript. Therefore, this opens up the possibility that perhaps not all export receptors are immediately removed from mRNPs upon translocation and multiple NPC–mRNP interactions are required for complete remodeling and cytoplasmic release, which may also be dependent on the transcript itself. For example, remodeling requirements may differ based on the size of the transcript, or if the transcript has undergone splicing to remove introns, both of which may alter mRNP composition.

Interestingly, here mRNP-scanning behavior was predominantly observed on the cytoplasmic face of the NPC, not at the nuclear face. This may suggest that for the *GFA1* transcript, under these growth conditions, mRNPs arriving in close proximity to NPCs are either rapidly remodeled here and/or do not require extensive remodeling and are largely export competent. In contrast, another study of live-cell mRNP dynamics in a yeast model did observe nuclear scanning of specific mRNPs (Saroufim et al., 2015). Again, these differences may be due to differences in the transcript itself being studied and even the requirement for expression of that transcript. Further investigation of other transcripts of many types will need to be carried out to determine if this is a common feature of mRNP export. Furthermore, evidence of distributive cytoplasmic scanning, may suggest that mRNP remodeling can be distributed across multiple NPCs and need not occur solely at the NPC that facilitated export. Given the large number of exporting substrates, which includes proteins, RNPs, and other molecules, this may be an advantageous mode for efficient RNP remodeling and clearance of NPCs for a continuous flux of substrates.

This scanning behavior is also consistent with the idea that rate-limiting mRNP remodeling occurs at either the nuclear or cytoplasmic faces of NPCs and perhaps not within the NPC channel itself. This is supported by previous analysis of NPC translocation kinetics of the β-

actin mRNA in mouse cells, which points to translocation through NPCs as not being the rate-limiting step (Grünwald and Singer, 2010). Rather, events close to the nucleo- and cytoplasmic face of the NPC were observed to contribute to the overall export times. This is consistent with data shown here for mRNP dwell times for the *GFA1* mRNP at the cytoplasmic face of NPCs, but not the nucleoplasmic face. However, the degree to which rearrangements occur during translocation for other types of mRNPs remains to be tested.

Yet another possibility for mRNP NE scanning in some instances, may be a requirement for NPC interactions important for events downstream of mRNP export, such as translation. In fact, a function in translation has been proposed for NPC-associated Dbp5p and the Nup Gle1p, which are key mRNP export factors required for remodeling (Gross et al., 2007; Bolger et al., 2008; Alcázar-Román et al., 2010; Bolger and Wente, 2011). Additionally, other factors loaded within an export competent mRNP are required for translation initiation (e.g. cap binding complex), further linking these processes (Lejeune et al., 2004; Maquat, 2004). Spatially where and when the first round of translation occurs in relation to NPCs and the completion of export is not known. EM images have shown that BR mRNPs from *C. tentans* in the process of export are often oriented to export 5′ cap first and the cytoplasmic portion of the exporting mRNP can be bound by ribosomes, which suggests that the mRNAs can associate with translation machinery coupled to the export process (Mehlin et al., 1995; Visa et al., 1996). However, this may be unique to this very large RNA. Whether this scanning behavior is indicative of general mRNP export coupled to translation initiation remains to be interrogated.

Direct evidence for the essential role of Mex67p in imparting directionality to mRNP export has been provided here. The *mex67-5* allele contains a histidine-to-tyrosine amino acid substitution at position 400, which is within the NTF2-like domain of Mex67p, required for interaction with Mtr2p, which then facilitates interactions with FG Nups. How this mutation alters protein structure of Mex67p and interactions with Mtr2p and/or FG Nups at a permissive temperature is not clear. However, previous studies have shown through RNA IP experiments that there is less mRNA associated with Mex67-5p as compared with Mex67p (Segref et al., 1997; Lund and Guthrie, 2005). Computational models of mRNA export suggest that the efficiency of mRNP export is highly sensitive to both the number and spacing of export factors along an mRNP (Azimi et al., 2014). As such, a reduced number and/or altered spacing of functional Mex67p molecules on the mRNA could lead to changes in mRNP architecture and

altered interactions with the NPC that may affect how efficiently the mRNP is transported and remodeled by the NPC. This could explain the resulting inefficiencies and failures in mRNP export reported here (e.g. delayed release), although further work will be required to characterize the molecular basis of these transport defects.

Future applications of this approach will include interrogating the function of the many other proteins (>80) involved in mRNP export, including Nups. The studies will be facilitated by the tractable genetics and the expansive knowledge of mRNP export and NPC function in yeast. Given that many of these factors overlap in functions to include roles in upstream mRNA transcription processing, splicing, and decay, these studies will also provide insight into how these processes are coupled and tightly regulated.

Chapter IV: A *nuclear role for the DEAD-box protein Dbp5p in tRNA export**

* Portions of this chapter have been published as Lari et al., 2019. Elife. pii:e48410. doi:10.7554/eLife.48410.

4.1 Overview

In eukaryotic cells, spatial separation of the transcriptional and translational processes necessitates transport of RNA and protein cargos across the NE via NPCs. Generally, mRNAs are transcribed and processed in the nucleus, transported across the NE, and then translated, stored, or decayed in the cytoplasm. ncRNA species, such as rRNA or tRNA, also undergo nuclear processing and export following transcription (Phizicky and Hopper, 2015; Zemp and Kutay, 2007). Throughout these events, RBPs interact with each RNA to form an RNP, with the protein constituents of each RNP mediating RNA processing and/or RNP functions within the cell (Moore, 2005).

DEAD-box proteins (DBPs) are a family of RBPs found in all domains of life, often displaying RNA-stimulated ATPase activity, with diverse roles in RNA biology (Linder and Jankowsky, 2011). For example, the DEAD-box protein Dbp5p (or DDX19B in humans) plays an essential role in eukaryotic mRNA metabolism by driving directional nuclear mRNP export (Hodge et al., 1999; Lund and Guthrie, 2005; Schmitt et al., 1999; Snay−Hodge et al., 1998; Tran et al., 2007; Tseng et al., 1998). Dbp5p, as a DEAD-box protein, is characteristically composed of two RecA-like domains that form the catalytic core of the enzyme, with identifiable sequence motifs that mediate RNA-binding, ATP-binding, and ATP hydrolysis (Collins et al., 2009; Dossani et al., 2009; Fan et al., 2009; Montpetit et al., 2011; Napetschnig et al., 2009; von Moeller et al., 2009). Dbp5p ATPase activity is further modulated by cytoplasmic oriented NPC proteins, Nup42p, Nup159p (NUP214 in humans) and Gle1p together with the endogenous small molecule co-factor, inositol hexakisphosphate ($InsP_6$) (Adams et al., 2017; Alcazar-Roman et al., 2006; Dossani et al., 2009; Hodge et al., 1999; Hodge et al., 2011; Montpetit et al., 2011; Napetschnig et al., 2009; Noble et al., 2011; Schmitt et al., 1999; von Moeller et al., 2009; Weirich et al., 2004, 2006; Wong et al., 2018).

Based on the localization of Dbp5p at NPCs and regulation by NPC components, models propose that Dbp5p encounters mRNPs at the cytoplasmic face of NPCs and remodels these substrates to enforce directionality as they enter the cytoplasm (Folkmann et al., 2011; Heinrich et al., 2017; Stewart, 2007). However, Dbp5p is dynamic at NPCs and is known to shuttle between the nuclear and cytoplasmic compartments (Estruch and Cole, 2003; Hodge et al., 1999; Izawa et al., 2005; Noble et al., 2011; Takemura et al., 2004; Zhao et al., 2002). This information

prompts an alternative model in which Dbp5p functions as a scaffold, binding the mRNA in the nucleoplasm and traveling with nuclear mRNPs to NPCs where remodeling occurs through interactions with Gle1p and Nup159p (Heinrich et al., 2017). While nuclear shuttling of Dbp5p is known, a mechanistic understanding of how nuclear transport is controlled and the relevance of this activity in the context of mRNP assembly and export is not.

Several additional roles for Dbp5p in gene expression have been proposed that point to functional pools of Dbp5p in the nuclear and cytoplasmic compartments. For example, studies have shown both physical and genetic interactions between Dbp5p and transcription initiation and translation termination machinery (Alcázar-Román et al., 2010; Beißel et al., 2019; Bolger et al., 2008; Estruch et al., 2012; Estruch and Cole, 2003; Gross et al., 2007). Additionally, a role for Dbp5p in the nuclear export of pre-ribosomal subunits has been identified (Neumann et al., 2016). Most recently, the mammalian and *Xenopus* homologs of Dbp5p, DDX19B, have been shown to stabilize ribosomal elongation and termination complexes *in vitro* and contribute to nuclear R-loop clearance upon replication or DNA damage stress (Hodroj et al., 2017; Mikhailova et al., 2016). These data suggest a broader role for Dbp5p in RNA metabolism and gene expression, but the mechanisms by which Dbp5p contributes to these various cellular processes remains largely undefined.

With the goal of understanding the cellular functions of Dbp5p, a comprehensive alanine scanning mutagenesis approach was employed to generate mutants encompassing residues 2-482 of Dbp5p, which is presented in this chapter. Combined with published Dbp5p structures, the resulting data provide a functional map of Dbp5p at a single amino acid resolution and mutant alleles that can be employed to detail mechanisms by which Dbp5p contributes to eukaryotic gene expression. This is exemplified by work here describing the identification of key residues within Dbp5p that facilitate nuclear transport and the discovery of a novel role for Dbp5p in nuclear tRNA export.

4.2 Results

4.2.1 Characterization of the *dbp5* mutant collection

An alanine scanning mutagenesis approach was used to generate single alanine (or glycine if the residue was an alanine) substitutions at positions 2-482 of Dbp5p, resulting in a collection of 481 plasmids carrying *dbp5* mutant alleles in frame with GFP at the N-terminus. To begin to address the functional status of the resulting mutants, a plasmid shuffle assay was used to generate strains solely expressing the mutant version of GFP-Dbp5p. Based on this selection, 25 alanine substitutions were identified as lethal (Table 4-1). Consistent with published biochemical and structural models of DBPs (Linder, 2006), the majority of the lethal substitutions identified in Dbp5p were in motifs known to be critical for RNA-binding, ATP-binding, and ATP hydrolysis (Figure 4-1). For example, lethal mutations included *Q119A*, which is within the highly conserved Q-motif and is known to be required for adenine recognition and ATP hydrolysis (Cordin et al., 2004). Similarly, lethal mutations included *D239A*, *E240A*, and *D242A* in motif II (or the Walker B motif), which are part of the namesake D-E-A-D amino acid sequence critical for ATP recognition and hydrolysis. Lethal mutations also mapped to regions of Dbp5p that participate in binding NPC regulators Gle1p and Nup159p, including residues R256, Y325, and K382 (Figure 4-2A) (Dossani et al., 2009; Montpetit et al., 2011; Weirich et al., 2004).

The collection of 456 *dbp5* mutant alleles that were viable with single amino acid substitutions in Dbp5p, were further employed in various phenotypic screens to assay Dbp5p functionality. First, temperature sensitive (Ts) alleles were identified by screening for a lack of growth at 37°C. The ability of each strain to grow was measured following two sequential rounds of plating at 37°C with a Ts phenotype defined as no observed growth on the second plate. This analysis resulted in the identification of 42 Ts alleles (Table 4-1). Similar to lethal mutations, many of the Ts mutations mapped to conserved regions of the protein important for hydrolysis and RNA-, ATP-, or regulator binding (Figure 4-1). However, several of the Ts mutations mapped to unstructured or surface-exposed regions of Dbp5p that have not been previously reported to facilitate known Dbp5p functions or activities, including residues L12 and L15, and a cluster of residues at 158-163 of Dbp5p (Figure 4-2B). One potential cause for a Ts phenotype is

Table 4-1. Summary of growth screening data for *dbp5* alleles

Lethal alleles	Temperature Sensitive (Ts) alleles at 37°C
dbp5-F94A	*dbp5-R6A*
dbp5-Q119A	*dbp5-D7A*
dbp5-N133A	*dbp5-L12A*
dbp5-G141A	*dbp5-L15A*
dbp5-G143A	*dbp5-V73A*
dbp5-K144A	*dbp5-F112A*
dbp5-F148A	*dbp5-K114A*
dbp5-R172A	*dbp5-P115A*
dbp5-E173A	*dbp5-S116A*
dbp5-D239A	*dbp5-I118A*
dbp5-E240A	*dbp5-P124A*
dbp5-D242A	*dbp5-L125A*
dbp5-R256A	*dbp5-H128A*
dbp5-Y325A	*dbp5-N129A*
dbp5-K340A	*dbp5-I135A*
dbp5-Y347A	*dbp5-Q137A*
dbp5-K349A	*dbp5-Q139A*
dbp5-R369A	*dbp5-S140A*
dbp5-K382A	*dbp5-T142A*
dbp5-T387A	*dbp5-V156A*
dbp5-N388A	*dbp5-P158A*
dbp5-R392A	*dbp5-E159A*
dbp5-G393A	*dbp5-A161G*
dbp5-R4236A	*dbp5-S162A*
dbp5-R429A	*dbp5-P163A*
	dbp5-P170A
	dbp5-R176A
	dbp5-F201A
	dbp5-K203A
	dbp5-M223A
	dbp5-R224A
	dbp5-F236A
	dbp5-L238A
	dbp5-L245A
	dbp5-F270A
	dbp5-H355A
	dbp5-I359A
	dbp5-D370A
	dbp5-V389A
	dbp5-L390A
	dbp5-R423A
	dbp5-G425A

Figure 4-1. Lethal and temperature sensitive (Ts) *dbp5* alleles. A. Primary amino acid sequence of yeast Dbp5p with lethal alleles (blue), Ts alleles (orange), and conserved motifs required for RNA-binding, ATP-binding, and hydrolysis (grey boxes).

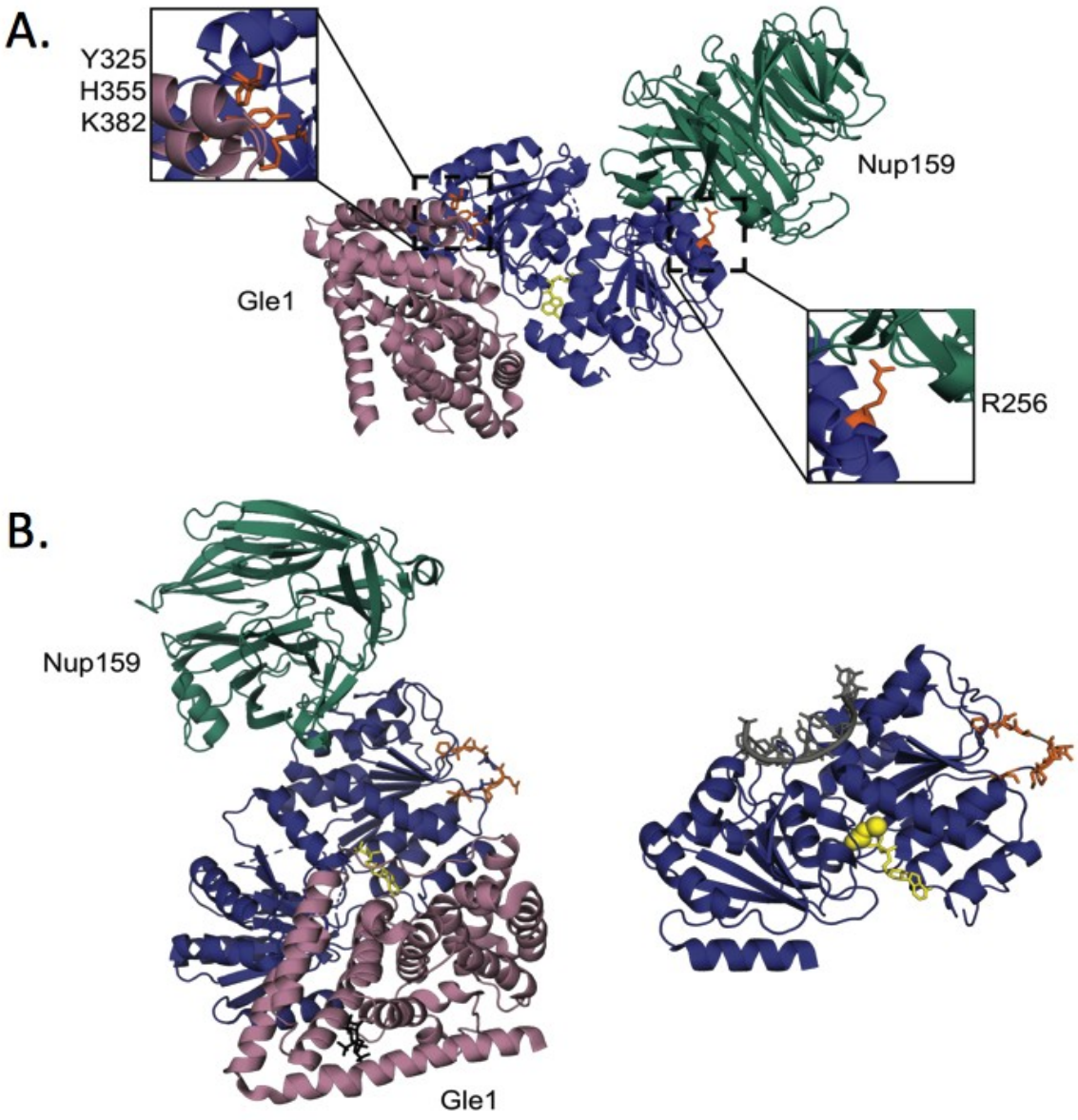

Figure 4-2. Key lethal and temperature sensitive (Ts) *dbp5* alleles mapped to structural models of Dbp5p. A. Structural model showing Dbp5p (blue) in complex with ADP (yellow), IP_6 (dark grey), and regulators Gle1p (reddish purple) and Nup159p (bluish green) with essential residues that mediate these interactions, R256 with Nup159p and Y325, H355, and K382 with Gle1p, highlighted in orange. Inset shows a zoomed in view of these residues. **B.** Residues V156, P158, E159, A161, S162, and P163 (orange) on a surface exposed region of Dbp5p in structural models showing (left) Dbp5p (blue) in complex with ADP (yellow), IP_6 (dark grey), and regulators Gle1p (reddish purple) and Nup159p (bluish green) or (right) Dbp5p (grey) in complex with RNA (blue) and ADP-BeF_x (yellow). Structural models in B and C taken from PDB 3RRM and 3PEY (Montpetit et al., 2011).

degradation of the protein at the restrictive temperature, but levels of GFP-Dbp5p in Ts mutants were largely comparable to the control strain after overnight growth at 37°C (Figure 4-3A).

To determine if observed Ts growth defects correlated with a disruption in nuclear mRNP export, fluorescent *in situ* hybridization (FISH) experiments were performed to detect poly(A)-RNA localization. In the control strain, 13% of cells displayed an observable accumulation of poly(A)-RNA in the nucleus after overnight growth at 37°C. In comparison, 26 of the 42 Ts mutants exhibited nuclear poly(A)-RNA accumulation in >50% of the population after overnight growth at 37°C; poly(A)-RNA accumulation in Ts strains ranged from 11% to 92% of cells (Table 4-2). These data suggest that in most cases the Ts phenotype is accompanied by a disruption in mRNP export; however, some Ts mutants showed a weak mRNP export defect at 37°C. This included *GFP-dbp5-V73A* and *GFP-dbp5-E159A,* suggesting that these particular mutants have alterations in essential Dbp5p functions that do not result in a strong mRNP export block (Figure 4-3B). These single amino acid substitutions represent particularly interesting alleles for study since they may specifically alter essential functions of Dbp5p outside of the mRNP export process.

4.2.2 Select *dbp5* mutants exhibit sensitivity to a translation inhibitor and DNA damage

The successful identification of Ts mutants that showed a range of poly(A)-RNA accumulation phenotypes, including alleles that were similar to the control, suggested that the mutant collection harbored separation-of-function alleles. To further identify such mutants, a screening strategy was employed with the entire viable mutant collection to identify strains that were hypersensitive to a translation inhibitor, Hygromycin B, or UV-induced DNA damage. These specific challenges were selected based on previous work linking Dbp5p to translation and findings that the metazoan homologue of Dbp5p transiently localizes to the nucleus upon DNA damage stress (Alcázar-Román et al., 2010; Beißel et al., 2019; Bolger et al., 2008; Gross et al., 2007; Hodroj et al., 2017). The rationale being that Dbp5p mutations that disrupt translation or the ability of cells to respond to DNA-damage would show hypersensitivity to these challenges.

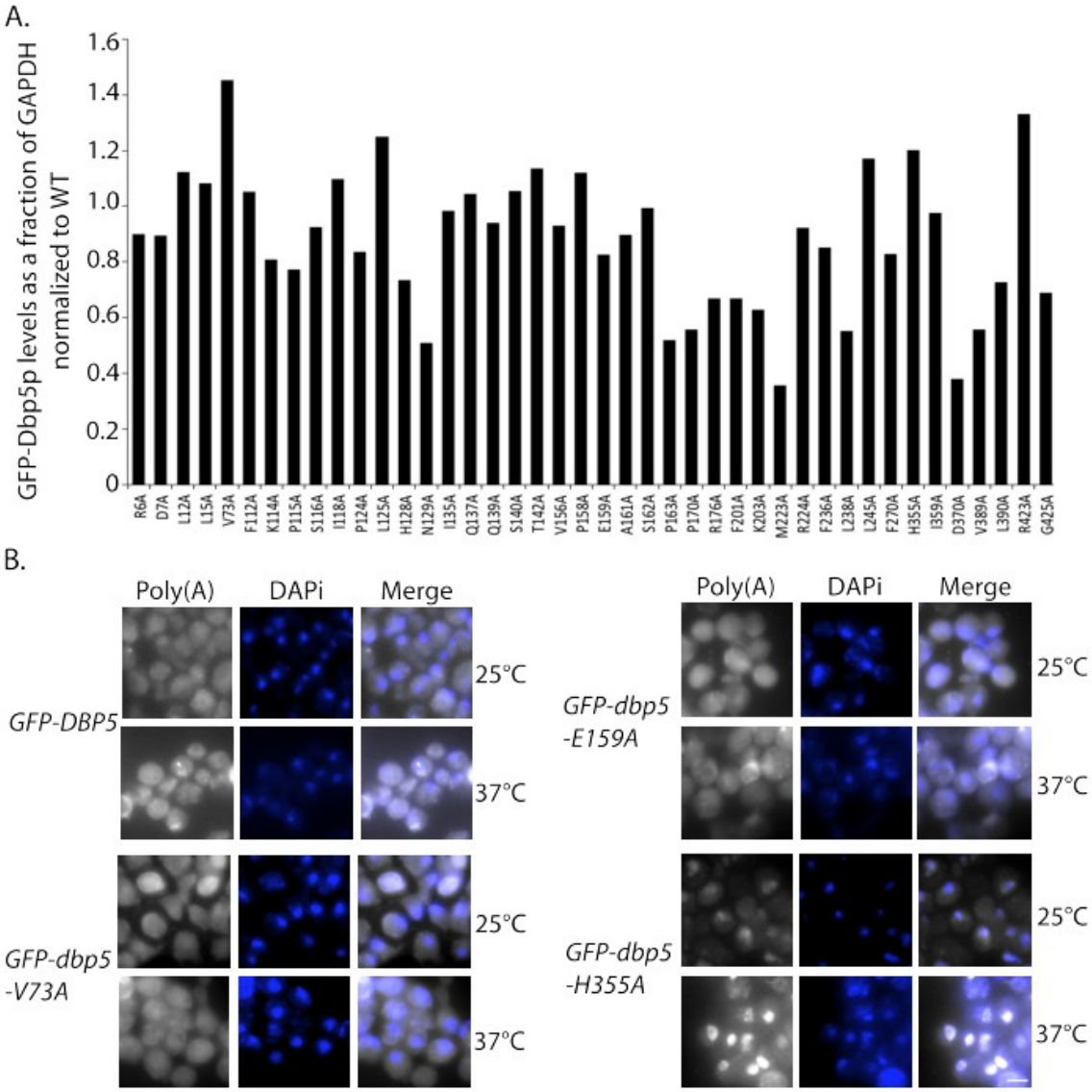

Figure 4-3. GFP-Dbp5p expression levels in *dbp5* temperature sensitive (Ts) mutants. A. Level of plasmid expressed GFP-Dbp5p in *dbp5* Ts mutants detected by western blotting before and after an overnight shift to 37°C. Bar graph shows GFP-Dbp5p levels in each mutant at 37°C normalized to the GAPDH loading control and to the level of GFP-Dbp5p in the wild-type strain. **B.** Images of strains carrying plasmid based *GFP-DBP5*, GFP-*dbp5-V73A,* GFP-*dbp5-E159A* and GFP-*dbp5-H355A* analyzed by FISH showing poly(A)-RNA (grey) and the DAPi stained DNA mass (blue) before and after an overnight shift to 37°C. Residue H335 mediates binding of Dbp5p to Gle1p (see Figure 4-1B) and is included here as a positive control. Scale bars = 2 □m. Immunoblotting performed by Rachel Montpetit.

Table 4-2. Quantification of poly(A) mRNA export defects in *dbp5* Ts strains

Mutant	% of cells with poly(A) mRNA export defects 25°C (n=200)	% of cells with poly(A) mRNA export defects 37°C (n=200)
DBP5	2%	13%
dbp5-R6A	0%	45%
dbp5-D7A	3%	58.50%
dbp5-L12A	8.50%	49%
dbp5-L15A	3.50%	41%
dbp5-V73A	2%	11%
dbp5-F112A	9%	81%
dbp5-K114A	21%	52%
dbp5-P115A	7%	42.50%
dbp5-S116A	10%	57.50%
dbp5-I118A	64.00%	56.50%
dbp5-P124A	43%	65.50%
dbp5-L125A	10%	35.50%
dbp5-H128A	4.50%	45%
dbp5-N129A	12.50%	29.50%
dbp5-I135A	4%	80%
dbp5-Q137A	8%	67%
dbp5-Q139A	5.50%	44%
dbp5-S140A	10%	53%
dbp5-T142A	4.50%	26%
dbp5-V156A	8.50%	51%
dbp5-P158A	13%	42%
dbp5-E159A	4.50%	25%
dbp5-A161G	3%	44%
dbp5-S162A	5%	42%
dbp5-P163A	5%	51%
dbp5-P170A	4.50%	62%
dbp5-R176A	15%	73%
dbp5-F201A	16.50%	57%
dbp5-K203A	8%	54%
dbp5-M223A	18%	62%
dbp5-R224A	29.50%	56%
dbp5-F236A	7.50%	43%
dbp5-L238A	1%	70%
dbp5-L245A	66%	92%
dbp5-F270A	12%	81%
dbp5-H355A	62.5	74%
dbp5-I359A	5.50%	68%
dbp5-D370A	21%	77%
dbp5-V389A	16.50%	72%
dbp5-L390A	32%	63%
dbp5-R423A	16%	83%
dbp5-G425A	26%	41%

From the Hygromycin B screen, 30 mutants were found to have increased sensitivity to the drug when compared to the wild-type strain at 25°C, of which 12 were also identified as Ts alleles (Table 4-3). Of the Ts alleles, GFP-*dbp5-V73A* was found to be sensitive to Hygromycin B (Figure 4-4A), which is of particular note since this Ts allele exhibited a minimal mRNP export defect based on poly(A)-RNA FISH at 25°C or 37°C (Table 4-2). Valine 73 is located within the N-terminal extension of Dbp5p, and when mutated to an alanine also caused slow growth at 25°C (Figure 4-4A). The Hygromycin B sensitivity suggests that V73 may be involved in mediating functions of Dbp5p in translation, which has been shown to involve interactions with the translation-release factor Sup45p (Beißel et al., 2019; Gross et al., 2007). To test the importance of V73 to this interaction, GFP-Dbp5p was immunoprecipitated from wild-type and GFP-*dbp5-V73A* strains and assayed for binding to Sup45p by western blotting; however, no significant changes in the Dbp5p interactions with Sup45p were observed with GFP-*dbp5-V73A,* as compared to wild-type (Figure 4-4B).

In the UV-induced DNA damage screen, five mutations were observed to exhibit sensitivity to UV-damage (Table 4-3). Of these, two mutations within motif VI of Dbp5p, GFP-*dbp5-R423A* and GFP-*dbp5-G425A,* were the most sensitive to UV-induced DNA damage. Sensitivity to UV-induced DNA damage was reproducible and GFP-*dbp5-R423A* and GFP-*dbp5-G425A* also showed sensitivity to another DNA-damaging agent, methyl methanesulfonate (MMS) (Figure 4-5A). To determine if DNA repair efficiency was impacted, the presence and resolution of DNA-repair centers were assayed by observing the number of Rad52p-YFP foci before and after treatment with MMS at 25°C. In cells carrying untagged and integrated *DBP5* or *dbp5-R423A*, similar numbers of repair foci were observed between both strains in both conditions tested suggesting that DNA damage is sensed and Rad52p foci are formed with comparable frequencies and kinetics (Figure 4-5B). This follow-up work with *dbp5-R423A* involved construction of an untagged integrated allele of *DBP5* at the endogenous locus. The *dbp5-R423A* strain grew comparably to wild-type and the GFP-tagged version of this allele at 25°C and 30°C, but was no longer Ts, nor did the strain show a nuclear poly(A)-RNA accumulation phenotype at 37°C (Figure 4-6A-B). These data indicate that the presence of GFP synergizes with the R423A mutation to enhance phenotypes, including growth and mRNP export defects at 37°C. This interpretation of the data is based on the fact that of the 456 viable GFP-

Table 4-3. ***dbp5 mutants sensitive to*** Hygromycin B or UV-induced DNA Damage

Hygromycin B Sensitive	**Temperature Sensitive (Ts) allele**	**UV Sensitive**	**Temperature Sensitive (Ts) allele**
dbp5-D10A	No	*dbp5-Q137A*	Yes
dbp5-L12A	Yes	*dbp5-H355A*	Yes
dbp5-L15A	Yes	*dbp5-I394A*	No
dbp5-L66A	No	*dbp5-R423A*	Yes
dbp5-V73A	Yes	*dbp5-G425A*	Yes
dbp5-I118A	Yes		
dbp5-M134A	No		
dbp5-I135A	Yes		
dbp5-A147G	No		
dbp5-N243A	No		
dbp5-L245A	Yes		
dbp5-D246A	No		
dbp5-M328A	No		
dbp5-I330A	No		
dbp5-V345A	No		
dbp5-L350A	No		
dbp5-L356A	No		
dbp5-H355A	Yes		
dbp5-S358A	No		
dbp5-I359A	Yes		
dbp5-L364A	No		
dbp5-Q365A	No		
dbp5-D370A	Yes		
dbp5-F376A	No		
dbp5-S381A	No		
dbp5-L390A	Yes		
dbp5-I394A	No		
dbp5-R423A	Yes		
dbp5-G425A	Yes		
dbp5-L480A	No		
dbp5-K481A	No		

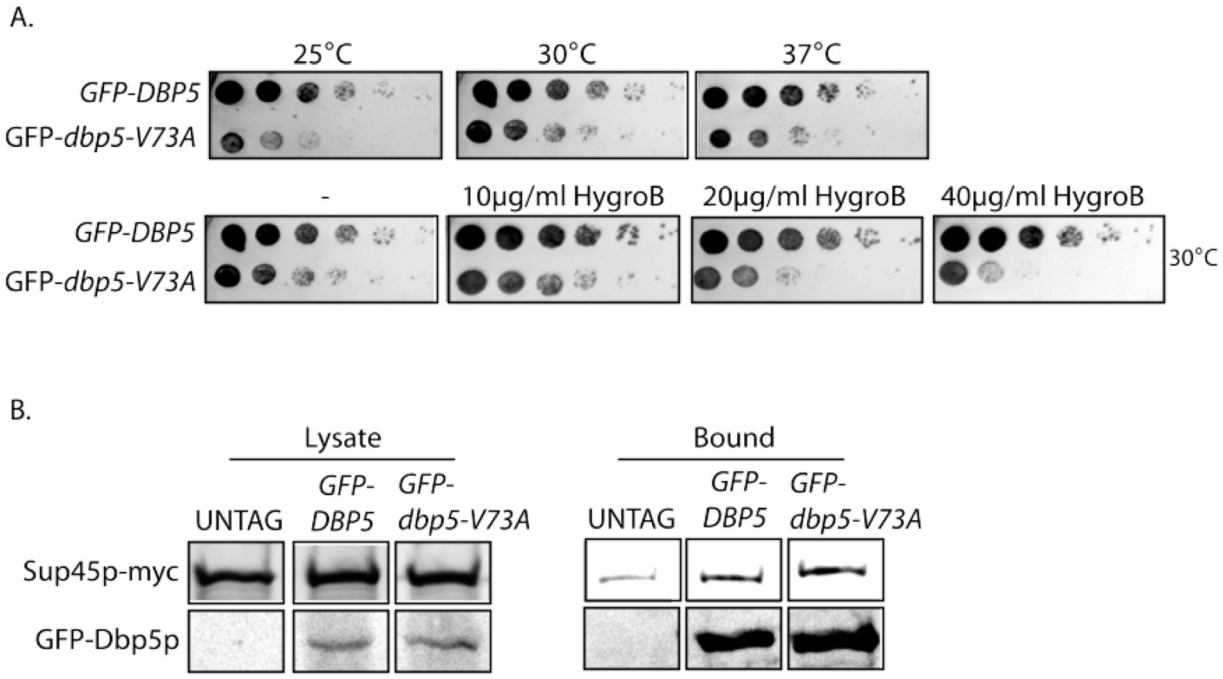

Figure 4-4. Characterization of Hygromycin B sensitive mutant, GFP-*dbp5-V73A*. A. Growth of yeast strains carrying plasmid based *GFP-DBP5* and GFP-*dbp5-V73A* at 25°C, 30°C, and 37°C or with Hygromycin B at 30°C for 2 days. **B**. Immunoprecipitation (IP) of GFP-Dbp5p from *GFP-DBP5* and *GFP-dbp5-V73A* strains. GFP-Dbp5p and Sup45p-myc bound to beads after IP from total cell lysates were detected by western blotting with anti-GFP and anti-myc antibodies. IPs performed by Rachel Montpetit.

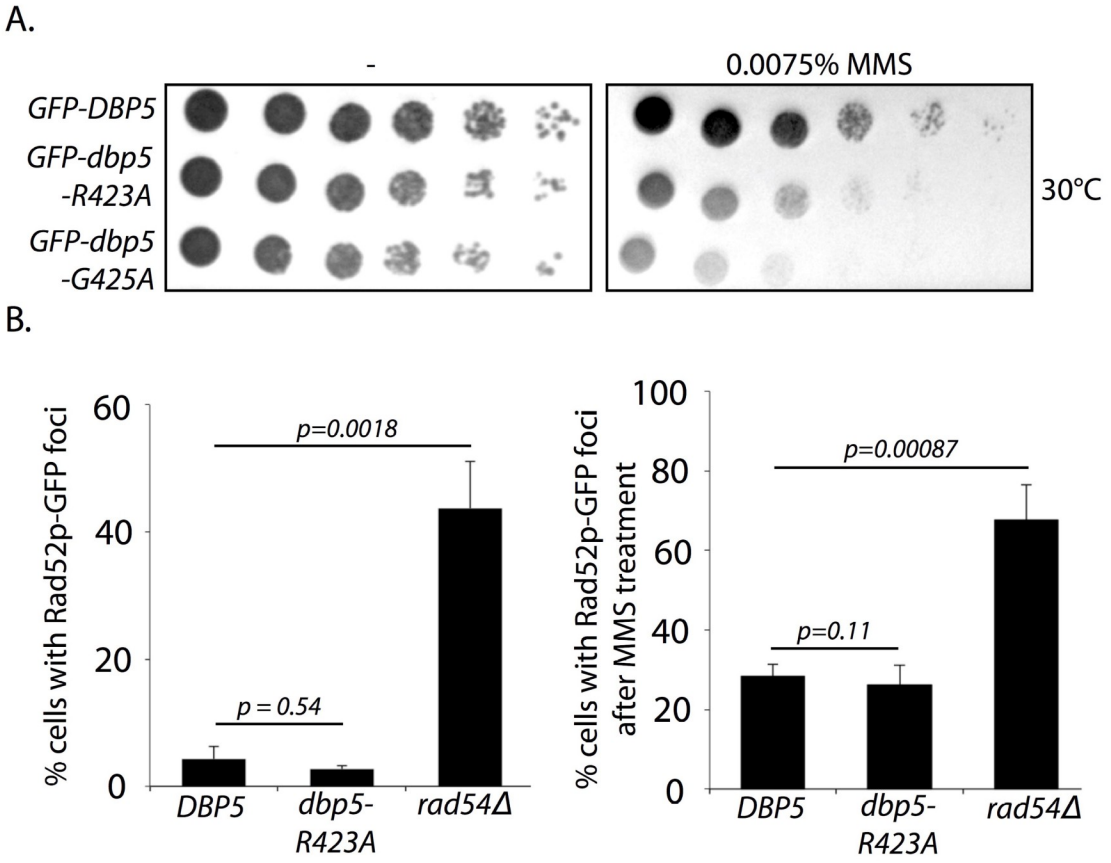

Figure 4-5. Characterization of *dbp5* mutants sensitive to MMS and UV-induced DNA-damage. A. Growth of yeast strains carrying plasmid based *GFP-DBP5,* GFP-*dbp5-R423A*, and GFP-*dbp5-G425A* at 30°C with or without 0.0075% MMS for 2 days. **B.** Quantification of Rad-52p-GFP foci in strains carrying untagged integrated copies of *DBP5*, *dbp5-R423A,* or *rad54Δ* before and after treatment with 0.5% MMS for 20 minutes. Bar graphs represent the percentage of cells in each strain with one or more Rad52p-GFP foci (3 biological replicates, n≥100, error bars represent standard deviation, p-value from unpaired t-test with two-tailed distribution shown). These experiments performed in collaboration with Rima Sandhu.

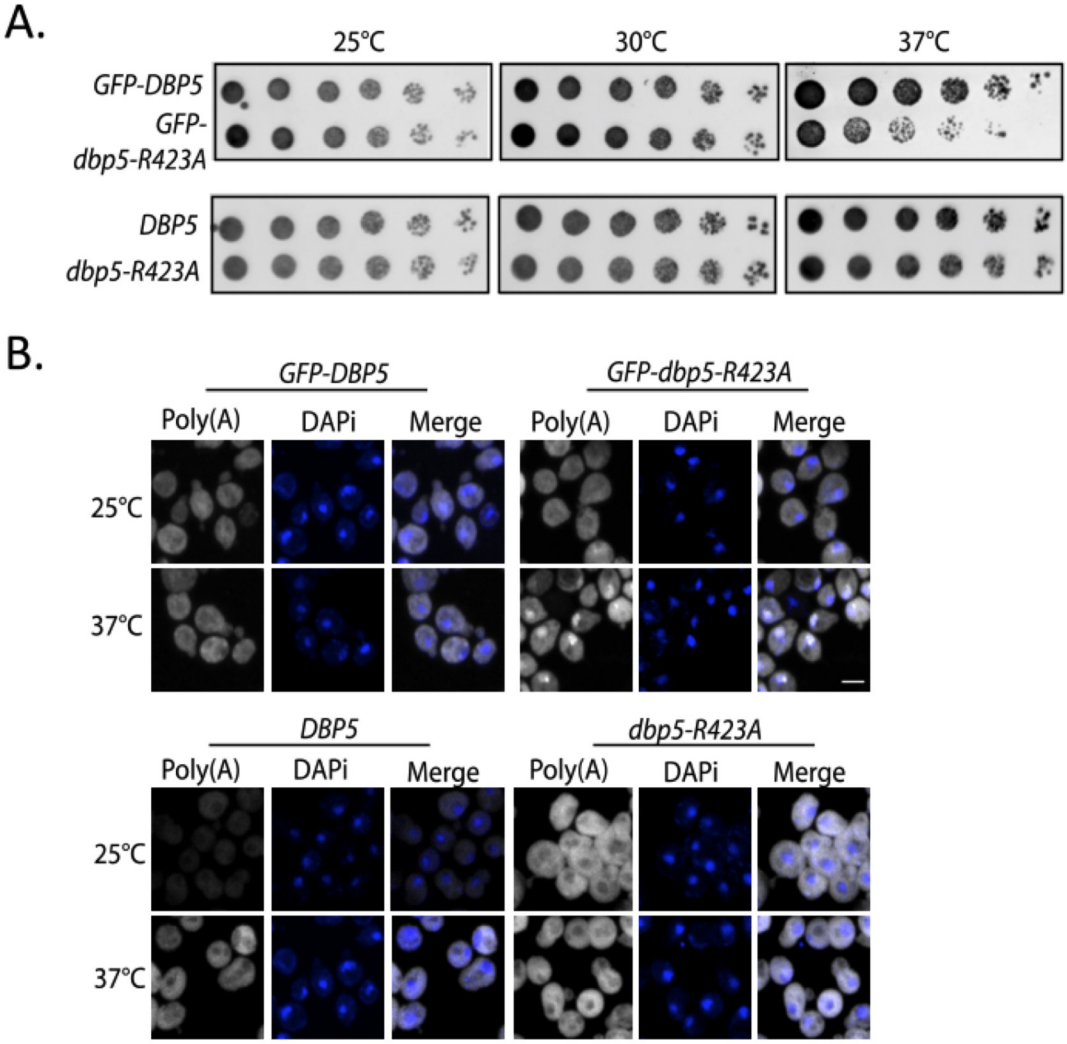

Figure 4-6. GFP-tagging of *dbp5-R423A* alters growth and mRNP export phenotypes. A. Growth of strains carrying plasmid-based versions of *GFP-DBP5* and GFP-*dbp5-R423A* compared to untagged integrated versions at 25°C, 30°C, and 37°C for 3 days. **B.** Images of yeast strains carrying plasmid-based versions of *GFP-DBP5* and GFP-*dbp5-R423A* compared to untagged integrated versions analyzed by FISH showing poly(A)-RNA (grey) and the DAPi stained DNA mass (blue) before and after a 3 hour shift to 37°C. Scale bars = 2 □m.

Dbp5p strains only 42 were identified as being Ts, and the wild-type strain did not show a strong Ts or mRNP export defect when N-terminally tagged with GFP at 37°C (Figure 4-6A-B). Importantly, the integrated *dbp5-R423A* strain retained sensitivity to MMS exposure, which was enhanced by growth at 37°C (Figure 4-7A). Similarly, *dbp5-V73A* retained Hygromycin B sensitivity when present as an untagged and integrated allele, but was also no longer slow growing at 25°C or Ts (Figure 4-7B). These findings indicate that the drug sensitivity phenotypes of *dbp5-V73A and dbp5-R423A* were not solely dependent on the presence of GFP, but rather they are enhanced by the presence of GFP, which must be taken into account when assaying this collection and interpreting the resulting data.

Finally, while the data presented here on Hygromycin B and UV-induced DNA damage do not resolve the mechanisms causing sensitivity to these stresses, the results demonstrate the potential utility of this collection to identify separation-of-function alleles. It is expected that such strategies could be further employed to investigate discrete functions of Dbp5p or used to identify individual residues in Dbp5p that mediate specific protein-protein interactions important to mRNP export and the other processes Dbp5p engages in.

4.2.3 Dbp5p contains an N-terminal nuclear export signal (NES)

Importantly, the inclusion of GFP in the mutant collection allowed for Dbp5p localization to be assayed in each point mutant. Under steady-state growth conditions, in the presence of a wild-type allele, GFP-Dbp5p expression was detectable for all 481-point mutations. The majority of the mutants displayed the expected localization pattern with enrichment of Dbp5p at NPCs with diffuse cytoplasmic and nuclear pools (Schmitt et al., 1999; Snay−Hodge et al., 1998; Weirich et al., 2004); however, two strains (*dbp5-L12A and dbp5-L15A*) showed a prominent nucleoplasmic localization of GFP-Dbp5p (Figure 4-8A). In these mutants, GFP-Dbp5p is found both in the nucleoplasm and nucleolus, as shown through co-localization of GFP-Dbp5p^{L12A} with the nucleolar protein Nop1p (Figure 4-8A). GFP-*dbp5-L12A and* GFP-*dbp5-L15A* were found to be Ts alleles and have poly(A)-RNA accumulation defects in ~49% and 41% of cells (Table 4-2). As described above, the presence of GFP can modify mutant phenotypes and

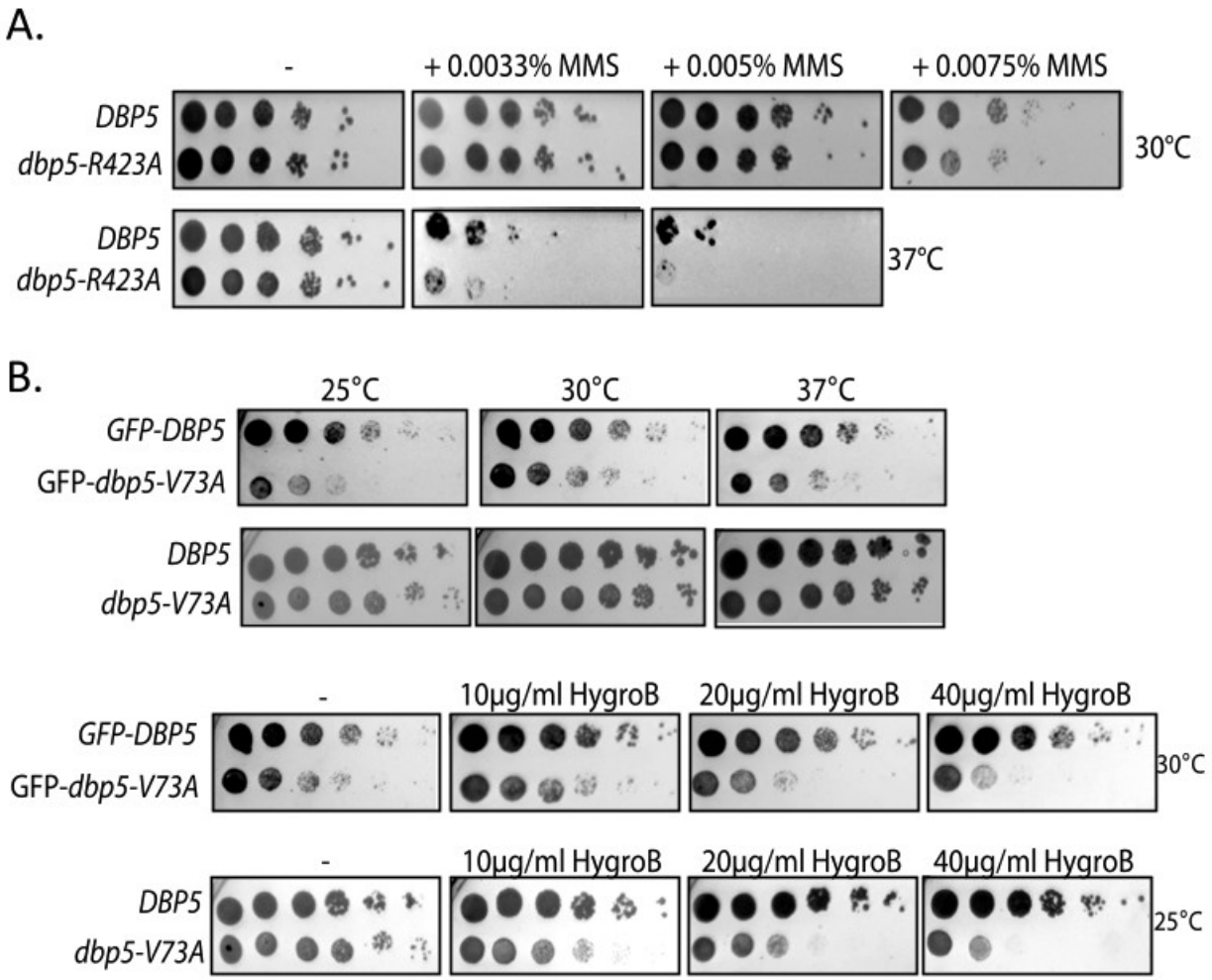

Figure 4-7. GFP-tagging of *dbp5-R423A* does not alter growth in the presence of drugs. A. Growth of yeast strains carrying untagged integrated versions of *DBP5* and *dbp5-R423A* at 30°C or 37°C for 2 days with various concentrations of MMS. **B.** Growth of yeast strains carrying plasmid based *GFP-DBP5* and GFP-*dbp5-V73A* compared to untagged integrated versions at 25°C, 30°C, and 37°C or with Hygromycin B at 30°C or 25°C for 2 days.

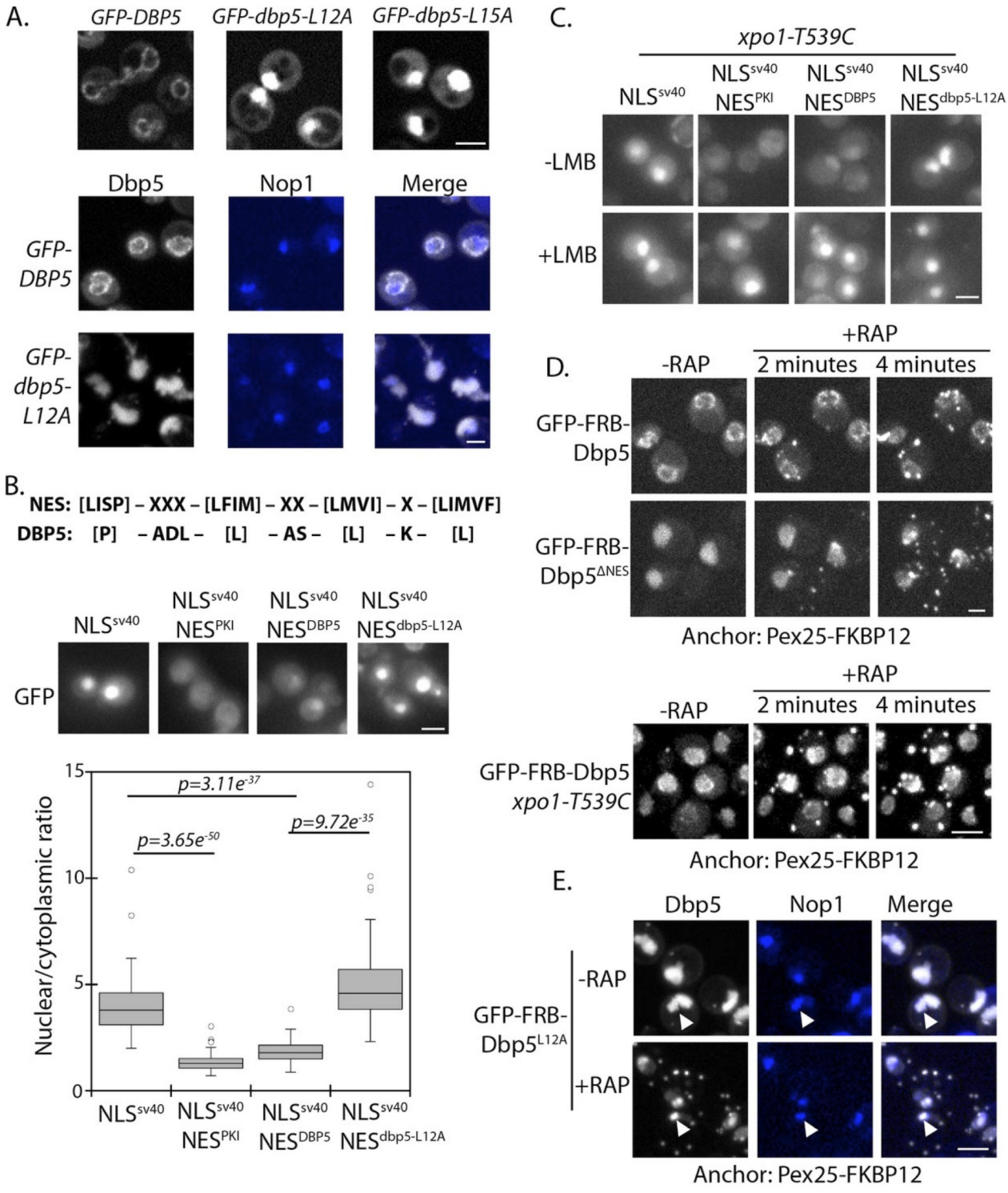

Figure 4-8. Identification of N-terminal nuclear export signal in Dbp5p

Figure 4-8. Identification of N-terminal nuclear export signal in Dbp5p. **A**. Fluorescent images showing localization of GFP-Dbp5p in plasmid based *GFP-DBP5*, *GFP-dbp5-L12A,* and *GFP-dbp5-L15A* strains (top panel). Bottom panel shows GFP-Dbp5p (gray) co-localization with the nucleolar marker Nop1-RFP (blue). **B**. Schematic at the top shows the overall sequence composition of verified NES motifs (la Cour et al., 2004), as compared to the Dbp5p N-terminal amino acid sequence. Fluorescent images show localization of 2xGFP-NLS^{SV40}-NES^{DBP5} reporters fused to residues 1–52 of *DBP5* or *dbp5-L12A* compared to a bona-fide NES (NES^{PKI}). Graph at the bottom shows the ratio between nuclear and cytoplasmic GFP signals measured for the various reporter constructs ($n \geq 100$, error bars represent standard deviation, p-value from unpaired t-test with two-tailed distribution shown). **C**. Fluorescent images show 2xGFP reporters as used in panel B in a strain carrying *xpo1-T539C* before and after addition of 100 ng/ml of LMB for 30 min to disrupt Xpo1p mediated export. **D**. Fluorescent images show localization of GFP-FRB-Dbp5p or GFP-FRB-$Dbp5p^{\Delta NES}$ in cells with a Pex25p-FKBP12 anchor prior to and following addition of 1 μg/ml rapamycin at 2 and 4 min. Bottom panel shows GFP-FRB-Dbp5p in cells with a Pex25-FKBP12 anchor and the *xpo1-539C* mutation to allow disruption of Xpo1p mediated export with LMB. Imaging was performed after treatment with 100 ng/ml of LMB for 7 min and following addition of rapamycin at 2 and 4 min. **E**. Fluorescent images show localization of GFP-FRB-$Dbp5p^{L12A}$ (gray) in reference to Nop1p-RFP (blue) in cells with a Pex25p-FKBP12 anchor before and after addition of rapamycin for 10 min. Co-localization of GFP-FRB-$Dbp5p^{L12A}$ and Nop1-RFP indicated by white arrows. Scale bars = 2 μm.

again it was observed that removal of GFP resolved the Ts and poly(A)-RNA accumulation phenotypes of *dbp5-L12A* (Figure 4-9A-B). To ensure that the presence of GFP did not contribute to the localization defect, an integrated and untagged version of *dbp5-L12A* was also assessed by immunofluorescence (IF). By this measure, while the NPC associated pool of Dbp5p could not be visualized in wild-type during the IF procedure, Dbp5p^{L12A} was enriched in the nucleoplasm (Figure 4-9C).

Residues surrounding L12 and L15 are hydrophobic and follow a consensus pattern similar to a nuclear export signal (NES) sequence (Figure 4-8B) (La Cour et al., 2004). To determine if this region was sufficient to function as an NES, residues 1 to 52 of Dbp5p were appended to a 2xGFP reporter with an SV40 nuclear localization signal (NLS ^{SV40}) sequence. The addition of the N-terminal region of Dbp5p antagonized the NLS ^{SV40} and facilitated export of the GFP reporter, which was abolished by the *L12A* substitution (Figure 4-8B). To test if export activity was dependent on Xpo1p, the major karyopherin involved in nuclear export, the same assay was repeated in strains expressing Xpo1p^{T539C}, which can be inhibited by Leptomycin B (LMB) treatment (Maurer et al., 2001; Neville and Rosbash, 1999). Upon addition of LMB, the GFP-NLS^{SV40}-NES^{DBP5} reporter accumulated in the nucleus (Figure 4-8C), which is consistent with previous work showing that Dbp5p accumulated in the nucleus of a Ts *xpo1-1* strain (Hodge et al., 1999). Together, these data show that the N-terminus of Dbp5p harbors an NES signal, which is sufficient to function as an Xpo1p-dependent NES.

As sole copy, GFP-*dbp5-L12A* at 25°C lacks poly(A)-RNA accumulation or a growth defect despite the prominent nucleoplasmic localization of GFP-Dbp5p^{L12A}, as does the integrated and untagged version at any temperature (Figure 4-9A-B). Given the essential function of Dbp5p at the cytoplasmic face of NPCs for mRNP export, these data suggest that only a small and/or dynamic pool of Dbp5p^{L12A} fulfills essential activities at NPCs. To test for the possibility that GFP-Dbp5p^{L12A} still accesses the cytoplasm, an anchor-away system was used with a peroxisomal anchor, Pex25p-FKB12, to anchor GFP-FRB-Dbp5p^{L12A} to peroxisomes in a rapamycin-dependent manner (Haruki et al., 2008). In wild-type cells, GFP-FRB-Dbp5p rapidly accumulated on peroxisomes after rapamycin addition, resulting in strong depletion of the GFP signal from the NE within ~4 minutes (Figure 4-8D). Dbp5p with alanine substitutions at L12, L15, and I17, referred to as GFP-FRB-*dbp5ΔNES*, also showed similar dynamics (Figure 4-8D), suggesting that any shuttling predicted for GFP-FRB-Dbp5p^{L12A} would not be due to residual

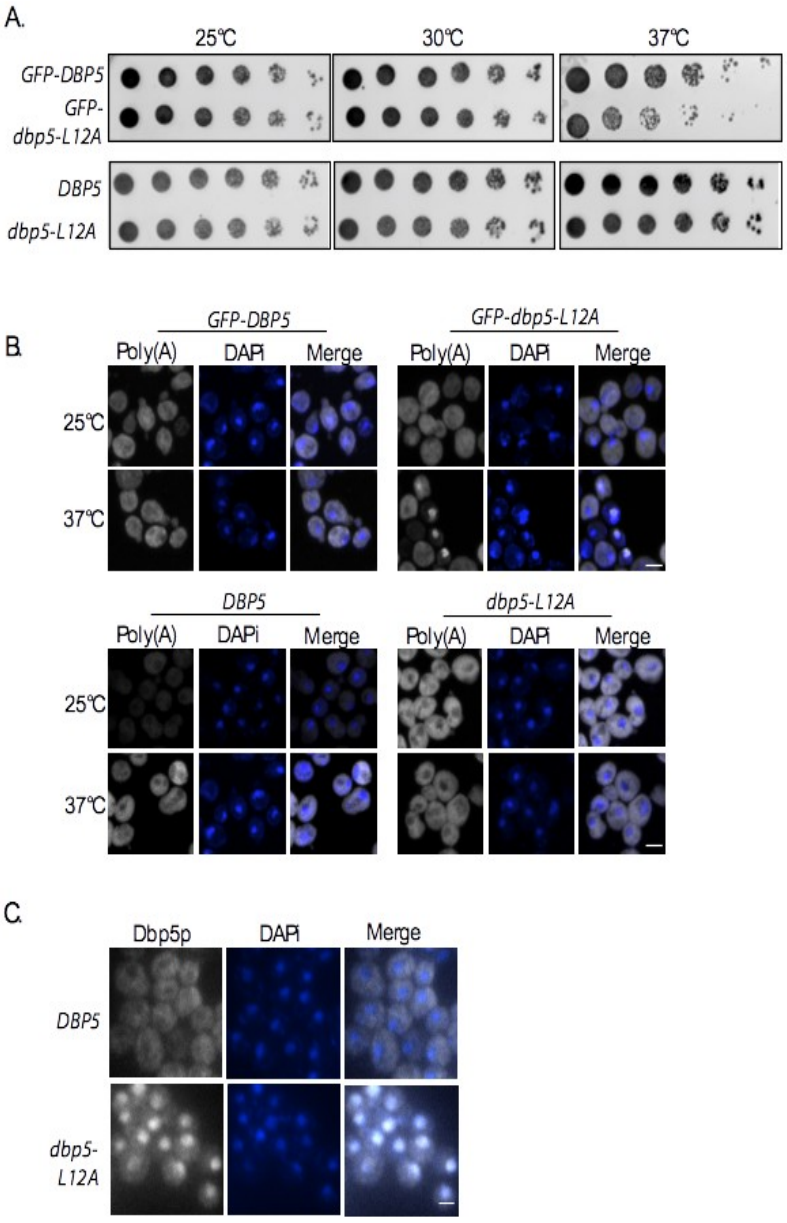

Figure 4-9. GFP-tagging of *dbp5-L12A* alters growth and mRNP export phenotypes. A. Growth of yeast strains with plasmid based *GFP-DBP5* and GFP-*dbp5-L12A* compared to untagged integrated versions at 25°C, 30°C, and 37°C for 3 days. **B.** Images of yeast strains carrying plasmid based versions of *GFP-DBP5* and GFP-*dbp5-L12A* compared to untagged integrated versions analyzed by FISH showing poly(A)-RNA (grey) and the DAPi stained DNA mass (blue) before and after a 3-hour shift to 37°C. Scale bars = 2 □m. **C.** Images showing Dbp5p localization in yeast strains expressing untagged integrated versions of *DBP5* and *dbp5-L12A* analyzed by immunofluorescence using an anti-Dbp5p antibody (grey) and DAPi to stain the DNA mass (blue). Scale bars = 2 □m.

NES activity. Quantitation of the nuclear GFP-FRB-Dbp5p$^{\Delta NES}$ showed that the nuclear signal was 63 ± 9 % and 58 ± 7% of the original at 2 and 4 minutes after rapamycin treatment, indicating that GFP-FRB-Dbp5p$^{\Delta NES}$ shuttles and remains able to access the cytoplasm. This assay was also performed with wild-type GFP-FRB-Dbp5p in the background of an *xpo1-T539C* strain. Following treatment with LMB for 7 minutes to allow GFP-FRB-Dbp5p to accumulate in the nucleus, rapamycin was added, but in this scenario GFP-FRB-Dbp5p remained largely nucleoplasmic (Figure 4-8D, bottom panel). Levels in the nucleoplasm measured 100 ± 23 %, 99.5± 24 %, and 103 ± 18% at 2, 4, and 10 minutes after rapamycin addition as compared to levels just prior to rapamycin addition. These results show that Dbp5p export dynamics are Xpo1p-dependent. As such, Dbp5p must engage the Xpo1p export pathway through both an N-terminal NES and through at least one other means that is independent of this NES. It was also observed that a pool of GFP-FRB-Dbp5p$^{\Delta NES}$ remained in the nucleus of most cells following rapamycin addition, and based on co-localization of GFP-FRB-Dbp5p^{L12A} with Nop1, this pool of Dbp5p is associated with the nucleolus (Figure 4-8E). This suggests that there are at least two distinct nuclear populations of GFP-FRB-Dbp5p^{L12A}; one population that is dynamic enters the cytoplasm through a mechanism dependent on Xpo1p and a second population that is stably associated with the nucleolus.

4.2.4 Dbp5p^{R423A} shows altered nuclear import

To further identify mutants with altered Dbp5p nuclear transport, localization of GFP-Dbp5p was determined for the complete mutant collection, in the background of a wild-type copy of Dbp5p, following exposure to 12% ethanol. Acute ethanol shock is a condition whereby Dbp5p re-localizes to the nucleoplasm (Izawa et al., 2005; Takemura et al., 2004) and was used here as a tool to address Dbp5p nuclear localization. Using this assay, mutations in a stretch of residues within and near motif VI (422-434) were found to disrupt GFP-Dbp5p nuclear accumulation in ethanol (Figure 4-10), including the GFP-*dbp5-R423A* mutant (Figure 4-11A). The accumulation of Dbp5p in the nucleoplasm of ethanol-treated cells has been reported to result from a disruption in nuclear export via Xpo1p (Takemura et al., 2004). Given the dependence of Dbp5p on Xpo1p for nuclear export, this suggested that failure of GFP-Dbp5p^{R423A} to accumulate in the nucleus during ethanol stress resulted from a defect in nuclear

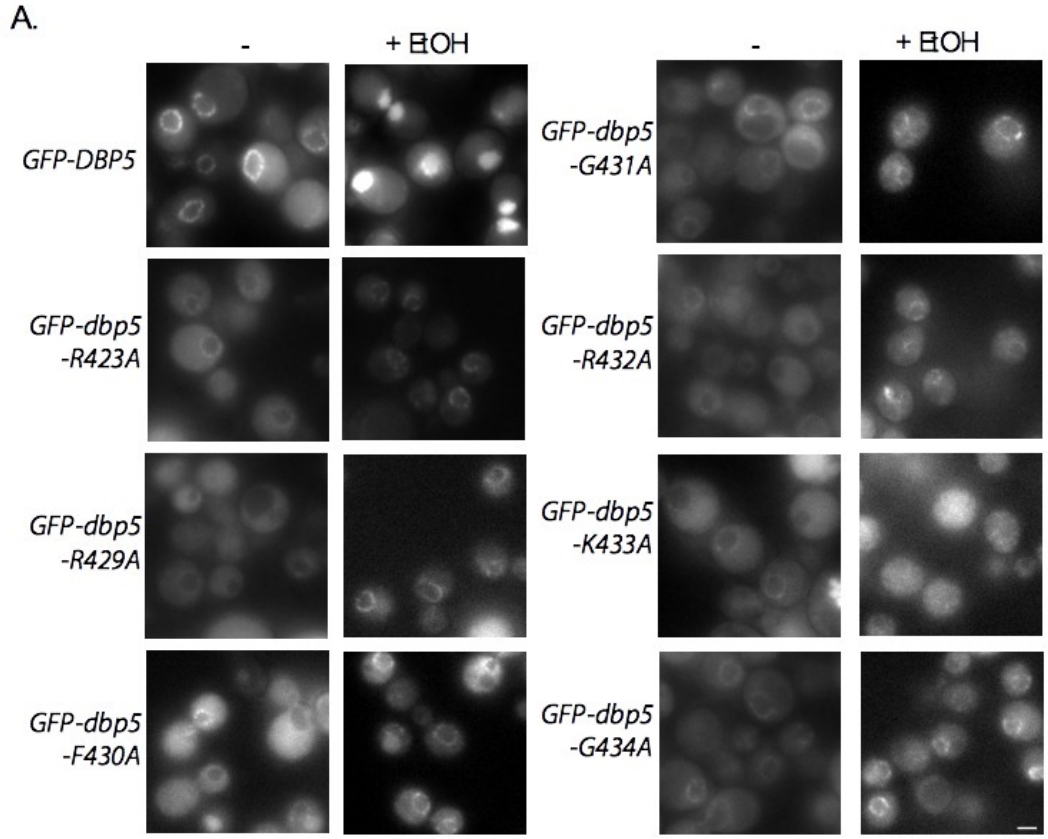

Figure 4-10. Altered nuclear import kinetics of *dbp5* mutants in response to ethanol stress. **A.** Images of yeast strains expressing plasmid based GFP-Dbp5p in *GFP-DBP5* and GFP-*dbp5* mutants in and around motif VI before and after a shift to media containing 12% ethanol for 20 minutes. Scale bars = 2 □m.

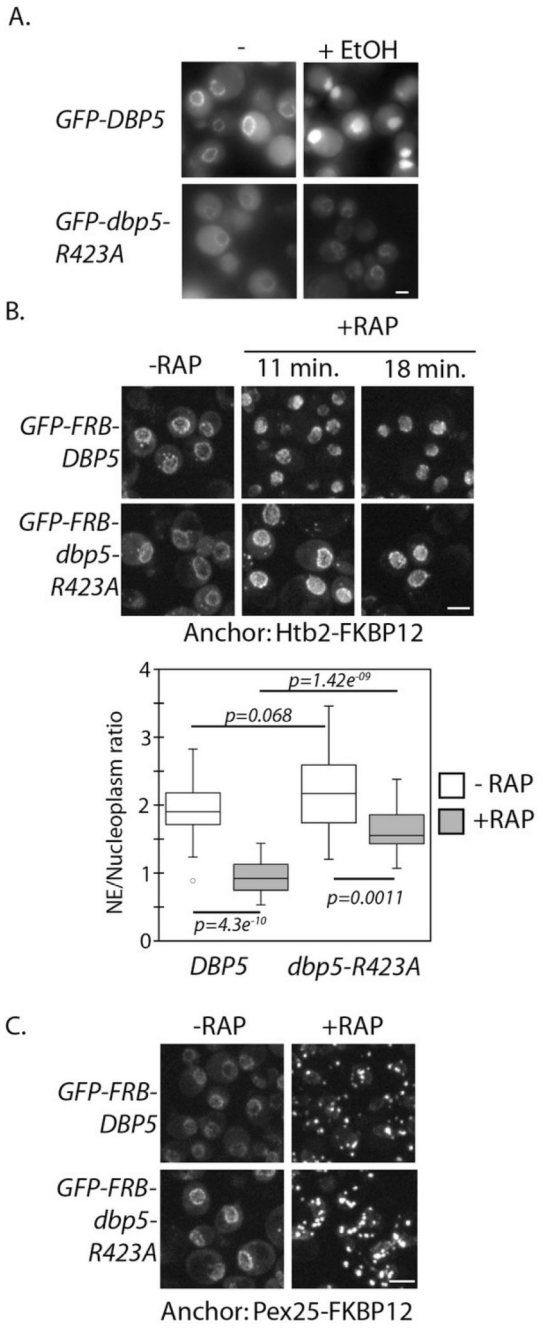

Figure 4-11. Altered import kinetics of Dbp5p^{R423A}. **A**. Fluorescent images showing localization of plasmid expressed GFP-Dbp5p in *GFP-DBP5* and *GFP-dbp5-R423A* strains pre- and post-shift to media with 12% ethanol for 30 min. **B**. Fluorescent images showing localization of GFP-FRB-Dbp5p or GFP-FRB-Dbp5p^{R423A} in cells with the nuclear Htb2p-FKBP12 anchor following addition of 1 μg/ml rapamycin at the indicated time points. Graph shows quantification of the nuclear envelope signal intensity vs. nucleoplasm (n = 23, error bars indicate standard deviation, p-value from paired or unpaired t-test with two-tailed distribution shown). **C**. Fluorescent images showing localization of GFP-FRB-Dbp5p or GFP-FRB-Dbp5p^{R423A} in cells with the Pex25p-FKBP12 anchor following addition of 1 μg/ml rapamycin for 4 min. Scale bars = 2 μm.

import. The region surrounding R423 is similar in sequence and charge to known NLS sequences (Kosugi et al., 2009); however, this region remains to be tested to determine if it is sufficient to drive nuclear import. This suggests that other regions of Dbp5p may act in concert with R423 to mediate import, or the mutation of this residue may alter intra- or inter-molecular Dbp5p interactions that impact nuclear import efficiency.

To assay Dbp5p^{R423A} nuclear import by another means, the anchor-away technique was employed with a histone protein anchor (Htb2p-FKB12) to address nuclear access of wild-type or R423A versions of GFP-FRB-Dbp5p when present as sole copy. Upon addition of rapamycin, GFP-FRB-Dbp5p moved to the nucleoplasm, resulting in complete depletion of the GFP signal at the NE within ~11 minutes (Figure 4-11B). GFP-FRB-Dbp5^{R423A} also accumulated in the nucleus following rapamycin addition, but a significant proportion also remained at the NE for the entire length of the 18-minute imaging series (Figure 4-11B). To test for the possibility that GFP-FRB-Dbp5p^{R423A} was stably bound to NPCs, the anchor-away system was again employed with the peroxisomal anchor (Pex25p-FKB12). In both wild-type cells and *dbp5-R423A* strains, GFP-FRB-Dbp5p rapidly accumulated on peroxisomes after rapamycin addition, resulting in complete depletion of the GFP signal from the NE in both strains in ~4 minutes (Figure 4-11C). Note the nuclear accumulation defect seen here was not as severe as with ethanol (Figure 4-11A). A major difference between these two assays is the presence of a wild-type copy of Dbp5p. The presence of wild-type Dbp5p may exacerbate the Dbp5p^{R423A} nuclear import defect, which is suggestive of competition for nuclear transport, which remains to be tested. These results show that GFP-FRB-Dbp5p^{R423A} remains dynamic in the cytoplasm, but Dbp5p^{R423A} import efficiency is altered.

Overall, the altered import kinetics of the *dbp5-R423A* allele and discovery of an N-terminal NES within Dbp5 provide needed insights and tools to investigate the mechanics and functional importance of Dbp5p nuclear shuttling. Markedly, the lack of an mRNP export defect in *dbp5-L12A,* where Dbp5p is predominantly nucleoplasmic, or *dbp5-R423A,* where Dbp5p nuclear access is altered, suggests that neither a large cytoplasmic pool of Dbp5p or rapid shuttling of Dbp5p through the nucleus is required to maintain steady-state nuclear mRNP export.

4.2.5 Gene expression in *dbp5-L12A* and *dbp5-R423A* at steady-state and in response to MMS

Strains with integrated versions of *dbp5-L12A* and *dbp5-R423A* show altered Dbp5p localizations, nuclear shuttling changes, and sensitivity to stress, but no discernible mRNP export defects by FISH. A possible reason for these observations is that shuttling of Dbp5p supports the biogenesis and export of a small subset of mRNAs during steady-state growth or stress, which could be related to reported functions of Dbp5p within the nucleus (Estruch et al., 2012; Estruch and Cole, 2003; Scarcelli et al., 2008; Zhao et al., 2002). However, transcript binding and export preferences for Dbp5p remain unknown preventing this postulate from being directly tested. As such, poly(A)-RNA localization was determined following MMS treatment to see if during the cellular response to DNA damage these mutants show export defects, especially since this stress involves genome-wide remodeling of the transcriptional program involving thousands of genes (Natarajan et al., 2001). Under these conditions, no accumulation of poly(A)-RNA was observed in wild-type, *dbp5-L12A*, or *dbp5-R423A* (Figure 4-12).

To probe gene expression at levels beyond mRNP export status, RNA-seq analysis was carried out to assess the cellular transcriptome of *dbp5-L12A* and *dbp5-R423A* during steady-state growth at 25°C and following exposure to a 30-minute treatment with MMS. The rationale of these experiments being that subtle alterations in transcription, mRNA processing, export, or other aspects of gene expression that are perturbed by mutations in Dbp5p may be detected at the level of transcript abundance at steady-state or after rapid reprogramming of gene expression. Analysis of the resulting RNA-seq data showed that gene expression at steady-state was highly similar in all strains, with *dbp5-L12A* and *dbp5-R423A* having no significantly differentially expressed genes when compared to wild-type.

In response to MMS treatment, gene expression patterns clustered based on the stress treatment, not strain, with transcriptome changes similar to what has been previous reported during MMS treatment (Natarajan et al., 2001). Of the 775 genes showing a two-fold or higher induction in the wild-type strain, 89% (688) and 80% (622) of these genes were also induced in *dbp5-L12A* and *dbp5-R423A* (Figure 4-13A and see Table 6-1 in *Appendix*). Similarly, of the 872 genes repressed two-fold or more upon MMS exposure in the wild-type strain, 80% (698) and

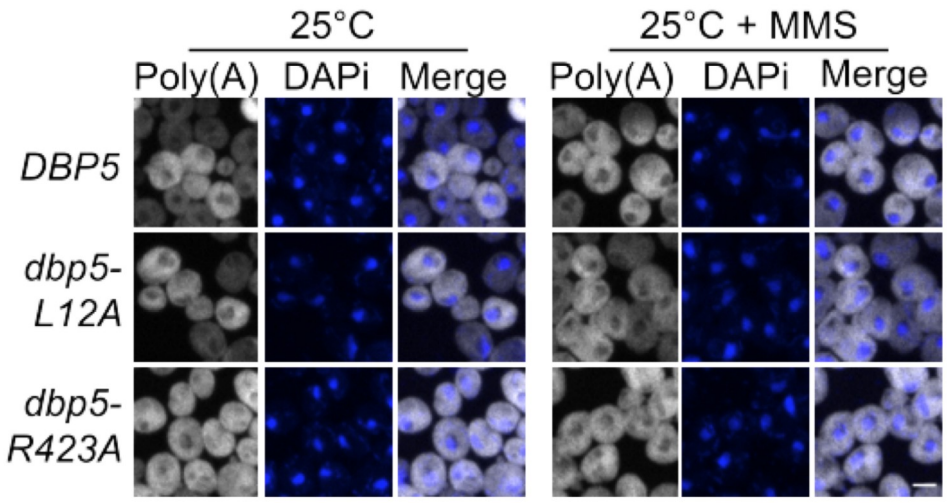

Figure 4-12. Poly(A)-RNA export status in *dbp5* mutants in response to MMS induced DNA-damage. Images of yeast strains carrying untagged and integrated versions of *DBP5*, *dbp5-L12A,* and *dbp5-R423A* strains analyzed by FISH showing poly(A)-RNA (grey) and the DAPi stained DNA mass (blue) with and without exposure to 0.5% MMS for 30 minutes. Scale bars = 2 μm. FISH performed by Rima Sandhu.

72% (624) of these genes were also repressed in *dbp5-L12A* and *dbp5-R423A* (Figure 4-13A and see Table 6-2 in *Appendix*). Gene ontology (GO) analyses showed that no GO terms were over represented within any of the sets of differentially repressed genes or the genes found not to be induced in both mutants or *dbp5-L12A* alone. In contrast, the unique set of 88 genes not induced in *dbp5-R423A* was enriched for GO terms "ribosomal small subunit biogenesis" (FDR=$8.72e^{-03}$), "tRNA modification" (FDR=$5.13e^{-03}$), and "RNA methylation" (FDR=$2.47e^{-03}$). Conversely, there were 88 genes in *dbp5-L12A* and 39 genes in *dbp5-R423A* that were uniquely induced two-fold or more by MMS exposure in that single strain alone, i.e. not induced in the other mutant or wild-type strain. GO analyses on these sets of genes revealed that there were no GO terms over represented in induced genes from *dbp5-R423A*, but the set of genes induced in *dbp5-L12A* was enriched for GO terms that also included "RNA methylation" (FDR=$6.42e^{-03}$) and "ribosomal small subunit biogenesis" (FDR=$1.74e^{-02}$). Clustering of gene expression data for all genes within the parent GO term categories "RNA modification" and "rRNA processing" produced three unique gene clusters that display alternate expression patterns in the mutant strains as compared to the wild-type (Figure 4-13B and see 6-2 in *Appendix*). These data highlight the fact that *dbp5-L12A* and *dbp5-R423A* cause opposite changes in gene expression within the same GO term categories and are suggestive of a role for nuclear shuttling in modulating the MMS-induced stress response, given that these mutations have opposing impacts on Dbp5p nucleocytoplasmic transport. Together, these data reveal that disruptions in Dbp5p shuttling and localization caused by *dbp5-L12A* and *dbp5-R423A* does not largely reshape the cellular transcriptome at steady-state, nor do these changes greatly impact the ability of cells to reprogram gene expression following stress at the level of transcriptional induction, gene repression, or the expression level of individual gene transcripts at the time points tested. Rather, these data suggest that during the MMS-induced DNA damage response, Dbp5p nuclear shuttling supports, directly or indirectly, regulated gene expression of a select subset of genes function in ncRNA biology.

4.2.6 *dbp5-L12A* and *dbp5-R423A* genetic interaction profiles

Towards a better understanding of the functional consequence of biasing Dbp5p localization to the nucleus (i.e. *dbp5-L12A*) or altering nuclear access (i.e. *dbp5-R423A*), a synthetic gene array

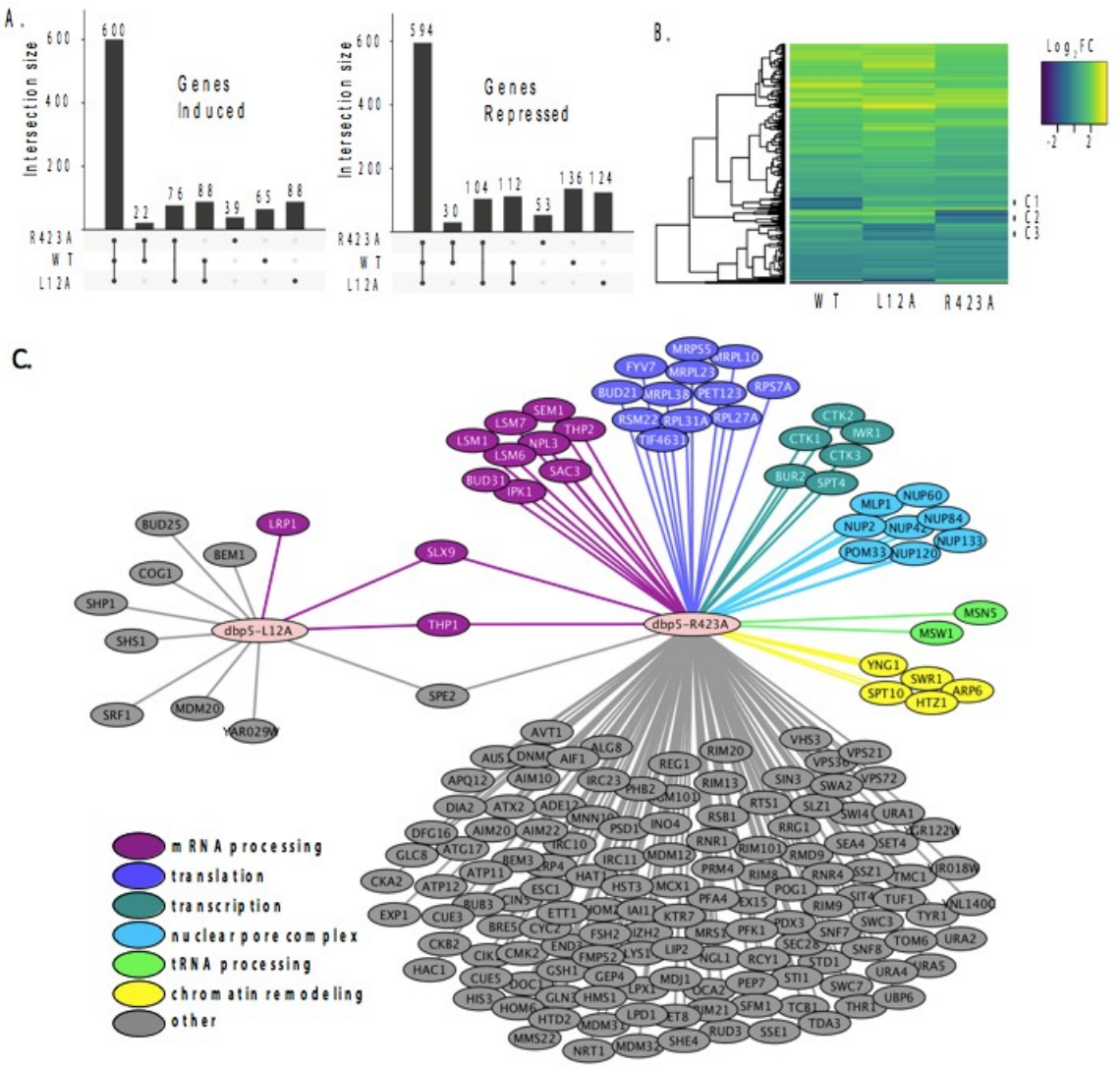

Figure 4-13. RNA-seq and genetic interaction analyses of *dbp5* mutants. A. UpSet plots showing the number of intersecting genes that are induced (left) or repressed (right) with at least a two-fold change ($\log_2$ FC = 1) across *DBP5*, *dbp5-L12A*, and *dbp5-R423A* strains in response to 0.5% MMS for 30 minutes as measured by 3′-TAG-RNA-seq. **B.** Heat map showing hierarchical two-dimensional clustering of all genes found in GO categories RNA modification and rRNA processing using gene expression data for *DBP5*, *dbp5-L12A*, and *dbp5-R423A* strains after exposure to 0.5% MMS for 30 minutes. Heat map shows normalized $\log_2$ FC values mapping to the selected set of genes (arranged on the y-axis) for each strain. Log2 FC values are color correlated from blue (lowest) to yellow (highest). Clusters marked 1-3 as discussed in the results section. See **Table 6-2 in *Appendix*** for the list of genes used and those found in each cluster. **C.** Identified synthetic interactions by SGA analysis in *dbp5-L12A* and *dbp5-R423A* strains. Gene deletions are grouped based on gene ontology (magenta- mRNA processing, purple- translation, teal- transcription, blue- nuclear pore complex, green- tRNA export, yellow- chromatin remodelling, grey- other). RNA-Seq analyses carried out in collaboration with Taylor Reiter and Rima Sandhu, and SGA carried out in collaboration with Barry Young and Chris Loewen (UBC).

(SGA) screen was carried out to identify potential genetic interactions between these alleles and non-essential gene mutants. SGA screens have been carried out previously with the *DBP5* Ts allele *rat8-2*, yielding 108 potential synthetic interactions, encompassing proteins involved in chromatin remodeling, transcription, mRNA metabolism, and mRNP export (Scarcelli et al., 2008). In contrast, the screen with *dbp5-L12A* only found 12 potential synthetic interactions (Figure 4-13C & see Table 6-3 in *Appendix*), which included the exosome-associated LRP1 and the TREX-2 complex component THP1. No gene ontology terms were enriched within this gene set, and most notably, no genetic interactions were identified with the many non-essential components of the mRNP export pathway, NPCs, or translation machinery. These results support the conclusion that having the majority of Dbp5p in the nucleus at steady-state is not detrimental to the processes of mRNP export, translation, or overall cellular fitness.

The SGA screen with *dbp5-R423A* yielded 176 potential genetic interactions that were more consistent with a previously reported SGA screen (Scarcelli et al., 2008), including interactions with non-essential components of NPCs (e.g. MLP1, NUP2, NUP42, NUP60, NUP84, NUP120, NUP133 and POM33) and both mRNA and ncRNA export pathways (e.g. MSN5, NPL3, SAC3, SEM1, SLX9, THP1, and THP2) (Figure 4-13C & see Table 6-3 in *Appendix*). These genetic interactions, combined with the observed poly(A)-RNA export defect only upon GFP tagging and growth at high temperature, suggest that when combined with other perturbations Dbp5p^{R423A} activity can be limiting for RNA export. This idea is supported by the fact that a threshold level of Dbp5 ATPase activity has been determined to be required for mRNP export (Dossani et al., 2009). Indeed, the location of residue R423 in motif VI, a DEAD-box motif generally involved in nucleotide binding and hydrolysis, would be expected to alter enzymatic activity (Hilbert et al., 2009; Linder and Jankowsky, 2011). These facts prompted investigations to determine how the R423A substitution impacts ATPase activity, which may lead to synthetic interactions in the presence of other perturbations to the gene expression apparatus (e.g. deletions impacting the mRNP export apparatus) or the function of Dbp5p (e.g. N-terminal GFP tag). Using an *in vitro* ATPase assay, the basal ATPase rate of Dbp5p^{R423A} was found to be similar to wild-type, but in the presence of saturating levels of RNA, Dbp5p^{R423A} exhibited an activity only 47 ±7 % of wild-type (Figure 4-14). These results were the same at 37°C with Dbp5p^{R423A} RNA-stimulated ATPase activity at 46±2% of wild-type. It is expected that the inability of Dbp5p^{R423A} to be fully stimulated by the presence of RNA results in the

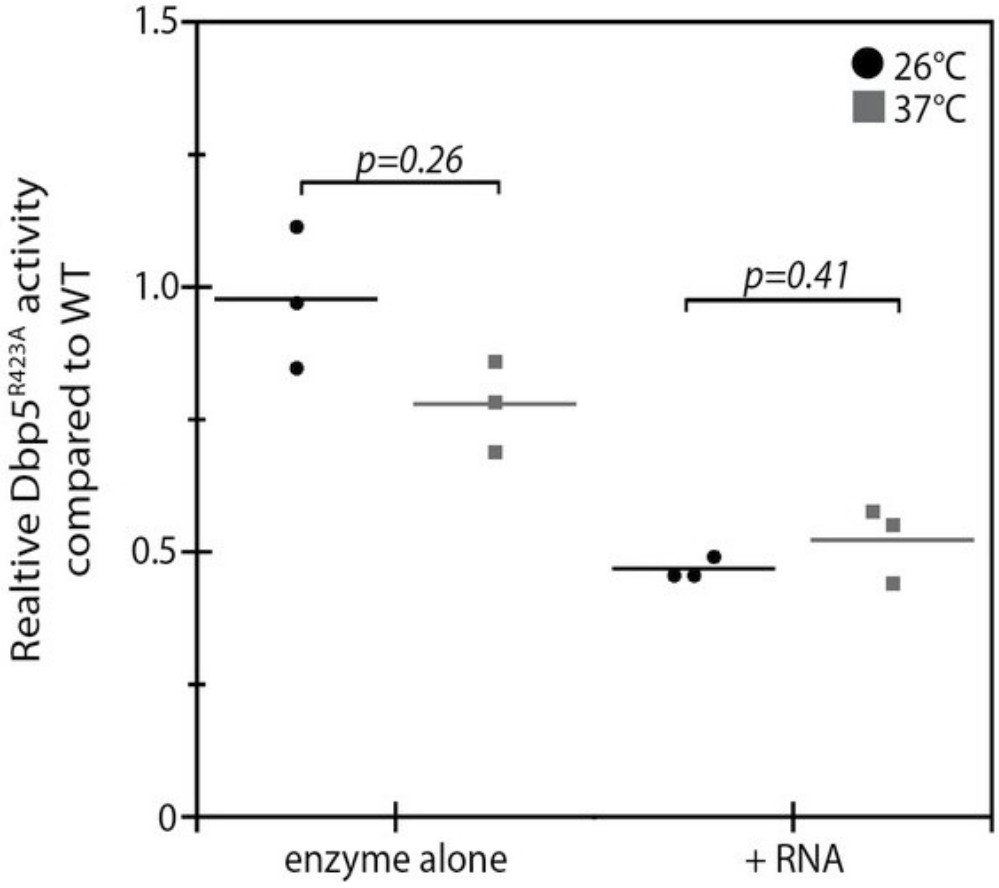

Figure 4-14. Dbp5p^{R423A} ATPase assays. Steady state in vitro ATPase assays performed with purified Dbp5p and Dbp5p^{R423A} at 26°C or 37°C. Graph shows the average ATPase rate measured for Dbp5p^{R423A} as a percentage of Dbp5p activity, with or without RNA stimulation (n = 3, error bars represent standard deviation, p-value from paired t-test with two-tailed distribution shown).

observed genetic interactions with other gene mutations that perturb RNP export and gene expression.

4.2.7 Dbp5p functions in tRNA export within the nucleus

Recent work has linked Dbp5p to the export of ncRNAs, including ribosomal and telomerase RNAs (Neumann et al., 2016; Wu et al., 2014b). Here, SGA screens have identified potential genetic interactions with factors that participate in rRNA (i.e. SLX9 and LRP1) and tRNA (i.e. MSN5 and MSW1) processing and export (Figure 4-13C & see Table 6-3 in *Appendix*). RNA-seq analyses have also identified altered expression of genes functioning in ncRNA pathways in response to MMS in both *dbp5-L12A* and *dbp5-R423A* (See Table 6-2 in *Appendix*). Similarly, the Dbp5p trans-activator Nup159p and mRNP export factor Mex67p were recently identified in a screen for proteins involved in nuclear tRNA biogenesis and export (Wu et al., 2015). The expression and localization of several RNA species, including rRNAs and tRNAs, are also modulated under cellular stress conditions (Baßler and Hurt, 2019; Huang and Hopper, 2016). Given these facts, and that strains with integrated *dbp5-L12A* and *dbp5-R423A* showed sensitivity to cellular stress with no obvious defects in mRNA biogenesis and export, investigations were extended to include the processing and export of ncRNA species.

In the case of tRNAs, primary tRNA transcript processing involves removal of 5′ and 3′ ends of the tRNA in the nucleus, transport across the nuclear envelope, and splicing of intron containing tRNAs in the cytoplasm to produce functionally mature tRNAs (Phizicky and Hopper, 2015). The aberrant accumulation of tRNA intermediates signifies a breakdown in tRNA processing and/or export. To detect such intermediates, northern blotting was performed with a probe against the $tRNA^{Ile}_{UAU}$ in wild-type, *dbp5-L12A*, and *dbp5-R423A* strains. The probe spans the 5′ exon and first 30 nucleotides of the $tRNA^{Ile}_{UAU}$ intron to allow detection of the primary transcript and processing intermediates. The intensity ratio between the intron containing intermediate (I) and precursor transcript (P) normalized to wild-type is used as a measure of tRNA processing, with altered ratios indicating a defect (Wu et al., 2015). At 25°C, the ratio between the precursor and intron containing tRNA in *dbp5-L12A* (1.00±0.1) was comparable to the wild-type strain, while a small but consistent accumulation of the intron-containing tRNA intermediate was observed in *dbp5-R423A* (1.4±0.1) (Figure 4-15A). This defect was further

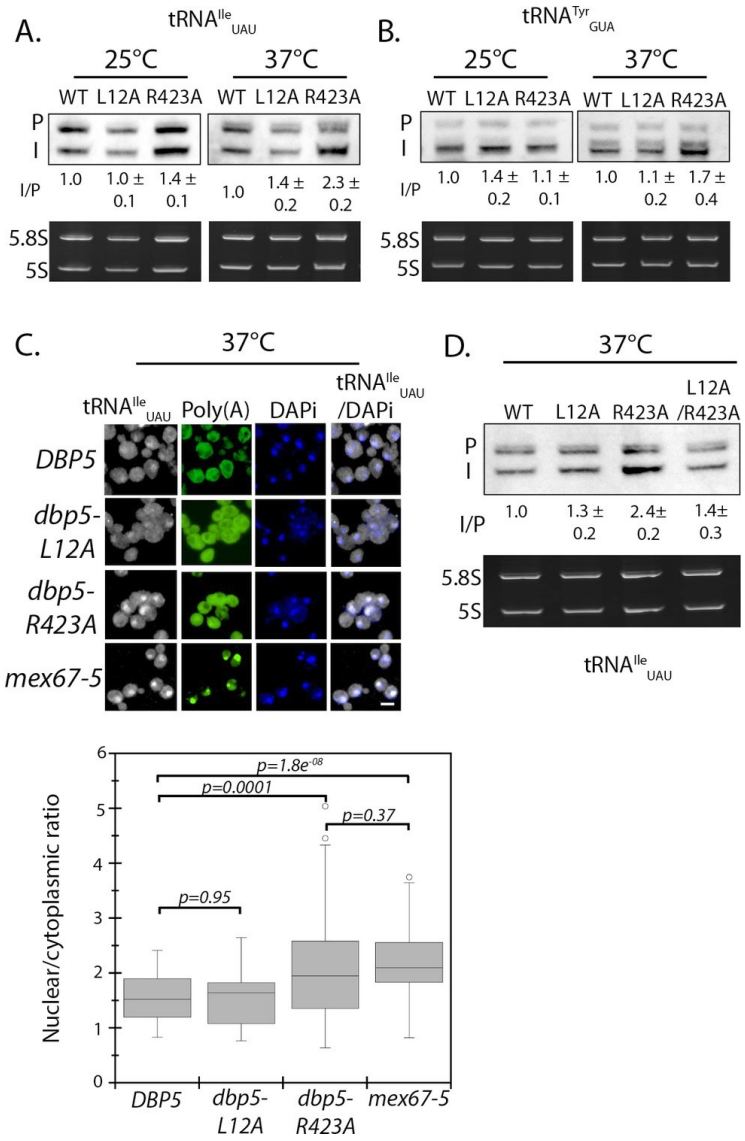

Figure 4-15. Dbp5p is required for tRNA export. A. Northern blot analysis of tRNA$^{Ile}_{UAU}$ (Probe1) in integrated and untagged *DBP5 (WT)*, *dbp5-L12A*, and *dbp5-R423A* strains before and after a 2 hr temperature shift to 37°C. The primary tRNA transcript is denoted as (P), and the end-matured intron-containing tRNA is denoted as (I). Ratio of mean integrated intensity between (I) and (P) species is measured and normalized to the wild type value (n = 3, error represents standard deviation). Ethidium bromide stained gel shows 5.8S and 5S rRNA species in bottom panel as a loading control. **B**. Northern blot analysis as in panel A using tRNA$^{Tyr}_{GUA}$ (Probe KC031). **C**. Localization of tRNA$^{Ile}_{UAU}$ determined by FISH in integrated and untagged *dbp5-L12A* and *dbp5-R423A* strains after a 4 hr shift to 37°C. Cells were probed with a Cy3 end-labeled tRNA$^{Ile}_{UAU}$ probe (SRIM04, gray) and DAPi (blue). Scale bar = 2 μm. Graph shows the ratio between nuclear and cytoplasmic tRNA$^{Ile}_{UAU}$ signals ($n \geq 50$, error bars represent standard deviation, p-value from unpaired t-test with two-tailed distribution shown). **D**. Northern blot analysis of tRNA$^{Ile}_{UAU}$ (Probe1) as performed in panel A, including an integrated and untagged *dbp5-L12A/R423A* double mutant strain.

increased after two hours at 37°C in *dbp5-R423A* (2.3±0.2), while the ratio only increased slightly in *dbp5-L12A* (1.4±0.2) (Figure 4-15A). To verify that these defects went beyond a single tRNA species, northern blotting was also carried out with a probe against $tRNA^{Tyr}_{GUA}$, which also showed an accumulation of the intron containing species in *dbp5-R423A* (1.7±0.4) at 37°C (Figure 4-15B). These measures suggest that tRNA processing or export is perturbed in the *dbp5-R423A* mutant.

Intron-containing tRNAs require transport to the cytoplasm to be spliced, therefore accumulation of intron containing intermediates in *dbp5-R423A* by northern blotting are suggestive of a defect in tRNA export (Phizicky and Hopper, 2015). Using a probe that binds all forms of $tRNA^{Ile}_{UAU}$, a significantly increased amount of $tRNA^{Ile}_{UAU}$ was observed in the nucleus of the *dbp5-R423A* strain at 37°C by FISH, as compared to wild-type strain and *dbp5-L12A* (Figure 4-15C). Note that under these conditions using integrated untagged alleles, no poly(A)-RNA export is observed in either *dbp5-L12A* or *dbp5-R423A*. The export defect in *dbp5-R423A* was similar to the level seen in the *mex67-5* strain, which has been previously identified to disrupt tRNA export (Chatterjee et al., 2017).

$Dbp5p^{R423A}$ has reduced ATPase activity in the presence of RNA and altered nuclear access, either or both of which could influence tRNA export. To address this issue, the double mutant *dbp5-L12A/R423A* was generated with the idea that the L12A mutation would decrease the amount of Dbp5p in the cytoplasm and increase the amount in the nucleus. As a result, if the R423A mutation causes tRNA export defects by limiting Dbp5p ATPase activity in the cytoplasm, the L12A mutation would be expected to worsen this phenotype by reducing cytoplasmic levels of Dbp5p. Alternatively, if Dbp5p nuclear access and activity within the nucleus is required to support tRNA export, the L12A mutation could improve defects in *dbp5-R423A* by increasing the amount of Dbp5p in the nucleus. Importantly, a strain expressing GFP-$Dbp5p^{L12A/R423A}$ is viable and shows a strong nuclear localization, i.e. an increased nuclear pool of Dbp5p as compared to R423A (Figure 4-16A). Further, the untagged and integrated version of *dbp5-L12A/R423A* does not exhibit mRNP export or temperature-dependent growth defects (Figure 4-16B-C). Using the double mutant, northern blotting was performed with probes against the $tRNA^{Ile}_{UAU}$ at 37°C (Figure 4-15D). As compared to *dbp5-R423A* (2.2±0.2), accumulation of the intron containing tRNA intermediate was reduced in *dbp5-L12A/R423A* (1.4±0.3), suggesting that increasing the nuclear pool of Dbp5p through inclusion of the L12A mutation largely rescues

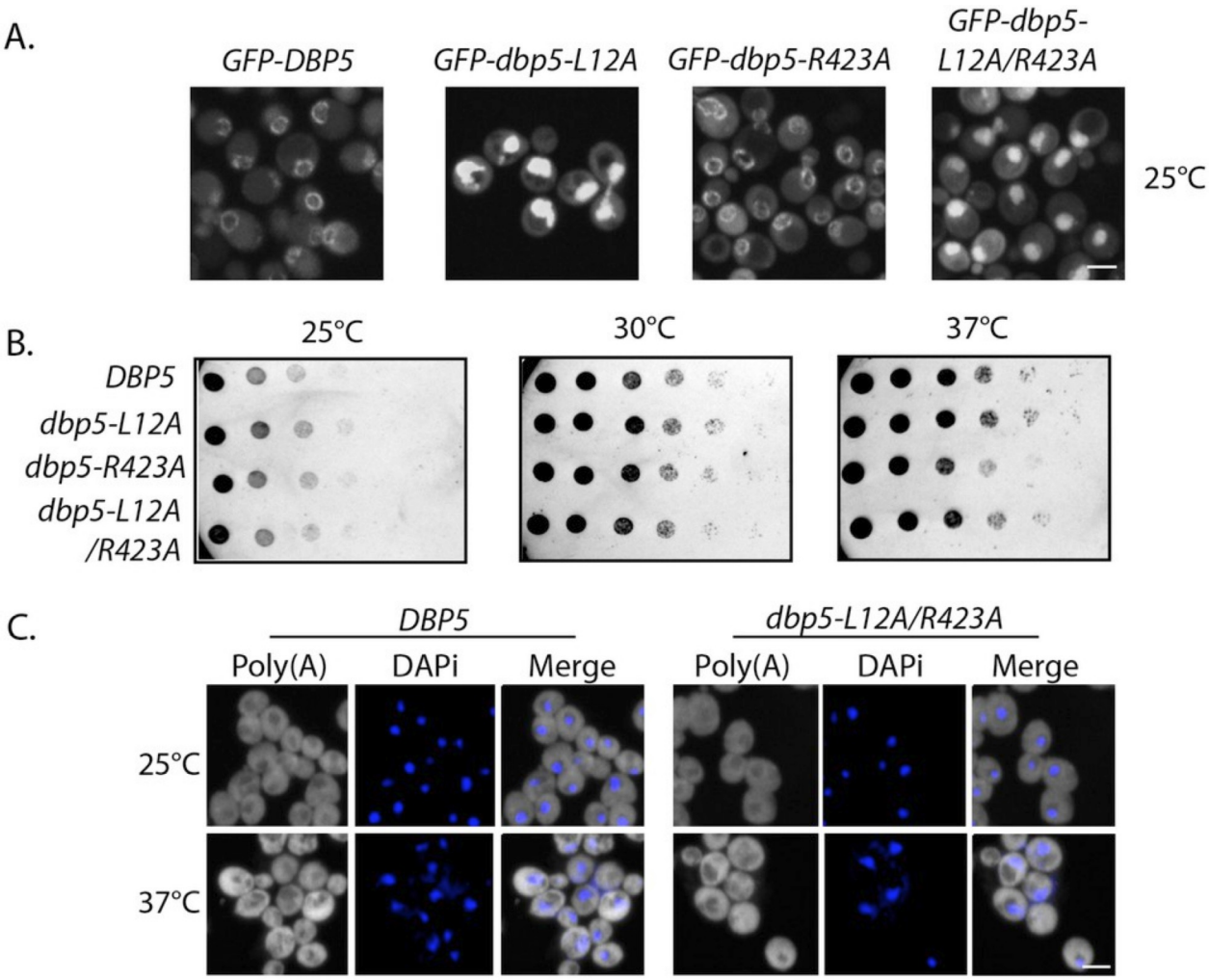

Figure 4-16. Characterization of *dbp5-L12A-R423A*. A. Images showing Dbp5p localization in strains carrying plasmid based versions of *GFP-DBP5*, GFP-*dbp5-L12A,* GFP-*dbp5-R423A,* and GFP-*dbp5-L12A-R423A*. **B.** Growth of integrated and untagged *DBP5*, *dbp5-L12A, dbp5-R423A,* and *dbp5-L12A/R423A* at 25°C, 30°C, and 37°C for 1 day. **C.** Images of integrated and untagged *DBP5* and *dbp5-L12A/R423A* analyzed by FISH showing poly(A)-RNA (grey) and the DAPi stained DNA mass (blue) before and after a 4 hour shift to 37°C. Scale bars = 2 □m. Scale bars = 2 μm.

the tRNA processing defects. Combined, the SGA, gene expression, northern, and in situ data employing the *dbp5-L12A* and *dbp5-R423A* mutations to alter Dbp5p nuclear levels are strongly supportive of Dbp5p functioning in tRNA export within the nucleus.

4.2.8 Gle1p is required for tRNA processing

Reported defects in tRNA processing in *nup159-1* (Wu et al., 2015), which are similar to those observed in *dbp5-R423A,* suggest a possible relationship between Dbp5p regulation at NPCs and Dbp5p functions in tRNA export. This prompted investigation of Gle1p in tRNA processing, given that Gle1p is also an NPC-associated regulator of Dbp5p. In these assays, *dbp5-1* was included, since upon temperature shift this mutant has a strong mRNP export block similar to *nup159-1, gle1-4,* and *mex67-5* (Gorsch et al., 1995; Murphy and Wente, 1996; Tseng et al., 1998; Segref et al., 1997). By northern blotting, the *dbp5-1* and *gle1-4* Ts mutants had a strong $tRNA^{Ile}_{UAU}$ processing defect at 37°C that was comparable to *nup159-1* and *mex67-5* (Figure 4-17A). tRNA processing defects are also apparent in all four mutants at 25°C, which is a condition where mRNP export is not severely perturbed. These data demonstrate that Dbp5p and both regulators linked to Dbp5p, Nup159p and Gle1p, support tRNA processing and/or export as does the RNA export adaptor Mex67p (Chatterjee et al., 2017), under conditions that do not involve a strong mRNP export block.

Given the known role for these proteins in mRNP export and the function of Gle1p and Nup159p at NPCs with Dbp5p, the localization of Dbp5p was considered in *gle1-4* and *nup159-1* as a possible cause for a shared tRNA processing defect. The localization of GFP-$Dbp5p^{L12A}$ was assayed at 25°C and at the same time point used for northern blotting (i.e. 2 hours at 37°C) leveraging the strong nuclear signal of GFP-$Dbp5p^{L12A}$ to assess Dbp5p nuclear localization. Under these conditions, it was observed that nuclear GFP-$Dbp5p^{L12A}$ localization was reduced in *gle1-4* at 37°C, but remained largely unchanged in *nup159-1* or *mex67-5* at 25°C or 37°C (Figure 4-17B). These data suggest that Gle1p and Nup159p influence tRNA export through a mechanism that goes beyond altering Dbp5p nuclear access.

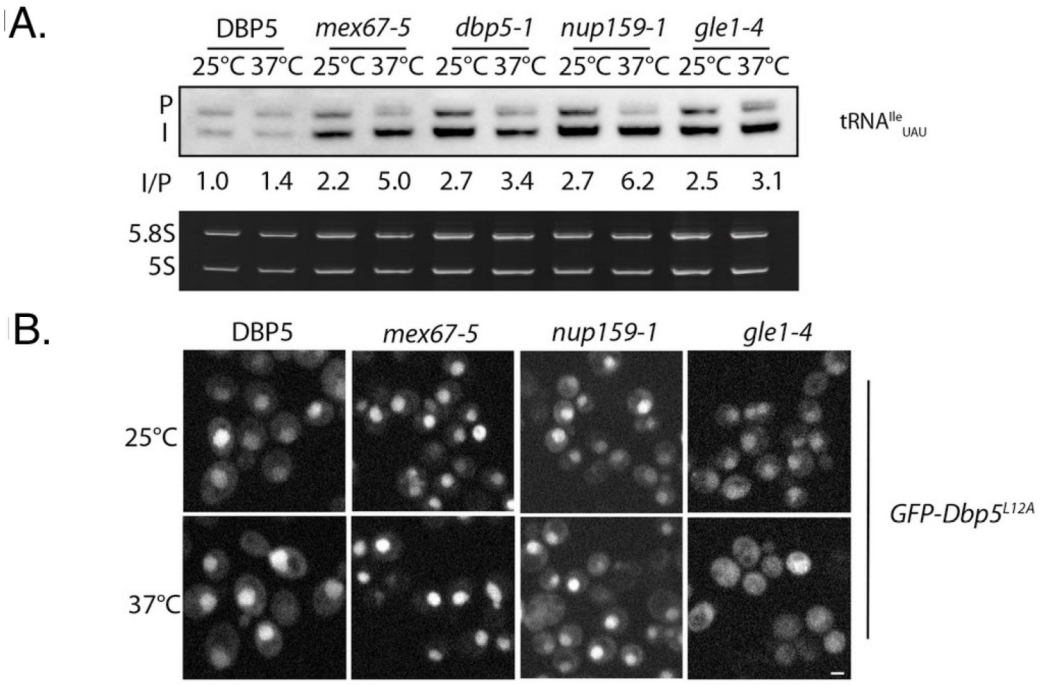

Figure 4-17. tRNA processing status in mRNP export mutants. A. Northern blot analysis of tRNA$^{Ile}_{UAU}$ (Probe1) in *DBP5* (WT), *mex67-5*, *dbp5-1*, *nup159-1,* and *gle1-4* strains before and after a 2 hour temperature shift to 37°C. Primary tRNA transcript is denoted as (P), and the end-matured intron-containing tRNA is denoted as (I). Ratio of mean integrated intensity between (I) and (P) species is measured and normalized to the wild type value. Ethidium bromide stained gel shows 5.8s and 5S rRNA species in bottom panel as a loading control. **B.** GFP-Dbp5p^{L12A} localization in *DBP5*, *mex67-5*, *nup159-1,* and *gle1-4* strains before and after a 2 hour temperature shift to 37°C. Scale bars = 2 μm.

4.2.9 Dbp5p supports re-export of mature tRNAs following nutritional stress

The screening of the *DBP5* mutant collection for sensitivity to a translational inhibitor and UV induced DNA-damage also revealed that *dbp5-R423A* was sensitive to these treatments. Interestingly, tRNA shuttling dynamics are altered during translational stress and UV induced DNA-damage (Ghavidel et al., 2007; Huang and Hopper, 2016). It is also known that re-export of mature tRNAs to the cytoplasm in response to nutrient availability involves the β-importin family member Exportin-5 (yeast Msn5p) (Bohnsack et al., 2002; Calado et al., 2002; Murthi et al., 2010; Takano et al., 2015). The *msn5Δ*/*dbp5-R423A* double mutant was identified here as being synthetic sick by SGA (see Table 6-3 in *Appendix*), which is suggestive of a potential relationship between Dbp5p, tRNA re-export, and *dbp5-R423A* sensitivity to stress.

A well characterized stress causing rapid and reversible re-localization of mature tRNAs to the nucleus is acute nutritional starvation using $tRNA^{Tyr}_{GUA}$ (Whitney et al., 2007). To determine if regulated tRNA shuttling was altered in *dbp5-R423A,* $tRNA^{Tyr}_{GUA}$ localization was assessed in strains subjected to a ten-minute amino-acid starvation followed by re-feeding through the addition of rich media. Under amino acid starvation, $tRNA^{Tyr}_{GUA}$ rapidly accumulated in the nuclei of both *dbp5-L12A* and *dbp5-R423A* cells in a manner comparable to the wild-type strain, indicating that nuclear tRNA import was not perturbed in these mutants (Figure 4-18). Following re-feeding, nuclear tRNA levels returned to near pre-stress conditions by 10 minutes in the integrated and untagged versions of the wild-type (15 ± 8) and *dbp5-L12A* (31 ± 5) strains; however, in *dbp5-R423A* the majority of cells at 10 minutes still showed elevated levels of nuclear tRNA (74 ± 9). This defect was largely rescued in the *dbp5-L12A/R423A* double mutant (43 ± 7), returning to levels that were not significantly different from the d*bp5-L12A* mutant alone (Figure 4-18). These observations, plus the genetic interaction with an *msn5Δ*, support the conclusion that nuclear Dbp5p supports the re-export of mature tRNAs following stress. The smaller but significant perturbation in the re-export of tRNAs in *dbp5-L12A* also suggests that efficient nucleocytoplasmic shuttling mediated by the N-terminal NES is important in the context of tRNA re-export.

To further validate these roles for Dbp5p in tRNA export, *in vivo* co-immunoprecipitation experiments with protein-A (PrA) tagged Dbp5p followed by RT-qPCR analyses were performed to determine if Dbp5p forms a complex with tRNAs. Using this approach, PrA-Dbp5p-RNA

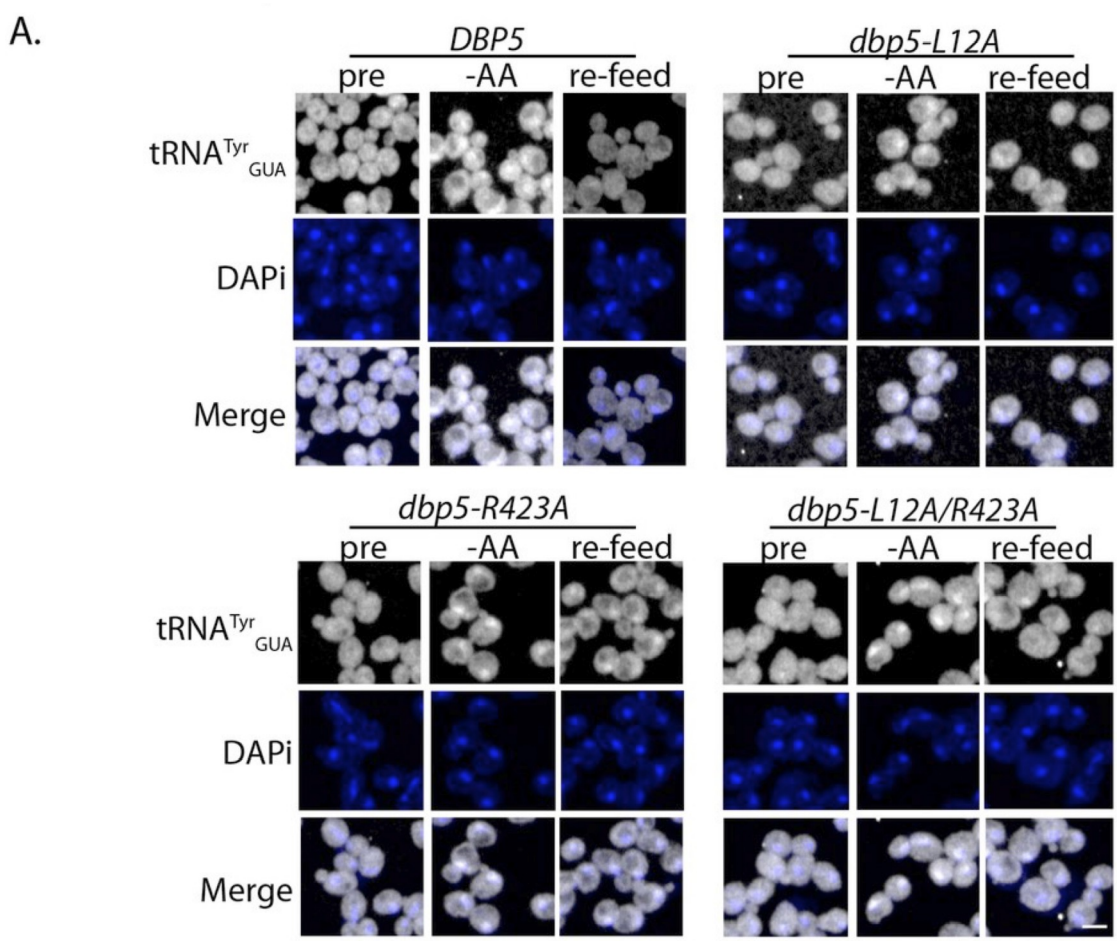

% of cells nuclear tRNA accumulation	DBP5			dbp5-L12A			dbp5-R423A			dbp5-L12A/R423A		
	pre	-AA	re-feed	pre	-AA	re-feed	pre	-AA	re-feed	pre	-AA	re-feed
	1±1	96±5	15±8	6±4	88±2	31±5	7±2	91±1	74±9	8±4	92±3	43 ±7

p=0.034
p=0.00078
p=0.059
p=0.32
p=0.045

Figure 4-18. Dbp5p supports re-export of mature tRNAs following nutritional stress. A. Localization of tRNA^{Tyr} determined by FISH at 25°C in integrated and untagged *DBP5*, *dbp5-L12A*, *dbp5-R423A,* and *dbp5-L12A/R423A* strains prior to (pre), during a 10 min starvation for amino acids (-AA), and 15 min after reintroduction of amino acids through addition of rich media (re-feed). Cells were probed with a Cy3 end-labeled tRNA^{Tyr} probe (SRIM15, gray) and DAPi (blue). Scale bar = 2 μm. Percent of cells determined to have increased levels of nuclear tRNA (i.e. nuclear signal >than cytoplasmic) under each condition are indicated below (three biological replicates, n = 100, error represents standard deviation, p-value from unpaired t-test with two-tailed distribution shown).

interactions were enriched for unspliced and spliced versions of $tRNA^{Ile}_{UAU}$, as compared to an untagged control strain (Figure 4-19A-C) PrA-$Dbp5p^{R423A}$ interactions appeared reduced with unspliced $tRNA^{Ile}_{UAU}$, but these reductions were not significant at the $p<0.05$ level (Figure 4-19A-C). In contrast, PrA-$Dbp5p^{L12A}$ interactions were significantly increased with unspliced $tRNA^{Ile}_{UAU}$ (Figure 4-19A-C). These patterns of $tRNA^{Ile}_{UAU}$ binding parallel both the observed export defects in $Dbp5^{R423A}$ and alterations in nuclear transport of both $Dbp5^{L12A}$ and $Dbp5^{R423A}$. In comparison, the highly abundant mitochondrial encoded mRNA *COX1* was not detected by RT-qPCR in any of the co-immunoprecipitation experiments above the background found in negative reverse transcriptase (-RT) controls (Figure 4-19D). Overall, the physical interaction of Dbp5 with tRNAs and the observed tRNA export defects in *dbp5-R423A,* which can both be modulated by altering the level of nuclear Dbp5 through use of the L12A mutation, provide strong evidence for Dbp5 functioning within the nucleus in tRNA export.

4.3 Discussion

4.3.1 Identification of novel functional domains within Dbp5p

The work presented here uses a comprehensive mutagenesis strategy to identify separation-of-function alleles in an essential DBP, which contributes to various processes within the gene expression program. Knowledge from these experiments can be combined with structural and biochemical data to understand the structure-function relationships between Dbp5p and gene expression. Furthermore, the mutant collection represents a resource that can be employed to identify alleles of value to the study of Dbp5p in particular contexts, and more broadly, to understand DBPs in general. For example, growth and fitness data in this study support the functional importance of critical residues within highly conserved motifs of DBPs critical for RNA-binding, ATP-binding, and hydrolysis. In short, this mutational analysis demonstrates the functional importance of all known motifs in this DBP *in vivo* based on a Ts or lethal phenotype (Figure 4-1). In addition, the binding sites of Dbp5p specific regulators, Gle1p and Nup159p, were identified as lethal or Ts when mutated, in agreement with biochemical and

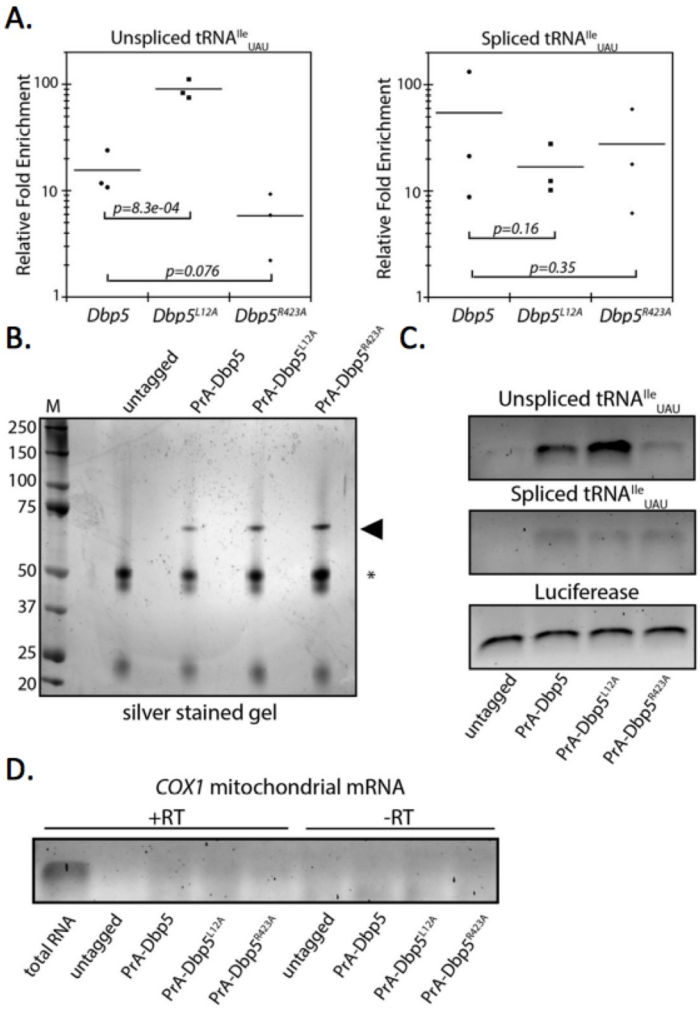

Figure 4-19. Co-immunoprecipitation analyses show tRNAs co-purify with Dbp5p. **A**. Graph showing relative fold enrichment (log scale) of associated unspliced or spliced $tRNA^{Ile}_{UAU}$ with PrA-Dbp5p in *DBP5, dbp5-L12A,* and *dbp5-R423A* strains as compared to the untagged control. Data generated by co-immunoprecipitation of PrA-Dbp5p followed by RT-qPCR using formaldehyde cross-linked cells (three biological replicates, p-value from unpaired t-test with two-tailed distribution using delta Ct values). **B.** Representative silver stained gel showing proteins present in co-immunoprecipitations of untagged control, PrA-Dbp5p, PrA-Dbp5p^{L12A}, or PrA-Dbp5p^{R423A}. Black arrowhead denotes Dbp5p and asterisk denotes IgG heavy chain. **C.** Representative agarose gel showing RT-qPCR products for $tRNA^{Ile}_{UAU}$, co-immunoprecipitations in untagged control, PrA-Dbp5p, PrA-Dbp5p^{L12A}, and PrA-Dbp5p^{R423A} RIPs, as well as the luciferase spike in control used for normalization. **D.** Agarose gel showing RT-qPCR products for the *COX1* mitochondrial mRNA in cDNA libraries made from total RNA vs. input RNA from RIPs. PCR products from reactions with (+RT) and without (-RT) addition of reverse transcriptase during cDNA library preparation are shown. Note that measured delta Ct values for *COX1* were similar to the levels found in -RT reactions suggesting only background detection of low levels of contaminating genomic DNA, which negates the calculation of relative fold change

structural models describing Dbp5p regulation (Alcazar-Roman et al., 2006; Dossani et al., 2009; Hodge et al., 2011; Montpetit et al., 2011; Noble et al., 2011; Weirich et al., 2006, 2004).

The strong correlation between lethal and Ts mutations with regulator binding sites and DBP motifs make the identification of Ts mutations in residues that have no known functional relevance to Dbp5p of particular interest. These included residues L12 and L15 within the extended N-terminal region of Dbp5p, which when analyzed in detail, were found to be part of an NES sequence (Figure 4-8). Other DBPs also contain NES sequences at their N-terminus, including multiple *DED1/DDX3* homologs and *DDX28* (Askjaer et al., 1999; Brennan et al., 2018; Senissar et al., 2014; Valgardsdottir and Prydz, 2003). A cluster of residues at position 158-162 is also notable, located between motif I and Ia, these residues are not highly conserved among DEAD-box proteins; however, many DBPs contain a serine and/or charged residues in this region, similar to Dbp5p. Based on the structure of Dbp5p bound to RNA, or in complex with known regulators (Montpetit et al., 2011), this region is a flexible surface accessible loop (Figure 4-1). Previous work has shown that this same region is also functionally important in other DEAD-box proteins. For example, in Mss116p the serine present in this loop is essential, resisting mutation *in vivo* (Mohr et al., 2011), and in human DDX3 this exposed loop contains an NLS sequence required for nuclear shuttling (Brennan et al., 2018). Although it remains unclear how these residues support the function of Mss116p and Dbp5p, it is enticing to speculate that this exposed loop represents a common surface in DBPs to engage trans-acting factors. In fact, a previous proteomics study has identified S162 within Dbp5p to be phosphorylated during DNA damage (Albuquerque et al., 2008), making this site of particular importance for future study.

Screening of the *DBP5* mutant collection against various cellular stresses, and for altered Dbp5p localization, served as another method to identify residues that could mediate distinct activities of Dbp5p. For example, this work identified several *DBP5* mutants with weak mRNP export defects that were found to be sensitive to a specific stress, including *dbp5-V73A* being sensitive to a translation inhibitor. These types of mutants are particularly informative since they appear to uncouple mRNP export defects from other events in the gene expression program. It is important to note that the inclusion of GFP within the mutant collection did result in the modification of mutant phenotypes, which was observed as a Ts and poly(A)-RNA accumulation phenotype at 37°C. This appears to have the benefit of further sensitizing mutants to particular perturbations, but also complicates the interpretation of mutant traits, requiring dissection of the

contributions of the mutation vs. GFP to an observed phenotype. For those phenotypes studied in detail here, this was done using an untagged version of the allele integrated at the endogenous *DBP5* locus and expressed from the native promoter. In doing this, localization and drug sensitivity phenotypes found at 25°C were verified for various alleles (e.g. L12A, V73A, and R423A). Nonetheless, work following on these screens, or found in future screens, must take note of these results and verify findings in the absence of GFP.

4.3.2 Nuclear shuttling of Dbp5p and mRNP export

The inclusion of GFP in this collection and subsequent identification of specific mutants that impact nuclear shuttling of Dbp5p was critical to establishing the nuclear function of Dbp5p reported here. This was accomplished through screening the mutant collection in the presence and absence of ethanol stress, which led to the identification of the Xpo1p dependent N-terminal NES sequence in Dbp5p (Figure 4-8). Interestingly, characterization of these mutants showed that Dbp5p NES-mediated nuclear export is not essential, and that a large cytoplasmic pool of Dbp5p is not required to support normal cellular functions in the growth conditions tested. This is based on the fact that an integrated *dbp5-L12A* allele had no growth defect at 25°C or 37°C, no mRNP export defect detectable by FISH, a transcriptome highly similar to control cells, and minimal genetic interactions as measured by SGA. Given previous reports of Dbp5p functioning in translation control (Beißel et al., 2019; Gross et al., 2007), this raises questions as to the exact requirement for Dbp5p in the cytoplasm and when the translation-related functions of Dbp5p are needed. It is expected that phenotypic and chemical genomic screening with the *dbp5-L12A* allele may allow insights in these questions. Analyses using the *dbp5-L12A* allele, as well as artificial means to direct Dbp5p localization, further showed that Dbp5p nuclear export does not rely on the N-terminal NES alone; however, the data show that export is still dependent on Xpo1p. Based on these findings, it is expected that Dbp5p shuttles in complex with other factors that also engage the Xpo1p transport system.

Localization screening further led to the identification of a stretch of residues in and around motif VI (422-434) required for efficient nuclear import (Figure 4-10), which combined with *dbp5-L12A* have provided critical reagents to investigate and characterize the nuclear function(s) of Dbp5p. Importantly, deconvolving the influence of GFP on Dbp5p function in the

presence of the L12A and R423A mutations allows for the general conclusion that Dbp5p nuclear shuttling is not central to Dbp5p mRNP export functions. Data supporting this conclusion includes the finding that strains carrying *dbp5-L12A* and *dbp5-R423A* integrated alleles have no poly(A)-RNA accumulation phenotype at 37°C, have a transcriptomic profile largely similar to the wild-type strain under steady-state growth conditions or following exposure to MMS, and *dbp5-L12A* has a weak genetic interaction profile as measured by SGA (Figure 4-13). Instead, both the transcriptomic profiling and SGA data provided indications that these mutants more specifically impact ncRNA biology. Interestingly, transcriptome profiling experiments showed that *dbp5-L12A* and *dbp5-R423A* impact distinct clusters of genes in the opposite manner (Figure 4-13). In *dbp5-L12A*, where Dbp5p is largely nucleoplasmic, a set of genes involved in ncRNA processes were largely induced in response to stress. In *dbp5-R423A*, where Dbp5p nuclear access is altered, expression of these same genes does not change or they are repressed. This suggests a nuclear role for Dbp5p in modulating gene in response to stress, which requires efficient nuclear access or shuttling.

Notably, the collected data on *dbp5-L12A* and *dbp5-R423A* provides information that can be used to discern current models in the field related to the function of Dbp5p during mRNP export (Heinrich et al., 2017). In the Dbp5p "scaffold" model of export, Dbp5p functions as a scaffold required for proper mRNP formation in the nucleus and travels with the mRNP to the cytoplasmic face of the NPC. At NPCs, the Dbp5p interaction with the mRNA would be altered by the presence of co-regulators, Gle1p and Nup159p, resulting in release of the mRNP into the cytoplasm. In this model, efficient shuttling of Dbp5p through the nucleus would be critical for the function of Dbp5p in mRNP export. The alternative "RNPase" model postulates that Dbp5p first encounters translocating mRNPs at the cytoplasmic face of the NPC and remodels these substrates at this location, an activity that would be independent of a nuclear pool of Dbp5p. In this model, a constant pool of Dbp5p at NPCs would be central to mRNP export and altering the residual nuclear or cytoplasmic pools of Dbp5p would have less of an impact on mRNP export. Indeed, the data presented here showed that mRNP export is relatively insensitive to changes in Dbp5p steady-state localization and shuttling, which supports the RNPase model and suggests that the nuclear role of Dbp5p may be more critical for activities relating to ncRNA processing and export.

4.3.3 Dbp5p acts within the nucleus to support tRNA export

Given that Dbp5p has been shown to be required for the export of ncRNA substrates, including pre-40s and pre-60s ribosomal subunits and the telomerase RNA *TLC1* (Neumann et al., 2016; Wu et al., 2014b), one hypothesis could be that perturbation in Dbp5p shuttling efficiency impacts these activities. Additionally, export of ncRNA species, such as pre-ribosomal subunits, largely occurs through Xpo1p mediated export (Kohler and Hurt, 2007), and identification of an Xpo1p mediated NES in Dbp5p provides a mode for Dbp5p to act as an export receptor for these ncRNA substrates. However, pre-ribosomal subunit export defects in *DBP5* shuttling mutants (*dbp5-L12A* or *dbp5-R423A*) were not observed under the conditions tested. This may partly be due to multiple redundant pathways that contribute to pre-ribosomal subunit export, which includes Arx1p, and the essential non-karyopherin transport receptor required for mRNP export, Mex67p (TAP or NXF1) (Bradatsch et al., 2007; Faza et al., 2012b; Hung et al., 2008; W Yao et al., 2007). The lack of a discernible phenotype is also in agreement with work from Neumann et al. (2016), which suggests that Dbp5p activity in relation to rRNA export is occurring at the cytoplasmic face of NPCs, similar to mRNP export. Given that both Dbp5p^{L12A} and Dbp5p^{R423A} still access the nuclear envelope, a block in rRNA may not be expected.

Instead, this work identified a requirement for efficient Dbp5p nuclear shuttling in supporting tRNA export (Figure 4-15 and 4-18). Specifically, analyses of wild-type and *dbp5-R423A* strains provided evidence for a direct role for Dbp5p in tRNA export, including a physical interaction between Dbp5p and tRNA transcripts in both the spliced and unprocessed forms. tRNA export defects being most apparent in an integrated *dbp5-R423A* strain after a temperature shift to 37°C or after re-introduction of nutrients (e.g. glucose or amino acids) to starved cells. Re-introduction of nutrients being a condition that induces rapid export of a large nuclear pool of mature tRNAs that accumulate during nutrient starvation (Whitney et al., 2007), which was found to be delayed in *dbp5-R423A*. Given that Dbp5p^{R423A} has reduced access to the nuclear compartment, and increasing nuclear levels through introduction of the L12A mutation rescued tRNA export defects, it is most likely that Dbp5p functions within the nucleus to support tRNA export.

Notably, a synthetic genetic interaction with *MSN5* was observed by SGA with *dbp5-R423A*, Msn5p being known to promote tRNA re-export following nutrient stress (Huang and Hopper, 2015; Murthi et al., 2010). Interestingly, a significantly increased interaction between Dbp5p^{L12A}, which is largely nucleoplasmic, and spliced tRNAs was identified, which further supports a nuclear function for Dbp5p in the re-export of mature tRNAs. In the case of Dbp5p^{R423A}, binding interactions with tRNAs were not lost indicating that tRNA export defects in *dbp5-R423A* arise in part through another mechanism. Moreover, the *dbp5-L12A/R423A* double mutant did not fully rescue tRNA processing defects or fully restore tRNA re-export kinetics following nutrient stress to wild-type levels. This is likely due to the RNA-stimulated ATPase defect seen in Dbp5p^{R423A}, as it is expected that the ATP hydrolysis cycle of Dbp5p would be central to modulating all RNA-dependent cellular functions of Dbp5p. Interestingly, the lack of an mRNP export defect in the *dbp5-R423A* mutant suggests that the R423A mutation alters Dbp5p in a manner that impacts tRNA export specifically and/or tRNA export during a temperature shift or recovery from nutrient stress requires a higher overall level of Dbp5p ATPase activity. Future studies will pursue mechanisms by which Dbp5p mediates tRNA export, especially in response to changes in nutrient availability, and how these functions of Dbp5p are specifically impacted in *dbp5-R423A*.

Previous work had identified a role for the mRNP export factor Mex67p and the Dbp5p regulator Nup159p in the export of tRNA substrates (Chatterjee et al., 2017; Wu et al., 2015). Here, the role of another Dbp5p regulator, Gle1p, in tRNA export was identified. The fact that these four proteins, which function together to support mRNP export (Folkmann et al., 2011; Heinrich et al., 2017a; Stewart, 2007), also show tRNA export defects raises the possibility that this machinery works together to facilitate the export of multiple transcript classes. Importantly, while *nup159-1*, *gle1-4*, and *dbp5-1* Ts alleles have strong mRNP export defects at 37°C, *dbp5-R423A* does not. In addition, tRNA export defects are apparent in *gle1-4*, *nup159-1*, and *dbp5-1* strains at 25°C in the absence of a block to mRNP export. This lends support to the postulate that Dbp5p, and both regulators Gle1p and Nup159p, have roles in tRNA export that are independent of a block in mRNP export.

Given this work, many questions emerge surrounding the function(s) Dbp5p performs, and how this activity is modulated *in vivo,* to support mRNA, tRNA, and rRNA export. For example, does Dbp5p generally function to remodel all RNP complexes exiting NPCs or does

Dbp5p function in a distinct manner for each type of substrate (e.g. an RNPase vs. a clamp)? Do the NPC associated Dbp5p regulators, Gle1p and Nup159p, support all of these activities? Or does disruption of Nup159p and Gle1p directed activities feedback to disrupt other Dbp5p and Mex67p driven processes? Notably, Mex67p is known to support the export of mRNA, tRNA and rRNA substrates (Bradatsch et al., 2007; Hurt et al., 2000; A Segref et al., 1997; Wu et al., 2015), and biochemical evidence suggests that Dbp5p targets Mex67p on mRNPs (Lund and Guthrie, 2005). As such, does Dbp5p target Mex67p bound to all RNA substrates? Finally, what is the role of Dbp5p during nutrient stress and recovery? Do these activities of Dbp5p during a stress response extend to other RNA substrates as well to more globally regulate the gene expression program? Further work is required to address these important questions and it is expected that the mutants characterized here, and potentially others within the collection, will serve as a rich resource to probe such questions in detail.

Chapter V: *Perspectives**

* A portion of this chapter has been reproduced from Heinrich, Derrer, Lari *et al., BioEssays,* 2017, 39: 1600124.

5.1 Synopsis

The spatial and temporal regulation of dozens of RBPs is critical for successful mRNP export and accurate coupling to both upstream and downstream processes within mRNA metabolism. The work presented in this thesis establishes the use of a live-cell single particle-imaging platform in yeast to interrogate the spatial and temporal regulation of mRNP export factors. Using this approach, mRNP export kinetics were determined, cytoplasmic scanning of mRNPs was identified, and the essential role for the principal mRNP export factor, Mex67p, was demonstrated through analysis of mRNP export dynamics in a *mex67-5* mutant. Furthermore, work in this thesis assessed roles of the DEAD-box ATPase, Dbp5p, in the eukaryotic gene expression program. Using a comprehensive mutagenesis approach, separation-of-function alleles of *dbp5* were identified, an Xpo1p dependent NES was identified in Dbp5p, and further insight into shuttling dynamics of this protein were established. Ultimately through characterization of mutants that altered the subcellular localization of Dbp5p, a novel nuclear role for Dbp5p in tRNA export was discovered. The following sections will focus on discussing these results in a broader context to speculate on the future directions that arise from these findings.

5.2 mRNP export kinetics

Analyses of mRNP export kinetics across multiple cellular systems, including studies presented here in yeast (section 3.2.2), have determined that export occurs anywhere from 11 ms to 20 seconds. These studies have utilized various different imaging approaches and focused on a multitude of different transcripts that range in size from 1.5kb to 15kb (reviewed in Heinrich et al., 2017). Although the machinery and mechanisms required for mRNP export are conserved between yeast and metazoans (Nino et al., 2013), the degree to which kinetics are conserved still remains to be tested. Future studies should largely focus on investigations to determine the export kinetics of a multitude of different transcript types using a consistent imaging approach. There are several transcript features and conditions that are predicted to alter mRNP export kinetics.

Firstly, transcript size is likely to affect the number and spacing of RBPs that can bind the transcript, which may require more or less remodeling during export, and therefore may affect the

kinetics of the process. In fact, computation models of mRNP export have predicted this (Azimi et al., 2014). In yeast, mRNA transcript size can range from ~0.4kb to 15kb, thus mRNP export kinetics of many other transcripts must be determined to understand the affect of size on the dynamics of this process. (Hurowitz and Brown, 2004).

Secondly, the presence of introns in a transcript may affect mRNP export kinetics. Transcripts that undergo splicing require the activity of a unique subset of RBPs in the nucleus resulting in an mRNP architecture that may demand altered remodeling requirements (Tuck and Tollervey, 2013). Although splicing occurs prior to mRNP export, there are RBPs such as Sub2p that support the coupling of splicing to export (Johnson et al., 2011, 2009; Sträßer et al., 2002; Zenklusen et al., 2002). Thus, splicing requirements may affect downstream mRNP export kinetics. In yeast only a small number of predicted protein coding genes contains introns and many of these genes contain only a single intron (Parenteau et al., 2008). However, the number of intron containing genes and the number of introns in a single gene are vastly increased in humans and necessitates even more complexity in these pathways (e.g. alternative splicing) (Nilsen and Graveley, 2010). Thus, it will be interesting to study the impact of splicing on mRNP export in a human cell model.

Lastly, the cellular conditions in which an mRNA is expressed may affect mRNP export kinetics. For example, under conditions of heat shock in yeast, mRNP export is rapidly modulated to prevent the export of "housekeeping" mRNAs to promote the export and rapid expression of heat shock (HS) mRNAs required for survival (Saavedra et al., 1996). Recent studies have also shown that HS specific mRNAs exhibit a paired down mRNP composition, lacking Mex67p adaptor proteins such as Nab2p and Npl3p (Zander et al., 2016). This may promote rapid expression of these mRNAs by speeding up export competent mRNP formation and export itself, which remains to be tested.

Importantly, Tuck and Tollervey, 2013 have utilized a systematic, transcriptome-wide approach to categorize RNAPII transcripts into 10 classes, which includes mRNP composition. This serves as another approach to define distinct types of mRNAs, and export kinetics for these distinct classes can be identified and correlated with mRNP composition. Ultimately, understanding the basal mRNP export kinetics of a multitude of mRNAs will be important to understand the role of RBPs and mechanisms driving the dynamics of this essential process, and furthermore how this is modulated in response to changing cellular conditions.

5.3 Spatial and temporal regulation of mRNP export

Large-scale approaches that utilize crosslinking RNA IPs with RNA seq analysis (e.g. crosslinking and analysis of cDNA–CRAC) have been tremendously powerful in identifying a host of RBPs that interact with mRNAs in the cell. However, the vast majority of these data do not capture the temporal changes an mRNP undergoes as a result of moving through different stages of biogenesis or between different subcellular compartments. As a result, the RNA-binding profile for each RBP reflects interactions occurring across multiple stages of mRNA biogenesis (i.e. an ensemble average), which may encompass multiple functions and binding interactions due to changes in mRNP architecture. For example, some RBPs transiently interact with the mRNA only within the nucleus or cytoplasm, and others accompany the mRNA from the nucleus to cytoplasm (Köhler and Hurt, 2007). Once in the cytoplasm, some RBPs are removed immediately after transition through the NPC, such as the export factor Mex67p (Lund and Guthrie, 2005), while others, like the nucleocytoplasmic shuttling RBP Npl3p, accompany mRNA transcripts for a longer time in the cytoplasm and may be further involved in cytoplasmic events such as translation.

As such, there is still a requirement to interrogate the spatial and temporal functions of the more than 30 RBPs that have been identified to play a role in mRNP export through complementary approaches such as live-cell single particle imaging. Analysis of mRNP export dynamics in a conditional mutant (*mex67-5*) of the major mRNP export factor Mex67p presented here demonstrates the requirement for this factor in release of mRNPs from NPCs and directionality of transport (Section 3.2.5). Future studies will need to focus on defining the spatial and temporal functions of other mRNP export factors such as those loaded within the nucleus and likely to be present in most nuclear mRNPs (e.g. Yra1p and Nab2p). Aberrant functioning of these factors would be expected to result in failures in the early stages of mRNP export such as initial mRNP docking to NPCs. Furthermore, the spatial functions of the essential machinery required for remodeling exporting mRNPs at the cytoplasmic face of NPCs (Dbp5p, Nup159p, Gle1p) should also be investigated. Mutations in these factors would be expected to affect late stages of mRNP export such as release from NPCs and consequently directionality of transport.

Importantly, these types of analyses could further resolve models for how Dbp5p functions in mRNP export (discussed in section 1.3.7). For example in a *dbp5* mutant, if the scaffold model

is correct, transcripts may not dock to the nuclear basket of NPCs or ever leave the nucleus due to failures in mRNP assembly, whereas in an RNPase model the mRNP would dock and transit through the NPC, but show release and/or directional transport defects due to failures in mRNP remodeling. Of course, it is possible that Dbp5p functions in multiple ways to facilitate export and that this may in part depend on the transcript being exported.

Notably, many mRNP export factors are essential and also function in processes both upstream and downstream of export such as transcription, 3′ end processing, splicing, and translation (Nino et al., 2013). This poses a unique challenge when assessing the direct spatial defects due to mutations in these factors. To mitigate this, and determine the most direct spatial defect associated with loss of these factors, future studies can employ methods to rapidly deplete the cellular pool of these proteins. One such approach that has been utilized successfully in yeast is an auxin-inducible degron (AID) system (Mendoza−Ochoa et al., 2019). mRNP export factors can be rapidly targeted for proteosomal degradation in the presence of auxin through AID-tagging. This provides a rapid and tunable approach to deplete these proteins and is conducive to live-cell imaging.

5.4 mRNP export coupled to translation

Analysis of mRNP dynamics reported here in a wild-type strain revealed that mRNPs are frequently confined near the cytoplasmic face of NPCs following export (Section 3.2.3). Scanning in general remains poorly understood and has so far only been reported for a few transcripts (Grünwald and Singer, 2010; Saroufim et al., 2015; Smith et al., 2015). This raises questions as to why some mRNPs are exported immediately and others are not. This may involve differential remodeling requirements for distinct transcripts, which could be resolved through analysis of mRNP dynamics of different transcript classes as discussed in section 5.2. Alternatively, scanning may be indicative of mRNP export coupled to downstream processes such as translation and/or cytoplasmic quality control. During the pioneer round of translation, mRNAs are subject to quality control to ensure upstream biogenesis events have successfully completed. Key to the surveillance process are the presence of factors in the mRNP that were loaded in the nucleus (e.g. exon-junction complex - EJC), which interact with cytoplasmic

components to provide an opportunity for crosstalk between nuclear and cytoplasmic processes for the purposes of quality control (Maquat et al., 2010). Thus, future studies depleting the function of the EJC or translation through the use of chemical inhibitors (e.g. cycloheximide or hippuristanol) and observing potential alterations in this scanning behavior of mRNPs will provide insight into the function of scanning. However, development of improved live-cell imaging approaches will be paramount for imaging mRNPs through longer lived events together such as mRNP export, scanning, and translation.

5.5 Improved live-cell quantitative imaging approaches in budding yeast

Successful detection and tracking of single particles, such as mRNPs, in live cells requires a sufficient SNR (Waters, 2009). Current mRNA labeling approaches suffer from low SNR when used to follow dynamic processes due to the requirement of short exposure times (~10–20 ms) and photobleaching over an imaging series. Consequently, in these studies 24 repeats of the PP7-specific RNA hairpins were introduced into the GFA1 mRNA to achieve the required SNR. The fluorescently tagged PP7-coat protein (PP7-FP-CP) binds as a dimer, therefore, up to 48 FP-CP can bind to an array of 24 RNA hairpins, adding significant protein mass to the labeled mRNP. This must be taken into consideration to ensure that the mRNP retains its functionality. Also, several studies have reported that the presence of multiple MS2 hairpins, another RNA-aptamer based tagging approach, can lead to the stabilization of MS2-containing decay fragments, which may act as false-positive signals in imaging experiments (Garcia and Parker, 2016, 2015; Haimovich et al., 2016; Heinrich et al., 2017c). Consequently improved versions of these RNA hairpins have been developed to minimize these decay fragments and should be utilized for future studies (Tutucci et al., 2018, 2017). To reduce the number of hairpins needed to visualize transcripts, fluorophores with improved brightness, and photostability also provide an attractive labeling alternative. Examples include fluorescent proteins such as the far-red variant mKATE or GFP variants such as mNeonGreen (Shaner et al., 2013; Shcherbo et al., 2007).

In addition to RNA labeling strategies, advancements in imaging technology are instrumental to the improved imaging of mRNPs *in vivo* with high spatial precision and temporal resolution. Single particle imaging systems have to balance imaging speed, sufficient SNR to

reliably detect particles over background, and illumination intensities that minimize photobleaching and phototoxic effects over time. Specialized single particle microscope systems, such as the widefield fluorescence setup described in this study, were developed to meet these criteria. However, to extract positional information of single particles relative to distinct subcellular or sub-organelle structures will require both high spatial precision and development of multi-color imaging. A solution to these challenges may be achieved through the use of light sheet microscopy (Follain et al., 2017). Light sheet microscopy, in its various forms, allows for long-term imaging and high 3D resolution via fast sectioning along the optical z-axis. For example, development of this technology allows for long-term tracking of mRNPs to include mRNP export and downstream processes such as translation. Therefore these developments can provide insight into the function of particle behaviors such as scanning, and how these processes are coupled both spatially and temporally.

5.6 Dbp5p activity in mRNP export

The spatial regulation of Dbp5p activity through the activity of co-regulators (Nup159p and Gle1p-Ip_6) that are located at the cytoplasmic side of NPCs has largely supported a role for Dbp5p in mRNP export through RNPase activity. However as discussed in section 1.3.7, several pieces of evidence complicate this model, such as Dbp5p nucleocytoplasmic shuttling and interactions with nuclear machinery such as transcription factors. Through characterization of mutants that alter the nucleocytoplasmic shuttling dynamics of Dbp5p presented here (section 4.2.3-4), these data suggest that efficient shuttling of Dbp5p is not critical for mRNP export, thus supporting an RNPase model for the essential Dbp5p activity in mRNP export (see Figure 5-1). Using both poly(A)-RNA FISH and RNA-seq approaches, evidence for mRNP export defects could not be identified in mutants that alter Dbp5p localization to being nucleoplasmic (*dbp5-L12A*) or affect efficient import of Dbp5p into the nucleus (*dbp5-R423A*). In both these mutants, Dbp5p could efficiently access the NE to support this role in mRNP export, and only a small proportion of the cellular pool of Dbp5p is required to support this function. If Dbp5p functioned as a scaffold within the nucleus to aid in export, *dbp5-R423A* would be predicted to exhibit mRNP export defects, which was not the case. Ultimately to further resolve these models of

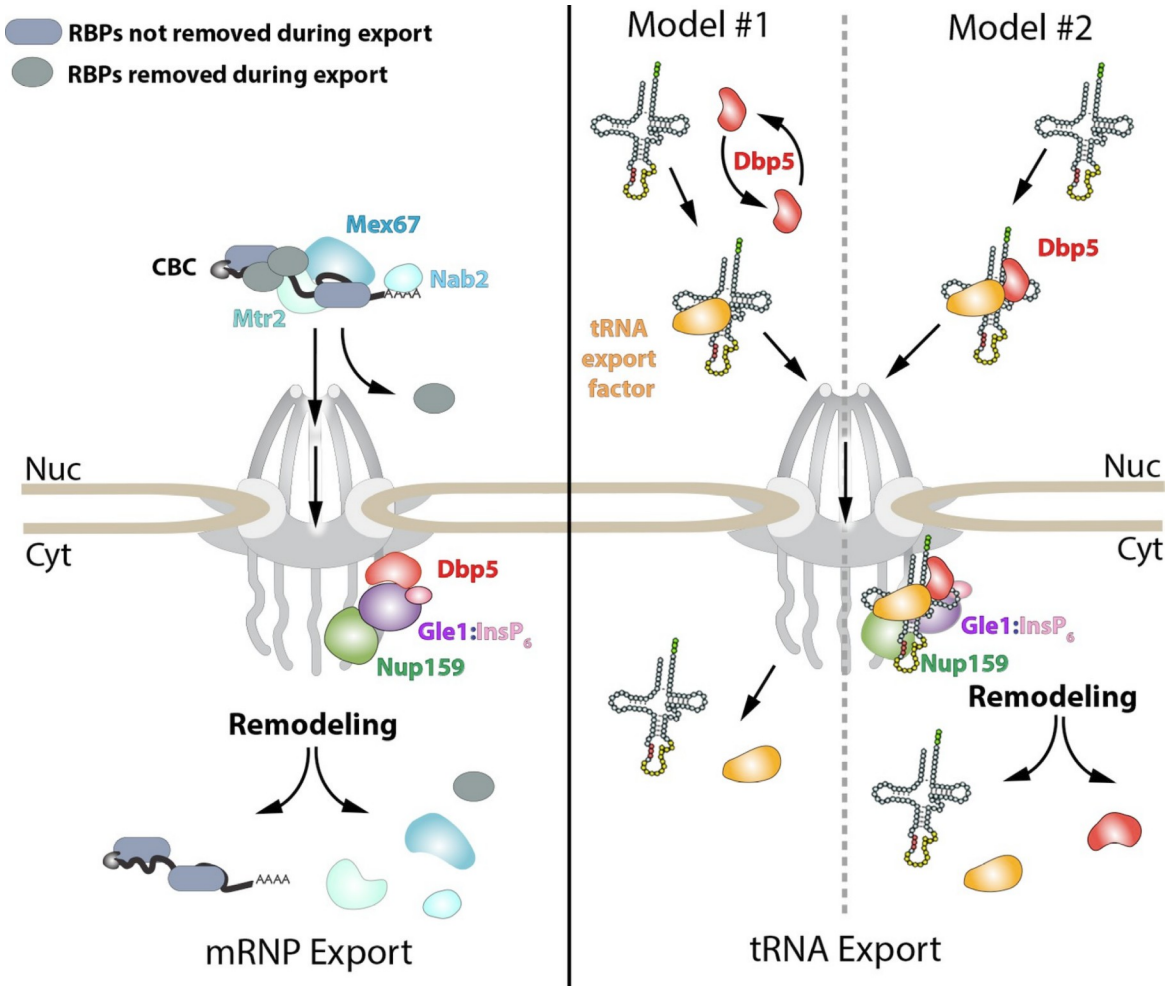

Figure 5-1. Roles for Dbp5p activity in RNP export. Data from this work suggest that Dbp5p shuttling is not critical to mRNP export, supporting a model in which Dbp5p acts at NPCs to facilitate export. In such a model (schematic on left), mRNPs assembled in the nucleus would be expected to include the cap binding complex (CBC), export factors Mex67p-Mtr2p, Nabp2, and various other RBPs. Following transport out of the nucleus, the activity of Dbp5p at the cytoplasmic face of the NPC in the context of Gle1p:$InsP_6$ and Nup159p would promote remodeling of RNA-RBP interactions to enforce directional transport (e.g. RNPase model). For tRNAs, a nuclear pool of Dbp5p is involved in export suggesting two broad models of Dbp5p function (schematic on right). In model #1, Dbp5p would act solely within the nucleus to support tRNA processing and export by facilitating events, potentially as an RNPase, that ultimately lead to a tRNA being exported with a tRNA export factor (e.g. Los1p or Mex67p). In model #2, Dbp5p engages a tRNA in the nucleus and travels with tRNAs from the nucleus to the cytoplasm in complex with the tRNA and tRNA export factor (e.g. scaffold model), and upon entering the cytoplasm, these interactions would be remodeled in the context of the NPC and Dbp5p regulators. The second model provides a rationale for tRNA export defects in mutants of Dbp5p co-regulators (Nup159p and Gle1p), whereas in model #1 the impact of mutations in Dbp5 co-regulators would act through an indirect and/or independent mechanism.

Dbp5p activity, a live-cell imaging approach could be used to determine the spatial mRNP export defects of *dbp5* mutants, as discussed in section 5.3.

Interestingly, although Dbp5p^{L12A} is predominantly nucleoplasmic, no evidence for perturbations in activities downstream of export, such as translation, were identified through screening with *dbp5-L12A* (section 4.2.6). Dbp5p has been linked to a direct role in translation (Beißel et al., 2019; Bolger et al., 2008; Gross et al., 2007), however these data suggest that Dbp5p either plays a redundant role in translation, or only a small transient pool of Dbp5p is required for this activity. As such, it remains pertinent to assess whether translation defects in any *dbp5* mutant are indirect results of upstream mRNP export defects.

Conversely, R423 is located within the highly conserved DBP motif VI of Dbp5p, which is required for ATP-binding and hydrolysis and RNA binding, and is expectedly more sensitive to other perturbations in mRNA metabolism as observed through genetic interactions identified through SGA screening with *dbp5-R423A*. Furthermore, Dbp5^{R423A} does exhibit altered ATPase activity, through a decrease in stimulation by RNA. However, under steady state conditions, this reveals that the Dbp5p ATPase activity within mRNP export can withstand some level of dysfunction, which may speak to what work Dbp5p is actually carrying out on mRNA substrates. For example, perhaps an RNPase type activity at NPCs may buffer a level of decreased RNA-dependent stimulation of ATPase activity, while a scaffold type function in the nucleus in the absence of co-regulators would not. Future studies should focus on determining the ATPase activity requirements for Dbp5p in roles for mRNP export or export of other RNA substrates (see section 5.6).

Finally, a mechanism for Dbp5p import into the nucleus still remains elusive, and requires future work to resolve. This may be due to multiple redundant Kaps that mediate import of Dbp5p under various conditions. Evidence of reduced nuclear import of Dbp5p^{R423A} also suggests that import is likely dependent on the enzymatic state of Dbp5p, which is dependent on the activity of co-regulators, Gle1p and Nup159p.

Ultimately to address many of the outstanding questions regarding the function of Dbp5p in mRNP export, it is paramount to identify the transcript binding preferences for Dbp5p. Future studies should focus on determining which mRNAs Dbp5p binds and if there is any specificity in binding across a transcript. This can be achieved through cross-linking IP and transcriptome wide RNA seq approaches (e.g. CRAC or CLIP). Furthermore, it will be interesting to determine

which subset of mRNAs (or other RNAs) Dbp5p interacts with and how the binding profile of Dbp5p correlated with other mRNP export factors such as Mex67p. These transcripts can be studied in more detail to determine how mRNP composition in altered with or without Dbp5p activity *in vivo*.

5.7 Dbp5p activity in tRNA export

Although efficient nuclear import of Dbp5p is not critical for bulk mRNP export, it is however required for efficient tRNA processing and export. Data presented here using northern blotting and tRNA FISH (section 4.2.7), show that the export of intron-containing pre-tRNAs, and re-export of mature tRNAs following nutrient starvation were affected in *dbp5-R423A*. Furthermore, upon increasing the nuclear pool of Dbp5p^{R423A} through generation of a double mutant allele (*dbp5-L12A-R423A*), export of tRNAs were no longer disrupted; thus, suggesting a nuclear role for Dbp5p in tRNA processing and export. Given that the known regulators of Dbp5p ATPase activity (Gle1p and Nup159p) do not localize to the nucleus, Dbp5p may be playing an alternative role here in the nucleus when compared to mRNP export (see Figure 5-1). One potential model is that Dbp5p acts as an RNPase solely in the nucleus to support nuclear tRNA processing and export competency. Dbp5p activy may be required in the nucleus to unload various protein maturation factors off the tRNA, and/or load factors required for export competency to support interactions with NPCs. A second possibility is that Dbp5p is acting as a scaffold for RNP assembly in the nucleus and then traveling with the tRNA to the cytoplasm. It is not uncommon for a DBP to function in this capacity, for example the EJC complex, which contains the DBP eIFAIII functions in this way. It is loaded onto mRNAs during splicing in the nucleus and is stably bound to mRNPs through export into the cytoplasm to further promote quality control mechanisms there (Boehm and Gehring, 2016). The EJC serves as a stable platform to which other proteins, such as RBPs required for export, can bind. Therefore, it can be hypothesized that Dbp5p may also be functioning in a similar capacity on tRNAs in the nucleus to promote export. However, these findings are not mutually exclusive with an RNPase role for Dbp5p activity within nuclear tRNA processing to generate export competent tRNAs, and/or at NPCs to support directionality of tRNA export similar to activity within mRNP export.

Consistent with this are the findings that mutants of NUP159 (identified previously by Wu et al., 2015), and GLE1 also show tRNA export defects.

There are many outstanding questions with regards to the role(s) Dbp5p is playing to support tRNA export. If Dbp5p is playing an RNPase role to remodel protein-tRNA complexes in the nucleus or at NPCs, what are the targets for this activity? Recently, the major mRNP export factor, the Mex67p-Mtr2p heterodimer, has been implicated in a direct role in tRNA export (Chatterjee et al., 2017). Similar to the predicted Dbp5p dependent mRNP remodeling at NPCs (Lund and Guthrie, 2005), does Dbp5p target Mex67p on tRNA substrates also? tRNA export is also supported by several different exportins including Los1p and Msn5p (Hopper, 2013), and Dbp5p activity could also be targeting these factors for remodeling following export through NPCs to enforce directionality. Future biochemical studies must be carried out to determine the extent to which Dbp5p supports remodeling of these factors on tRNAs. Similar to understanding the role of Dbp5p in mRNP export, transcriptome wide approaches in understanding the tRNA transcript binding preferences of Dbp5p will be critical in determining the extent to which Dbp5p is directly required for tRNA processing and export. This may also inform what role Dbp5p is carrying out on these substrates. For example, Dbp5p may be more biased in binding intron-containing pre-tRNAs, which suggests a more nuclear role for Dbp5p.

Dbp5p has also been linked to the export of other ncRNAs such as pre-ribosomal subunits and the telomerase RNA, *TLC1* (Neumann et al., 2016; Wu et al., 2014). Again, it remains unclear what activities Dbp5p is carrying out on these substrates, if these roles are direct, and whether this activity is required in the nucleus, at NPCs, or at both. The Mex67p-Mtr2 heterodimer has also been linked to pre-ribosomal subunit export (Faza et al., 2012; Yao et al., 2007), which again prompts the question; Does Dbp5p target Mex67p for remodeling on rRNAs also? Ultimately, this prompts even further questions regarding how all these RNP export activities of Dbp5p are coordinated in the cell, including how are cellular pools of Dbp5p allocated and differentiated to function in all these processes? Mechanisms that should be further investigated could include other binding partners of Dbp5p that are spatially constrained to particular compartments (nucleoplasm vs. NPCs vs. cytoplasm) or even post-translational modifications (PTMs) on Dbp5p or other RBPs. PTMs provide the advantage of rapidly modulating protein-protein and protein-RNA interactions in a reversible manner (Deribe et al., 2010; Tutucci and Stutz, 2011). These modifications have been implicated in regulating mRNP

metabolism by weakening contacts between proteins, thereby contributing to mRNP remodeling. Ultimately this may change mRNP composition and promote distinct interactions.

5.8 Role of mRNP export machinery as general RNP export factors

To date, Dbp5p, Nup159p, Gle1p and Mex67p, which are essential and critical factors required for mRNP export, have also been linked to roles in tRNA export and telomerase RNA export (Chatterjee et al., 2017; Wu et al., 2014). Dbp5p, Nup159p, and Mex67p have also been linked to roles in pre-ribosomal subunit export (Faza et al., 2012; Neumann et al., 2016; Yao et al., 2007). The reoccurrence for the requirement of this machinery for efficient export of many types of RNPs suggests that potentially these factors may function as general RNP export factors. The notion of general and redundant export receptors in the cell is an attractive model, given the large number of RNPs that need to be exported from the nucleus at any given time to sustain critical downstream RNA metabolism and gene expression processes.

Of these factors, Mex67p has been the most well characterized to be playing direct roles in mRNP, tRNA, and pre-ribosomal subunit export, providing strong evidence for its role as a general RNP export receptor. The data presented here (section 4.2.7), which includes a direct physical interaction with tRNAs, also suggests that Dbp5p plays a direct role in mRNP export and tRNA export. In the case of Nup159p and Gle1p, a direct requirement for these factors in tRNA export remains elusive and requires future investigation. Mutations in NUP159 and GLE1 could impact tRNA export in at least three capacities. Firstly, mutations in these factors result in robust mRNP export defects, which could indirectly affect tRNA export (Gorsch et al., 1995; Murphy and Wente, 1996). This could occur by lowering expression of factors required for tRNA export, or by physically blocking NPCs with non-functional mRNPs and preventing export of other substrates such as tRNAs. Secondly, these mutations could affect nuclear import of Dbp5p, and thus spatially separate Dbp5p from a nuclear role in tRNA processing and export leading to these defects. In fact, mutations that affect Dbp5p binding to Nup159p render Dbp5p localization to be cytoplasmic (Napetschnig et al., 2009; Noble et al., 2011; Schmitt et al., 1999; Weirich et al., 2004), and shown here Dbp5p localization is observed to be more cytoplasmic in a *gle1-4* mutant (section 4.2.8). Finally, in a more direct capacity these mutations could affect stimulation

and recycling of Dbp5p ATPase activity, which may be required for remodeling tRNAs at NPCs in the cytoplasm. Although the idea of Dbp5p, Gle1p, and Nup159p functioning as a complex for general RNP export is an enticing model, future investigations will need to focus on the direct versus indirect requirement of activity of these factors in relation to the export of various RNP substrates to ultimately determine if this model is supported.

References

Adams RL, Mason AC, Glass L, Aditi, Wente SR. 2017. Nup42 and IP $_6$ coordinate Gle1 stimulation of Dbp5/DDX19B for mRNA export in yeast and human cells. *Traffic* **18**:776–790. doi:10.1111/tra.12526.

Aebi M, Kirchner G, Chen JY, Vijayraghavan U, Jacobson A, Martin NC, Abelson J. 1990. Isolation of a temperature-sensitive mutant with an altered tRNA nucleotidyltransferase and cloning of the gene encoding tRNA nucleotidyltransferase in the yeast Saccharomyces cerevisiae. *J Biol Chem* **265**:16216–16220.

Aitchison JD, Rout MP. 2012. The Yeast Nuclear Pore Complex and Transport Through It. *Genetics* **190**:855 LP-883. doi:10.1534/genetics.111.127803.

Albuquerque CP, Smolka MB, Payne SH, Bafna V, Eng J, Zhou H. 2008. A Multidimensional Chromatography Technology for In-depth Phosphoproteome Analysis. *Mol Cell Proteomics* **7**:1389–1396. doi:10.1074/mcp.M700468-MCP200.

Alcázar-Román AR, Bolger TA, Wente SR. 2010. Control of mRNA export and translation termination by inositol hexakisphosphate requires specific interaction with Gle. *J Biol Chem* **285**:16683–16692. doi:10.1074/jbc.M109.082370.

Alcazar-Roman AR, Tran EJ, Guo S, Wente SR. 2006. Inositol hexakisphosphate and Gle1 activate the DEAD-box protein Dbp5 for nuclear mRNA export. *Nat Cell Biol* **8**:711–716.

Amberg DC, Goldstein AL, Cole CN. 1992. Isolation and characterization of RAT1: an essential gene of Saccharomyces cerevisiae required for the efficient nucleocytoplasmic trafficking of mRNA. *Genes Dev* **6**:1173–1189. doi:10.1101/gad.6.7.1173.

Arts G, Kuersten S, Romby P, Ehresmann B, Mattaj IW. 1998. The role of exportin-t in selective nuclear export of mature tRNAs. *EMBO J* **17**:7430 LP-7441. doi:10.1093/emboj/17.24.7430.

Askjaer P, Bachi A, Wilm M, Bischoff FR, Weeks DL, Ogniewski V, Ohno M, Niehrs C, Kjems J, Mattaj IW, Fornerod M. 1999. RanGTP-regulated interactions of CRM1 with nucleoporins and a shuttling DEAD-box helicase. *Mol Cell Biol* **19**:6276–85. doi:10.1128/MCB.19.9.6276.

Azimi M, Bulat E, Weis K, Mofrad MRK. 2014. An agent-based model for mRNA export through the nuclear pore complex. *Mol Biol Cell* **25**:3643–3653. doi:10.1091/mbc.E14-06-1065.

Baejen C, Torkler P, Gressel S, Essig K, Söding J, Cramer P. 2014. Transcriptome Maps of mRNP Biogenesis Factors Define Pre-mRNA Recognition. *Mol Cell* **55**:745–757. doi:https://doi.org/10.1016/j.molcel.2014.08.005.

Baker Brachmann C, Davies A, Cost GJ, Caputo E, Li J, Hieter P, Boeke JD. 1998. Designer deletion strains derived from Saccharomyces cerevisiae S288C: A useful set of strains and plasmids for PCR-mediated gene disruption and other applications. *Yeast* **14**:115–132. doi:10.1002/(SICI)1097-0061(19980130)14:2<115::AID-YEA204>3.0.CO;2-2.

Barhoom S, Kaur J, Cooperman BS, Smorodinsky NI, Smilansky Z, Ehrlich M, Elroy-Stein O. 2011. Quantitative single cell monitoring of protein synthesis at subcellular resolution using fluorescently labeled tRNA. *Nucleic Acids Res* **39**:e129–e129. doi:10.1093/nar/gkr601.

Baßler J, Hurt E. 2019. Eukaryotic Ribosome Assembly. *Annu Rev Biochem* **88**:8.1–8.26. doi:10.1146/annurev-biochem-013118-110817.

Batisse J, Batisse C, Budd A, Böttcher B, Hurt E. 2009. Purification of nuclear poly(A)-binding protein Nab2 reveals association with the yeast transcriptome and a messenger ribonucleoprotein core structure. *J Biol Chem* **284**:34911–7. doi:10.1074/jbc.M109.062034.

Beach DL, Salmon ED, Bloom K. 1999. Localization and anchoring of mRNA in budding yeast. *Curr Biol* **9**:569-S1. doi:https://doi.org/10.1016/S0960-9822(99)80260-7.

Bear J, Tan W, Zolotukhin AS, Tabernero C, Hudson EA, Felber BK. 1999. Identification of Novel Import and Export Signals of Human TAP, the Protein That Binds to the Constitutive Transport Element of the Type D Retrovirus mRNAs. *Mol Cell Biol* **19**:6306 LP-6317. doi:10.1128/MCB.19.9.6306.

Beißel C, Neumann B, Uhse S, Hampe I, Karki P, Krebber H. 2019. Translation termination depends on the sequential ribosomal entry of eRF1 and eRF3. *Nucleic Acids Reseach* **47**:9.4798-4813**.** doi:10.1093/nar/gkz177.

Bentley DL. 2014. Coupling mRNA processing with transcription in time and space. *Nat Rev Genet* **15**:163.

Bertrand E, Chartrand P, Schaefer M, Shenoy SM, Singer RH, Long RM. 1998a. Localization of ASH1 mRNA Particles in Living Yeast. *Mol Cell* **2**:437–445. doi:10.1016/S1097-2765(00)80143-4

Bertrand E, Chartrand P, Schaefer M, Shenoy SM, Singer RH, Long RM. 1998b. Localization of ASH1 mRNA Particles in Living Yeast. *Mol Cell* **2**:437–445.

doi:https://doi.org/10.1016/S1097-2765(00)80143-4.

Björk P, Wieslander L. 2014. Mechanisms of mRNA export. *Semin Cell Dev Biol* **32**:47–54. doi:https://doi.org/10.1016/j.semcdb.2014.04.027.

Boehm V, Gehring NH. 2016. Exon Junction Complexes: Supervising the Gene Expression Assembly Line. *Trends Genet* **32**:724–735. doi:10.1016/j.tig.2016.09.003.

Bohnsack MT, Regener K, Schwappach B, Saffrich R, Paraskeva E, Hartmann E, Görlich D. 2002. Exp5 exports eEF1A via tRNA from nuclei and synergizes with other transport pathways to confine translation to the cytoplasm. *EMBO J* **21**:6205 LP-6215. doi:10.1093/emboj/cdf613.

Bolger TA, Folkmann AW, Tran EJ, Wente SR. 2008. The mRNA Export Factor Gle1 and Inositol Hexakisphosphate Regulate Distinct Stages of Translation. *Cell* **134**:624–633. doi:http://dx.doi.org/10.1016/j.cell.2008.06.027.

Bonnet A, Palancade B. 2014. Regulation of mRNA Trafficking by Nuclear Pore Complexes 767–791. doi:10.3390/genes5030767.

Bossie MA, DeHoratius C, Barcelo G, Silver P. 1992. A mutant nuclear protein with similarity to RNA binding proteins interferes with nuclear import in yeast. *Mol Biol Cell* **3**:875–893. doi:10.1091/mbc.3.8.875.

Bradatsch B, Katahira J, Kowalinski E, Bange G, Yao W, Sekimoto T, Baumgärtel V, Boese G, Bassler J, Wild K, Peters R, Yoneda Y, Sinning I, Hurt E. 2007. Arx1 Functions as an Unorthodox Nuclear Export Receptor for the 60S Preribosomal Subunit. *Mol Cell* **27**:767–779. doi:10.1016/j.molcel.2007.06.034.

Brennan R, Haap-Hoff A, Gu L, Gautier V, Long A, Schröder M. 2018. Investigating nucleo-cytoplasmic shuttling of the human DEAD-box helicase DDX3. *Eur J Cell Biol*. doi:10.1016/J.EJCB.2018.08.001.

Brockmann C, Soucek S, Kuhlmann SI, Mills-Lujan K, Kelly SM, Yang J-C, Iglesias N, Stutz F, Corbett AH, Neuhaus D, Stewart M. 2012. Structural Basis for Polyadenosine-RNA Binding by Nab2 Zn Fingers and Its Function in mRNA Nuclear Export. *Structure* **20**:1007–1018. doi:https://doi.org/10.1016/j.str.2012.03.011.

Brohawn SG, Partridge JR, Whittle JRR, Schwartz TU. 2009. The nuclear pore complex has entered the atomic age. *Structure* **17**:1156–1168. doi:10.1016/j.str.2009.07.014.

Calado A, Treichel N, Müller E, Otto A, Kutay U. 2002. Exportin-5-mediated nuclear export of

eukaryotic elongation factor 1A and tRNA. *EMBO J* **21**:6216 LP-6224. doi:10.1093/emboj/cdf620.

Calero G, Wilson KF, Ly T, Rios-Steiner JL, Clardy JC, Cerione RA. 2002. Structural basis of m7GpppG binding to the nuclear cap-binding protein complex. *Nat Struct Biol* **9**:912–917. doi:10.1038/nsb874.

Caruthers JM, McKay DB. 2002. Helicase structure and mechanism. *Curr Opin Struct Biol* **12**:123–133. doi:https://doi.org/10.1016/S0959-440X(02)00298-1.

Chan PP, Lowe TM. 2008. GtRNAdb: a database of transfer RNA genes detected in genomic sequence. *Nucleic Acids Res* **37**:D93–D97. doi:10.1093/nar/gkn787.

Chang TH, Arenas J, Abelson J. 1990. Identification of five putative yeast RNA helicase genes. *Proc Natl Acad Sci* **87**:1571 LP-1575. doi:10.1073/pnas.87.4.1571.

Chao J a, Patskovsky Y, Almo SC, Singer RH. 2008. Structural basis for the coevolution of a viral RNA-protein complex. *Nat Struct Mol Biol* **15**:103–105. doi:10.1038/nsmb1327.

Chatterjee K, Majumder S, Wan Y, Shah V, Wu J, Huang H-Y, Hopper AK. 2017. Sharing the load: Mex67–Mtr2 cofunctions with Los1 in primary tRNA nuclear export. *Genes Dev* **31**:2186–2198. doi:10.1101/gad.305904.117.

Chen J, McSwiggen D, Ünal E. 2018. Single Molecule Fluorescence In Situ Hybridization (smFISH) Analysis in Budding Yeast Vegetative Growth and Meiosis. *JoVE* e57774. doi:doi:10.3791/57774.

Chen Y, Varani G. 2005. Protein families and RNA recognition. *FEBS J* **272**:2088–2097. doi:10.1111/j.1742-4658.2005.04650.x.

Cole CN, Heath CV, Hodge CA, Hammell CM, Amberg DCBT-M in E. 2002. Analysis of RNA exportGuide to Yeast Genetics and Molecular and Cell Biology Part C. Academic Press. pp. 568–587. doi:https://doi.org/10.1016/S0076-6879(02)51869-3.

Collins R, Karlberg T, Lehtiö L, Schütz P, van den Berg S, Dahlgren L-G, Hammarström M, Weigelt J, Schüler H. 2009. The DEXD/H-box RNA helicase DDX19 is regulated by an {alpha}-helical switch. *J Biol Chem* **284**:10296–300. doi:10.1074/jbc.C900018200.

Colquhoun D, G. HA, Bernard K. 1982. On the stochastic properties of bursts of single ion channel openings and of clusters of bursts. *Philos Trans R Soc London B, Biol Sci* **300**:1–59. doi:10.1098/rstb.1982.0156.

Cook AG, Fukuhara N, Jinek M, Conti E. 2009. Structures of the tRNA export factor in the

nuclear and cytosolic states. *Nature* **461**:60.

Cordin O, Tanner NK, Doère M, Linder P, Banroques J. 2004. The newly discovered Q motif of DEAD-box RNA helicases regulates RNA-binding and helicase activity. *EMBO J* **23**:2478 LP-2487.

Deribe YL, Pawson T, Dikic I. 2010. Post-translational modifications in signal integration. *Nat Struct &Amp; Mol Biol* **17**:666.

Dever TE, Green R. 2012. The Elongation, Termination, and Recycling Phases of Translation in Eukaryotes. *Cold Spring Harb Perspect Biol* **4**. doi:10.1101/cshperspect.a013706.

Dhungel N, Hopper AK. 2012. Beyond tRNA cleavage: novel essential function for yeast tRNA splicing endonuclease unrelated to tRNA processing. *Genes Dev* **26**:503–514. doi:10.1101/gad.183004.111.

Dieppois G, Stutz F. 2010. Connecting the transcription site to the nuclear pore: a multi-tether process that regulates gene expression. *J Cell Sci* **123**:1989–1999. doi:10.1242/jcs.053694

Dossani ZY, Weirich CS, Erzberger JP, Berger JM, Weis K. 2009. Structure of the C-terminus of the mRNA export factor Dbp5 reveals the interaction surface for the ATPase activator Gle1. *Proc Natl Acad Sci U S A* **106**:16251–16256. doi:10.1073/pnas.0902251106.

Egloff S, Dienstbier M, Murphy S. 2012. Updating the RNA polymerase CTD code: adding gene-specific layers. *Trends Genet* **28**:333–341. doi:https://doi.org/10.1016/j.tig.2012.03.007.

Estruch F, Cole CN. 2003. An Early Function during Transcription for the Yeast mRNA Export Factor Dbp5p / Rat8p Suggested by Its Genetic and Physical Interactions with Transcription Factor IIH Components **14**:1664–1676. doi:10.1091/mbc.E02.

Estruch F, Hodge C, Gómez-Navarro N, Peiró-Chova L, Heath C V, Cole CN. 2012. Insights into mRNP biogenesis provided by new genetic interactions among export and transcription factors. *BMC Genet* **13**:80. doi:10.1186/1471-2156-13-80.

Fahrenkrog B, Aebi U. 2003. The nuclear pore complex: nucleocytoplasmic transport and beyond. *Nat Rev Mol Cell Biol* **4**:757–766. doi:10.1038/nrm1230.

Fairman-Williams ME, Guenther U-P, Jankowsky E. 2010. SF1 and SF2 : family matters **20**:313–324. doi:10.1016/j.sbi.2010.03.011.SF1.

Fan JS, Cheng Z, Zhang J, Noble C, Zhou Z, Song H, Yang D. 2009. Solution and crystal structures of mRNA exporter Dbp5p and its interaction with nucleotides. *J Mol Biol* **388**:1–

10. doi:10.1016/j.jmb.2009.03.004.

Faza MB, Chang Y, Occhipinti L, Kemmler S, Panse VG. 2012. Role of Mex67-Mtr2 in the Nuclear Export of 40S Pre-Ribosomes. *PLoS Genet* **8**:16–21. doi:10.1371/journal.pgen.1002915.

Feaver WJ, Svejstrup JQ, Bardwell L, Bardwell AJ, Buratowski S, Gulyas KD, Donahue TF, Friedberg EC, Kornberg RD. 1993. Dual roles of a multiprotein complex from S. cerevisiae in transcription and DNA repair. *Cell* **75**:1379–1387. doi:https://doi.org/10.1016/0092-8674(93)90624-Y.

Femino AM, Fay FS, Fogarty K, Singer RH. 1998. Visualization of Single RNA Transcripts in Situ. *Science (80-)* **280**:585 LP-590. doi:10.1126/science.280.5363.585.

Feng Q, Düring L, de Mayolo AA, Lettier G, Lisby M, Erdeniz N, Mortensen UH, Rothstein R. 2007. Rad52 and Rad59 exhibit both overlapping and distinct functions. *DNA Repair (Amst)* **6**:27–37. doi:10.1016/J.DNAREP.2006.08.007.

Floch AG, Palancade B, Doye V. 2014. Chapter 1 - Fifty Years of Nuclear Pores and Nucleocytoplasmic Transport Studies: Multiple Tools Revealing Complex Rules In: Doye V, editor. Nuclear Pore Complexes and Nucleocytoplasmic Transport - Methods, Methods in Cell Biology. Academic Press. pp. 1–40. doi:https://doi.org/10.1016/B978-0-12-417160-2.00001-1.

Folkmann A, Noble K, Cole C, Wente S. 2011. Dbp5, Gle1-IP6 and Nup159: a working model for mRNP export. *Nucleus* **2**:540–8. doi:10.4161/nucl.2.6.17881.

Follain G, Mercier L, Osmani N, Harlepp S, Goetz JG. 2017. Seeing is believing – multi-scale spatio-temporal imaging towards in vivo cell biology. *J Cell Sci* **130**:23 LP-38. doi:10.1242/jcs.189001.

Fornerod M, Ohno M, Yoshida M, Mattaj IW. 1997. CRM1 Is an Export Receptor for Leucine-Rich Nuclear Export Signals. *Cell* **90**:1051–1060. doi:10.1016/S0092-8674(00)80371-2

Fribourg S, Braun IC, Izaurralde E, Conti E. 2001. Structural Basis for the Recognition of a Nucleoporin FG Repeat by the NTF2-like Domain of the TAP/p15 mRNA Nuclear Export Factor. *Mol Cell* **8**:645–656. doi:https://doi.org/10.1016/S1097-2765(01)00348-3.

Fried H, Kutay U. 2003. Nucleocytoplasmic transport: taking an inventory. *Cell Mol Life Sci C* **60**:1659–1688. doi:10.1007/s00018-003-3070-3.

Fromont-Racine M, Senger B, Saveanu C, Fasiolo F. 2003. Ribosome assembly in eukaryotes.

Gene **313**:17–42. doi:https://doi.org/10.1016/S0378-1119(03)00629-2.

Fukuda M, Asano S, Nakamura T, Adachi M, Yoshida M, Yanagida M, Nishida E. 1997. CRM1 is responsible for intracellular transport mediated by the nuclear export signal. *Nature* **390**:308–311. doi:10.1038/36894.

Galy V, Gadal O, Fromont-Racine M, Romano A, Jacquier A, Nehrbass U. 2004. Nuclear Retention of Unspliced mRNAs in Yeast Is Mediated by Perinuclear Mlp1. *Cell* **116**:63–73. doi:https://doi.org/10.1016/S0092-8674(03)01026-2.

Garcia JF, Parker R. 2016. Ubiquitous accumulation of 3′ mRNA decay fragments in Saccharomyces cerevisiae mRNAs with chromosomally integrated MS2 arrays. *RNA* **22**:657–659. doi:10.1261/rna.056325.116.

Garcia JF, Parker R. 2015. MS2 coat proteins bound to yeast mRNAs block 5′ to 3′ degradation and trap mRNA decay products: Implications for the localization of mRNAs by MS2-MCP system. *Rna* **21**:1393–1395. doi:10.1261/rna.051797.115.

Geisberg J V, Holstege FC, Young RA, Struhl K. 2001. Yeast NC2 Associates with the RNA Polymerase II Preinitiation Complex and Selectively Affects Transcription In Vivo. *Mol Cell Biol* **21**:2736 LP-2742. doi:10.1128/MCB.21.8.2736-2742.2001.

Ghavidel A, Kislinger T, Pogoutse O, Sopko R, Jurisica I, Emili A. 2007. Impaired tRNA Nuclear Export Links DNA Damage and Cell-Cycle Checkpoint. *Cell* **131**:915–926. doi:10.1016/j.cell.2007.09.042.

Gibbons JD, Chakraborti S. 2011. Nonparametric Statistical Inference BT - International Encyclopedia of Statistical Science In: Lovric M, editor. Berlin, Heidelberg: Springer Berlin Heidelberg. pp. 977–979. doi:10.1007/978-3-642-04898-2_420.

Gietz RD, Woods RA. 2002. Transformation of yeast by lithium acetate/single-stranded carrier DNA/polyethylene glycol method. *Methods Enzymol* **350**:87–96. doi:10.1016/S0076-6879(02)50957-5.

Gleizes P-E, Noaillac-Depeyre J, Léger-Silvestre I, Teulières F, Dauxois J-Y, Pommet D, Azum-Gelade M-C, Gas N. 2001. Ultrastructural localization of rRNA shows defective nuclear export of preribosomes in mutants of the Nup82p complex. *J Cell Biol* **155**:923 LP-936. doi:10.1083/jcb.200108142.

Glisovic T, Bachorik JL, Yong J, Dreyfuss G. 2008. RNA-binding proteins and post-transcriptional gene regulation. *FEBS Lett* **582**:1977–1986.

doi:10.1016/j.febslet.2008.03.004.

Glover-Cutter K, Kim S, Espinosa J, Bentley DL. 2007. RNA polymerase II pauses and associates with pre-mRNA processing factors at both ends of genes. *Nat Struct &Amp; Mol Biol* **15**:71.

Gorbalenya AE, Koonin E V. 1993. Helicases: amino acid sequence comparisons and structure-function relationships. *Curr Opin Struct Biol* **3**:419–429. doi:https://doi.org/10.1016/S0959-440X(05)80116-2.

Görlich D, Kutay U. 1999. Transport Between the Cell Nucleus and the Cytoplasm. *Annu Rev Cell Dev Biol* **15**:607–660. doi:10.1146/annurev.cellbio.15.1.607.

Gorsch LC, Dockendorff TC, Cole CN. 1995. A conditional allele of the novel repeat-containing yeast nucleoporin RAT7/NUP159 causes both rapid cessation of mRNA export and reversible clustering of nuclear pore complexes. *J Cell Biol* **129**:939 LP-955.

Granneman S, Baserga SJ. 2004. Ribosome biogenesis: of knobs and RNA processing. *Exp Cell Res* **296**:43–50. doi:https://doi.org/10.1016/j.yexcr.2004.03.016.

Green DM, Johnson CP, Hagan H, Corbett AH. 2003. The C-terminal domain of myosin-like protein 1 (Mlp1p) is a docking site for heterogeneous nuclear ribonucleoproteins that are required for mRNA export. *Proc Natl Acad Sci U S A* **100**:1010–1015. doi:10.1073/pnas.0336594100.

Gross T, Siepmann A, Sturm D, Windgassen M, Scarcelli JJ, Seedorf M, Cole CN, Krebber H. 2007. The DEAD-box RNA helicase Dbp5 functions in translation termination. *Science* **315**:646–9. doi:10.1126/science.1134641.

Grünwald D, Singer RH. 2010. In vivo imaging of labelled endogenous β-actin mRNA during nucleocytoplasmic transport. *Nature* **467**:604–7. doi:10.1038/nature09438.

Grüter P, Tabernero C, von Kobbe C, Schmitt C, Saavedra C, Bachi A, Wilm M, Felber BK, Izaurralde E. 1998. TAP, the Human Homolog of Mex67p, Mediates CTE-Dependent RNA Export from the Nucleus. *Mol Cell* **1**:649–659. doi:https://doi.org/10.1016/S1097-2765(00)80065-9.

Güldener U, Heck S, Fiedler T, Beinhauer J, Hegemann JH, Gießen J, Straße F. 1996. <KanMX-loxP.pdf> **24**:2519–2524.

Haim L, Zipor G, Aronov S, Gerst JE. 2007. A genomic integration method to visualize localization of endogenous mRNAs in living yeast. *Nat Methods* **4**:409–412.

doi:10.1038/nmeth1040.

Haimovich G, Zabezhinsky D, Haas B, Slobodin B, Purushothaman P, Fan L, Levin JZ, Nusbaum C, Gerst JE. 2016. Use of the MS2 aptamer and coat protein for RNA localization in yeast: A response to "MS2 coat proteins bound to yeast mRNAs block 5′ to 3′ degradation and trap mRNA decay products: implications for the localization of mRNAs by MS2-MCP system." *RNA* **22**:660–666. doi:10.1261/rna.055095.115 .

Halstead JM, Lionnet T, Wilbertz JH, Wippich F, Ephrussi A, Singer RH, Chao JA. 2015. An RNA biosensor for imaging the first round of translation from single cells to living animals. *Science (80)* **347**:1367 LP-1671. doi:10.1126/science.aaa3380.

Haruki H, Nishikawa J, Laemmli UK. 2008. The Anchor-Away Technique: Rapid, Conditional Establishment of Yeast Mutant Phenotypes. *Mol Cell* **31**:925–932. doi:10.1016/j.molcel.2008.07.020.

Heinrich S, Derrer CP, Lari A, Weis K, Montpetit B. 2017a. Temporal and spatial regulation of mRNA export: Single particle RNA-imaging provides new tools and insights. *BioEssays* **39**. doi:10.1002/bies.201600124.

Heinrich S, Sidler CL, Azzalin CM, Weis K. 2017. Stem-loop RNA labeling can affect nuclear and cytoplasmic mRNA processing. *Rna* **23**:134–141. doi:10.1261/rna.057786.116

Hellmuth K, Lau DM, Bischoff FR, Künzler M, Hurt E, Simos G. 1998. Yeast Los1p Has Properties of an Exportin-Like Nucleocytoplasmic Transport Factor for tRNA. *Mol Cell Biol* **18**:6374 LP-6386. doi:10.1128/MCB.18.11.6374.

Henn A, Cao W, Hackney DD, De La Cruz EM. 2008. The ATPase Cycle Mechanism of the DEAD-box rRNA Helicase, DbpA. *J Mol Biol* **377**:193–205. doi:https://doi.org/10.1016/j.jmb.2007.12.046.

Hieronymus H, Yu MC, Silver PA. 2004. Genome-wide mRNA surveillance is coupled to mRNA export. *Genes Dev* **18**:2652–2662. doi:10.1101/gad.1241204.

Hilbert M, Karow AR, Klostermeier D. 2009. The mechanism of ATP-dependent RNA unwinding by DEAD box proteins. *Biol Chem* **390**:1237–1250. doi:10.1515/BC.2009.135

Hocine S, Raymond P, Zenklusen D, Chao JA, Singer RH. 2013. Single-molecule analysis of gene expression using two-color RNA labeling in live yeast. *Nat Meth* **10**:119–121.

Hodge C, Colot HV, Stafford P, Cole CN. 1999. Rat8p/Dbp5p is a shuttling transport factor that interacts with Rat7p/Nup159p and Gle1p and suppresses the mRNA export defect of xpo1-1

cells. *EMBO J* **18**:5778–88. doi:10.1093/emboj/18.20.5778.

Hodge CA, Tran EJ, Noble KN, Alcazar-Roman AR, Ben-Yishay R, Scarcelli JJ, Folkmann AW, Shav-Tal Y, Wente SR, Cole CN. 2011. The Dbp5 cycle at the nuclear pore complex during mRNA export I: Dbp5 mutants with defects in RNA binding and ATP hydrolysis define key steps for Nup159 and Gle1. *Genes Dev* **25**:1052–1064. doi:10.1101/gad.2041611.

Hodroj D, Recolin B, Serhal K, Martinez S, Tsanov N, Abou Merhi R, Maiorano D. 2017. An ATR-dependent function for the Ddx19 RNA helicase in nuclear R-loop metabolism. *EMBO J*. **6**(9):1182-1198. doi: 10.15252/embj.201695131.

Hogan DJ, Riordan DP, Gerber AP, Herschlag D, Brown PO. 2008. Diverse RNA-Binding Proteins Interact with Functionally Related Sets of RNAs, Suggesting an Extensive Regulatory System. *PLOS Biol* **6**:e255.

Hopper AK. 2013. Transfer RNA Post-Transcriptional Processing, Turnover, and Subcellular Dynamics in the Yeast Saccharomyces cerevisiae *Genetics* **194**:43 LP-67.

Hopper AK, Phizicky EM. 2003. tRNA transfers to the limelight. *Genes Dev* **17**:162–180. doi:10.1101/gad.1049103.

Hopper AK, Schultz LD, Shapiro RA. 1980. Processing of intervening sequences: a new yeast mutant which fails to excise intervening sequences from precursor tRNAs. *Cell* **19**:741–751. doi:10.1016/S0092-8674(80)80050-X.

Hsin J-P, Manley JL. 2012. The RNA polymerase II CTD coordinates transcription and RNA processing. *Genes Dev* **26**:2119–2137. doi:10.1101/gad.200303.112.

Huang H-Y, Hopper A. 2016. Multiple Layers of Stress-Induced Regulation in tRNA Biology. *Life* **6**:16. doi:10.3390/life6020016.

Huang HY, Hopper AK. 2015. In vivo biochemical analyses reveal distinct roles of Beta-importins and eEF1A in tRNA subcellular traffic. *Genes Dev* **29**:772–783. doi:10.1101/gad.258293.115.

Huh W-K, Falvo J V, Gerke LC, Carroll AS, Howson RW, Weissman JS, O'Shea EK. 2003. Global analysis of protein localization in budding yeast. *Nature* **425**:686–691. doi:10.1038/nature02026.

Hung N-J, Lo K-Y, Patel SS, Helmke K, Johnson AW. 2008. Arx1 is a nuclear export receptor for the 60S ribosomal subunit in yeast. *Mol Biol Cell* **19**:735–744. doi:10.1091/mbc.e07-09-

0968.

Hurowitz EH, Brown PO. 2004. Genome-wide analysis of mRNA lengths in Saccharomyces cerevisiae. *Genome Biol* **5**:R2–R2. doi:10.1186/gb-2003-5-1-r2.

Hurt E, Hannus S, Schmelzl B, Lau D, Tollervey D, Simos G. 1999. A Novel In Vivo Assay Reveals Inhibition of Ribosomal Nuclear Export in Ran-Cycle and Nucleoporin Mutants. *J Cell Biol* **144**:389 LP-401. doi:10.1083/jcb.144.3.389.

Hurt E, Strasser K, Segref A, Bailer S, Schlaich N, Presutti C, Tollervey D, Jansen R. 2000. Mex67p mediates nuclear export of a variety of RNA polymerase II transcripts. *J Biol Chem* **275**:8361–8368.

Iglesias N, Tutucci E, Gwizdek C, Vinciguerra P, Von Dach E, Corbett AH, Dargemont C, Stutz F. 2010. Ubiquitin-mediated mRNP dynamics and surveillance prior to budding yeast mRNA export. *Genes Dev* **24**:1927–1938. doi:10.1101/gad.583310.

Izawa S, Takemura R, Ikeda K, Fukuda K, Wakai Y, Inoue Y. 2005. Characterization of Rat8 localization and mRNA export in Saccharomyces cerevisiae during the brewing of Japanese sake. *Appl Microbiol Biotechnol* **69**:86–91. doi:10.1007/s00253-005-1954-x.

Janke C, Magiera MM, Rathfelder N, Taxis C, Reber S, Maekawa H, Moreno-Borchart A, Doenges G, Schwob E, Schiebel E, Knop M. 2004. A versatile toolbox for PCR-based tagging of yeast genes: new fluorescent proteins, more markers and promoter substitution cassettes. *Yeast* **21**:947–962. doi:10.1002/yea.1142.

Jarmoskaite I, Russell R. 2011. DEAD-box proteins as RNA helicases and chaperones. *Wiley Interdiscip Rev RNA* **2**:135–152. doi:10.1002/wrna.50.

Johnson AW, Lund E, Dahlberg J. 2002. Nuclear export of ribosomal subunits. *Trends Biochem Sci* **27**:580–585. doi:10.1016/S0968-0004(02)02208-9.

Johnson SA, Cubberley G, Bentley DL. 2009. Cotranscriptional Recruitment of the mRNA Export Factor Yra1 by Direct Interaction with the 3′ End Processing Factor Pcf11. *Mol Cell* **33**:215–226. doi:https://doi.org/10.1016/j.molcel.2008.12.007.

Johnson SA, Kim H, Erickson B, Bentley DL. 2011. The export factor Yra1 modulates mRNA 3′ end processing. *Nat Struct &Amp; Mol Biol* **18**:1164.

Kaffman A, Rank NM, O'Neill EM, Huang LS, O'Shea EK. 1998. The receptor Msn5 exports the phosphorylated transcription factor Pho4 out of the nucleus. *Nature* **396**:482–486. doi:10.1038/24898.

Kang Y, Cullen BR. 1999. The human Tap protein is a nuclear mRNA export factor that contains novel RNA-binding and nucleocytoplasmic transport sequences. *Genes Dev* **13**:1126–1139.

Karkusiewicz I, Turowski TW, Graczyk D, Towpik J, Dhungel N, Hopper AK, Boguta M. 2011. Maf1 Protein, Repressor of RNA Polymerase III, Indirectly Affects tRNA Processing. *J Biol Chem* **286**:39478–39488. doi:10.1074/jbc.M111.253310 .

Katahira J, Sträßer K, Podtelejnikov A, Mann M, Jung JU, Hurt E. 1999. The Mex67p-mediated nuclear mRNA export pathway is conserved from yeast to human. *EMBO J* **18**:2593 LP-2609. doi:10.1093/emboj/18.9.2593.

Kay SM. 1993. Fundamentals of Statistical Signal Processing, Volume **I**: Estimation Theory. Prentice Hall, Upper Saddle River, NJ**.** 625 pp.

Kelly SM, Leung SW, Apponi LH, Bramley AM, Tran EJ, Chekanova JA, Wente SR, Corbett AH. 2010. Recognition of Polyadenosine RNA by the Zinc Finger Domain of Nuclear Poly(A) RNA-binding Protein 2 (Nab2) Is Required for Correct mRNA 3′-End Formation*. *J Biol Chem* **285**:26022–26032. doi:10.1074/jbc.M110.141127.

Kikuma T, Ohtsu M, Utsugi T, Koga S, Okuhara K, Eki T, Fujimori F, Murakami Y. 2004. Dbp9p, a Member of the DEAD Box Protein Family, Exhibits DNA Helicase Activity. *J Biol Chem* **279**:20692–20698. doi:10.1074/jbc.M400231200.

Kohler A, Hurt E. 2007. Exporting RNA from the nucleus to the cytoplasm. *Nat Rev Mol Cell Biol* **8**:761–773. doi:10.1038/nrm2255

Köhler A, Hurt E. 2007. Exporting RNA from the nucleus to the cytoplasm. *Nat Rev Mol Cell Biol* **8**:761–73. doi:10.1038/nrm2255.

Kosugi S, Hasebe M, Matsumura N, Takashima H, Miyamoto-Sato E, Tomita M, Yanagawa H. 2009. Six classes of nuclear localization signals specific to different binding grooves of importin?? *J Biol Chem* **284**:478–485. doi:10.1074/jbc.M807017200.

Kressler D, Linder P. 1999. MINIREVIEW Protein trans -Acting Factors Involved in Ribosome Biogenesis in Saccharomyces cerevisiae **19**:7897–7912.

Kubitscheck U, Grünwald D, Hoekstra A, Rohleder D, Kues T, Siebrasse JP, Peters R. 2005. Nuclear transport of single molecules. *J Cell Biol* **168**:233 LP-243. doi:10.1083/jcb.200411005.

Kühn U, Wahle E. 2004. Structure and function of poly(A) binding proteins. *Biochim Biophys Acta - Gene Struct Expr* **1678**:67–84. doi:https://doi.org/10.1016/j.bbaexp.2004.03.008.

La Cour T, Kiemer L, Mølgaard A, Gupta R, Skriver K, Brunak S. 2004. Analysis and prediction of leucine-rich nuclear export signals. *Protein Eng Des Sel* **17**:527–536. doi:10.1093/protein/gzh062.

Lapetina DL, Ptak C, Roesner UK, Wozniak RW. 2017. Yeast silencing factor Sir4 and a subset of nucleoporins form a complex distinct from nuclear pore complexes. *J Cell Biol* **216**:3145 LP-3159.

Lari A, Arul Nambi Rajan A, Sandhu R, Reiter T, Montpetit R, Young BP, Loewen CJR, Montpetit B. 2019. A nuclear role for the DEAD-box protein Dbp5 in tRNA export. *Elife* **8**:e48410. doi:10.7554/eLife.48410.

Larson DR, Zenklusen D, Wu B, Chao JA, Singer RH. 2011. Real-Time Observation of Transcription Initiation and Elongation on an Endogenous Yeast Gene. *Science (80-)* **332**:475 LP-478. doi:10.1126/science.1202142.

Lee SJ, Jiko C, Yamashita E, Tsukihara T. 2011. Selective nuclear export mechanism of small RNAs. *Curr Opin Struct Biol* **21**:101–108. doi:https://doi.org/10.1016/j.sbi.2010.11.004.

Lejeune F, Ranganathan AC, Maquat LE. 2004. eIF4G is required for the pioneer round of translation in mammalian cells. *Nat Struct Mol Biol* **11**:992–1000. doi:10.1038/nsmb824.

Lévesque L, Guzik B, Guan T, Coyle J, Black BE, Rekosh D, Hammarskjöld M-L, Paschal BM. 2001. RNA Export Mediated by Tap Involves NXT1-dependent Interactions with the Nuclear Pore Complex. *J Biol Chem* **276**:44953–44962. doi:10.1074/jbc.M106558200.

Lewis A, Felberbaum R, Hochstrasser M. 2007. A nuclear envelope protein linking nuclear pore basket assembly, SUMO protease regulation, and mRNA surveillance. *J Cell Biol* **178**:813 LP-827. doi:10.1083/jcb.200702154.

Li Z, Deutscher MP. 1996. Maturation Pathways for E. coli tRNA Precursors: A Random Multienzyme Process In Vivo. *Cell* **86**:503–512. doi:10.1016/S0092-8674(00)80123-3.

Li Z, Vizeacoumar FJ, Bahr S, Li J, Warringer J, Vizeacoumar FS, Min R, VanderSluis B, Bellay J, DeVit M, Fleming JA, Stephens A, Haase J, Lin Z-Y, Baryshnikova A, Lu H, Yan Z, Jin K, Barker S, Datti A, Giaever G, Nislow C, Bulawa C, Myers CL, Costanzo M, Gingras A-C, Zhang Z, Blomberg A, Bloom K, Andrews B, Boone C. 2011. Systematic exploration of essential yeast gene function with temperature-sensitive mutants. *Nat Biotechnol* **29**:361.

Liker E, Fernandez E, Izaurralde E, Conti E. 2000. The structure of the mRNA export factor TAP reveals a cis arrangement of a non-canonical RNP domain and an

LRR domain. *EMBO J* **19**:5587 LP-5598. doi:10.1093/emboj/19.21.5587.

Lin D, Yin X, Wang X, Zhou P, Guo F-B. 2013. Re-Annotation of Protein-Coding Genes in the Genome of Saccharomyces cerevisiae Based on Support Vector Machines. *PLoS One* **8**:e64477.

Linder P. 2006. Dead-box proteins: A family affair - Active and passive players in RNP-remodeling. *Nucleic Acids Res* **34**:4168–4180. doi:10.1093/nar/gkl468.

Linder P, Jankowsky E. 2011. From unwinding to clamping - the DEAD box RNA helicase family. *Nat Rev Mol Cell Biol* **12**:505–16. doi:10.1038/nrm3154.

Lipowsky G, Bischoff FR, Izaurralde E, Kutay U, Schafer S, Gross HJ, Beier H, Gorlich D. 1999. Coordination of tRNA nuclear export with processing of tRNA. *RNA* **5**:539–549. doi:DOI: 10.1017/S1355838299982134.

Listerman I, Sapra AK, Neugebauer KM. 2006. Cotranscriptional coupling of splicing factor recruitment and precursor messenger RNA splicing in mammalian cells. *Nat Struct Mol Biol* **13**:815–822. doi:10.1038/nsmb1135.

Livak KJ, Schmittgen TD. 2001. Analysis of Relative Gene Expression Data Using Real-Time Quantitative PCR and the 2−ΔΔCT Method. *Methods* **25**:402–408. doi:https://doi.org/10.1006/meth.2001.1262.

Logan J, Falck-Pedersen E, Darnell JE, Shenk T. 1987. A poly(A) addition site and a downstream termination region are required for efficient cessation of transcription by RNA polymerase II in the mouse beta maj-globin gene. *Proc Natl Acad Sci* **84**:8306 LP-8310. doi:10.1073/pnas.84.23.8306.

Longtine MS, Mckenzie III A, Demarini DJ, Shah NG, Wach A, Brachat A, Philippsen P, Pringle JR. 1998. Additional modules for versatile and economical PCR-based gene deletion and modification in Saccharomyces cerevisiae. *Yeast* **14**:953–961. doi:10.1002/(SICI)1097-0061(199807)14:10<953::AID-YEA293>3.0.CO;2-U,

Lund MK, Guthrie C. 2005. The DEAD-box protein Dbp5p is required to dissociate Mex67p from exported mRNPs at the nuclear rim. *Mol Cell* **20**:645–51. doi:10.1016/j.molcel.2005.10.005.

Lunde BM, Moore C, Varani G. 2007. RNA-binding proteins: modular design for efficient function. *Nat Rev Mol Cell Biol* **8**:479.

Ma J, Liu Z, Michelotti N, Pitchiaya S, Veerapaneni R, Androsavich JR, Walter NG, Yang W.

2013. High-resolution three-dimensional mapping of mRNA export through the nuclear pore. *Nat Commun* **4**:2414.

Mangus DA, Evans MC, Jacobson A. 2003. Poly(A)-binding proteins: multifunctional scaffolds for the post-transcriptional control of gene expression. *Genome Biol* **4**:223. doi:10.1186/gb-2003-4-7-223.

Maquat LE. 2004. Nonsense-mediated mRNA decay: splicing, translation and mRNP dynamics. *Nat Rev Mol Cell Biol* **5**:89–99. doi:10.1038/nrm1310.

Maquat LE, Tarn W-Y, Isken O. 2010. The Pioneer Round of Translation: Features and Functions. *Cell* **142**:368–374. doi:https://doi.org/10.1016/j.cell.2010.07.022.

Matsuoka S, Ballif BA, Smogorzewska A, McDonald ER, Hurov KE, Luo J, Bakalarski CE, Zhao Z, Solimini N, Lerenthal Y, Shiloh Y, Gygi SP, Elledge SJ. 2007. ATM and ATR Substrate Analysis Reveals Extensive Protein Networks Responsive to DNA Damage. *Science (80-)* **316**:1160 LP-1166. doi:10.1126/science.1140321.

Maurer P, Redd M, Solsbacher J, Bischoff FR, Greiner M, Podtelejnikov A V, Mann M, Stade K, Weis K, Schlenstedt G. 2001. The nuclear export receptor Xpo1p forms distinct complexes with NES transport substrates and the yeast Ran binding protein 1 (Yrb1p). *Mol Biol Cell* **12**:539–49.

Mazza C, Segref A, Mattaj IW, Cusack S. 2002. Large-scale induced fit recognition of an m⁷GpppG cap analogue by the human nuclear cap-binding complex. *EMBO J* **21**:5548 LP-5557. doi:10.1093/emboj/cdf538.

Mehlin H, Daneholt B, Skoglund U. 1995. Structural interaction between the nuclear pore complex and a specific translocating RNP particle. *J Cell Biol* **129**:1205 LP-1216. doi:10.1083/jcb.129.5.1205.

Mendoza-Ochoa GI, Barrass JD, Terlouw BR, Maudlin IE, Lucas S, Sani E, Aslanzadeh V, Reid JAE, Beggs JD. 2019. A fast and tuneable auxin-inducible degron for depletion of target proteins in budding yeast. *Yeast* **36**:75–81. doi:10.1002/yea.3362.

Mikhailova T, Shuvalova E, Ivanov A, Susorov D, Shuvalov A, Kolosov PM, Alkalaeva E. 2016. RNA helicase DDX19 stabilizes ribosomal elongation and termination complexes. *Nucleic Acids Res* gkw1239-. doi:10.1093/nar/gkw1239.

Miller AL, Suntharalingam M, Johnson SL, Audhya A, Emr SD, Wente SR. 2004. Cytoplasmic inositol hexakisphosphate production is sufficient for mediating the Gle1-mRNA export

pathway. *J Biol Chem* **279**:51022–32. doi:10.1074/jbc.M409394200.

Miller C, Schwalb B, Maier K, Schulz D, Dümcke S, Zacher B, Mayer A, Sydow J, Marcinowski L, Dölken L, Martin DE, Tresch A, Cramer P. 2011. Dynamic transcriptome analysis measures rates of mRNA synthesis and decay in yeast. *Mol Syst Biol* **7**:458. doi:10.1038/msb.2010.112.

Miyagawa R, Mizuno R, Watanabe K, Ijiri K. 2012. Formation of tRNA granules in the nucleus of heat-induced human cells. *Biochem Biophys Res Commun* **418**:149–155. doi:https://doi.org/10.1016/j.bbrc.2011.12.150.

Mohr G, Del Campo M, Turner KG, Gilman B, Wolf RZ, Lambowitz AM. 2011. High-Throughput Genetic Identification of Functionally Important Regions of the Yeast DEAD-Box Protein Mss116p. *J Mol Biol* **413**:952–972. doi:10.1016/J.JMB.2011.09.015.

Montpetit B, Thomsen ND, Helmke KJ, Seeliger MA, Berger JM, Weis K. 2011. A conserved mechanism of DEAD-box ATPase activation by nucleoporins and InsP6 in mRNA export. *Nature* **472**:238–242.

Moore MJ. 2005. From birth to death: the complex lives of eukaryotic mRNAs. *Science (80-)* **309**:1514–1518.

Mor A, Suliman S, Ben-Yishay R, Yunger S, Brody Y, Shav-Tal Y. 2010. Dynamics of single mRNP nucleocytoplasmic transport and export through the nuclear pore in living cells. *Nat Cell Biol* **12**:543–552. doi:10.1038/ncb2056

Mori T, Ogasawara C, Inada T, Englert M, Beier H, Takezawa M, Endo T, Yoshihisa T. 2010. Dual Functions of Yeast tRNA Ligase in the Unfolded Protein Response: Unconventional Cytoplasmic Splicing of HAC1 Pre-mRNA Is Not Sufficient to Release Translational Attenuation. *Mol Biol Cell* **21**:3722–3734. doi:10.1091/mbc.e10-08-0693.

Müller-McNicoll M, Neugebauer KM. 2013. How cells get the message: dynamic assembly and function of mRNA–protein complexes. *Nat Rev Genet* **14**:275.

Munchel SE, Shultzaberger RK, Takizawa N, Weis K. 2011. Dynamic profiling of mRNA turnover reveals gene-specific and system-wide regulation of mRNA decay. *Mol Biol Cell* **22**:2787–2795. doi:10.1091/mbc.e11-01-0028.

Murphy R, Wente SR. 1996. An RNA-export mediator with an essential nuclear export signal. *Nature* **383**:357–360.

Murthi A, Shaheen HH, Huang H-Y, Preston MA, Lai T-P, Phizicky EM, Hopper AK. 2010.

Regulation of tRNA bidirectional nuclear-cytoplasmic trafficking in Saccharomyces cerevisiae. *Mol Biol Cell* **21**:639–649. doi:10.1091/mbc.E09-07-0551.

Musser SM, Grünwald D. 2016. Deciphering the Structure and Function of Nuclear Pores Using Single-Molecule Fluorescence Approaches. *J Mol Biol* **428**:2091–2119. doi:https://doi.org/10.1016/j.jmb.2016.02.023.

Napetschnig J, Kassube S a, Debler EW, Wong RW, Blobel G, Hoelz A. 2009. Structural and functional analysis of the interaction between the nucleoporin Nup214 and the DEAD-box helicase Ddx19. *Proc Natl Acad Sci U S A* **106**:3089–94. doi:10.1073/pnas.0813267106.

Natarajan K, Meyer MR, Belinda M, Slade D, Roberts C, Alan G, Marton MJ, Jackson BM, Hinnebusch AG. 2001. Transcriptional Profiling Shows that Gcn4p Is a Master Regulator of Gene Expression during Amino Acid Starvation in Yeast Transcriptional Profiling Shows that Gcn4p Is a Master Regulator of Gene Expression during Amino Acid Starvation in Yeast. *Mol Cell Biol* **21**:4347–4368. doi:10.1128/MCB.21.13.4347.

Nazar R. 2004. Ribosomal RNA Processing and Ribosome Biogenesis in Eukaryotes. *IUBMB Life* **56**:457–465. doi:10.1080/15216540400010867.

Neumann B, Wu H, Hackmann A, Krebber H. 2016. Nuclear export of pre-ribosomal subunits requires Dbp5, but not as an RNA-helicase as for mRNA export. *PLoS One* **11**. doi:10.1371/journal.pone.0149571.

Neville M, Rosbash M. 1999. The NES–Crm1p export pathway is not a major mRNA export route in Saccharomyces cerevisiae *EMBO J* **18**:3746 LP-3756.

Nilsen TW, Graveley BR. 2010. Expansion of the eukaryotic proteome by alternative splicing. *Nature* **463**:457.

Niño CA, Hérissant L, Babour A, Dargemont C. 2013. mRNA Nuclear Export in Yeast. *Chem Rev* **113**:8523–8545. doi:10.1021/cr400002g.

Noble KN, Tran EJ, Alcázar-Román AR, Hodge C a, Cole CN, Wente SR. 2011. The Dbp5 cycle at the nuclear pore complex during mRNA export II: Nucleotide cycling and mRNP remodeling by Dbp5 are controlled by Nup159 and Gle1. *Genes Dev* **25**:4065–1077. doi:10.1101/gad.2040611.

O'Connor J., Peebles CL. 1991. In vivo pre-tRNA processing in Saccharomyces cerevisiae. *Mol Cell Biol* **11**:425 LP-439. doi:10.1128/MCB.11.1.425.

Oeffinger M, Montpetit B. 2015. Emerging properties of nuclear RNP biogenesis and export.

Curr Opin Cell Biol **34**:46–53. doi:10.1016/j.ceb.2015.04.007.

Oeffinger M, Zenklusen D. 2012. To the pore and through the pore: A story of mRNA export kinetics. *Biochim Biophys Acta - Gene Regul Mech* **1819**:494–506. doi:10.1016/j.bbagrm.2012.02.011.

Ohira T, Suzuki T. 2011. Retrograde nuclear import of tRNA precursors is required for modified base biogenesis in yeast. *Proc Natl Acad Sci* **108**:10502 LP-10507. doi:10.1073/pnas.1105645108.

Ossareh-Nazari B, Bachelerie F, Dargemont C. 1997. Evidence for a Role of CRM1 in Signal-Mediated Nuclear Protein Export. *Science (80)* **278**:141 LP-144. doi:10.1126/science.278.5335.141.

Palancade B, Zuccolo M, Loeillet S, Nicolas A, Doye V. 2005. Pml39, a Novel Protein of the Nuclear Periphery Required for Nuclear Retention of Improper Messenger Ribonucleoparticles. *Mol Biol Cell* **16**:5258–5268. doi:10.1091/mbc.e05-06-0527.

Parenteau J, Durand M, Véronneau S, Lacombe A-A, Morin G, Guérin V, Cecez B, Gervais-Bird J, Koh C-S, Brunelle D, Wellinger RJ, Chabot B, Abou Elela S. 2008. Deletion of many yeast introns reveals a minority of genes that require splicing for function. *Mol Biol Cell* **19**:1932–1941. doi:10.1091/mbc.E07-12-1254.

Park HY, Lim H, Yoon YJ, Follenzi A, Nwokafor C, Lopez-Jones M, Meng X, Singer RH. 2014. Visualization of Dynamics of Single Endogenous mRNA Labeled in Live Mouse. *Science (80-)* **343**:422 LP-424. doi:10.1126/science.1239200.

Parker R, Sheth U. 2007. P Bodies and the Control of mRNA Translation and Degradation. *Mol Cell* **25**:635–646. doi:https://doi.org/10.1016/j.molcel.2007.02.011.

Patro R, Duggal G, Love MI, Irizarry RA, Kingsford C. 2017. Salmon provides fast and bias-aware quantification of transcript expression. *Nat Methods* **14**:417–419. doi:10.1038/nmeth.4197.

Paul B, Montpetit B. 2016. Altered RNA processing and export lead to retention of mRNAs near transcription sites and nuclear pore complexes or within the nucleolus. *Mol Biol Cell* **27**:2742–2756. doi:10.1091/mbc.E16-04-0244.

Pemberton LF, Paschal BM. 2005. Mechanisms of Receptor-Mediated Nuclear Import and Nuclear Export. *Traffic* **6**:187–198. doi:10.1111/j.1600-0854.2005.00270.x.

Perales R, Bentley D. 2009. "Cotranscriptionality": The Transcription Elongation Complex as a

Nexus for Nuclear Transactions. *Mol Cell* **36**:178–191. doi:https://doi.org/10.1016/j.molcel.2009.09.018.

Phizicky EM, Alfonzo JD. 2010. Do all modifications benefit all tRNAs? *FEBS Lett* **584**:265–271. doi:10.1016/j.febslet.2009.11.049.

Phizicky EM, Hopper AK. 2015. tRNA processing , modification , and subcellular dynamics : past , present , and future 483–485. doi:10.1261/rna.049932.115.

Phizicky EM, Hopper AK. 2010. tRNA biology charges to the front. *Genes Dev* **24**:1832–1860. doi:10.1101/gad.1956510.

Preibisch S, Saalfeld S, Tomancak P. 2009. Globally optimal stitching of tiled 3D microscopic image acquisitions. *Bioinformatics* **25**:1463–1465. doi:10.1093/bioinformatics/btp184.

Prelich G. 1997. Saccharomyces cerevisiae BUR6 encodes a DRAP1/NC2alpha homolog that has both positive and negative roles in transcription in vivo. *Mol Cell Biol* **17**:2057 LP-2065. doi:10.1128/MCB.17.4.2057.

Pyle AM. 2008. Translocation and Unwinding Mechanisms of RNA and DNA Helicases. *Annu Rev Biophys* **37**:317–336. doi:10.1146/annurev.biophys.37.032807.125908.

Quan X, Yu J, Bussey H, Stochaj U. 2007. The localization of nuclear exporters of the importin-β family is regulated by Snf1 kinase, nutrient supply and stress. *Biochim Biophys Acta - Mol Cell Res* **1773**:1052–1061. doi:https://doi.org/10.1016/j.bbamcr.2007.04.014,

Raj A, Peskin CS, Tranchina D, Vargas DY, Tyagi S. 2006. Stochastic mRNA Synthesis in Mammalian Cells. *PLOS Biol* **4**:e309.

Robinson MD, McCarthy DJ, Smyth GK. 2010. edgeR: a Bioconductor package for differential expression analysis of digital gene expression data. *Bioinformatics* **26**. doi:10.1093/bioinformatics/btp616,

Rougemaille M, Dieppois G, Kisseleva-Romanova E, Gudipati RK, Lemoine S, Blugeon C, Boulay J, Jensen TH, Stutz F, Devaux F, Libri D. 2008. THO/Sub2p Functions to Coordinate 3′-End Processing with Gene-Nuclear Pore Association. *Cell* **135**:308–321. doi:https://doi.org/10.1016/j.cell.2008.08.005.

Russell I, Tollervey D. 1995. Yeast Nop3p has structural and functional similarities to mammalian pre-mRNA binding proteins. *Eur J Cell Biol* **66**:293—301.

Saavedra C, Tung KS, Amberg DC, Hopper AK, Cole CN. 1996. Regulation of mRNA export in response to stress in Saccharomyces cerevisiae. *Genes Dev* **10**:1608–1620.

doi:10.1101/gad.10.13.1608.

Santos-Rosa H, Moreno H, Simos G, Segref A, Fahrenkrog B, Panté N, Hurt E. 1998. Nuclear mRNA Export Requires Complex Formation between Mex67p and Mtr2p at the Nuclear Pores. *Mol Cell Biol* **18**:6826 LP-6838. doi:10.1128/MCB.18.11.6826

Sarkar S, Hopper AK. 1998. tRNA Nuclear Export in Saccharomyces cerevisiae: In Situ Hybridization Analysis. *Mol Biol Cell* **9**:3041–3055. doi:10.1091/mbc.9.11.3041.

Saroufim MA, Bensidoun P, Raymond P, Rahman S, Krause MR, Oeffinger M, Zenklusen D. 2015. The nuclear basket mediates perinuclear mRNA scanning in budding yeast. *J Cell Biol* **211**:1131–1140. doi:10.1083/jcb.201503070.

Scarcelli JJ, Viggiano S, Hodge CA, Heath C V., Amberg DC, Cole CN. 2008. Synthetic genetic array analysis in Saccharomyces cerevisiae provides evidence for an interaction between RAT8/DBP5 and genes encoding P-body components. *Genetics* **179**:1945–1955. doi:10.1534/genetics.108.091256.

Schindelin J, Arganda-Carreras I, Frise E, Kaynig V, Longair M, Pietzsch T, Preibisch S, Rueden C, Saalfeld S, Schmid B, Tinevez J-Y, White DJ, Hartenstein V, Eliceiri K, Tomancak P, Cardona A. 2012. Fiji: an open-source platform for biological-image analysis. *Nat Methods* **9**:676.

Schmitt C, von Kobbe C, Bachi A, Panté N, Rodrigues JP, Boscheron C, Rigaut G, Wilm M, Séraphin B, Carmo-Fonseca M, Izaurralde E. 1999. Dbp5, a DEAD-box protein required for mRNA export, is recruited to the cytoplasmic fibrils of nuclear pore complex via a conserved interaction with CAN/Nup159p. *EMBO J* **18**:4332–47. doi:10.1093/emboj/18.15.4332.

Scott RJ, Cairo L V, Van de Vosse DW, Wozniak RW. 2009. The nuclear export factor Xpo1p targets Mad1p to kinetochores in yeast. *J Cell Biol* **184**:21–29. doi:10.1083/jcb.200804098.

Segref A, Sharma K, Doye V, Hellwig A, Huber J, Lührmann R, Hurt E. 1997. Mex67p, a novel factor for nuclear mRNA export. Binds to both poly(A)+ RNA and nuclear pores. *EMBO J* **16**:3256–3271. doi:10.1093/emboj/16.11.3256.

Senger B, Simos G, Bischoff FR, Podtelejnikov A, Mann M, Hurt E. 1998. Mtr10p functions as a nuclear import receptor for the mRNA-binding protein Npl3p. *EMBO J* **17**:2196 LP-2207. doi:10.1093/emboj/17.8.2196.

Sengoku T, Nureki O, Nakamura A, Kobayashi S, Yokoyama S. 2006. Structural Basis for RNA

Unwinding by the DEAD-Box Protein Drosophila Vasa. *Cell* **125**:287–300. doi:https://doi.org/10.1016/j.cell.2006.01.054.

Senissar M, Le Saux A, Belgareh-Touzé N, Adam C, Banroques J, Tanner NK. 2014. The DEAD-box helicase Ded1 from yeast is an mRNP cap-associated protein that shuttles between the cytoplasm and nucleus. *Nucleic Acids Res* **42**:10005–10022. doi:10.1093/nar/gku584.

Shaheen HH, Hopper AK. 2005. Retrograde movement of tRNAs from the cytoplasm to the nucleus in Saccharomyces cerevisiae. *Proc Natl Acad Sci U S A* **102**:11290–11295. doi:10.1073/pnas.0503836102.

Shaheen HH, Horetsky RL, Kimball SR, Murthi A, Jefferson LS, Hopper AK. 2007. Retrograde nuclear accumulation of cytoplasmic tRNA in rat hepatoma cells in response to amino acid deprivation. *Proc Natl Acad Sci* **104**:8845 LP-8850. doi:10.1073/pnas.0700765104.

Shaner NC, Lambert GG, Chammas A, Ni Y, Cranfill PJ, Baird MA, Sell BR, Allen JR, Day RN, Israelsson M, Davidson MW, Wang J. 2013. A bright monomeric green fluorescent protein derived from Branchiostoma lanceolatum. *Nat Methods* **10**:407.

Shcherbo D, Merzlyak EM, Chepurnykh T V, Fradkov AF, Ermakova G V, Solovieva EA, Lukyanov KA, Bogdanova EA, Zaraisky AG, Lukyanov S, Chudakov DM. 2007. Bright far-red fluorescent protein for whole-body imaging. *Nat Methods* **4**:741.

Sheff MA, Thorn KS. 2004. Optimized cassettes for fluorescent protein tagging in Saccharomyces cerevisiae. *Yeast* **21**:661–670. doi:10.1002/yea.1130.

Sherman BF, Sherman MF, Enzymol M. 2003. Getting Started with Yeast. *Methods in Enzymology* **41**:3–41.

Siebrasse JP, Kaminski T, Kubitscheck U. 2012. Nuclear export of single native mRNA molecules observed by light sheet fluorescence microscopy. *Proc Natl Acad Sci* **109**:9426 LP-9431. doi:10.1073/pnas.1201781109.

Simpson CE, Lui J, Kershaw CJ, Sims PFG, Ashe MP. 2014. mRNA localization to Pbodies in yeast is biphasic with many mRNAs captured in a late Bfr1pdependent wave. *J Cell Sci* **127**:1254 LP-1262. doi:10.1242/jcs.139055.

Singleton DR, Chen S, Hitomi M, Kumagai C, Tartakoff AM. 1995. A yeast protein that bidirectionally affects nucleocytoplasmic transport. *J Cell Sci* **108**:265 LP-272.

Singleton MR, Dillingham MS, Wigley DB. 2007. Structure and Mechanism of Helicases and

Nucleic Acid Translocases. *Annu Rev Biochem* **76**:23–50. doi:10.1146/annurev.biochem.76.052305.115300.

Skružný M, Schneider C, Rácz A, Weng J, Tollervey D, Hurt E. 2009. An Endoribonuclease Functionally Linked to Perinuclear mRNP Quality Control Associates with the Nuclear Pore Complexes. *PLOS Biol* **7**:e1000008.

Smith C, Lari A, Derrer CP, Ouwehand A, Rossouw A, Huisman M, Dange T, Hopman M, Joseph A, Zenklusen D, Weis K, Grunwald D, Montpetit B. 2015. In vivo single-particle imaging of nuclear mRNA export in budding yeast demonstrates an essential role for Mex67p. *J Cell Biol* **211**:1121–1130. doi:10.1083/jcb.201503135.

Smith CS, Joseph N, Rieger B, Lidke KA. 2010. Fast, single-molecule localization that achieves theoretically minimum uncertainty. *Nat Methods* **7**:373–375. doi:10.1038/nmeth.1449

Snay-Hodge CA, Colot H V, Goldstein AL, Cole CN. 1998. Dbp5p/Rat8p is a yeast nuclear pore-associated DEAD-box protein essential for RNA export. *EMBO J* **17**:2663 LP-2676.

Song T, Zheng Y, Wang Y, Katz Z, Liu X, Chen S, Singer RH, Gu W. 2015. Specific interaction of KIF11 with ZBP1 regulates the transport of β-actin mRNA and cell motility. *J Cell Sci* **128**:1001 LP-1010. doi:10.1242/jcs.161679.

Stade K, Ford CS, Guthrie C, Weis K. 1997. Exportin 1 (Crm1p) Is an Essential Nuclear Export Factor. *Cell* **90**:1041–1050. doi:10.1016/S0092-8674(00)80370-0.

Stage-Zimmermann T, Schmidt U, Silver PA. 2000. Factors Affecting Nuclear Export of the 60S Ribosomal Subunit In Vivo. *Mol Biol Cell* **11**:3777–3789. doi:10.1091/mbc.11.11.3777.

Stewart M. 2007. Ratcheting mRNA out of the nucleus. *Mol Cell* **25**:327–330.

Sträßer K, Baßler J, Hurt E. 2000. Binding of the Mex67p/Mtr2p Heterodimer to Fxfg, Glfg, and Fg Repeat Nucleoporins Is Essential for Nuclear mRNA Export. *J Cell Biol* **150**:695 LP-706. doi:10.1083/jcb.150.4.695.

Sträßer K, Hurt E. 2000. Yra1p, a conserved nuclear RNA-binding protein, interacts directly with Mex67p and is required for mRNA export. *EMBO J* **19**:410 LP-420. doi:10.1093/emboj/19.3.410.

Sträßer K, Masuda S, Mason P, Pfannstiel J, Oppizzi M, Rodriguez-Navarro S, Rondón AG, Aguilera A, Struhl K, Reed R, Hurt E. 2002. TREX is a conserved complex coupling transcription with messenger RNA export. *Nature* **417**:304–308. doi:10.1038/nature746.

Ström AC, Weis K. 2001. Importin-beta-like nuclear transport receptors. *Genome Biol*

2:REVIEWS3008-REVIEWS3008.

Stutz F, Bachi A, Doerks T, Braun IC, Séraphin B, Wilm M, Bork P, Izaurralde E. 2000. REF, an evolutionary conserved family of hnRNP-like proteins, interacts with TAP/Mex67p and participates in mRNA nuclear export. *Rna* **6**:638–650. doi:10.1017/S1355838200000078.

Sun D, Ostermaier MK, Heydenreich FM, Mayer D, Jaussi R, Standfuss J, Veprintsev DB. 2013. AAscan, PCRdesign and MutantChecker: a suite of programs for primer design and sequence analysis for high-throughput scanning mutagenesis. *PLoS One* **8**:e78878. doi:10.1371/journal.pone.0078878.

Takano A, Endo T, Yoshihisa T. 2005. tRNA Actively Shuttles Between the Nucleus and Cytosol in Yeast. *Science (80-)* **309**:140 LP-142. doi:10.1126/science.1113346.

Takano A, Kajita T, Mochizuki M, Endo T, Yoshihisa T. 2015. Cytosolic Hsp70 and co-chaperones constitute a novel system for tRNA import into the nucleus. *Elife* **2015**:1–22. doi:10.7554/eLife.04659.

Takemura R, Inoue Y, Izawa S. 2004. Stress response in yeast mRNA export factor: reversible changes in Rat8p localization are caused by ethanol stress but not heat shock. *J Cell Sci* **117**:4189 LP-4197.

Terry LJ, Wente SR. 2007. Nuclear mRNA export requires specific FG nucleoporins for translocation through the nuclear pore complex. *J Cell Biol* **178**:1121–1132. doi:10.1083/jcb.200704174.

Thomsen R, Saguez C, Nasser T, Jensen TH. 2008. General, rapid, and transcription-dependent fragmentation of nucleolar antigens in S. cerevisiae mRNA export mutants. *RNA* **14**:706–716. doi:10.1261/rna.718708 .

Tong AHY, Boone C. 2007. 16 High-Throughput Strain Construction and Systematic Synthetic Lethal Screening in Saccharomyces cerevisiae. *Methods Microbiol* **36**. doi:10.1016/S0580-9517(06)36016-3.

Tran EJ, Zhou Y, Corbett AH, Wente SR. 2007. The DEAD-Box Protein Dbp5 Controls mRNA Export by Triggering Specific RNA:Protein Remodeling Events. *Mol Cell* **28**:850–859. doi:10.1016/j.molcel.2007.09.019.

Tschochner H, Hurt E. 2003. Pre-ribosomes on the road from the nucleolus to the cytoplasm. *Trends Cell Biol* **13**:255–263. doi:10.1016/S0962-8924(03)00054-0.

Tseng SS, Weaver PL, Liu Y, Hitomi M, Tartakoff a M, Chang TH. 1998. Dbp5p, a cytosolic

RNA helicase, is required for poly(A)+ RNA export. *EMBO J* **17**:2651–62. doi:10.1093/emboj/17.9.2651.

Tuck AC, Tollervey D. 2013. A Transcriptome-wide Atlas of RNP Composition Reveals Diverse Classes of mRNAs and lncRNAs. *Cell* **154**:996–1009. doi:10.1016/j.cell.2013.07.047.

Tutucci E, Stutz F. 2011. Keeping mRNPs in check during assembly and nuclear export. *Nat Rev Mol Cell Biol* **12**:377.

Tutucci E, Vera M, Biswas J, Garcia J, Parker R, Singer RH. 2017. An improved MS2 system for accurate reporting of the mRNA life cycle. *Nat Methods* **15**:81.

Tutucci E, Vera M, Singer RH. 2018. Single-mRNA detection in living S. cerevisiae using a re-engineered MS2 system. *Nat Protoc* **13**:2268–2296. doi:10.1038/s41596-018-0037-2.

Urbanek MO, Galka-Marciniak P, Olejniczak M, Krzyzosiak WJ. 2014. RNA imaging in living cells – methods and applications. *RNA Biol* **11**:1083–1095. doi:10.4161/rna.35506.

Valgardsdottir R, Prydz H. 2003. Transport signals and transcription-dependent nuclear localization of the putative DEAD-box helicase MDDX28. *J Biol Chem* **278**:21146–54. doi:10.1074/jbc.M300888200.

Venema J, Tollervey D. 1999. Ribosome Synthesis in Saccharomyces cerevisiae. *Annu Rev Genet* **33**:261–311. doi:10.1146/annurev.genet.33.1.261.

Verghese J, Abrams J, Wang Y, Morano KA. 2012. Biology of the Heat Shock Response and Protein Chaperones: Budding Yeast as a Model System. *Microbiol Mol Biol Rev* **76**:115 LP-158. doi:10.1128/MMBR.05018-11.

Vinciguerra P, Iglesias N, Camblong J, Zenklusen D, Stutz F. 2005. Perinuclear Mlp proteins downregulate gene expression in response to a defect in mRNA export. *EMBO J* **24**:813 LP-823. doi:10.1038/sj.emboj.7600527.

Visa N, Izaurralde E, Ferreira J, Daneholt B, Mattaj IW. 1996. A nuclear cap-binding complex binds Balbiani ring pre-mRNA cotranscriptionally and accompanies the ribonucleoprotein particle during nuclear export. *J Cell Biol* **133**:5 LP-14. doi:10.1083/jcb.133.1.5.

von Moeller H, Basquin C, Conti E. 2009. The mRNA export protein DBP5 binds RNA and the cytoplasmic nucleoporin NUP214 in a mutually exclusive manner. *Nat Struct Mol Biol* **16**:247–254.

Wang Z, Buratowski S, Svejstrup JQ, Feaver WJ, Wu X, Kornberg RD, Donahue TF, Friedberg EC. 1995. The yeast TFB1 and SSL1 genes, which encode subunits of transcription factor

IIH, are required for nucleotide excision repair and RNA polymerase II transcription. *Mol Cell Biol* **15**:2288 LP-2293. doi:10.1128/MCB.15.4.2288.

Waters JC. 2009. Accuracy and precision in quantitative fluorescence microscopy. *J Cell Biol* **185**:1135 LP-1148. doi:10.1083/jcb.200903097.

Weirich CS, Erzberger JP, Berger JM, Weis K. 2004. The N-terminal domain of Nup159 forms a beta-propeller that functions in mRNA export by tethering the helicase Dbp5 to the nuclear pore. *Mol Cell* **16**:749–60. doi:10.1016/j.molcel.2004.10.032.

Weirich CS, Erzberger JP, Flick JS, Berger JM, Thorner J, Weis K. 2006. Activation of the DExD/H-box protein Dbp5 by the nuclear-pore protein Gle1 and its coactivator InsP6 is required for mRNA export. *Nat Cell Biol* **8**:668–676.

Wente SR, Rout MP. 2010. The nuclear pore complex and nuclear transport. *Cold Spring Harb Perspect Biol* **2**:a000562–a000562. doi:10.1101/cshperspect.a000562.

Whitelaw E, Proudfoot N. 1986. a-Thalassaemia caused by a poly (A) site mutation reveals that transcriptional termination is linked to 3 ' end processing in the **5**:2915–2922.

Whitney ML, Hurto RL, Shaheen HH, Hopper AK. 2007. Rapid and reversible nuclear accumulation of cytoplasmic tRNA in response to nutrient availability. *Mol Biol Cell* **18**:2678–2686. doi:10.1091/mbc.e07-01-0006.

Wiegand HL, Coburn GA, Zeng Y, Kang Y, Bogerd HP, Cullen BR. 2002. Formation of Tap/NXT1 Heterodimers Activates Tap-Dependent Nuclear mRNA Export by Enhancing Recruitment to Nuclear Pore Complexes. *Mol Cell Biol* **22**:245 LP-256. doi:10.1128/MCB.22.1.245-256.2002.

Winey M, Yarar D, Giddings TH, Mastronarde DN. 1997. Nuclear Pore Complex Number and Distribution throughout theSaccharomyces cerevisiae Cell Cycle by Three-Dimensional Reconstruction from Electron Micrographs of Nuclear Envelopes. *Mol Biol Cell* **8**:2119–2132. doi:10.1091/mbc.8.11.2119.

Wong E V., Gray S, Cao W, Montpetit R, Montpetit B, De La Cruz EM. 2018. Nup159 Weakens Gle1 Binding to Dbp5 But Does Not Accelerate ADP Release. *J Mol Biol* **430**:2080–2095. doi:10.1016/j.jmb.2018.05.025.

Wozniak RW, Rout MP, Aitchison JD. 1998. Karyopherins and kissing cousins. *Trends Cell Biol* **8**:184–188. doi:10.1016/S0962-8924(98)01248-3.

Wu H, Becker D, Krebber H. 2014. Telomerase RNA TLC1 shuttling to the cytoplasm requires

mRNA export factors and is important for telomere maintenance. *Cell Rep* **8**:1630–1638. doi:10.1016/j.celrep.2014.08.021

Wu J, Bao A, Chatterjee K, Wan Y, Hopper AK. 2015. Genome-wide screen uncovers novel pathways for tRNA processing and nuclear–cytoplasmic dynamics. *Genes Dev* **29**:2633–2644. doi:10.1101/gad.269803.115.

Yao W, Roser D, Kohler A, Bradatsch B, Bassler J, Hurt E. 2007. Nuclear export of ribosomal 60S subunits by the general mRNA export receptor Mex67-Mtr2. *Mol Cell* **26**:51–62.

York JD, Odom AR, Murphy R, Ives EB, Wente SR. 1999. A Phospholipase C-Dependent Inositol Polyphosphate Kinase Pathway Required for Efficient Messenger RNA Export. *Science (80-)* **285**:96 LP-100. doi:10.1126/science.285.5424.96.

Yoshihisa T, Ohshima C, Yunoki-Esaki K, Endo T. 2007. Cytoplasmic splicing of tRNA in Saccharomyces cerevisiae. *Genes to Cells* **12**:285–297. doi:10.1111/j.1365-2443.2007.01056.x.

Yoshihisa T, Yunoki-Esaki K, Ohshima C, Tanaka N, Endo T. 2003. Possibility of Cytoplasmic pre-tRNA Splicing: the Yeast tRNA Splicing Endonuclease Mainly Localizes on the Mitochondria. *Mol Biol Cell* **14**:3266–3279. doi:10.1091/mbc.e02-11-0757.

Young BP, Loewen CJ. 2013. Balony:a software package for analysis of data generated by synthetic genetic array experiments. *BMC Bioinformatics* **14**:354. doi:10.1186/1471-2105-14-354.

Young BP, Shin JJH, Orij R, Chao JT, Li SC, Guan XL, Khong A, Jan E, Wenk MR, Prinz WA, Smits GJ, Loewen CJR. 2010. Phosphatidic acid is a pH biosensor that links membrane biogenesis to metabolism. *Science* **329**:1085–8. doi:10.1126/science.1191026.

Zander G, Hackmann A, Bender L, Becker D, Lingner T, Salinas G, Krebber H. 2016. mRNA quality control is bypassed for immediate export of stress-responsive transcripts. *Nature* **540**:593.

Zander G, Krebber H. 2017. Quick or quality? How mRNA escapes nuclear quality control during stress. *RNA Biol* **14**:1642–1648. doi:10.1080/15476286.2017.1345835.

Zaret KS, Sherman F. 1982. DNA sequence required for efficient transcription termination in yeast. *Cell* **28**:563–573. doi:https://doi.org/10.1016/0092-8674(82)90211-2.

Zemp I, Kutay U. 2007. Nuclear export and cytoplasmic maturation of ribosomal subunits. *FEBS Lett* **581**:2783–2793. doi:10.1016/J.FEBSLET.2007.05.013.

Zenklusen D, Larson DR, Singer RH. 2008. Single-RNA counting reveals alternative modes of gene expression in yeast. *Nat Struct &Amp; Mol Biol* **15**:1263.

Zenklusen D, Stutz F. 2001. Nuclear export of mRNA. *FEBS Lett* **498**:150–156. doi:10.1016/S0014-5793(01)02482-6.

Zenklusen D, Vinciguerra P, Strahm Y, Stutz F. 2001. The Yeast hnRNP-Like Proteins Yra1p and Yra2p Participate in mRNA Export through Interaction with Mex67p. *Mol Cell Biol* **21**:4219 LP-4232. doi:10.1128/MCB.21.13.4219-4232.2001.

Zenklusen D, Vinciguerra P, Wyss J-C, Stutz F. 2002. Stable mRNP Formation and Export Require Cotranscriptional Recruitment of the mRNA Export Factors Yra1p and Sub2p by Hpr1p. *Mol Cell Biol* **22**:8241 LP-8253. doi:10.1128/MCB.22.23.8241-8253.2002.

Zhao J, Jin S-B, Björkroth B, Wieslander L, Daneholt B. 2002. The mRNA export factor Dbp5 is associated with Balbiani ring mRNP from gene to cytoplasm. *EMBO J* **21**:1177–87. doi:10.1093/emboj/21.5.1177.

Appendix

Table 6-1. Gene expression changes in wild-type, *dbp5-L12A*, and *dbp5-R423A* strains in response to MMS treatment

(0=unchanged, 1=induced (>two fold higher), 2=repressed (<two fold lower))

Identifier	Common Name	wild-type	*dbp5-L12A*	*dbp5-R423A*
YBR027C		1	0	0
YLR459W	GAB1	1	0	0
YER019C-A	SBH2	1	0	0
YDL064W	UBC9	1	0	0
YIL040W	APQ12	1	0	0
YDL084W	SUB2	1	0	0
YGR260W	TNA1	1	0	0
YPR069C	SPE3	1	0	0
YPR020W	ATP2	1	0	0
YDR378C	LSM6	1	0	0
YPR138C	MEP3	1	0	0
YNL135C	FPR1	1	0	0
YIL015W	BAR1	1	0	0
YLR065C	ENV1	1	0	0
YJL166W	QCR8	1	0	0
YML054C	CYB2	1	0	0
YER023W	PRO3	1	0	0
YBR268W	MRPL37	1	0	0
YBR058C-A	TSC3	1	0	0
YOL012C	HTZ1	1	0	0
YKL110C	KTI12	1	0	0
YJR133W	XPT1	1	0	0
YJL087C	TRL1	1	0	0
YJL193W		1	0	0
YPR083W	MDM36	1	0	0

YNL246W	VPS75	1	0	0
YLR023C	IZH3	1	0	0
YOR253W	NAT5	1	0	0
YLR099W-A	MIM2	1	0	0
YHL014C	YLF2	1	0	0
YKL060C	FBA1	1	0	0
YDR050C	TPI1	1	0	0
YHR065C	RRP3	1	0	0
YJR129C	EFM3	1	0	0
YPL268W	PLC1	1	0	0
YBL043W	ECM13	1	0	0
YGR296W	YRF1-3	1	0	0
YDL085C-A		1	0	0
YBL009W	ALK2	1	0	0
YNR057C	BIO4	1	0	0
YFR005C	SAD1	1	0	0
YOR365C		1	0	0
YGR036C	CAX4	1	0	0
YOR144C	ELG1	1	0	0
YGL253W	HXK2	1	0	0
YPL193W	RSA1	1	0	0
YPL057C	SUR1	1	0	0
YPL133C	RDS2	1	0	0
YOR166C	SWT1	1	0	0
YKL048C	ELM1	1	0	0
YMR042W	ARG8	1	0	0
YLR364W	GRX8	1	0	0
YHL028W	WSC4	1	0	0
YGR057C	LST7	1	0	0
YIR021W	MRS1	1	0	0

YOR344C	TYE7	1	0	0
YAR028W		1	0	0
YOR044W	IRC23	1	0	0
YOR107W	RGS2	1	0	0
YIL092W		1	0	0
YEL064C	AVT2	1	0	0
YJL214W	HXT8	1	0	0
YCR005C	CIT2	1	0	0
YOR030W	DFG16	1	0	0
YGR212W	SLI1	1	0	0
YHR120W	MSH1	0	1	0
YPR052C	NHP6A	0	1	0
YER060W	FCY21	0	1	0
YNL227C	JJJ1	0	1	0
YOR154W	SLP1	0	1	0
YPL207W	TYW1	0	1	0
YJR124C		0	1	0
YEL016C	NPP2	0	1	0
YGR191W	HIP1	0	1	0
YPL163C	SVS1	0	1	0
YDR444W		0	1	0
YNR018W	RCF2	0	1	0
YGR264C	MES1	0	1	0
YDR524C	AGE1	0	1	0
YPR002W	PDH1	0	1	0
YLR287C-A	RPS3A	0	1	0
YMR266W	RSN1	0	1	0
YLR179C		0	1	0
YBR093C	PHO5	0	1	0
YNL068C	FKH2	0	1	0

YGR280C	PXR1	0	1	0
YGR095C	RRP46	0	1	0
YPL146C	NOP53	0	1	0
YDR156W	RPA14	0	1	0
YHR039C	MSC7	0	1	0
YKR043C	SHB17	0	1	0
YGR173W	RBG2	0	1	0
YOL076W	MDM2	0	1	0
YMR128W	ECM16	0	1	0
YDR339C	FCF1	0	1	0
YGR140W	CBF2	0	1	0
YDR161W	ACL4	0	1	0
YLL035W	GRC3	0	1	0
YLR353W	BUD8	0	1	0
YOR021C	SFM1	0	1	0
YER110C	KAP123	0	1	0
YBR056W-A		0	1	0
YGL176C		0	1	0
YNL162W-A		0	1	0
YPL266W	DIM1	0	1	0
YCL063W	VAC17	0	1	0
YOR001W	RRP6	0	1	0
YNL315C	ATP11	0	1	0
YOL144W	NOP8	0	1	0
YJL209W	CBP1	0	1	0
YDL150W	RPC53	0	1	0
YDL209C	CWC2	0	1	0
YOR119C	RIO1	0	1	0
YBR118W	TEF2	0	1	0
YIL104C	SHQ1	0	1	0

YKL143W	LTV1	0	1	0
YNL062C	GCD1	0	1	0
YKL081W	TEF4	0	1	0
YGL171W	ROK1	0	1	0
YBR210W	ERV15	0	1	0
YKL125W	RRN3	0	1	0
YFR032C-B		0	1	0
YBR239C	ERT1	0	1	0
YOL136C	PFK27	0	1	0
YLR293C	GSP1	0	1	0
YPL263C	KEL3	0	1	0
YPR144C	NOC4	0	1	0
YDR213W	UPC2	0	1	0
YNL175C	NOP13	0	1	0
YDR110W	FOB1	0	1	0
YLR017W	MEU1	0	1	0
YDR365C	ESF1	0	1	0
YOR339C	UBC11	0	1	0
YJR047C	ANB1	0	1	0
YOR188W	MSB1	0	1	0
YLR205C	HMX1	0	1	0
YJL033W	HCA4	0	1	0
YCR028C	FEN2	0	1	0
YOR063W	RPL3	0	1	0
YPL217C	BMS1	0	1	0
YJL194W	CDC6	0	1	0
YHR070W	TRM5	0	1	0
YMR229C	RRP5	0	1	0
YGL162W	SUT1	0	1	0
YNL065W	AQR1	0	1	0

YGL063W	PUS2	0	1	0
YGL188C-A		0	1	0
YMR306W	FKS3	0	1	0
YMR310C		0	1	0
YJR147W	HMS2	0	1	0
YKR015C		0	1	0
YPR195C		0	1	0
YJR160C	MPH3	0	1	0
YJR105W	ADO1	1	1	0
YPL028W	ERG1	1	1	0
YPR033C	HTS1	1	1	0
YMR259C	TRM732	1	1	0
YNL044W	YIP3	1	1	0
YDR222W		1	1	0
YNL010W		1	1	0
YLR367W	RPS22B	1	1	0
YNL255C	GIS2	1	1	0
YHR062C	RPP1	1	1	0
YBR233W-A	DAD3	1	1	0
YOR346W	REV1	1	1	0
YGL169W	SUA5	1	1	0
YHR020W		1	1	0
YDR529C	QCR7	1	1	0
YGR251W	NOP19	1	1	0
YLL014W	EMC6	1	1	0
YEL020W-A	TIM9	1	1	0
YKL014C	URB1	1	1	0
YLR075W	RPL1	1	1	0
YMR260C	TIF11	1	1	0
YHL039W	EFM1	1	1	0

YPL237W	SUI3	1	1	0
YBL068W	PRS4	1	1	0
YDR119W	VBA4	1	1	0
YPL241C	CIN2	1	1	0
YIR012W	SQT1	1	1	0
YBR121C	GRS1	1	1	0
YKR025W	RPC37	1	1	0
YHR064C	SSZ1	1	1	0
YOR243C	PUS7	1	1	0
YJR031C	GEA1	1	1	0
YER127W	LCP5	1	1	0
YBR192W	RIM2	1	1	0
YIL103W	DPH1	1	1	0
YEL027W	VMA3	1	1	0
YNL024C	EFM6	1	1	0
YPL245W		1	1	0
YJL010C	NOP9	1	1	0
YPR009W	SUT2	1	1	0
YHR170W	NMD3	1	1	0
YNR024W	MPP6	1	1	0
YNL207W	RIO2	1	1	0
YJL168C	SET2	1	1	0
YJL130C	URA2	1	1	0
YDL184C	RPL41A	1	1	0
YPL016W	SWI1	1	1	0
YPL253C	VIK1	1	1	0
YKR056W	TRM2	1	1	0
YPR163C	TIF3	1	1	0
YEL053C	MAK1	1	1	0
YOR108W	LEU9	1	1	0

YIL019W	FAF1	1	1	0
YOL061W	PRS5	1	1	0
YGR200C	ELP2	1	1	0
YCR016W		1	1	0
YHR088W	RPF1	1	1	0
YDL148C	NOP14	1	1	0
YML087C	AIM33	1	1	0
YDL153C	SAS1	1	1	0
YDR060W	MAK21	1	1	0
YGL111W	NSA1	1	1	0
YOR295W	UAF3	1	1	0
YJL109C	UTP1	1	1	0
YCR087C-A		1	1	0
YBL031W	SHE1	1	1	0
YDL240W	LRG1	1	1	0
YBR066C	NRG2	1	1	0
YDR165W	TRM82	1	1	0
YLR002C	NOC3	1	1	0
YOR272W	YTM1	1	1	0
YJL181W	RBH1	1	1	0
YCR051W		1	1	0
YMR239C	RNT1	1	1	0
YLR197W	NOP56	1	1	0
YKL216W	URA1	1	1	0
YIL008W	URM1	1	1	0
YDR020C	DAS2	1	1	0
YDR087C	RRP1	1	1	0
YJR002W	MPP1	1	1	0
YPL012W	RRP12	1	1	0
YMR049C	ERB1	1	1	0

YDL039C	PRM7	1	1	0
YOL093W	TRM1	1	1	0
YOR341W	RPA19	1	1	0
YGR245C	SDA1	1	1	0
YGL007C-A		1	1	0
YGR121W-A		1	1	0
YDR381W	YRA1	0	0	1
YGL257C	MNT2	0	0	1
YHR072W	ERG7	0	0	1
YDL236W	PHO13	0	0	1
YLR318W	EST2	0	0	1
YFL017C	GNA1	0	0	1
YKR054C	DYN1	0	0	1
YCL014W	BUD3	0	0	1
YJR092W	BUD4	0	0	1
YBR038W	CHS2	0	0	1
YER141W	COX15	0	0	1
YBR202W	MCM7	0	0	1
YNL277W	MET2	0	0	1
YLR121C	YPS3	0	0	1
YGR041W	BUD9	0	0	1
YLR057W	MNL2	0	0	1
YGR138C	TPO2	0	0	1
YOR159C	SME1	0	0	1
YEL061C	CIN8	0	0	1
YPL076W	GPI2	0	0	1
YDR179W-A	NVJ3	0	0	1
YMR059W	SEN15	0	0	1
YBR219C		0	0	1
YNL254C	RTC4	0	0	1

YOR387C		0	0	1
YGR096W	TPC1	0	0	1
YKL055C	OAR1	0	0	1
YAL040C	CLN3	0	0	1
YOL014W		0	0	1
YOR032C	HMS1	0	0	1
YBR292C		0	0	1
YOR334W	MRS2	0	0	1
YCR048W	ARE1	0	0	1
YCR081W	SRB8	0	0	1
YIL122W	POG1	0	0	1
YCR063W	BUD31	0	0	1
YPR158W-B		0	0	1
YNL124W	NAF1	0	0	1
YLR245C	CDD1	0	0	1
YFR033C	QCR6	1	0	1
YPL227C	ALG5	1	0	1
YKL008C	LAC1	1	0	1
YOR385W		1	0	1
YOR307C	SLY41	1	0	1
YPR156C	TPO3	1	0	1
YLL009C	COX17	1	0	1
YIL004C	BET1	1	0	1
YPL042C	SSN3	1	0	1
YHR215W	PHO12	1	0	1
YMR134W	ERG29	1	0	1
YDR451C	YHP1	1	0	1
YPL040C	ISM1	1	0	1
YPL026C	SKS1	1	0	1
YJL048C	UBX6	1	0	1

YNL211C	MRX7	1	0	1
YBL055C		1	0	1
YBR220C		1	0	1
YDR343C	HXT6	1	0	1
YBR157C	ICS2	1	0	1
YDR076W	RAD55	1	0	1
YHR172W	SPC97	1	0	1
YNR067C	DSE4	0	1	1
YMR122W-A		0	1	1
YPL274W	SAM3	0	1	1
YCR059C	YIH1	0	1	1
YPR031W	NTO1	0	1	1
YDR232W	HEM1	0	1	1
YML058W	SML1	0	1	1
YHR133C	NSG1	0	1	1
YNL070W	TOM7	0	1	1
YLR008C	PAM18	0	1	1
YPR053C		0	1	1
YGR024C	THG1	0	1	1
YDR123C	INO2	0	1	1
YDL217C	TIM22	0	1	1
YER001W	MNN1	0	1	1
YNR046W	TRM112	0	1	1
YDR312W	SSF2	0	1	1
YMR070W	MOT3	0	1	1
YPL075W	GCR1	0	1	1
YMR150C	IMP1	0	1	1
YCL037C	SRO9	0	1	1
YPL050C	MNN9	0	1	1
YHR026W	VMA16	0	1	1

YKR099W	BAS1	0	1	1
YOR065W	CYT1	0	1	1
YGR014W	MSB2	0	1	1
YJR016C	ILV3	0	1	1
YHR031C	RRM3	0	1	1
YDR044W	HEM13	0	1	1
YPL030W	TRM44	0	1	1
YNL095C		0	1	1
YKL109W	HAP4	0	1	1
YER156C		0	1	1
YOL128C	YGK3	0	1	1
YLR355C	ILV5	0	1	1
YEL046C	GLY1	0	1	1
YCR084C	TUP1	0	1	1
YJL158C	CIS3	0	1	1
YGL028C	SCW11	0	1	1
YMR205C	PFK2	0	1	1
YKL078W	DHR2	0	1	1
YHR206W	SKN7	0	1	1
YJL198W	PHO9	0	1	1
YGR188C	BUB1	0	1	1
YCR060W	TAH1	0	1	1
YGL125W	MET13	0	1	1
YKL023C-A		0	1	1
YOL149W	DCP1	0	1	1
YJR010C-A	SPC1	0	1	1
YOL059W	GPD2	0	1	1
YIL123W	SIM1	0	1	1
YLR210W	CLB4	0	1	1
YER165W	PAB1	0	1	1

YNL112W	DBP2	0	1	1
YDR277C	MTH1	0	1	1
YPL058C	PDR12	0	1	1
YGL139W	FLC3	0	1	1
YOL007C	CSI2	0	1	1
YLL012W	YEH1	0	1	1
YLL052C	AQY2	0	1	1
YDL211C		0	1	1
YAL024C	LTE1	0	1	1
YPL108W		0	1	1
YPL255W	BBP1	0	1	1
YGL209W	MIG2	0	1	1
YER038C	KRE29	0	1	1
YBL069W	AST1	0	1	1
YNL190W		0	1	1
YBL030C	PET9	0	1	1
YGR146C-A		0	1	1
YOR390W	FEX1	0	1	1
YJR012C		0	1	1
YGR221C	TOS2	0	1	1
YKR075C		0	1	1
YHL022C	SPO11	0	1	1
YCR065W	HCM1	0	1	1
YLR056W	ERG3	1	1	1
YNL111C	CYB5	1	1	1
YGR175C	ERG1	1	1	1
YMR241W	YHM2	1	1	1
YMR015C	ERG5	1	1	1
YGR060W	ERG25	1	1	1
YDR492W	IZH1	1	1	1

YBL003C	HTA2	1	1	1
YMR202W	ERG2	1	1	1
YBL002W	HTB2	1	1	1
YGL008C	PMA1	1	1	1
YNR043W	MVD1	1	1	1
YIL158W	AIM2	1	1	1
YHR007C	ERG11	1	1	1
YNL052W	COX5A	1	1	1
YER056C	FCY2	1	1	1
YDL227C	HO	1	1	1
YIL079C	AIR1	1	1	1
YCL005W-A	VMA9	1	1	1
YCR043C		1	1	1
YDL171C	GLT1	1	1	1
YER044C	ERG28	1	1	1
YLR388W	RPS29A	1	1	1
YGL077C	HNM1	1	1	1
YNR053C	NOG2	1	1	1
YGL225W	VRG4	1	1	1
YNL162W	RPL42A	1	1	1
YLR344W	RPL26A	1	1	1
YML056C	IMD4	1	1	1
YOR293W	RPS1A	1	1	1
YJR048W	CYC1	1	1	1
YLR084C	RAX2	1	1	1
YIL133C	RPL16A	1	1	1
YEL033W	MTC7	1	1	1
YBR252W	DUT1	1	1	1
YOR234C	RPL33B	1	1	1
YIL069C	RPS24B	1	1	1

YPR010C-A		1	1	1
YOR315W	SFG1	1	1	1
YDR471W	RPL27B	1	1	1
YPL117C	IDI1	1	1	1
YMR145C	NDE1	1	1	1
YEL034W	HYP2	1	1	1
YER049W	TPA1	1	1	1
YDL083C	RPS16B	1	1	1
YMR194W	RPL36A	1	1	1
YLR395C	COX8	1	1	1
YNL030W	HHF2	1	1	1
YCR024C-A	PMP1	1	1	1
YGR034W	RPL26B	1	1	1
YEL026W	SNU13	1	1	1
YOL121C	RPS19A	1	1	1
YCR024C-B		1	1	1
YOR356W	CIR2	1	1	1
YDL208W	NHP2	1	1	1
YDR500C	RPL37B	1	1	1
YKL096W-A	CWP2	1	1	1
YLR372W	ELO3	1	1	1
YGL055W	OLE1	1	1	1
YJL190C	RPS22A	1	1	1
YER074W-A	YOS1	1	1	1
YCL058W-A	ADF1	1	1	1
YDR418W	RPL12B	1	1	1
YMR230W	RPS1B	1	1	1
YLR048W	RPSB	1	1	1
YGL256W	ADH4	1	1	1
YHR010W	RPL27A	1	1	1

YKR057W	RPS21A	1	1	1
YLR363W-A		1	1	1
YML126C	ERG13	1	1	1
YNL280C	ERG24	1	1	1
YPL079W	RPL21B	1	1	1
YBR034C	HMT1	1	1	1
YBL018C	POP8	1	1	1
YLR325C	RPL38	1	1	1
YPR035W	GLN1	1	1	1
YOR096W	RPS7A	1	1	1
YDR120C	TRM1	1	1	1
YHL001W	RPL14B	1	1	1
YDR502C	SAM2	1	1	1
YDL061C	RPS29B	1	1	1
YLR448W	RPL6B	1	1	1
YBR092C	PHO3	1	1	1
YNL113W	RPC19	1	1	1
YLR186W	EMG1	1	1	1
YOR182C	RPS3B	1	1	1
YOR145C	PNO1	1	1	1
YKR094C	RPL4B	1	1	1
YKL156W	RPS27A	1	1	1
YML022W	APT1	1	1	1
YLR061W	RPL22A	1	1	1
YOR167C	RPS28A	1	1	1
YJR094W-A	RPL43B	1	1	1
YFR032C-A	RPL29	1	1	1
YKR093W	PTR2	1	1	1
YEL024W	RIP1	1	1	1
YDL130W	RPP1B	1	1	1

YGR214W	RPSA	1	1	1
YFL034C-A	RPL22B	1	1	1
YCR031C	RPS14A	1	1	1
YGR108W	CLB1	1	1	1
YCL054W-A	RDT1	1	1	1
YLR406C	RPL31B	1	1	1
YGR159C	NSR1	1	1	1
YOR294W	RRS1	1	1	1
YMR142C	RPL13B	1	1	1
YPL198W	RPL7B	1	1	1
YNL069C	RPL16B	1	1	1
YBR010W	HHT1	1	1	1
YGL220W	BOL2	1	1	1
YBR181C	RPS6B	1	1	1
YBR242W		1	1	1
YML026C	RPS18B	1	1	1
YML073C	RPL6A	1	1	1
YOR312C	RPL2B	1	1	1
YER056C-A	RPL34A	1	1	1
YDR225W	HTA1	1	1	1
YPL249C-A	RPL36B	1	1	1
YMR292W	GOT1	1	1	1
YEL054C	RPL12A	1	1	1
YGR049W	SCM4	1	1	1
YMR143W	RPS16A	1	1	1
YBL027W	RPL19B	1	1	1
YHR021C	RPS27B	1	1	1
YJL177W	RPL17B	1	1	1
YPL143W	RPL33A	1	1	1
YGL226C-A	OST5	1	1	1

YMR307W	GAS1	1	1	1
YGR027C	RPS25A	1	1	1
YHR128W	FUR1	1	1	1
YLR300W	EXG1	1	1	1
YNL248C	RPA49	1	1	1
YDR450W	RPS18A	1	1	1
YMR256C	COX7	1	1	1
YGL103W	RPL28	1	1	1
YER117W	RPL23B	1	1	1
YDL082W	RPL13A	1	1	1
YML024W	RPS17A	1	1	1
YLR304C	ACO1	1	1	1
YDL136W	RPL35B	1	1	1
YBR189W	RPS9B	1	1	1
YLR083C	EMP7	1	1	1
YPR113W	PIS1	1	1	1
YJL011C	RPC17	1	1	1
YNL301C	RPL18B	1	1	1
YBR078W	ECM33	1	1	1
YNL289W	PCL1	1	1	1
YGL135W	RPL1B	1	1	1
YBL028C		1	1	1
YEL040W	UTR2	1	1	1
YML106W	URA5	1	1	1
YER074W	RPS24A	1	1	1
YLR185W	RPL37A	1	1	1
YPL211W	NIP7	1	1	1
YKL180W	RPL17A	1	1	1
YDR144C	MKC7	1	1	1
YML052W	SUR7	1	1	1

YIL052C	RPL34B	1	1	1
YNL244C	SUI1	1	1	1
YGL255W	ZRT1	1	1	1
YKL006C-A	SFT1	1	1	1
YHR072W-A	NOP1	1	1	1
YNL302C	RPS19B	1	1	1
YER091C	MET6	1	1	1
YBR263W	SHM1	1	1	1
YDR064W	RPS13	1	1	1
YGR118W	RPS23A	1	1	1
YLL011W	SOF1	1	1	1
YGR085C	RPL11B	1	1	1
YJL208C	NUC1	1	1	1
YHR141C	RPL42B	1	1	1
YPL144W	POC4	1	1	1
YKL172W	EBP2	1	1	1
YOR206W	NOC2	1	1	1
YJL191W	RPS14B	1	1	1
YOR078W	BUD21	1	1	1
YMR199W	CLN1	1	1	1
YHR196W	UTP9	1	1	1
YMR242C	RPL2A	1	1	1
YPL093W	NOG1	1	1	1
YPR187W	RPO26	1	1	1
YBL087C	RPL23A	1	1	1
YPR043W	RPL43A	1	1	1
YHR051W	COX6	1	1	1
YGL187C	COX4	1	1	1
YMR243C	ZRC1	1	1	1
YGR177C	ATF2	1	1	1

YHR046C	INM1	1	1	1
YMR305C	SCW1	1	1	1
YDR025W	RPS11A	1	1	1
YNL002C	RLP7	1	1	1
YDR033W	MRH1	1	1	1
YLR051C	FCF2	1	1	1
YDR497C	ITR1	1	1	1
YKL006W	RPL14A	1	1	1
YPL090C	RPS6A	1	1	1
YDL075W	RPL31A	1	1	1
YML063W	RPS1B	1	1	1
YOL010W	RCL1	1	1	1
YOL092W	YPQ1	1	1	1
YBR162W-A	YSY6	1	1	1
YLR407W		1	1	1
YKR044W	UIP5	1	1	1
YNL067W	RPL9B	1	1	1
YLR153C	ACS2	1	1	1
YIL148W	RPL4A	1	1	1
YOL120C	RPL18A	1	1	1
YMR272C	SCS7	1	1	1
YGL078C	DBP3	1	1	1
YER053C-A		1	1	1
YIL018W	RPL2B	1	1	1
YJL136C	RPS21B	1	1	1
YPR062W	FCY1	1	1	1
YLR146W-A		1	1	1
YEL021W	URA3	1	1	1
YDR045C	RPC11	1	1	1
YDR367W	KEI1	1	1	1

YOL127W	RPL25	1	1	1
YDR447C	RPS17B	1	1	1
YHL011C	PRS3	1	1	1
YLR441C	RPS1A	1	1	1
YPR132W	RPS23B	1	1	1
YDR299W	BFR2	1	1	1
YLL045C	RPL8B	1	1	1
YJR063W	RPA12	1	1	1
YGL076C	RPL7A	1	1	1
YER131W	RPS26B	1	1	1
YIL091C	UTP25	1	1	1
YPL082C	MOT1	1	1	1
YBR084C-A	RPL19A	1	1	1
YKR081C	RPF2	1	1	1
YML043C	RRN11	1	1	1
YBR187W	GDT1	1	1	1
YER126C	NSA2	1	1	1
YPR137W	RRP9	1	1	1
YBR009C	HHF1	1	1	1
YLR333C	RPS25B	1	1	1
YAL003W	EFB1	1	1	1
YER102W	RPS8B	1	1	1
YJL122W	ALB1	1	1	1
YKL009W	MRT4	1	1	1
YPL220W	RPL1A	1	1	1
YBL092W	RPL32	1	1	1
YLR435W	TSR2	1	1	1
YNL169C	PSD1	1	1	1
YOL077W-A	ATP19	1	1	1
YLR003C	CMS1	1	1	1

YJL050W	MTR4	1	1	1
YDR224C	HTB1	1	1	1
YBL042C	FUI1	1	1	1
YNL300W	TOS6	1	1	1
YOR224C	RPB8	1	1	1
YMR319C	FET4	1	1	1
YOL039W	RPP2A	1	1	1
YLR129W	DIP2	1	1	1
YMR001C	CDC5	1	1	1
YDR524C-B		1	1	1
YER043C	SAH1	1	1	1
YGR148C	RPL24B	1	1	1
YHL033C	RPL8A	1	1	1
YHR001W-A	QCR1	1	1	1
YML018C		1	1	1
YOR246C	ENV9	1	1	1
YBR271W	EFM2	1	1	1
YOR210W	RPB1	1	1	1
YCL054W	SPB1	1	1	1
YDL167C	NRP1	1	1	1
YLR038C	COX12	1	1	1
YGR187C	HGH1	1	1	1
YLR222C	UTP13	1	1	1
YBR191W	RPL21A	1	1	1
YGL030W	RPL3	1	1	1
YFR031C-A	RPL2A	1	1	1
YGL031C	RPL24A	1	1	1
YJR070C	LIA1	1	1	1
YJL205C	NCE11	1	1	1
YPR170W-B		1	1	1

YLR009W	RLP24	1	1	1
YGL029W	CGR1	1	1	1
YMR116C	ASC1	1	1	1
YCR034W	ELO2	1	1	1
YKL082C	RRP14	1	1	1
YPR102C	RPL11A	1	1	1
YGL123W	RPS2	1	1	1
YBR021W	FUR4	1	1	1
YGL021W	ALK1	1	1	1
YPR080W	TEF1	1	1	1
YPL157W	TGS1	1	1	1
YDR454C	GUK1	1	1	1
YHR041C	SRB2	1	1	1
YDR385W	EFT2	1	1	1
YAL025C	MAK16	1	1	1
YGL033W	HOP2	1	1	1
YHR005C-A	TIM1	1	1	1
YOR276W	CAF2	1	1	1
YBR154C	RPB5	1	1	1
YLR073C	RFU1	1	1	1
YBR238C		1	1	1
YJR123W	RPS5	1	1	1
YHR085W	IPI1	1	1	1
YJL148W	RPA34	1	1	1
YJR112W	NNF1	1	1	1
YOR045W	TOM6	1	1	1
YDL063C	SYO1	1	1	1
YDR021W	FAL1	1	1	1
YOR369C	RPS12	1	1	1
YPL226W	NEW1	1	1	1

YKL099C	UTP11	1	1	1
YLR168C	UPS2	1	1	1
YLR405W	DUS4	1	1	1
YGR271C-A	EFG1	1	1	1
YGL189C	RPS26A	1	1	1
YIL127C	RRT14	1	1	1
YIL053W	GPP1	1	1	1
YNL119W	NCS2	1	1	1
YDL051W	LHP1	1	1	1
YDL212W	SHR3	1	1	1
YLR068W	FYV7	1	1	1
YNL308C	KRI1	1	1	1
YDR226W	ADK1	1	1	1
YDL191W	RPL35A	1	1	1
YPR112C	MRD1	1	1	1
YOR116C	RPO31	1	1	1
YDL081C	RPP1A	1	1	1
YPL037C	EGD1	1	1	1
YBR029C	CDS1	1	1	1
YNL209W	SSB2	1	1	1
YMR309C	NIP1	1	1	1
YBL039C	URA7	1	1	1
YPL189C-A	COA2	1	1	1
YGR081C	SLX9	1	1	1
YKR024C	DBP7	1	1	1
YHR183W	GND1	1	1	1
YHR052W	CIC1	1	1	1
YIL131C	FKH1	1	1	1
YBL071W-A	KTI11	1	1	1
YKL182W	FAS1	1	1	1

YGL147C	RPL9A	1	1	1
YBL072C	RPS8A	1	1	1
YJR097W	JJJ3	1	1	1
YKL056C	TMA19	1	1	1
YDL229W	SSB1	1	1	1
YKR063C	LAS1	1	1	1
YDL157C		1	1	1
YLR223C	IFH1	1	1	1
YDR514C		1	1	1
YLR262C-A	TMA7	1	1	1
YFL045C	SEC53	1	1	1
YJL189W	RPL39	1	1	1
YJL138C	TIF2	1	1	1
YHR203C	RPS4B	1	1	1
YKL144C	RPC25	1	1	1
YJR073C	OPI3	1	1	1
YJR145C	RPS4A	1	1	1
YDR297W	SUR2	1	1	1
YMR079W	SEC14	1	1	1
YHR068W	DYS1	1	1	1
YLR221C	RSA3	1	1	1
YKL181W	PRS1	1	1	1
YDR399W	HPT1	1	1	1
YML080W	DUS1	1	1	1
YLR167W	RPS31	1	1	1
YML123C	PHO84	1	1	1
YDL060W	TSR1	1	1	1
YPR010C	RPA135	1	1	1
YPL256C	CLN2	1	1	1
YLR029C	RPL15A	1	1	1

YGR283C		1	1	1
YML081C-A	ATP18	1	1	1
YNL178W	RPS3	1	1	1
YCL036W	GFD2	1	1	1
YMR001C-A		1	1	1
YDR321W	ASP1	1	1	1
YBR143C	SUP45	1	1	1
YIL047C	SYG1	1	1	1
YDR496C	PUF6	1	1	1
YNL110C	NOP15	1	1	1
YDR302W	GPI11	1	1	1
YKR059W	TIF1	1	1	1
YHR089C	GAR1	1	1	1
YHR143W-A	RPC1	1	1	1
YAL036C	RBG1	1	1	1
YDL049C	KNH1	1	1	1
YLR249W	YEF3	1	1	1
YDL121C		1	1	1
YLR175W	CBF5	1	1	1
YML075C	HMG1	1	1	1
YJL069C	UTP18	1	1	1
YMR014W	BUD22	1	1	1
YKR010C	TOF2	1	1	1
YJR077C	MIR1	1	1	1
YKR079C	TRZ1	1	1	1
YLR409C	UTP21	1	1	1
YPL131W	RPL5	1	1	1
YKR060W	UTP3	1	1	1
YOL013W-A		1	1	1
YNL141W	AAH1	1	1	1

YGR183C	QCR9	1	1	1
YML113W	DAT1	1	1	1
YEL017C-A	PMP2	1	1	1
YOR355W	GDS1	1	1	1
YOL142W	RRP4	1	1	1
YLR264W	RPS28B	1	1	1
YNL066W	SUN4	1	1	1
YPL081W	RPS9A	1	1	1
YMR215W	GAS3	1	1	1
YJL051W	IRC8	1	1	1
YDL181W	INH1	1	1	1
YNL186W	UBP1	1	1	1
YBR031W	RPL4A	1	1	1
YBL004W	UTP2	1	1	1
YPR016C	TIF6	1	1	1
YOR359W	VTS1	1	1	1
YDR091C	RLI1	1	1	1
YKL069W		1	1	1
YBR069C	TAT1	1	1	1
YML096W		1	1	1
YNR054C	ESF2	1	1	1
YJL157C	FAR1	1	1	1
YDR545W	YRF1-1	1	1	1
YER025W	GCD11	1	1	1
YJL121C	RPE1	1	1	1
YPL183C	RTT1	1	1	1
YDR101C	ARX1	1	1	1
YPR110C	RPC4	1	1	1
YPR190C	RPC82	1	1	1
YER036C	ARB1	1	1	1

YNR075W	COS1	1	1	1
YDL166C	FAP7	1	1	1
YDR382W	RPP2B	1	1	1
YHR148W	IMP3	1	1	1
YLR074C	BUD2	1	1	1
YOL077C	BRX1	1	1	1
YIL009W	FAA3	1	1	1
YJL125C	GCD14	1	1	1
YNL151C	RPC31	1	1	1
YCR020C-A	MAK31	1	1	1
YBR267W	REI1	1	1	1
YAL059W	ECM1	1	1	1
YDR184C	ATC1	1	1	1
YMR093W	UTP15	1	1	1
YLR196W	PWP1	1	1	1
YML093W	UTP14	1	1	1
YDL031W	DBP1	1	1	1
YOR287C	RRP36	1	1	1
YOR095C	RKI1	1	1	1
YPL271W	ATP15	1	1	1
YNL096C	RPS7B	1	1	1
YPR074C	TKL1	1	1	1
YOL139C	CDC33	1	1	1
YOR348C	PUT4	1	1	1
YKL191W	DPH2	1	1	1
YBR030W	RKM3	1	1	1
YDR300C	PRO1	1	1	1
YNR012W	URK1	1	1	1
YGR128C	UTP8	1	1	1
YDR234W	LYS4	1	1	1

YMR269W	TMA23	1	1	1
YJR041C	URB2	1	1	1
YGR090W	UTP22	1	1	1
YPL043W	NOP4	1	1	1
YHR066W	SSF1	1	1	1
YOL041C	NOP12	1	1	1
YNR038W	DBP6	1	1	1
YOL040C	RPS15	1	1	1
YBR247C	ENP1	1	1	1
YOR342C		1	1	1
YLR154C	RNH23	1	1	1
YJR143C	PMT4	1	1	1
YPR143W	RRP15	1	1	1
YBR048W	RPS11B	1	1	1
YOL124C	TRM11	1	1	1
YCR072C	RSA4	1	1	1
YLL034C	RIX7	1	1	1
YHR092C	HXT4	1	1	1
YNL075W	IMP4	1	1	1
YLL008W	DRS1	1	1	1
YOL052C	SPE2	1	1	1
YMR003W	AIM34	1	1	1
YKR092C	SRP4	1	1	1
YOL125W	TRM13	1	1	1
YER072W	VTC1	1	1	1
YOR306C	MCH5	1	1	1
YMR131C	RRB1	1	1	1
YHR032W	ERC1	1	1	1
YNR009W	NRM1	1	1	1
YJL025W	RRN7	1	1	1

YDR281C	PHM6	1	1	1
YMR230W-A		1	1	1
YGR079W		1	1	1
YHR197W	RIX1	1	1	1
YBR172C	SMY2	1	1	1
YDL014W	NOP1	1	1	1
YDR075W	PPH3	1	1	1
YOR064C	YNG1	1	1	1
YBL054W	TOD6	1	1	1
YLR432W	IMD3	1	1	1
YGL211W	NCS6	1	1	1
YNL182C	IPI3	1	1	1
YPL233W	NSL1	1	1	1
YBL024W	NCL1	1	1	1
YDR179C	CSN9	1	1	1
YKR013W	PRY2	1	1	1
YOR252W	TMA16	1	1	1
YGR109C	CLB6	1	1	1
YKL068W-A		1	1	1
YDL205C	HEM3	1	1	1
YDR449C	UTP6	1	1	1
YLR336C	SGD1	1	1	1
YMR127C	SAS2	1	1	1
YCR047C	BUD23	1	1	1
YBR061C	TRM7	1	1	1
YLR264C-A		1	1	1
YDL213C	NOP6	1	1	1
YHR099W	TRA1	1	1	1
YDR119W-A	COX26	1	1	1
YDR083W	RRP8	1	1	1

YCR057C	PWP2	1	1	1
YOR073W	SGO1	1	1	1
YML108W		1	1	1
YIL096C	BMT5	1	1	1
YMR225C	MRPL44	1	1	1
YOL109W	ZEO1	1	1	1
YDR384C	ATO3	1	1	1
YOR133W	EFT1	1	1	1
YGR123C	PPT1	1	1	1
YGR217W	CCH1	1	1	1
YHL015W	RPS2	1	1	1
YNL090W	RHO2	1	1	1
YIL064W	EFM4	1	1	1
YOR313C	SPS4	1	1	1
YKL004W	AUR1	1	1	1
YOR204W	DED1	1	1	1
YNL282W	POP3	1	1	1
YNL313C	EMW1	1	1	1
YHR144C	DCD1	1	1	1
YIL130W	ASG1	1	1	1
YHR169W	DBP8	1	1	1
YBL029W		1	1	1
YGL168W	HUR1	1	1	1
YNL061W	NOP2	1	1	1
YGL101W		1	1	1
YDL201W	TRM8	1	1	1
YDR412W	RRP17	1	1	1
YML009C	MRPL39	1	1	1
YGR030C	POP6	1	1	1
YLR067C	PET39	1	1	1

YDR324C	UTP4	1	1	1
YBR141C	BMT2	1	1	1
YMR217W	GUA1	1	1	1
YGL258W	VEL1	1	1	1
YMR006C	PLB2	1	1	1
YIL110W	HPM1	1	1	1
YOR025W	HST3	1	1	1
YER137C		1	1	1
YML027W	YOX1	1	1	1
YDR398W	UTP5	1	1	1
YFL002C	SPB4	1	1	1
YFL023W	BUD27	1	1	1
YLR413W	INA1	1	1	1
YOR310C	NOP58	1	1	1
YDR441C	APT2	1	1	1
YGR129W	SYF2	1	1	1
YOR129C	AFI1	1	1	1
YNL299W	TRF5	1	1	1
YBL098W	BNA4	1	1	1
YJL098W	SAP185	1	1	1
YDR345C	HXT3	1	1	1
YBR213W	MET8	1	1	1
YOL080C	REX4	1	1	1
YPR119W	CLB2	1	1	1
YCR098C	GIT1	1	1	1
YCL002C		1	1	1
YOR340C	RPA43	1	1	1
YCR085W		1	1	1
YJL118W		1	1	1
YLR150W	STM1	1	1	1

YPL279C	FEX2	1	1	1
YGR158C	MTR3	1	1	1
YHL048C-A		1	1	1
YNL132W	KRE33	1	1	1
YHR149C	SKG6	1	1	1
YOR101W	RAS1	1	1	1
YPL126W	NAN1	1	1	1
YLR180W	SAM1	1	1	1
YLR340W	RPP	1	1	1
YBL081W		1	1	1
YIL011W	TIR3	1	1	1
YEL042W	GDA1	1	1	1
YOR004W	UTP23	1	1	1
YIL119C	RPI1	1	1	1
YEL073C		1	1	1
YLR453C	RIF2	1	1	1
YMR290C	HAS1	1	1	1
YHR061C	GIC1	1	1	1
YLR401C	DUS3	1	1	1
YDR524W-C		1	1	1
YLR014C	PPR1	1	1	1
YJL153C	INO1	1	1	1
YLR044C	PDC1	1	1	1

Identifier	**Common name**	**wild-type**	***dbp5-L12A***	***dbp5-R423A***
YKR077W	MSA2	2	0	0
YDR153C	ENT5	2	0	0
YER017C	AFG3	2	0	0
YNL059C	ARP5	2	0	0
YBR260C	RGD1	2	0	0

YPL177C	CUP9	2	0	0
YLR248W	RCK2	2	0	0
YBR115C	LYS2	2	0	0
YNL236W	SIN4	2	0	0
YDR354W	TRP4	2	0	0
YER088C	DOT6	2	0	0
YKL032C	IXR1	2	0	0
YMR237W	BCH1	2	0	0
YMR285C	NGL2	2	0	0
YOR303W	CPA1	2	0	0
YPL023C	MET12	2	0	0
YER052C	HOM3	2	0	0
YFL013C	IES1	2	0	0
YLR396C	VPS33	2	0	0
YGR270W	YTA7	2	0	0
YMR124W	EPO1	2	0	0
YHR106W	TRR2	2	0	0
YBL016W	FUS3	2	0	0
YLR090W	XDJ1	2	0	0
YHR164C	DNA2	2	0	0
YOR316C	COT1	2	0	0
YLR099C	ICT1	2	0	0
YFR022W	ROG3	2	0	0
YGL179C	TOS3	2	0	0
YKL108W	SLD2	2	0	0
YLR046C		2	0	0
YDL103C	QRI1	2	0	0
YBR198C	TAF5	2	0	0
YPL124W	SPC29	2	0	0
YLL019C	KNS1	2	0	0

YDR477W	SNF1	2	0	0
YNR010W	CSE2	2	0	0
YBR223C	TDP1	2	0	0
YNL020C	ARK1	2	0	0
YIL095W	PRK1	2	0	0
YPL204W	HRR25	2	0	0
YER008C	SEC3	2	0	0
YAL043C	PTA1	2	0	0
YKL204W	EAP1	2	0	0
YDR113C	PDS1	2	0	0
YOL148C	SPT2	2	0	0
YLR133W	CKI1	2	0	0
YER119C	AVT6	2	0	0
YPL259C	APM1	2	0	0
YEL047C	FRD1	2	0	0
YDL123W	SNA4	2	0	0
YOL060C	MAM3	2	0	0
YIL109C	SEC24	2	0	0
YPL009C	RQC2	2	0	0
YDR405W	MRP2	2	0	0
YPL049C	DIG1	2	0	0
YGL066W	SGF73	2	0	0
YJR091C	JSN1	2	0	0
YIL146C	ATG32	2	0	0
YJR065C	ARP3	2	0	0
YIL137C	TMA18	2	0	0
YIL153W	RRD1	2	0	0
YHR158C	KEL1	2	0	0
YMR086W	SEG1	2	0	0
YOR074C	CDC21	2	0	0

YCR067C	SED4	2	0	0
YOR070C	GYP1	2	0	0
YPL180W	TCO89	2	0	0
YDR406W	PDR15	2	0	0
YBR016W		2	0	0
YDL045C	FAD1	2	0	0
YIR014W		2	0	0
YLR394W	CST9	2	0	0
YML114C	TAF8	2	0	0
YPL188W	POS5	2	0	0
YGR247W	CPD1	2	0	0
YJL079C	PRY1	2	0	0
YJR021C	REC17	2	0	0
YGR056W	RSC1	2	0	0
YLR273C	PIG1	2	0	0
YLR134W	PDC5	2	0	0
YFR029W	PTR3	2	0	0
YLR187W	SKG3	2	0	0
YJR019C	TES1	2	0	0
YAR020C	PAU7	2	0	0
YCR106W	RDS1	2	0	0
YCL004W	PGS1	2	0	0
YFR008W	FAR7	2	0	0
YPR093C	ASR1	2	0	0
YPR034W	ARP7	2	0	0
YOR014W	RTS1	2	0	0
YOR380W	RDR1	2	0	0
YNL128W	TEP1	2	0	0
YLL056C		2	0	0
YBL047C	EDE1	2	0	0

YHL047C	ARN2	2	0	0
YLR006C	SSK1	2	0	0
YPL089C	RLM1	2	0	0
YAR019C	CDC15	2	0	0
YGR097W	ASK1	2	0	0
YKL187C	FAT3	2	0	0
YGL035C	MIG1	2	0	0
YIR018C-A		2	0	0
YGR287C	IMA1	2	0	0
YOR290C	SNF2	2	0	0
YKR020W	VPS51	2	0	0
YDR169C	STB3	2	0	0
YLR070C	XYL2	2	0	0
YPL015C	HST2	2	0	0
YJL078C	PRY3	2	0	0
YJL106W	IME2	2	0	0
YJL159W	HSP15	2	0	0
YPL164C	MLH3	2	0	0
YNL107W	YAF9	2	0	0
YOR371C	GPB1	2	0	0
YFL020C	PAU5	2	0	0
YGL071W	AFT1	2	0	0
YDL210W	UGA4	2	0	0
YDL214C	PRR2	2	0	0
YKR102W	FLO1	2	0	0
YLR438W	CAR2	2	0	0
YPL258C	THI21	2	0	0
YMR206W		2	0	0
YIL072W	HOP1	2	0	0
YOL091W	SPO21	2	0	0

YIR019C	FLO11	2	0	0
YPL201C	YIG1	2	0	0
YDL197C	ASF2	2	0	0
YOL038C-A		2	0	0
YGR067C		2	0	0
YGL125W	MET13	2	0	0
YKL095W	YJU2	2	0	0
YGR292W	MAL12	2	0	0
YOR156C	NFI1	2	0	0
YDR402C	DIT2	2	0	0
YMR279C		2	0	0
YKL065C	YET1	0	2	0
YKL126W	YPK1	0	2	0
YDR391C		0	2	0
YGR186W	TFG1	0	2	0
YPR072W	NOT5	0	2	0
YDR067C	OCA6	0	2	0
YPL091W	GLR1	0	2	0
YMR121C	RPL15B	0	2	0
YHR012W	VPS29	0	2	0
YCL035C	GRX1	0	2	0
YPL154C	PEP4	0	2	0
YAL016W	TPD3	0	2	0
YMR113W	FOL3	0	2	0
YOR124C	UBP2	0	2	0
YHR027C	RPN1	0	2	0
YKL015W	PUT3	0	2	0
YJL210W	PEX2	0	2	0
YJL094C	KHA1	0	2	0
YMR092C	AIP1	0	2	0

YDL017W	CDC7	0	2	0
YHR017W	YSC83	0	2	0
YIL034C	CAP2	0	2	0
YMR022W	UBC7	0	2	0
YAL060W	BDH1	0	2	0
YFR042W	KEG1	0	2	0
YFR053C	HXK1	0	2	0
YPR057W	BRR1	0	2	0
YGR013W	SNU71	0	2	0
YOR352W	TFB6	0	2	0
YPL096W	PNG1	0	2	0
YNL200C	NNR1	0	2	0
YKL193C	SDS22	0	2	0
YJL047C	RTT11	0	2	0
YOR110W	TFC7	0	2	0
YMR077C	VPS2	0	2	0
YPL214C	THI6	0	2	0
YBR053C		0	2	0
YBR272C	HSM3	0	2	0
YPL147W	PXA1	0	2	0
YNL233W	BNI4	0	2	0
YIL033C	BCY1	0	2	0
YHR043C	DOG2	0	2	0
YBR255W	MTC4	0	2	0
YGL153W	PEX14	0	2	0
YDR103W	STE5	0	2	0
YBR137W		0	2	0
YJL103C	GSM1	0	2	0
YDR219C	MFB1	0	2	0
YDR265W	PEX1	0	2	0

YER045C	ACA1	0	2	0
YDR306C		0	2	0
YMR120C	ADE17	0	2	0
YML028W	TSA1	0	2	0
YLR085C	ARP6	0	2	0
YNL160W	YGP1	0	2	0
YER053C	PIC2	0	2	0
YNR061C		0	2	0
YPL060W	MFM1	0	2	0
YDR371W	CTS2	0	2	0
YOL117W	RRI2	0	2	0
YLR271W	CMG1	0	2	0
YMR029C	FAR8	0	2	0
YER104W	RTT15	0	2	0
YDL130W-A	STF1	0	2	0
YGL185C		0	2	0
YLR119W	SRN2	0	2	0
YCL048W-A		0	2	0
YDR387C	CIN1	0	2	0
YFR015C	GSY1	0	2	0
YJR106W	ECM27	0	2	0
YOL100W	PKH2	0	2	0
YPL099C	INA17	0	2	0
YPR160W	GPH1	0	2	0
YDR383C	NKP1	0	2	0
YGL130W	CEG1	0	2	0
YCR045C	RRT12	0	2	0
YGL196W	DSD1	0	2	0
YOR034C-A		0	2	0
YMR114C		0	2	0

YDR490C	PKH1	0	2	0
YDR282C	MRX1	0	2	0
YMR020W	FMS1	0	2	0
YJL132W		0	2	0
YIL077C		0	2	0
YEL062W	NPR2	0	2	0
YGL237C	HAP2	0	2	0
YGL090W	LIF1	0	2	0
YOR368W	RAD17	0	2	0
YDL027C	MRX9	0	2	0
YKL065W-A		0	2	0
YBL100W-C		0	2	0
YDR069C	DOA4	0	2	0
YEL039C	CYC7	0	2	0
YML029W	USA1	0	2	0
YIL071C	PCI8	0	2	0
YML118W	NGL3	0	2	0
YEL041W	YEF1	0	2	0
YER078W-A		0	2	0
YOL156W	HXT11	0	2	0
YPL236C	ENV7	0	2	0
YJR008W	MHO1	0	2	0
YGR174W-A		0	2	0
YAR023C		0	2	0
YFR026C	ULI1	0	2	0
YCR101C		0	2	0
YER039C	HVG1	0	2	0
YMR195W	ICY1	0	2	0
YNR069C	BSC5	0	2	0
YOL159C-A		0	2	0

YDR256C	CTA1	0	2	0
YFL058W	THI5	0	2	0
YIL029C		0	2	0
YGR289C	MAL11	0	2	0
YJR149W		0	2	0
YGL062W	PYC1	0	2	0
YOR113W	AZF1	0	2	0
YPR005C	HAL1	0	2	0
YIL134C-A		0	2	0
YIL172C	IMA3	0	2	0
YOR134W	BAG7	0	2	0
YBR294W	SUL1	0	2	0
YLR363C	NMD4	0	2	0
YBR033W	EDS1	0	2	0
YNL025C	SSN8	0	2	0
YER027C	GAL83	2	2	0
YJR125C	ENT3	2	2	0
YER162C	RAD4	2	2	0
YGR009C	SEC9	2	2	0
YPL110C	GDE1	2	2	0
YBR204C	LDH1	2	2	0
YBR269C	SDH8	2	2	0
YGL157W	ARI1	2	2	0
YER095W	RAD51	2	2	0
YPR040W	TIP41	2	2	0
YLR219W	MSC3	2	2	0
YOR043W	WHI2	2	2	0
YER101C	AST2	2	2	0
YKL025C	PAN3	2	2	0
YGR156W	PTI1	2	2	0

YFL054C	AQY3	2	2	0
YBR105C	VID24	2	2	0
YOR162C	YRR1	2	2	0
YIL050W	PCL7	2	2	0
YOR128C	ADE2	2	2	0
YJL042W	MHP1	2	2	0
YKR098C	UBP11	2	2	0
YFR030W	MET1	2	2	0
YOL016C	CMK2	2	2	0
YGL174W	BUD13	2	2	0
YNL125C	ESBP6	2	2	0
YKL168C	KKQ8	2	2	0
YGR002C	SWC4	2	2	0
YHR195W	NVJ1	2	2	0
YKL142W	MRP8	2	2	0
YHR176W	FMO1	2	2	0
YDL132W	CDC53	2	2	0
YOR185C	GSP2	2	2	0
YOL082W	ATG19	2	2	0
YGR268C	HUA1	2	2	0
YIR017C	MET28	2	2	0
YAL014C	SYN8	2	2	0
YOL135C	MED7	2	2	0
YJR093C	FIP1	2	2	0
YOR347C	PYK2	2	2	0
YDL223C	HBT1	2	2	0
YNL242W	ATG2	2	2	0
YLR095C	IOC2	2	2	0
YAL062W	GDH3	2	2	0
YJL060W	BNA3	2	2	0

YLR144C	ACF2	2	2	0
YOR383C	FIT3	2	2	0
YOR267C	HRK1	2	2	0
YMR181C		2	2	0
YOL067C	RTG1	2	2	0
YGL156W	AMS1	2	2	0
YER059W	PCL6	2	2	0
YNL304W	YPT11	2	2	0
YNL309W	STB1	2	2	0
YPL055C	LGE1	2	2	0
YBL022C	PIM1	2	2	0
YMR304W	UBP15	2	2	0
YJL020C	BBC1	2	2	0
YPL250C	ATG41	2	2	0
YCL052C	PBN1	2	2	0
YDR036C	EHD3	2	2	0
YPL222W	FMP4	2	2	0
YNL260C	LTO1	2	2	0
YKL035W	UGP1	2	2	0
YOR228C	MCP1	2	2	0
YOR062C		2	2	0
YFL029C	CAK1	2	2	0
YPR184W	GDB1	2	2	0
YHR159W	TDA11	2	2	0
YDR475C	JIP4	2	2	0
YKL096C-B		2	2	0
YKL059C	MPE1	2	2	0
YKL034W	TUL1	2	2	0
YJR033C	RAV1	2	2	0
YKL133C		2	2	0

YCL057W	PRD1	2	2	0
YLR011W	LOT6	2	2	0
YNR047W	FPK1	2	2	0
YDR293C	SSD1	2	2	0
YGR019W	UGA1	2	2	0
YNL293W	MSB3	2	2	0
YMR189W	GCV2	2	2	0
YDL057W		2	2	0
YPR036W-A	SPO24	2	2	0
YGL194C	HOS2	2	2	0
YGL197W	MDS3	2	2	0
YDR530C	APA2	2	2	0
YGR241C	YAP182	2	2	0
YOR393W	ERR1	2	2	0
YMR104C	YPK2	2	2	0
YGL081W		2	2	0
YPL223C	GRE1	2	2	0
YKR029C	SET3	2	2	0
YLR238W	FAR1	2	2	0
YLR337C	VRP1	2	2	0
YMR252C		2	2	0
YFL053W	DAK2	2	2	0
YNL196C	SLZ1	2	2	0
YPL278C		2	2	0
YCR091W	KIN82	2	2	0
YLR346C	CIS1	2	2	0
YLR157C-B		2	2	0
YOL085C		2	2	0
YBR128C	ATG14	2	2	0
YPL017C	IRC15	2	2	0

YCL026C-A	FRM2	2	2	0
YDL024C	DIA3	2	2	0
YOR100C	CRC1	2	2	0
YGL096W	TOS8	2	2	0
YKR106W	GEX2	2	2	0
YPL202C	AFT2	2	2	0
YDR043C	NRG1	2	2	0
YKL010C	UFD4	0	0	2
YNL026W	SAM5	0	0	2
YLR137W	RKM5	0	0	2
YBR045C	GIP1	0	0	2
YDR092W	UBC13	0	0	2
YDR117C	TMA64	0	0	2
YER028C	MIG3	0	0	2
YJR084W		0	0	2
YER163C	GCG1	0	0	2
YNL193W		0	0	2
YER055C	HIS1	0	0	2
YGL080W	MPC1	0	0	2
YKR009C	FOX2	0	0	2
YPL031C	PHO85	0	0	2
YIL030C	SSM4	0	0	2
YDR305C	HNT2	0	0	2
YOR087W	YVC1	0	0	2
YJL071W	ARG2	0	0	2
YOL123W	HRP1	0	0	2
YGL060W	YBP2	0	0	2
YNL008C	ASI3	0	0	2
YIL003W	CFD1	0	0	2
YDL088C	ASM4	0	0	2

YOL068C	HST1	0	0	2
YDR138W	HPR1	0	0	2
YNL051W	COG5	0	0	2
YJL066C	MPM1	0	0	2
YMR201C	RAD14	0	0	2
YPR179C	HDA3	0	0	2
YLL063C	AYT1	0	0	2
YDL139C	SCM3	0	0	2
YDR515W	SLF1	0	0	2
YGR109W-B		0	0	2
YMR160W		0	0	2
YOR288C	MPD1	0	0	2
YER041W	YEN1	0	0	2
YGR144W	THI4	0	0	2
YGR278W	CWC22	0	0	2
YHR116W	COX23	0	0	2
YLR126C		0	0	2
YHR048W	YHK8	0	0	2
YJR078W	BNA2	0	0	2
YER185W	PUG1	0	0	2
YOR391C	HSP33	0	0	2
YJL023C	PET13	0	0	2
YGR120C	COG2	0	0	2
YDR523C	SPS1	0	0	2
YDR403W	DIT1	0	0	2
YAR031W	PRM9	0	0	2
YOR186W		0	0	2
YER121W		0	0	2
YDL244W	THI13	0	0	2
YDR253C	MET32	0	0	2

YDR476C		2	0	2
YDL070W	BDF2	2	0	2
YIL143C	SSL2	2	0	2
YER161C	SPT2	2	0	2
YJL128C	PBS2	2	0	2
YDR145W	TAF12	2	0	2
YHL008C		2	0	2
YKR002W	PAP1	2	0	2
YKL195W	MIA4	2	0	2
YPR106W	ISR1	2	0	2
YNL251C	NRD1	2	0	2
YPR024W	YME1	2	0	2
YMR192W	GYL1	2	0	2
YCL049C		2	0	2
YLR115W	CFT2	2	0	2
YKL159C	RCN1	2	0	2
YDL193W	NUS1	2	0	2
YKL124W	SSH4	2	0	2
YML032C	RAD52	2	0	2
YLR343W	GAS2	2	0	2
YDR207C	UME6	2	0	2
YNL314W	DAL82	2	0	2
YGL051W	MST27	2	0	2
YGR240C-A		2	0	2
YCL016C	DCC1	2	0	2
YPL153C	RAD53	2	0	2
YIR009W	MSL1	2	0	2
YER096W	SHC1	2	0	2
YHL037C		2	0	2
YKL071W		2	0	2

YKL007W	CAP1	0	2	2
YKR049C	FMP46	0	2	2
YDL099W	BUG1	0	2	2
YOL064C	MET22	0	2	2
YIL065C	FIS1	0	2	2
YML069W	POB3	0	2	2
YJR052W	RAD7	0	2	2
YCR011C	ADP1	0	2	2
YGL095C	VPS45	0	2	2
YNR035C	ARC35	0	2	2
YGR101W	PCP1	0	2	2
YOR362C	PRE1	0	2	2
YLR199C	PBA1	0	2	2
YJL070C		0	2	2
YFR055W	IRC7	0	2	2
YMR110C	HFD1	0	2	2
YDL010W	GRX6	0	2	2
YER004W	FMP52	0	2	2
YNL265C	IST1	0	2	2
YLR257W		0	2	2
YOR138C	RUP1	0	2	2
YML088W	UFO1	0	2	2
YKL206C	ADD66	0	2	2
YFR014C	CMK1	0	2	2
YGL048C	RPT6	0	2	2
YGR135W	PRE9	0	2	2
YBR059C	AKL1	0	2	2
YGR250C	RIE1	0	2	2
YJL001W	PRE3	0	2	2
YKL079W	SMY1	0	2	2

YNL157W	IGO1	0	2	2
YML062C	MFT1	0	2	2
YKL213C	DOA1	0	2	2
YER094C	PUP3	0	2	2
YBL041W	PRE7	0	2	2
YGL121C	GPG1	0	2	2
YDR329C	PEX3	0	2	2
YNL181W	PBR1	0	2	2
YMR271C	URA1	0	2	2
YOL017W	ESC8	0	2	2
YOL083W	ATG34	0	2	2
YDR353W	TRR1	0	2	2
YDL110C	TMA17	0	2	2
YLR352W		0	2	2
YLL001W	DNM1	0	2	2
YNL006W	LST8	0	2	2
YJL102W	MEF2	0	2	2
YDR202C	RAV2	0	2	2
YGR070W	ROM1	0	2	2
YER042W	MXR1	0	2	2
YBR139W		0	2	2
YDR131C		0	2	2
YLR408C	BLS1	0	2	2
YJR086W	STE18	0	2	2
YDR058C	TGL2	0	2	2
YHL010C	ETP1	0	2	2
YDR392W	SPT3	0	2	2
YMR313C	TGL3	0	2	2
YDL021W	GPM2	0	2	2
YBR278W	DPB3	0	2	2

YGR053C		0	2	2
YOR075W	UFE1	0	2	2
YOL031C	SIL1	0	2	2
YJR104C	SOD1	0	2	2
YNL222W	SSU72	0	2	2
YDL190C	UFD2	0	2	2
YDL180W		0	2	2
YDR231C	COX2	0	2	2
YNL142W	MEP2	0	2	2
YGL154C	LYS5	0	2	2
YMR053C	STB2	0	2	2
YIR028W	DAL4	0	2	2
YAL063C	FLO9	0	2	2
YNL294C	RIM21	0	2	2
YLL057C	JLP1	0	2	2
YMR210W	MGL2	0	2	2
YIL170W	HXT12	0	2	2
YHR007C-A		0	2	2
YNL253W	TEX1	0	2	2
YOR022C	DDL1	0	2	2
YDR244W	PEX5	0	2	2
YPL261C		0	2	2
YHR075C	PPE1	0	2	2
YPL191C		0	2	2
YPR081C	GRS2	0	2	2
YPL120W	VPS3	0	2	2
YMR040W	YET2	0	2	2
YMR232W	FUS2	0	2	2
YER066W	RRT13	0	2	2
YIR005W	IST3	0	2	2

YKL221W	MCH2	0	2	2
YCR010C	ADY2	0	2	2
YJL206C		0	2	2
YHR140W		0	2	2
YLR031W		0	2	2
YGL240W	DOC1	0	2	2
YNL214W	PEX17	0	2	2
YGR225W	AMA1	0	2	2
YML058W-A	HUG1	0	2	2
YDR255C	RMD5	0	2	2
YGL205W	POX1	0	2	2
YLR281C		0	2	2
YLL062C	MHT1	0	2	2
YDL247W	MPH2	0	2	2
YBR244W	GPX2	2	2	2
YKL086W	SRX1	2	2	2
YER143W	DDI1	2	2	2
YOR226C	ISU2	2	2	2
YDR453C	TSA2	2	2	2
YFR017C	IGD1	2	2	2
YKR034W	DAL8	2	2	2
YBR101C	FES1	2	2	2
YER175C	TMT1	2	2	2
YJL036W	SNX4	2	2	2
YOL151W	GRE2	2	2	2
YGR142W	BTN2	2	2	2
YDL025C	RTK1	2	2	2
YHR030C	SLT2	2	2	2
YDR394W	RPT3	2	2	2
YFL056C	AAD6	2	2	2

YNL335W	DDI3	2	2	2
YLL029W	FRA1	2	2	2
YER142C	MAG1	2	2	2
YPL092W	SSU1	2	2	2
YOL158C	ENB1	2	2	2
YGR048W	UFD1	2	2	2
YKL091C		2	2	2
YBL064C	PRX1	2	2	2
YPL247C		2	2	2
YOR052C	TMC1	2	2	2
YAL061W	BDH2	2	2	2
YHL035C	VMR1	2	2	2
YJL101C	GSH1	2	2	2
YMR062C	ARG7	2	2	2
YBR047W	FMP23	2	2	2
YOL119C	MCH4	2	2	2
YDL234C	GYP7	2	2	2
YJR130C	STR2	2	2	2
YDL020C	RPN4	2	2	2
YGR161C	RTS3	2	2	2
YLR177W		2	2	2
YIR034C	LYS1	2	2	2
YKR052C	MRS4	2	2	2
YHR097C		2	2	2
YCL030C	HIS4	2	2	2
YDR533C	HSP31	2	2	2
YBL033C	RIB1	2	2	2
YML007W	YAP1	2	2	2
YGR209C	TRX2	2	2	2
YPL171C	OYE3	2	2	2

YLR387C	REH1	2	2	2
YNR014W		2	2	2
YBR280C	SAF1	2	2	2
YER035W	EDC2	2	2	2
YDL182W	LYS2	2	2	2
YJR096W		2	2	2
YGR130C		2	2	2
YNL036W	NCE13	2	2	2
YOR382W	FIT2	2	2	2
YJL057C	IKS1	2	2	2
YJR109C	CPA2	2	2	2
YNL134C		2	2	2
YNL195C		2	2	2
YFR004W	RPN11	2	2	2
YNR068C		2	2	2
YDR425W	SNX41	2	2	2
YMR031C	EIS1	2	2	2
YDL007W	RPT2	2	2	2
YBR046C	ZTA1	2	2	2
YHL021C	AIM17	2	2	2
YDR436W	PPZ2	2	2	2
YGR223C	HSV2	2	2	2
YGR258C	RAD2	2	2	2
YDL169C	UGX2	2	2	2
YGR043C	NQM1	2	2	2
YMR261C	TPS3	2	2	2
YFR010W	UBP6	2	2	2
YDR074W	TPS2	2	2	2
YDR423C	CAD1	2	2	2
YDR001C	NTH1	2	2	2

YGL117W		2	2	2
YJL165C	HAL5	2	2	2
YOL032W	OPI1	2	2	2
YAR007C	RFA1	2	2	2
YOL058W	ARG1	2	2	2
YLR327C	TMA1	2	2	2
YKR023W		2	2	2
YDR003W-A		2	2	2
YGL091C	NBP35	2	2	2
YML130C	ERO1	2	2	2
YKR076W	ECM4	2	2	2
YPR107C	YTH1	2	2	2
YBR256C	RIB5	2	2	2
YIL101C	XBP1	2	2	2
YMR004W	MVP1	2	2	2
YFR003C	YPI1	2	2	2
YPL230W	USV1	2	2	2
YDR270W	CCC2	2	2	2
YOR173W	DCS2	2	2	2
YDL059C	RAD59	2	2	2
YGR194C	XKS1	2	2	2
YOR130C	ORT1	2	2	2
YDR011W	SNQ2	2	2	2
YBR170C	NPL4	2	2	2
YDR171W	HSP42	2	2	2
YLR149C		2	2	2
YGL141W	HUL5	2	2	2
YOR059C	LPL1	2	2	2
YNL194C		2	2	2
YGL181W	GTS1	2	2	2

YOR223W	DSC3	2	2	2
YMR087W		2	2	2
YLR025W	SNF7	2	2	2
YBR212W	NGR1	2	2	2
YBL086C		2	2	2
YNL305C	BXI1	2	2	2
YOR181W	LAS17	2	2	2
YHL002W	HSE1	2	2	2
YDR380W	ARO1	2	2	2
YMR115W	MGR3	2	2	2
YEL065W	SIT1	2	2	2
YBL058W	SHP1	2	2	2
YKL100C	YPF1	2	2	2
YPL100W	ATG21	2	2	2
YPL152W	RRD2	2	2	2
YGL122C	NAB2	2	2	2
YJL144W		2	2	2
YDL147W	RPN5	2	2	2
YMR258C	ROY1	2	2	2
YIL036W	CST6	2	2	2
YIL066C	RNR3	2	2	2
YOR259C	RPT4	2	2	2
YDR258C	HSP78	2	2	2
YEL060C	PRB1	2	2	2
YCL039W	GID7	2	2	2
YLL026W	HSP14	2	2	2
YML131W		2	2	2
YBL101C	ECM21	2	2	2
YHL036W	MUP3	2	2	2
YDR229W	IVY1	2	2	2

YMR067C	UBX4	2	2	2
YBR214W	SDS24	2	2	2
YBR114W	RAD16	2	2	2
YOR261C	RPN8	2	2	2
YAL034C	FUN19	2	2	2
YMR173W	DDR48	2	2	2
YOR221C	MCT1	2	2	2
YDL022W	GPD1	2	2	2
YJL155C	FBP26	2	2	2
YFL007W	BLM1	2	2	2
YDL204W	RTN2	2	2	2
YDL131W	LYS21	2	2	2
YLR214W	FRE1	2	2	2
YNL183C	NPR1	2	2	2
YLR362W	STE11	2	2	2
YHR138C		2	2	2
YLR258W	GSY2	2	2	2
YIL055C		2	2	2
YNR006W	VPS27	2	2	2
YEL012W	UBC8	2	2	2
YOR023C	AHC1	2	2	2
YPL084W	BRO1	2	2	2
YIL116W	HIS5	2	2	2
YCL044C	MGR1	2	2	2
YHR096C	HXT5	2	2	2
YHR199C	AIM46	2	2	2
YDL222C	FMP45	2	2	2
YMR314W	PRE5	2	2	2
YBR279W	PAF1	2	2	2
YMR311C	GLC8	2	2	2

YDL113C	ATG2	2	2	2
YJL016W	TPH3	2	2	2
YIR025W	MND2	2	2	2
YDL072C	YET3	2	2	2
YFL061W	DDI2	2	2	2
YFR052W	RPN12	2	2	2
YPL196W	OXR1	2	2	2
YGR237C		2	2	2
YLL039C	UBI4	2	2	2
YGL180W	ATG1	2	2	2
YOL084W	PHM7	2	2	2
YLR225C		2	2	2
YML057W	CMP2	2	2	2
YLR345W		2	2	2
YIL165C		2	2	2
YOR076C	SKI7	2	2	2
YOR131C		2	2	2
YOR161C	PNS1	2	2	2
YKR011C		2	2	2
YFR050C	PRE4	2	2	2
YNL115C		2	2	2
YLR034C	SMF3	2	2	2
YDR168W	CDC37	2	2	2
YPR178W	PRP4	2	2	2
YMR090W		2	2	2
YIL136W	OM45	2	2	2
YDL243C	AAD4	2	2	2
YDR320C	SWA2	2	2	2
YDR427W	RPN9	2	2	2
YPL249C	GYP5	2	2	2

YGL011C	SCL1	2	2	2
YML116W	ATR1	2	2	2
YHR104W	GRE3	2	2	2
YNL317W	PFS2	2	2	2
YKL218C	SRY1	2	2	2
YLR247C	IRC2	2	2	2
YHL019C	APM2	2	2	2
YLL023C	POM33	2	2	2
YNL007C	SIS1	2	2	2
YOR069W	VPS5	2	2	2
YML092C	PRE8	2	2	2
YGR248W	SOL4	2	2	2
YDR358W	GGA1	2	2	2
YJL088W	ARG3	2	2	2
YMR096W	SNZ1	2	2	2
YHR209W	CRG1	2	2	2
YDL097C	RPN6	2	2	2
YER012W	PRE1	2	2	2
YPL119C-A		2	2	2
YDR132C		2	2	2
YDR263C	DIN7	2	2	2
YHR137W	ARO9	2	2	2
YBR072W	HSP26	2	2	2
YPR185W	ATG13	2	2	2
YMR105C	PGM2	2	2	2
YGR136W	LSB1	2	2	2
YOR036W	PEP12	2	2	2
YOR220W	RCN2	2	2	2
YLR270W	DCS1	2	2	2
YGL036W		2	2	2

YOR250C	CLP1	2	2	2
YLR178C	TFS1	2	2	2
YBR126C	TPS1	2	2	2
YFR024C-A	LSB3	2	2	2
YGL227W	VID3	2	2	2
YIR007W	EGH1	2	2	2
YJR059W	PTK2	2	2	2
YAL017W	PSK1	2	2	2
YCL055W	KAR4	2	2	2
YML004C	GLO1	2	2	2
YIL097W	FYV1	2	2	2
YFL016C	MDJ1	2	2	2
YER067W	RGI1	2	2	2
YDL149W	ATG9	2	2	2
YKL103C	APE1	2	2	2
YBR173C	UMP1	2	2	2
YFL042C	LAM5	2	2	2
YIL105C	SLM1	2	2	2
YLR350W	ORM2	2	2	2
YDR070C	FMP16	2	2	2
YJL149W	DAS1	2	2	2
YOR292C		2	2	2
YKL146W	AVT3	2	2	2
YBR273C	UBX7	2	2	2
YNL312W	RFA2	2	2	2
YMR107W	SPG4	2	2	2
YMR095C	SNO1	2	2	2
YJL141C	YAK1	2	2	2
YCL034W	LSB5	2	2	2
YER021W	RPN3	2	2	2

YOR155C	ISN1	2	2	2
YKL026C	GPX1	2	2	2
YDR035W	ARO3	2	2	2
YDR246W	TRS23	2	2	2
YHR029C	YHI9	2	2	2
YML100W	TSL1	2	2	2
YIL155C	GUT2	2	2	2
YNL215W	IES2	2	2	2
YLR303W	MET17	2	2	2
YIL117C	PRM5	2	2	2
YLR356W	ATG33	2	2	2
YGR080W	TWF1	2	2	2
YBR001C	NTH2	2	2	2
YHL030W	ECM29	2	2	2
YEL011W	GLC3	2	2	2
YMR262W		2	2	2
YLR151C	PCD1	2	2	2
YOR117W	RPT5	2	2	2
YBR231C	SWC5	2	2	2
YBR241C		2	2	2
YLR260W	LCB5	2	2	2
YGL013C	PDR1	2	2	2
YPL260W	CUB1	2	2	2
YNR032W	PPG1	2	2	2
YGL037C	PNC1	2	2	2
YMR058W	FET3	2	2	2
YMR275C	BUL1	2	2	2
YIR039C	YPS6	2	2	2
YDR330W	UBX5	2	2	2
YPR108W	RPN7	2	2	2

YLR108C		2	2	2
YCL026C-B	HBN1	2	2	2
YLR251W	SYM1	2	2	2
YNR033W	ABZ1	2	2	2
YBR108W	AIM3	2	2	2
YOR120W	GCY1	2	2	2
YOR374W	ALD4	2	2	2
YDR122W	KIN1	2	2	2
YDR085C	AFR1	2	2	2
YJR005C-A	LSO1	2	2	2
YPL056C	LCL1	2	2	2
YDR273W	DON1	2	2	2
YHR161C	YAP181	2	2	2
YKR058W	GLG1	2	2	2
YML070W	DAK1	2	2	2
YMR196W		2	2	2
YMR103C		2	2	2
YER079W		2	2	2
YCL008C	STP22	2	2	2
YKL129C	MYO3	2	2	2
YIR003W	AIM21	2	2	2
YLR072W	LAM6	2	2	2
YLR206W	ENT2	2	2	2
YPR103W	PRE2	2	2	2
YKL163W	PIR3	2	2	2
YIL135C	VHS2	2	2	2
YIL026C	IRR1	2	2	2
YMR175W	SIP18	2	2	2
YGL093W	SPC15	2	2	2
YEL005C	VAB2	2	2	2

YPR158W	CUR1	2	2	2
YIL075C	RPN2	2	2	2
YGL163C	RAD54	2	2	2
YML049C	RSE1	2	2	2
YGR234W	YHB1	2	2	2
YDR251W	PAM1	2	2	2
YFR027W	ECO1	2	2	2
YOR132W	VPS17	2	2	2
YBR233W	PBP2	2	2	2
YMR041C	ARA2	2	2	2
YDL085W	NDE2	2	2	2
YOR157C	PUP1	2	2	2
YDL215C	GDH2	2	2	2
YDR003W	RCR2	2	2	2
YDR018C		2	2	2
YGL110C	CUE3	2	2	2
YKR091W	SRL3	2	2	2
YBL078C	ATG8	2	2	2
YBR117C	TKL2	2	2	2
YOR329C	SCD5	2	2	2
YAR027W	UIP3	2	2	2
YGL025C	PGD1	2	2	2
YML117W	NAB6	2	2	2
YDR019C	GCV1	2	2	2
YDR204W	COQ4	2	2	2
YOL073C	DSC2	2	2	2
YHR102W	KIC1	2	2	2
YPL004C	LSP1	2	2	2
YHR171W	ATG7	2	2	2
YLR299W	ECM38	2	2	2

YDL091C	UBX3	2	2	2
YOR298C-A	MBF1	2	2	2
YIR011C	STS1	2	2	2
YLR136C	TIS11	2	2	2
YNL155W	CUZ1	2	2	2
YDL239C	ADY3	2	2	2
YCL064C	CHA1	2	2	2
YMR219W	ESC1	2	2	2
YAL013W	DEP1	2	2	2
YPL123C	RNY1	2	2	2
YKR089C	TGL4	2	2	2
YMR085W		2	2	2
YGL010W	MPO1	2	2	2
YPR079W	MRL1	2	2	2
YBR056W		2	2	2
YOR019W		2	2	2
YHR087W	RTC3	2	2	2
YNL094W	APP1	2	2	2
YBL048W	RRT1	2	2	2
YDR059C	UBC5	2	2	2
YDL238C	GUD1	2	2	2
YDR479C	PEX29	2	2	2
YLL060C	GTT2	2	2	2
YDR501W	PLM2	2	2	2
YDL233W	MFG1	2	2	2
YKL151C	NNR2	2	2	2
YOL018C	TLG2	2	2	2
YDL089W	NUR1	2	2	2
YER033C	ZRG8	2	2	2
YPR167C	MET16	2	2	2

YDL230W	PTP1	2	2	2
YDL054C	MCH1	2	2	2
YMR152W	YIM1	2	2	2
YNL274C	GOR1	2	2	2
YML112W	CTK3	2	2	2
YDR295C	HDA2	2	2	2
YMR139W	RIM11	2	2	2
YNL074C	MLF3	2	2	2
YLR392C	ART1	2	2	2
YOR289W		2	2	2
YBR043C	QDR3	2	2	2
YIL099W	SGA1	2	2	2
YCL040W	GLK1	2	2	2
YDL115C	IWR1	2	2	2
YDL101C	DUN1	2	2	2
YIL087C	AIM19	2	2	2
YLR369W	SSQ1	2	2	2
YGL114W		2	2	2
YOL162W		2	2	2
YPL022W	RAD1	2	2	2
YGR008C	STF2	2	2	2
YKL023W		2	2	2
YJL163C		2	2	2
YML042W	CAT2	2	2	2
YLR324W	PEX3	2	2	2
YGL053W	PRM8	2	2	2
YER054C	GIP2	2	2	2
YKR067W	GPT2	2	2	2
YBR284W		2	2	2
YOR227W	HER1	2	2	2

YIL154C	IMP2'	2	2	2
YGL224C	SDT1	2	2	2
YDL161W	ENT1	2	2	2
YGR243W	MPC3	2	2	2
YGL059W	PKP2	2	2	2
YLR267W	BOP2	2	2	2
YGL184C	STR3	2	2	2
YCR030C	SYP1	2	2	2
YDL019C	OSH2	2	2	2
YOR042W	CUE5	2	2	2
YHR018C	ARG4	2	2	2
YPR145W	ASN1	2	2	2
YGL073W	HSF1	2	2	2
YPR155C	NCA2	2	2	2
YDR182W-A		2	2	2
YIL113W	SDP1	2	2	2
YPL213W	LEA1	2	2	2
YDR151C	CTH1	2	2	2
YMR118C	SHH3	2	2	2
YDR162C	NBP2	2	2	2
YJR039W		2	2	2
YGL250W	RMR1	2	2	2
YPR025C	CCL1	2	2	2
YHR200W	RPN1	2	2	2
YPL003W	ULA1	2	2	2
YGL047W	ALG13	2	2	2
YGL128C	CWC23	2	2	2
YNR034W-A	EGO4	2	2	2
YLR176C	RFX1	2	2	2
YJL031C	BET4	2	2	2

YPL240C	HSP82	2	2	2
YFL041W-A		2	2	2
YHL040C	ARN1	2	2	2
YDR411C	DFM1	2	2	2
YDL124W		2	2	2
YMR140W	SIP5	2	2	2
YJL053W	PEP8	2	2	2
YGL219C	MDM34	2	2	2
YBR062C		2	2	2
YML128C	MSC1	2	2	2
YBR290W	BSD2	2	2	2
YOR208W	PTP2	2	2	2
YFR020W	CSS2	2	2	2
YPL113C		2	2	2
YOL038W	PRE6	2	2	2
YGR028W	MSP1	2	2	2
YAL028W	FRT2	2	2	2
YHR008C	SOD2	2	2	2
YGL104C	VPS73	2	2	2
YBR085C-A		2	2	2
YBL075C	SSA3	2	2	2
YGR127W		2	2	2
YJL084C	ALY2	2	2	2
YPR026W	ATH1	2	2	2
YOL048C	RRT8	2	2	2
YGR256W	GND2	2	2	2
YIL007C	NAS2	2	2	2
YDR516C	EMI2	2	2	2
YPL186C	UIP4	2	2	2
YBL015W	ACH1	2	2	2

YMR174C	PAI3	2	2	2
YNL054W	VAC7	2	2	2
YBR008C	FLR1	2	2	2
YBL091C-A	SCS22	2	2	2
YDR034W-B		2	2	2
YBR169C	SSE2	2	2	2
YOL111C	MDY2	2	2	2
YNR007C	ATG3	2	2	2
YMR028W	TAP42	2	2	2
YDR435C	PPM1	2	2	2
YGL222C	EDC1	2	2	2
YNR034W	SOL1	2	2	2
YOR028C	CIN5	2	2	2
YIL045W	PIG2	2	2	2
YHR139C	SPS1	2	2	2
YLR162W-A	RRT15	2	2	2
YNR002C	ATO2	2	2	2
YPL119C	DBP1	2	2	2
YMR276W	DSK2	2	2	2
YBL029C-A		2	2	2
YMR197C	VTI1	2	2	2
YMR135C	GID8	2	2	2
YDR259C	YAP6	2	2	2
YER020W	GPA2	2	2	2
YMR068W	AVO2	2	2	2
YIL107C	PFK26	2	2	2
YIL152W		2	2	2
YNL234W		2	2	2
YKL211C	TRP3	2	2	2
YKL162C		2	2	2

YGR010W	NMA2	2	2	2
YDL216C	RRI1	2	2	2
YPL054W	LEE1	2	2	2
YLR080W	EMP46	2	2	2
YOR018W	ROD1	2	2	2
YER103W	SSA4	2	2	2
YOR381W	FRE3	2	2	2
YJL045W		2	2	2
YAL051W	OAF1	2	2	2
YJL161W	FMP33	2	2	2
YDL199C		2	2	2
YBR006W	UGA2	2	2	2
YAL015C	NTG1	2	2	2
YNL223W	ATG4	2	2	2
YMR169C	ALD3	2	2	2
YGR197C	SNG1	2	2	2
YDR513W	GRX2	2	2	2
YDL183C		2	2	2
YGL164C	YRB3	2	2	2
YMR250W	GAD1	2	2	2
YDR014W-A	HED1	2	2	2
YNL014W	HEF3	2	2	2
YNL104C	LEU4	2	2	2
YPL203W	TPK2	2	2	2
YJL085W	EXO7	2	2	2
YIL164C	NIT1	2	2	2
YOR054C	VHS3	2	2	2
YHR016C	YSC84	2	2	2
YLR164W	SHH4	2	2	2
YPL070W	MUK1	2	2	2

YBR147W	RTC2	2	2	2
YIL160C	POT1	2	2	2
YNR064C		2	2	2
YNL241C	ZWF1	2	2	2
YKL107W		2	2	2
YNL011C		2	2	2
YER150W	SPI1	2	2	2
YDR484W	VPS52	2	2	2
YLR216C	CPR6	2	2	2
YMR158C-A		2	2	2
YOR005C	DNL4	2	2	2
YNL092W		2	2	2
YDL142C	CRD1	2	2	2
YJL199C	MBB1	2	2	2
YLL058W		2	2	2
YMR175W-A		2	2	2
YGL208W	SIP2	2	2	2
YKL121W	DGR2	2	2	2
YJR036C	HUL4	2	2	2
YJR083C	ACF4	2	2	2
YPL228W	CET1	2	2	2
YJL164C	TPK1	2	2	2
YOR377W	ATF1	2	2	2
YER179W	DMC1	2	2	2
YOR152C	ATG4	2	2	2
YDR421W	ARO8	2	2	2
YKL105C	SEG2	2	2	2
YOR114W		2	2	2
YFL014W	HSP12	2	2	2
YLR109W	AHP1	2	2	2

YBL049W	MOH1	2	2	2
YBR285W		2	2	2
YIL056W	VHR1	2	2	2
YER037W	PHM8	2	2	2
YNL117W	MLS1	2	2	2
YHL016C	DUR3	2	2	2
YPL229W		2	2	2
YOL052C-A	DDR2	2	2	2
YLR102C	APC9	2	2	2
YDL106C	PHO2	2	2	2
YKR097W	PCK1	2	2	2
YIL024C		2	2	2
YNR049C	MSO1	2	2	2
YIL017C	VID28	2	2	2
YHR189W	PTH1	2	2	2
YGR066C		2	2	2
YOL024W		2	2	2
YBR119W	MUD1	2	2	2
YPR015C		2	2	2
YMR159C	ATG16	2	2	2
YOR027W	STI1	2	2	2
YCR102C		2	2	2
YPL166W	ATG29	2	2	2
YHL024W	RIM4	2	2	2
YJL219W	HXT9	2	2	2
YLR312C	ATG39	2	2	2
YIR041W	PAU15	2	2	2
YGR154C	GTO1	2	2	2
YOL126C	MDH2	2	2	2
YDR374C	PHO92	2	2	2

YOR394W	PAU21	2	2	2
YGR236C	SPG1	2	2	2
YOL131W		2	2	2
YJR156C	THI11	2	2	2
YJL089W	SIP4	2	2	2
YLR460C		2	2	2
YCR099C		2	2	2
YCL027W	FUS1	2	2	2

Table 6-2. Clusters of ncRNA genes differentially expressed in dbp5 mutatants in response to MMS treatment

Complete list of genes used for cluster analysis		**Cluster 1 genes**		**Cluster 2 genes**		**Cluster 3 genes**	
Identifier	**Common name**	**Identifier**	**Common name**	**Identifier**	**Common name**	**Identifier**	**Common name**
YBR236C	ABD1	YDL175C	AIR2	YOL077C	BRX1	YLR063W	BMT6
YOR239W	ABP140	YFL009W	CDC4	YHR052W	CIC1	YKL078W	DHR2
YDL175C	AIR2	YIL003W	CFD1	YNL232W	CSL4	YPL086C	ELP3
YOR335C	ALA1	YOL021C	DIS3	YJL125C	GCD14	YGR145W	ENP2
YAL020C	ATS1	YLR192C	HCR1	YHR085W	IPI1	YJL033W	HCA4
YDR299W	BFR2	YPL204W	HRR25	YNR024W	MPP6	YNL075W	IMP4
YPL217C	BMS1	YPL135W	ISU1	YER006W	NUG1	YCL059C	KRR1
YBR141C	BMT2	YBR057C	MUM2	YMR239C	RNT1	YKL110C	KTI12
YIL096C	BMT5	YGL091C	NBP35	YDR500C	RPL37b	YFR001W	LOC1
YLR063W	BMT6	YMR285C	NGL2	YDR087C	RRP1	YHR081W	LRP1
YOL077C	BRX1	YBR279W	PAF1	YDR412W	RRP17	YKL021C	MAK11
YOR078W	BUD21	YHR034C	PIH1	YGR095C	RRP46	YPR144C	NOC4
YMR014W	BUD22	YLR107W	REX3	YHL025W	SNF6	YDL213C	NOP6
YCR047C	BUD23	YLR145W	RMP1	YDR478W	SNM1	YOL115W	PAP2
YGR262C	BUD32	YML127	RSC9	YDL112	TRM3	YKR095	PCC1

		W		W		W−A	
YLR175W	CBF5	YLR430W	SEN1	YBR061C	TRM7	YPL212C	PUS1
YKL208W	CBT1	YNL224C	SQS1	YDL060W	TSR1	YGL063W	PUS2
YFL009W	CDC4	YHR111W	UBA4	YOL022C	TSR4	YNL292W	PUS4
YIL003W	CFD1			YDR324C	UTP4	YGR280C	PXR1
YML036W	CGI121			YGL173C	XRN1	YGL246C	RAI1
YGL029W	CGR1					YOR001W	RRP6
YDR267C	CIA1					YNR015W	SMM1
YHR052W	CIC1					YHR070W	TRM5
YIL035C	CKA1					YGL050W	TYW3
YOR061W	CKA2						
YGL019W	CKB1						
YOR039W	CKB2						
YNL232W	CSL4						
YDL031W	DBP10						
YNL112W	DBP2						
YGL078C	DBP3						
YNR038W	DBP6						
YKR024C	DBP7						
YHR169W	DBP8						
YLR276C	DBP9						
YFL001W	DEG1						
YKL078W	DHR2						
YPL266W	DIM1						
YLR129W	DIP2						
YOL021C	DIS3						
YLL008W	DRS1						
YML080W	DUS1						
YLR401C	DUS3						
YLR405W	DUS4						
YKL172W	EBP2						

YMR128W	ECM16
YGR271C-A	EFG1
YGR200C	ELP2
YPL086C	ELP3
YPL101W	ELP4
YMR312W	ELP6
YLR186W	EMG1
YBR247C	ENP1
YGR145W	ENP2
YMR049C	ERB1
YDR365C	ESF1
YNR054C	ESF2
YIL019W	FAF1
YDR021W	FAL1
YDL166C	FAP7
YDR339C	FCF1
YLR051C	FCF2
YAL035W	FUN12
YLR068W	FYV7
YHR089C	GAR1
YNL062C	GCD10
YJL125C	GCD14
YOR205C	GEP3
YER133W	GLC7
YLL035W	GRC3
YLR293C	GSP1
YMR290C	HAS1
YJL033W	HCA4
YLR192C	HCR1
YJR055W	HIT1
YPL204W	HRR25
YHR187W	IKI1

YLR384C	IKI3
YHR148W	IMP3
YNL075W	IMP4
YHR085W	IPI1
YNL182C	IPI3
YPL135W	ISU1
YOR226C	ISU2
YNL227C	JJJ1
YKR038C	KAE1
YNL132W	KRE33
YNL308C	KRI1
YCL059C	KRR1
YBL071W-A	KTI11
YKL110C	KTI12
YKR063C	LAS1
YER127W	LCP5
YFR001W	LOC1
YHR081W	LRP1
YBL026W	LSM2
YLR438C-A	LSM3
YER112W	LSM4
YER146W	LSM5
YDR378C	LSM6
YNL147W	LSM7
YJR022W	LSM8
YKL021C	MAK11
YAL025C	MAK16
YBR142W	MAK5
YLR106C	MDN1
YOR274W	MOD5
YPL082C	MOT1
YJR002W	MPP10

YNR024W	MPP6
YPR112C	MRD1
YOR201C	MRM1
YGL136C	MRM2
YNL306W	MRPS18
YBR146W	MRPS9
YKL009W	MRT4
YMR023C	MSS1
YGL236C	MTO1
YJL050W	MTR4
YBR057C	MUM2
YNL124W	NAF1
YPL126W	NAN1
YGL091C	NBP35
YBL024W	NCL1
YNL119W	NCS2
YGL211W	NCS6
YCL017C	NFS1
YMR285C	NGL2
YDL208W	NHP2
YPL211W	NIP7
YOR056C	NOB1
YLR002C	NOC3
YPR144C	NOC4
YPL093W	NOG1
YDL014W	NOP1
YHR072W-A	NOP10
YOL041C	NOP12
YDL148C	NOP14
YNL110C	NOP15
YER002W	NOP16
YGR251W	NOP19

YNL061W	NOP2
YPL043W	NOP4
YPL146C	NOP53
YLR197W	NOP56
YOR310C	NOP58
YDL213C	NOP6
YGR103W	NOP7
YJL010C	NOP9
YDR432W	NPL3
YER126C	NSA2
YGR159C	NSR1
YER006W	NUG1
YBR279W	PAF1
YOL115W	PAP2
YKR095W-A	PCC1
YHR034C	PIH1
YOR145C	PNO1
YNL282W	POP3
YBR257W	POP4
YAL033W	POP5
YGR030C	POP6
YBR167C	POP7
YBL018C	POP8
YGL120C	PRP43
YPL212C	PUS1
YGL063W	PUS2
YNL292W	PUS4
YLR165C	PUS5
YGR169C	PUS6
YOR243C	PUS7
YDL036C	PUS9
YLR196W	PWP1

YCR057C	PWP2
YGR280C	PXR1
YDL104C	QRI7
YGL246C	RAI1
YOR048C	RAT1
YOL010W	RCL1
YNL022C	RCM1
YLR059C	REX2
YLR107W	REX3
YOL080C	REX4
YOL066C	RIB2
YOR119C	RIO1
YNL207W	RIO2
YMR283C	RIT1
YHR197W	RIX1
YDR091C	RLI1
YNL002C	RLP7
YLR145W	RMP1
YGR276C	RNH70
YMR239C	RNT1
YGL171W	ROK1
YHR088W	RPF1
YKR081C	RPF2
YKL180W	RPL17a
YJL177W	RPL17b
YPL220W	RPL1a
YGL135W	RPL1b
YGL030W	RPL30
YDL136W	RPL35b
YLR185W	RPL37a
YDR500C	RPL37b
YGL076C	RPL7a

YPL198W	RPL7b
YHL033C	RPL8a
YLL045C	RPL8b
YHR062C	RPP1
YGR214W	RPS0a
YLR048W	RPS0b
YDR025W	RPS11a
YBR048W	RPS11b
YDR064W	RPS13
YCR031C	RPS14a
YJL191W	RPS14b
YMR143W	RPS16a
YDL083C	RPS16b
YDR450W	RPS18a
YML026C	RPS18b
YLR441C	RPS1a
YML063W	RPS1b
YGL123W	RPS2
YHL015W	RPS20
YKR057W	RPS21a
YJL136C	RPS21b
YGR118W	RPS23a
YPR132W	RPS23b
YER074W	RPS24a
YIL069C	RPS24b
YKL156W	RPS27a
YHR021C	RPS27b
YOR167C	RPS28a
YLR264W	RPS28b
YLR167W	RPS31
YPL090C	RPS6a
YBR181C	RPS6b

YOR096W	RPS7a
YNL096C	RPS7b
YBL072C	RPS8a
YER102W	RPS8b
YPL081W	RPS9a
YBR189W	RPS9b
YMR131C	RRB1
YDR087C	RRP1
YPL012W	RRP12
YKL082C	RRP14
YPR143W	RRP15
YDR412W	RRP17
YHR065C	RRP3
YOR287C	RRP36
YHR069C	RRP4
YOL142W	RRP40
YDL111C	RRP42
YCR035C	RRP43
YDR280W	RRP45
YGR095C	RRP46
YMR229C	RRP5
YOR001W	RRP6
YCL031C	RRP7
YDR083W	RRP8
YPR137W	RRP9
YOR294W	RRS1
YML127W	RSC9
YHR087W	RTC3
YPL235W	RVB2
YJL098W	SAP185
YKR028W	SAP190
YDL153C	SAS10

YLR430W	SEN1
YDL047W	SIT4
YGR195W	SKI6
YDL033C	SLM3
YGR081C	SLX9
YNL196C	SLZ1
YNR015W	SMM1
YHL025W	SNF6
YDR478W	SNM1
YEL026W	SNU13
YOR308C	SNU66
YLL011W	SOF1
YCL054W	SPB1
YFL002C	SPB4
YNL224C	SQS1
YCR018C	SRD1
YNL209W	SSB2
YHR066W	SSF1
YHR064C	SSZ1
YGL169W	SUA5
YNR004W	SWM2
YGL243W	TAD1
YJL035C	TAD2
YLR316C	TAD3
YGL232W	TAN1
YHR003C	TCD1
YKL027W	TCD2
YPL157W	TGS1
YGR024C	THG1
YPR016C	TIF6
YDR117C	TMA64
YDR457W	TOM1

YDR120C	TRM1
YOL093W	TRM10
YOL124C	TRM11
YNR046W	TRM112
YML005W	TRM12
YOL125W	TRM13
YKR056W	TRM2
YDL112W	TRM3
YPL030W	TRM44
YHR070W	TRM5
YBR061C	TRM7
YMR259C	TRM732
YDL201W	TRM8
YDR165W	TRM82
YML014W	TRM9
YDL060W	TSR1
YLR435W	TSR2
YOR006C	TSR3
YOL022C	TSR4
YOR251C	TUM1
YPL207W	TYW1
YGL050W	TYW3
YHR111W	UBA4
YJR041C	URB2
YIL008W	URM1
YJL109C	UTP10
YKL099C	UTP11
YLR222C	UTP13
YML093W	UTP14
YMR093W	UTP15
YJL069C	UTP18
YBL004W	UTP20

YLR409C	UTP21
YGR090W	UTP22
YOR004W	UTP23
YIL091C	UTP25
YKR060W	UTP30
YDR324C	UTP4
YDR398W	UTP5
YDR449C	UTP6
YER082C	UTP7
YGR128C	UTP8
YHR196W	UTP9
YGL173C	XRN1
YOR272W	YTM1
YGR285C	ZUO1

Table 6-3. Synthetic gene array analysis of *dbp5-L12A* and *dbp5-R423A*

Term:	Description:
Gene	Standard gene name
Ctr	Average normalized colony size of control strain
Exp	Average normalized colony size of double mutant
Ratio	Average ratio of Exp to Ctr
Ratio <p	Number of replicates in which the ratio is below the low cut-off value (*p*)
Diff	Average normalized experimental colony size minus average normalized colony size
p-value	p-value from a paired t-test
Hit	When the ratio is below the low cut-off value (p) in 3/3 (L12A) or 5/6 (R423A) of the independent SGA replicates and p-value is <0.05

dbp5-L12A SGA results:

Gene	Ctrl	Exp	Ratio	Ratio < p	Diff	p-value	Hit?	Description
SRF1	1.057	0.050	0.047	3/3	-1.057	3.3E-04	Yes	Regulator of phospholipase D (Spo14p); interacts with Spo14p and regulates its catalytic activity; capable of buffering the toxicity of C16:0 platelet activating factor, a lipid that accumulates intraneuronally in Alzheimer's patients
YAR029W	0.636	0.050	0.079	3/3	-0.636	1.3E-02	Yes	Member of DUP240 gene family but contains no transmembrane domains; green fluorescent protein (GFP)-fusion protein localizes to the cytoplasm in a punctate pattern
BEM1	0.567	0.050	0.088	3/3	-0.567	6.6E-03	Yes	Protein containing SH3-domains, involved in establishing cell polarity and morphogenesis; functions as a scaffold protein for complexes that include Cdc24p, Ste5p, Ste20p, and Rsr1p
LRP1	0.791	0.404	0.511	3/3	-0.387	6.0E-03	Yes	Nuclear exosome-associated nucleic acid binding protein; involved in RNA processing, surveillance, degradation, tethering, and export; homolog of mammalian nuclear matrix protein C1D involved in regulation of DNA repair and recombination
THP1	0.839	0.507	0.604	3/3	-0.332	1.6E-02	Yes	Nuclear pore-associated protein, forms a complex with Sac3p that is involved in transcription and in mRNA export from the nucleus; contains a PAM domain implicated in protein-protein binding
SLX9	0.898	0.615	0.685	3/3	-0.283	4.5E-03	Yes	Protein required for pre-rRNA processing; associated with the 90S pre-ribosome and 43S small ribosomal subunit precursor; interacts with U3 snoRNA; deletion mutant has synthetic fitness defect with an sgs1 deletion mutant
SHS1	0.237	0.050	0.211	3/3	-0.237	6.2E-03	Yes	One of five related septins (Cdc3p, Cdc10p, Cdc11p, Cdc12p, Shs1p) that form a cortical filamentous collar at the mother-bud neck which is necessary for normal morphogenesis and cytokinesis
BUD25	0.930	0.726	0.781	3/3	-0.204	8.2E-03	Yes	Protein involved in bud-site selection; diploid mutants display a random budding pattern instead of the wild-type bipolar pattern
COG1	0.302	0.154	0.509	3/3	-0.148	1.7E-03	Yes	Essential component of the conserved oligomeric Golgi complex (Cog1p through Cog8p), a cytosolic tethering complex that functions in protein trafficking to mediate

								fusion of transport vesicles to Golgi compartments
SHP1	0.448	0.324	0.724	3/3	-0.124	1.6E-02	Yes	UBX (ubiquitin regulatory X) domain-containing protein that regulates Glc7p phosphatase activity and interacts with Cdc48p; interacts with ubiquitylated proteins in vivo and is required for degradation of a ubiquitylated model substrate
MDM20	0.381	0.259	0.679	3/3	-0.122	1.2E-02	Yes	Non-catalytic subunit of the NatB N-terminal acetyltransferase, which catalyzes N-acetylation of proteins with specific N-terminal sequences; involved in mitochondrial inheritance and actin assembly
SPE2	0.265	0.169	0.639	3/3	-0.096	4.7E-02	Yes	S-adenosylmethionine decarboxylase, required for the biosynthesis of spermidine and spermine; cells lacking Spe2p require spermine or spermidine for growth in the presence of oxygen but not when grown anaerobically

dbp5-R423A SGA results:

Gene	Ctrl	Exp	Ratio	Ratio < p	Diff	p-value	Hit?	Description
STD1	1.0655	0.050	0.047	6/6	-1.016	1.6E-08	Yes	Protein involved in control of glucose-regulated gene expression; interacts with kinase Snf1p, glucose sensors Snf3p and Rgt2p, TATA-binding Spt15p; regulator of transcription factor Rgt1p; interactions with Pma1p appear to propagate [GAR+]; STD1 has a paralog, MTH1, that arose from the whole genome duplication
SLX9	0.9942	0.065	0.065	6/6	-0.929	4.5E-08	Yes	Protein required for pre-rRNA processing; associated with the 90S pre-ribosome and 43S small ribosomal subunit precursor; interacts with U3 snoRNA; deletion mutant has synthetic fitness defect with an sgs1 deletion mutant
RSB1	1.0754	0.163	0.155	6/6	-0.912	9.6E-05	Yes	Putative sphingoid long-chain base (LCB) efflux transporter; integral membrane transporter that localizes to the plasma membrane and may transport long chain bases (LCBs) from the cytoplasmic side toward the extracytoplasmic side of the membrane; role in glycerophospholipid translocation; suppressor of the sphingoid LCB sensitivity of an LCB-lyase mutation
NUP120	1.0493	0.165	0.161	6/6	-0.885	7.7E-04	Yes	Subunit of the Nup84p subcomplex of the nuclear pore complex (NPC); contributes to nucleocytoplasmic transport and NPC biogenesis and is involved in establishment of a normal nucleocytoplasmic concentration gradient of the GTPase Gsp1p; also plays roles in several processes that may require localization of genes or chromosomes at the nuclear periphery,

								including double-strand break repair, transcription and chromatin silencing; homologous to human NUP160
CIN5	1.0838	0.326	0.300	6/6	-0.758	6.5E-03	Yes	Basic leucine zipper (bZIP) transcription factor of the yAP-1 family; physically interacts with the Tup1-Cyc8 complex and recruits Tup1p to its targets; mediates pleiotropic drug resistance and salt tolerance; nuclearly localized under oxidative stress and sequestered in the cytoplasm by Lot6p under reducing conditions; CIN5 has a paralog, YAP6, that arose from the whole genome duplication
ETT1	1.0435	0.290	0.287	6/6	-0.753	5.9E-03	Yes	Nuclear protein that inhibits replication of Brome mosaic virus; S. cerevisiae is a model system for studying replication of positive-strand RNA viruses in their natural hosts; deletion increases stop codon readthrough
YNL140C	1.1134	0.367	0.339	6/6	-0.746	5.5E-03	Yes	Protein of unknown function; expressed at both mRNA and protein levels; partially overlaps THO2/YNL139C
NUP60	1.0476	0.383	0.365	6/6	-0.664	4.2E-07	Yes	FG-nucleoporin component of central core of the nuclear pore complex; contributes directly to nucleocytoplasmic transport and maintenance of the nuclear pore complex (NPC) permeability barrier and is involved in gene tethering at the nuclear periphery; relocalizes to the cytosol in response to hypoxia; both NUP1 and NUP60 are homologous to human NUP153
SAC3	0.9978	0.341	0.339	6/6	-0.657	3.6E-03	Yes	mRNA export factor; required for biogenesis of the small ribosomal subunit; component of TREX-2 complex (Sac3p-Thp1p-Sus1p-Cdc31p) involved in transcription elongation and mRNA export from the nucleus; involved in post-transcriptional tethering of active genes to the nuclear periphery and to non-nascent mRNP; similar to the human germinal center-associated nuclear protein (GANP)
NUP84	0.8211	0.182	0.224	6/6	-0.639	2.4E-05	Yes	Subunit of the Nup84p subcomplex of the nuclear pore complex (NPC); contributes to nucleocytoplasmic transport and NPC biogenesis; also plays roles in several processes that may require localization of genes or chromosomes at the nuclear periphery, including double-strand break repair, transcription and chromatin silencing; homologous to human NUP107
THP2	1.0088	0.380	0.396	5/6	-0.629	2.0E-02	Yes	Subunit of the THO and TREX complexes; THO connects transcription elongation and mitotic recombination, and TREX is recruited to activated genes and couples transcription to mRNA export; involved in telomere maintenance
VHS3	1.0174	0.398	0.393	6/6	-0.619	1.2E-02	Yes	Negative regulatory subunit of protein phosphatase 1 Ppz1p; involved in coenzyme A biosynthesis; subunit of the phosphopantothenoylcysteine decarboxylase (PPCDC; Cab3p, Sis2p, Vhs3p) complex and the CoA-Synthesizing Protein Complex (CoA-

								SPC: Cab2p, Cab3p, Cab4p, Cab5p, Sis2p and Vhs3p)
PFA4	1.0722	0.465	0.434	6/6	-0.607	1.0E-02	Yes	Palmitoyltransferase with autoacylation activity; required for palmitoylation of amino acid permeases containing a C-terminal Phe-Trp-Cys site; required for modification of Chs3p; member of the DHHC family of putative palmitoyltransferases
TMC1	1.0509	0.449	0.426	5/6	-0.602	2.1E-02	Yes	AN1-type zinc finger protein, effector of proteotoxic stress response; stress-inducible transcriptional target of Rpn4p; induced by nitrogen limitation, weak acid, misfolded proteins; short-lived protein, degraded by proteasome; may protect cells from trivalent metalloid induced proteotoxicity; contains PACE promoter element; ortholog of human AIRAP, which stimulates proteasome activity in response to arsenic; protein abundance increases under DNA replication stress
IRC23	1.0739	0.472	0.449	6/6	-0.601	1.2E-02	Yes	Protein of unknown function; green fluorescent protein (GFP)-fusion localizes to the ER; null mutant displays increased levels of spontaneous Rad52p foci; IRC23 has a paralog, BSC2, that arose from the whole genome duplication
HST3	0.8805	0.292	0.345	6/6	-0.589	7.2E-03	Yes	Member of the Sir2 family of NAD(+)-dependent protein deacetylases; involved along with Hst4p in telomeric silencing, cell cycle progression, radiation resistance, genomic stability and short-chain fatty acid metabolism
CUE5	1.1679	0.600	0.517	6/6	-0.567	7.3E-04	Yes	Ubiquitin-binding protein; functions as ubiquitin-Atg8p adaptor in ubiquitin-dependent autophagy; serves as proteaphagy receptor for inactivated 26S proteasomes; contains CUE domain that binds ubiquitin, which may facilitate intramolecular monoubiquitination; CUE5 has a paralog, DON1, that arose from the whole genome duplication; human TOLLIP is a functional CUE-domain homolog, can complement yeast null mutant, rescuing hypersensitivity of cue5 null mutant cells to Htt-96Q
AUS1	1.0622	0.510	0.483	6/6	-0.552	2.0E-02	Yes	Plasma membrane sterol transporter of the ATP-binding cassette family; required, along with Pdr11p, for uptake of exogenous sterols and their incorporation into the plasma membrane; activity is stimulated by phosphatidylserine; sterol uptake is required for anaerobic growth because sterol biosynthesis requires oxygen; AUS1 has a paralog, PDR11, that arose from the whole genome duplication
CKA2	0.9955	0.458	0.461	6/6	-0.537	1.5E-02	Yes	Alpha' catalytic subunit of casein kinase 2 (CK2); CK2 is a Ser/Thr protein kinase with roles in cell growth and proliferation; CK2, comprised of CKA1, CKA2, CKB1 and CKB2, has many substrates including transcription factors and all RNA polymerases; protein abundance increases in response to DNA replication stress; regulates

								Fkh1p-mediated donor preference during mating-type switching
HTZ1	0.8711	0.340	0.388	6/6	-0.531	2.4E-03	Yes	Histone variant H2AZ; exchanged for histone H2A in nucleosomes by the SWR1 complex; involved in transcriptional regulation through prevention of the spread of silent heterochromatin; Htz1p-containing nucleosomes facilitate RNA Pol II passage by affecting correct assembly and modification status of RNA Pol II elongation complexes and by favoring efficient nucleosome remodeling
CTK3	0.6016	0.072	0.120	6/6	-0.529	2.4E-05	Yes	Gamma subunit of C-terminal domain kinase I; CTDK-I phosphorylates RNA polymerase II subunit Rpo21p to affect transcription and pre-mRNA 3' end processing, and also phosphorylates ribosomal protein Rps2p to increase translational fidelity; protein abundance increases in response to DNA replication stress
YOR029W	1.0221	0.499	0.490	5/6	-0.523	2.2E-02	Yes	Putative protein of unknown function; conserved among S. cerevisiae strains; YOR029W is not an essential gene
STI1	1.0788	0.559	0.521	6/6	-0.520	2.7E-02	Yes	Hsp90 cochaperone; regulates spatial organization of amyloid-like proteins in the cytosol, thereby buffering the proteotoxicity caused by amyloid-like proteins; interacts with the Ssa group of the cytosolic Hsp70 chaperones and activates Ssa1p ATPase activity; interacts with Hsp90 chaperones and inhibits their ATPase activity; homolog of mammalian Hop
LSM1	1.0461	0.539	0.517	6/6	-0.507	7.4E-04	Yes	Lsm (Like Sm) protein; forms heteroheptameric complex (with Lsm2p, Lsm3p, Lsm4p, Lsm5p, Lsm6p, and Lsm7p) involved in degradation of cytoplasmic mRNAs; also enters the nucleus and positively regulates transcription initiation; unlike most Sm-like proteins, Lsm1p requires both its SM-domain and C-terminal domain for RNA-binding; binds to mRNAs under glucose starvation, most often in the 3' UTR; forms cytoplasmic foci upon DNA replication stress
MDM12	0.8337	0.327	0.389	5/6	-0.507	8.2E-03	Yes	Mitochondrial outer membrane protein, ERMES complex subunit; required for transmission of mitochondria to daughter cells; required for mitophagy; may influence import and assembly of outer membrane beta-barrel proteins; ERMES complex is often co-localized with peroxisomes and with concentrated areas of pyruvate dehydrogenase
HMS1	1.0894	0.596	0.548	6/6	-0.494	1.5E-02	Yes	bHLH protein with similarity to myc-family transcription factors; overexpression confers hyperfilamentous growth and suppresses the pseudohyphal filamentation defect of a diploid mep1 mep2 homozygous null mutant
CYC2	0.9400	0.452	0.487	5/6	-0.488	2.4E-02	Yes	Mitochondrial peripheral inner membrane protein; contains a FAD cofactor in a domain exposed in the intermembrane space; exhibits redox activity in vitro; likely participates in

								ligation of heme to acytochromes c and c1 (Cyc1p and Cyt1p)
TOM6	1.0780	0.599	0.554	5/6	-0.479	2.2E-02	Yes	Component of the TOM (translocase of outer membrane) complex; responsible for recognition and initial import steps for all mitochondrially directed proteins; promotes assembly and stability of the TOM complex
FMP52	0.5847	0.110	0.164	5/5	-0.475	2.0E-03	Yes	Protein of unknown function; localized to the mitochondrial outer membrane; induced by treatment with 8-methoxypsoralen and UVA irradiation
EXP1	0.9367	0.484	0.521	6/6	-0.452	3.2E-03	Yes	Putative protein of unknown function; green fluorescent protein (GFP)-fusion protein localizes to the endoplasmic reticulum; YDL121C is not an essential protein
YOR019W	1.1366	0.688	0.601	6/6	-0.448	3.5E-02	Yes	Protein of unknown function; may interact with ribosomes, based on co-purification experiments; YOR019W has a paralog, JIP4, that arose from the whole genome duplication
THR1	0.9054	0.457	0.507	6/6	-0.448	5.2E-03	Yes	Homoserine kinase; conserved protein required for threonine biosynthesis; long-lived protein that is preferentially retained in mother cells and forms cytoplasmic filaments; expression is regulated by the GCN4-mediated general amino acid control pathway
LPX1	1.1128	0.667	0.599	6/6	-0.446	1.9E-02	Yes	Peroxisomal matrix-localized lipase; required for normal peroxisome morphology; contains a peroxisomal targeting signal type 1 (PTS1) and a lipase motif; peroxisomal import requires the PTS1 receptor, Pex5p and self-interaction; transcriptionally activated by Yrm1p along with genes involved in multidrug resistance; oleic acid inducible
DFG16	0.8809	0.436	0.493	6/6	-0.445	1.4E-04	Yes	Probable multiple transmembrane protein; involved in diploid invasive and pseudohyphal growth upon nitrogen starvation; is glycosylated and phosphorylated; interacts with Rim21p and Rim9p in the plasma membrane to form a pH-sensing complex in the Rim101 pathway and is required to maintain Rim21p levels; required for accumulation of processed Rim101p
ALG8	0.9755	0.532	0.549	6/6	-0.443	1.9E-02	Yes	Glucosyl transferase; involved in N-linked glycosylation; adds glucose to the dolichol-linked oligosaccharide precursor prior to transfer to protein during lipid-linked oligosaccharide biosynthesis; similar to Alg6p; human homolog ALG8 can complement yeast null mutant
SHE4	0.7142	0.272	0.397	5/6	-0.442	1.0E-02	Yes	Protein containing a UCS (UNC-45/CRO1/SHE4) domain; binds to myosin motor domains to regulate myosin function; involved in endocytosis, polarization of the actin cytoskeleton, and asymmetric mRNA localization
SET4	0.9362	0.500	0.495	5/6	-0.436	3.7E-02	Yes	Protein of unknown function, contains a SET domain; SET4 has a paralog, SET3, that arose from the whole genome duplication
RTS1	0.826	0.40	0.50	5/6	-	2.4E	Yes	B-type regulatory subunit of protein

	4	7	2		0.420	-02		phosphatase 2A (PP2A); Rts1p and Cdc55p are alternative regulatory subunits for PP2A catalytic subunits, Pph21p and Pph22p; PP2A-Rts1p protects cohesin when recruited by Sgo1p to the pericentromere; highly enriched at centromeres in the absence of Cdc55p; required for maintenance of septin ring organization during cytokinesis, for ring disassembly in G1 and for dephosphorylation of septin, Shs1p; homolog of the mammalian B' subunit of PP2A
YNG1	1.0927	0.673	0.622	5/6	-0.419	4.7E-02	Yes	Subunit of the NuA3 histone acetyltransferase complex; this complex acetylates histone H3; contains PHD finger domain that interacts with methylated histone H3; shares significant sequence identity with the human candidate tumor suppressor p33-ING1 in C-terminal region
CTK1	0.6064	0.189	0.314	6/6	-0.418	2.1E-04	Yes	Catalytic (alpha) subunit of C-terminal domain kinase I (CTDK-I); phosphorylates both RNA pol II subunit Rpo21p to affect transcription and pre-mRNA 3' end processing, and ribosomal protein Rps2p to increase translational fidelity; required for H3K36 trimethylation but not dimethylation by Set2p; suggested stimulatory role in 80S formation during translation initiation; similar to the Drosophila dCDK12 and human CDK12 and probably CDK13
CTK2	0.6322	0.217	0.348	6/6	-0.415	3.5E-04	Yes	Beta subunit of C-terminal domain kinase I (CTDK-I); which phosphorylates both RNA pol II subunit Rpo21p to affect transcription and pre-mRNA 3' end processing, and ribosomal protein Rps2p to increase translational fidelity; relocalizes to the cytosol in response to hypoxia
SFM1	1.1207	0.707	0.631	6/6	-0.414	3.9E-02	Yes	SPOUT methyltransferase; catalyzes omega-monomethylation of Rps3p on Arg-146; not an essential gene; predicted to be involved in rRNA processing and ribosome biogenesis and in biopolymer catabolism
NUP133	0.9059	0.494	0.557	6/6	-0.412	4.7E-03	Yes	Subunit of Nup84p subcomplex of nuclear pore complex (NPC); contributes to nucleocytoplasmic transport, NPC biogenesis; is involved in establishment of a normal nucleocytoplasmic concentration gradient of GTPase Gsp1p; also plays roles in several processes that may require localization of genes or chromosomes at nuclear periphery, including double-strand break repair, transcription and chromatin silencing; relocalizes to cytosol in response to hypoxia; homolog of human NUP133
GEP4	0.6402	0.230	0.357	6/6	-0.411	1.1E-03	Yes	Mitochondrial phosphatidylglycerophosphatase (PGP phosphatase); dephosphorylates phosphatidylglycerolphosphate to generate phosphatidylglycerol, an essential step during cardiolipin biosynthesis; null mutant is sensitive to tunicamycin, DTT

CKB2	0.8091	0.404	0.500	6/6	-0.406	3.0E-03	Yes	Beta' regulatory subunit of casein kinase 2 (CK2); a Ser/Thr protein kinase with roles in cell growth and proliferation; CK2, comprised of CKA1, CKA2, CKB1 and CKB2, has many substrates including transcription factors and all RNA polymerase
BUD31	0.8811	0.477	0.549	6/6	-0.404	1.1E-02	Yes	Component of the SF3b subcomplex of the U2 snRNP; increases efficiency of first and second step pre-mRNA splicing; diploid mutants display a random budding pattern instead of the wild-type bipolar pattern; facilitates passage through G1/S Start, but is not required for G2/M transition or exit from mitosis
MRPL10	0.7248	0.332	0.451	5/5	-0.393	2.3E-02	Yes	Mitochondrial ribosomal protein of the large subunit; appears as two protein spots (YmL10 and YmL18) on two-dimensional SDS gels
PET8	1.1583	0.769	0.657	6/6	-0.390	3.7E-02	Yes	S-adenosylmethionine transporter of the mitochondrial inner membrane; member of the mitochondrial carrier family; required for biotin biosynthesis and respiratory growth
LPD1	1.0799	0.691	0.643	6/6	-0.389	3.4E-02	Yes	Dihydrolipoamide dehydrogenase; the lipoamide dehydrogenase component (E3) of the pyruvate dehydrogenase and 2-oxoglutarate dehydrogenase multi-enzyme complexes; PDH complex is concentrated in spots within the mitochondrial matrix, often near the ERMES complex and near peroxisomes; LPD1 has a paralog, IRC15, that arose from the whole genome duplication
RPL27A	0.6048	0.223	0.372	6/6	-0.382	5.0E-03	Yes	Ribosomal 60S subunit protein L27A; homologous to mammalian ribosomal protein L27, no bacterial homolog; RPL27A has a paralog, RPL27B, that arose from the whole genome duplication
MDM31	0.6984	0.325	0.505	6/6	-0.373	8.7E-03	Yes	Mitochondrial protein that may have a role in phospholipid metabolism; inner membrane protein with similarity to Mdm32p; required for normal mitochondrial morphology and inheritance; interacts genetically with MMM1, MMM2, MDM10, MDM12, and MDM34
IPK1	0.8291	0.456	0.553	6/6	-0.373	3.8E-04	Yes	Inositol 1,3,4,5,6-pentakisphosphate 2-kinase; nuclear protein required for synthesis of 1,2,3,4,5,6-hexakisphosphate (phytate), which is integral to cell function; has 2 motifs conserved in other fungi; ipk1 gle1 double mutant is inviable; human IPPK can complement ipk1 null mutant
BUB3	0.7929	0.426	0.531	6/6	-0.367	8.6E-03	Yes	Kinetochore checkpoint WD40 repeat protein; localizes to kinetochores during prophase and metaphase, delays anaphase in the presence of unattached kinetochores; forms complexes with Mad1p-Bub1p and with Cdc20p, binds Mad2p and Mad3p; functions at kinetochore to activate APC/C-Cdc20p for normal mitotic progression
YOR015W	1.0519	0.686	0.654	5/6	-0.36	4.7E-02	Yes	Putative protein of unknown function; conserved among S. cerevisiae strains;

					6			YOR015W is not an essential gene
SWR1	0.8760	0.510	0.596	6/6	-0.366	7.7E-03	Yes	Swi2/Snf2-related ATPase; structural component of the SWR1 complex, which exchanges histone variant H2AZ (Htz1p) for chromatin-bound histone H2A; relocalizes to the cytosol in response to hypoxia; chronological aging factor that mediates lifespan extension by dietary restriction
IZH2	1.1036	0.739	0.673	6/6	-0.365	2.3E-02	Yes	Plasma membrane receptor for plant antifungal osmotin; involved in zinc ion homeostasis, apoptosis; negatively regulates ZRT1 and other functionally divergent genes through CCCTC promoter motif (IzRE); modulates FET3 activity in iron-independent manner; affects gene expression by influencing balance of competition between Msn2p/ Msn4p and Nrg1p/Nrg2p for binding to IzRE; transcription regulated by Zap1p, zinc, fatty acid levels; homolog of mammalian adiponectin receptor
VPS72	0.9264	0.562	0.607	6/6	-0.365	4.0E-04	Yes	Htz1p-binding component of the SWR1 complex; exchanges histone variant H2AZ (Htz1p) for chromatin-bound histone H2A; may function as a lock that prevents removal of H2AZ from nucleosomes; required for vacuolar protein sorting
PFK1	0.4294	0.067	0.161	6/6	-0.362	8.2E-05	Yes	Alpha subunit of heterooctameric phosphofructokinase; involved in glycolysis, indispensable for anaerobic growth, activated by fructose-2,6-bisphosphate and AMP, mutation inhibits glucose induction of cell cycle-related genes
BUR2	0.4045	0.050	0.125	6/6	-0.354	4.5E-06	Yes	Cyclin for the Sgv1p (Bur1p) protein kinase; Sgv1p and Bur2p comprise the CDK-cyclin BUR kinase complex which is involved in transcriptional regulation through its phosphorylation of the carboxy-terminal domain (CTD) of the largest subunit of RNA polymerase II (Rpo21p); BUR kinase is also involved in the recruitment of Spt6p to the CTD at the onset of transcription
RCY1	0.4201	0.073	0.192	6/6	-0.347	6.9E-04	Yes	F-box protein involved in recycling endocytosed proteins; involved in recycling plasma membrane proteins internalized by endocytosis; localized to sites of polarized growth; direct interaction with C-terminal cytoplasmic region of Drs2p plays an important role for Drs2p function in endocytic recycling pathway
APQ12	0.8188	0.473	0.580	6/6	-0.346	1.7E-03	Yes	Nuclear envelope/ER integral membrane protein; interacts and functions with Brr6p and Brl1p in lipid homeostasis; mutants are defective in nuclear pore complex biogenesis, nuclear envelope morphology, mRNA export from the nucleus and are sensitive to sterol biosynthesis inhibitors and membrane fluidizing agents; exhibits synthetic lethal genetic interactions with genes involved in lipid metabolism
NUP2	1.229	0.89	0.73	6/6	-	4.2E	Yes	Nucleoporin involved in

	8	3	0		0.337	-04		nucleocytoplasmic transport; binds to either the nucleoplasmic or cytoplasmic faces of the nuclear pore complex depending on Ran-GTP levels; also has a role in chromatin organization
THP1	0.8407	0.512	0.613	6/6	-0.328	6.5E-03	Yes	Nuclear pore-associated protein; component of TREX-2 complex (Sac3p-Thp1p-Sus1p-Cdc31p) involved in transcription elongation and mRNA export from the nucleus; involved in post-transcriptional tethering of active genes to the nuclear periphery and to non-nascent mRNP; contains a PAM domain implicated in protein-protein binding
RPS7A	0.4983	0.193	0.387	6/6	-0.306	8.3E-04	Yes	Protein component of the small (40S) ribosomal subunit; interacts with Kti11p; deletion causes hypersensitivity to zymocin; homologous to mammalian ribosomal protein S7, no bacterial homolog; RPS7A has a paralog, RPS7B, that arose from the whole genome duplication
PEP7	0.8661	0.564	0.652	6/6	-0.302	4.1E-05	Yes	Adaptor protein involved in vesicle-mediated vacuolar protein sorting; multivalent adaptor protein; facilitates vesicle-mediated vacuolar protein sorting by ensuring high-fidelity vesicle docking and fusion, which are essential for targeting of vesicles to the endosome; required for vacuole inheritance
SPT10	0.8298	0.535	0.657	5/6	-0.295	2.1E-03	Yes	Histone H3 acetylase with a role in transcriptional regulation; sequence-specific activator of histone genes, binds specifically and cooperatively to pairs of UAS elements in core histone promoters, functions at or near TATA box; involved in S phase-specific acetylation of H3K56 at histone promoters, which is required for recruitment of SWI/SNF nucleosome remodeling complex and subsequent transcription
ARP6	0.9615	0.667	0.693	6/6	-0.295	3.6E-04	Yes	Actin-related protein that binds nucleosomes; a component of the SWR1 complex, which exchanges histone variant H2AZ (Htz1p) for chromatin-bound histone H2A
MDM32	0.5332	0.243	0.456	6/6	-0.290	6.4E-04	Yes	Mitochondrial inner membrane protein with similarity to Mdm31p; required for normal mitochondrial morphology and inheritance; interacts genetically with MMM1, MDM10, MDM12, and MDM34; variation between SK1 and S288C at residues 182 and 262 impacts invasive growth and mitochondrial network structure
LIP2	0.8901	0.609	0.689	6/6	-0.282	9.9E-04	Yes	Lipoyl ligase; involved in the modification of mitochondrial enzymes by the attachment of lipoic acid groups
SIT4	0.4430	0.162	0.370	6/6	-0.281	2.2E-03	Yes	Ceramide-activated, type 2A-related serine-threonine phosphatase; functions in G1/S transition of mitotic cycle; controls lifespan, mitochondrial function, cell cycle progression by regulating HXK2 phosphorylation; regulator of COPII coat dephosphorylation; required for ER to

								Golgi traffic; interacts with Hrr25p kinase; cytoplasmic and nuclear protein that modulates functions mediated by Pkc1p including cell wall and actin cytoskeleton organization; similar to human PP6
IWR1	0.5114	0.235	0.449	6/6	-0.276	3.3E-03	Yes	RNA polymerase II transport factor, conserved from yeast to humans; also has a role in transporting RNA polymerase III into the nucleus; interacts with most of the RNAP II subunits; nucleo-cytoplasmic shuttling protein; deletion causes hypersensitivity to K1 killer toxin; protein increases in abundance and relocalizes from nucleus to cytoplasm upon DNA replication stress
SEM1	0.9216	0.647	0.706	6/6	-0.275	8.0E-03	Yes	19S proteasome regulatory particle lid subcomplex component; role in Ub-dependent proteolysis and proteasome stability; involved in TREX-2 mediated mRNA export, and in the prevention of transcription-associated genome instability; ubiquitinated by Nedd4-like E3-ligase, Rsp5p; human ortholog DSS1, a BRCA1 binding protein implicated in cancer, complements the yeast null; drives trinucleotide repeat expansion; protein abundance increases in response to DNA replication stress
PSD1	0.6977	0.424	0.611	6/6	-0.273	1.1E-03	Yes	Phosphatidylserine decarboxylase of the mitochondrial inner membrane; converts phosphatidylserine to phosphatidylethanolamine; regulates mitochondrial fusion and morphology by affecting lipid mixing in the mitochondrial membrane and by influencing the ratio of long to short forms of Mgm1p; partly exposed to the mitochondrial intermembrane space; autocatalytically processed
IRC10	1.1399	0.869	0.766	5/6	-0.271	1.3E-02	Yes	Protein of unknown function; subunit of the leading edge protein (LEP) complex (Ssp1-Ady3-Don1-Irc10) that forms a ring-like structure at the leading edge of the prospore membrane during meiosis II; null mutant displays increased levels of spontaneous Rad52p foci
SPT4	0.3616	0.095	0.298	5/5	-0.267	7.6E-03	Yes	Spt4p/5p (DSIF) transcription elongation factor complex subunit; the Spt4/5 complex binds to ssRNA in a sequence-specific manner, and along with RNAP I and II has multiple roles regulating transcriptional elongation, RNA processing, quality control, and transcription-coupled repair; localizes to kinetochores and heterochromatin, influencing chromosomal dynamics and silencing; required for transcription through long trinucleotide repeats in ORFs and non-protein coding regions
BRE5	0.9540	0.691	0.723	6/6	-0.263	4.1E-03	Yes	Ubiquitin protease cofactor; forms deubiquitination complex with Ubp3p that coregulates anterograde and retrograde transport between the endoplasmic reticulum and Golgi compartments; null is sensitive to brefeldin A
MCX1	1.116	0.86	0.77	6/6	-	2.0E	Yes	Non-proteolytic ATPase of the AAA

	7	3	3		0.254	-03		family; stimulates incorporation of the pyridoxal phosphate cofactor into Hem1p (5-aminolevulinic acid synthase); localized to the mitochondrial matrix; ortholog of vertebrate CLPX, which promotes erythropoiesis
DIA2	0.6694	0.419	0.629	6/6	-0.251	4.4E-03	Yes	Origin-binding F-box protein; forms SCF ubiquitin ligase complex with Skp1p and Cdc53p; functions in ubiquitination of silent chromatin structural protein Sir4p; required to target Cdc6p for destruction during G1 phase; required for deactivation of Rad53 checkpoint kinase, completion of DNA replication during recovery from DNA damage, assembly of RSC complex, RSC-mediated transcription regulation, and nucleosome positioning; involved in invasive and pseudohyphal growth
SWI4	1.1445	0.898	0.790	5/6	-0.247	8.7E-03	Yes	DNA binding component of the SBF complex (Swi4p-Swi6p); a transcriptional activator that in concert with MBF (Mbp1-Swi6p) regulates late G1-specific transcription of targets including cyclins and genes required for DNA synthesis and repair; Slt2p-independent regulator of cold growth; acetylation at two sites, K1016 and K1066, regulates interaction with Swi6p
SIN3	0.6604	0.414	0.642	5/6	-0.246	1.4E-02	Yes	Component of both the Rpd3S and Rpd3L histone deacetylase complexes; involved in transcriptional repression and activation of diverse processes, including mating-type switching and meiosis; involved in the maintenance of chromosomal integrity
RIM21	0.8731	0.629	0.723	6/6	-0.244	8.8E-04	Yes	pH sensor molecule, component of the RIM101 pathway; has a role in cell wall construction and alkaline pH response; is glycosylated and phosphorylated; interacts with Dfg16p and Rim9p to form a pH-sensing complex; localization to the plasma membrane is dependent on Dfg16p and Rim9p; has similarity to A. nidulans PalH
RRG1	0.4365	0.193	0.452	6/6	-0.243	9.1E-03	Yes	Protein of unknown function; required for vacuolar acidification and mitochondrial genome maintenance; the authentic, non-tagged protein is detected in highly purified mitochondria in high-throughput studies
FSH2	0.8312	0.594	0.714	6/6	-0.237	1.2E-04	Yes	Putative serine hydrolase that localizes to the cytoplasm; sequence is similar to S. cerevisiae Fsh1p and Fsh3p and the human candidate tumor suppressor OVCA2
END3	1.0950	0.859	0.784	6/6	-0.236	1.2E-04	Yes	EH domain-containing protein involved in endocytosis; actin cytoskeletal organization and cell wall morphogenesis; forms a complex with Sla1p and Pan1p
AIF1	1.2724	1.038	0.817	6/6	-0.234	3.4E-04	Yes	Mitochondrial cell death effector; translocates to the nucleus in response to apoptotic stimuli, homolog of mammalian Apoptosis-Inducing Factor, putative reductase
HTD2	0.874	0.64	0.74	5/6	-	1.1E	Yes	Mitochondrial 3-hydroxyacyl-thioester

	6	4	1		0.230	-02		dehydratase; involved in fatty acid biosynthesis, required for respiratory growth and for normal mitochondrial morphology
MLP1	1.1559	0.928	0.803	6/6	-0.228	2.5E-05	Yes	Myosin-like protein associated with the nuclear envelope; nuclear basket protein that connects the nuclear pore complex with the nuclear interior; involved with Tel1p in telomere length control; involved with Pml1p and Pml39p in nuclear retention of unspliced mRNAs; MLP1 has a paralog, MLP2, that arose from the whole genome duplication
ADE12	0.5244	0.297	0.523	6/6	-0.228	5.7E-03	Yes	Adenylosuccinate synthase; catalyzes the first step in synthesis of adenosine monophosphate from inosine 5'monophosphate during purine nucleotide biosynthesis; exhibits binding to single-stranded autonomously replicating (ARS) core sequence
RIM20	0.8628	0.636	0.742	6/6	-0.227	2.2E-03	Yes	Protein involved in proteolytic activation of Rim101p; part of response to alkaline pH; PalA/AIP1/Alix family member; interaction with the ESCRT-III subunit Snf7p suggests a relationship between pH response and multivesicular body formation
SWA2	0.8410	0.615	0.733	5/6	-0.226	5.6E-03	Yes	Auxilin-like protein involved in vesicular transport; clathrin-binding protein required for uncoating of clathrin-coated vesicles
DOC1	0.8287	0.605	0.738	5/6	-0.224	1.9E-02	Yes	Processivity factor; required for the ubiquitination activity of the anaphase promoting complex (APC), mediates the activity of the APC by contributing to substrate recognition; involved in cyclin proteolysis; contains a conserved DOC1 homology domain
NUP42	1.0267	0.809	0.802	5/6	-0.218	4.4E-02	Yes	FG-nucleoporin component of central core of the nuclear pore complex; also part of the nuclear pore complex (NPC) cytoplasmic filaments; contributes directly to nucleocytoplasmic transport and maintenance of the NPC permeability barrier and is involved in gene tethering at the nuclear periphery; interacts with Gle1p
VPS36	0.3051	0.092	0.320	6/6	-0.214	2.1E-03	Yes	Component of the ESCRT-II complex; contains the GLUE (GRAM Like Ubiquitin binding in EAP45) domain which is involved in interactions with ESCRT-I and ubiquitin-dependent sorting of proteins into the endosome; plays a role in the formation of mutant huntingtin (Htt) aggregates in yeast
TYR1	1.4145	1.202	0.855	5/6	-0.213	7.4E-03	Yes	Prephenate dehydrogenase involved in tyrosine biosynthesis; expression is dependent on phenylalanine levels
NPL3	0.3223	0.113	0.342	5/5	-0.209	2.9E-04	Yes	RNA-binding protein; promotes elongation, regulates termination, and carries poly(A) mRNA from nucleus to cytoplasm; represses translation initiation by binding eIF4G; required for pre-mRNA splicing; interacts with E3 ubiquitin ligase Bre1p, linking histone ubiquitination to mRNA processing; may have role in telomere maintenance; dissociation from mRNAs promoted by

								Mtr10p; phosphorylated by Sky1p in cytoplasm; protein abundance increases in response to DNA replication stress
RIM101	0.8764	0.670	0.768	5/6	-0.206	6.2E-03	Yes	Cys2His2 zinc-finger transcriptional repressor; involved in alkaline responsive gene repression as part of adaptation to alkaline conditions; involved in cell wall assembly; required for alkaline pH-stimulated haploid invasive growth and sporulation; activated by alkaline-dependent proteolytic processing which results in removal of the C-terminal tail; similar to A. nidulans PacC
RIM13	0.8815	0.678	0.770	6/6	-0.203	3.1E-05	Yes	Calpain-like cysteine protease; involved in proteolytic activation of Rim101p in response to alkaline pH; localizes to punctate structures in alkaline conditions and in vps4 mutant; has similarity to A. nidulans palB
TCB1	1.0271	0.826	0.806	6/6	-0.201	7.4E-04	Yes	Lipid-binding ER protein involved in ER-plasma membrane tethering; one of 6 proteins (Ist2p, Scs2p, Scs22p, Tcb1p, Tcb2p, Tcb3p) that connect ER to plasma membrane and regulate PI4P levels by controlling access of Sac1p phosphatase to its substrate PI4P in PM; contains 3 calcium and lipid binding domains; non-tagged protein also localizes to mitochondria; C-termini of Tcb1p, Tcb2p and Tcb3p interact; TCB1 has a paralog, TCB2, that arose from the whole genome duplication
SNF7	0.2568	0.057	0.223	5/5	-0.200	2.2E-04	Yes	One of four subunits of the ESCRT-III complex; involved in the sorting of transmembrane proteins into the multivesicular body (MVB) pathway; recruited from the cytoplasm to endosomal membranes; ESCRT-III stands for endosomal sorting complex required for transport III
SWC3	0.9301	0.732	0.789	5/6	-0.199	1.5E-02	Yes	Protein of unknown function; component of the SWR1 complex, which exchanges histone variant H2AZ (Htz1p) for chromatin-bound histone H2A; required for formation of nuclear-associated array of smooth endoplasmic reticulum known as karmellae
TUF1	0.4749	0.279	0.607	6/6	-0.196	7.5E-03	Yes	Mitochondrial translation elongation factor Tu (EF-Tu); involved in fundamental pathway of mtDNA homeostasis; comprises both GTPase and guanine nucleotide exchange factor activities, while these activities are found in separate proteins in S. pombe and humans; rare mutations in human mitochondrial elongation factor Tu (EFTu) associated with severe lactic acidosis, rapidly progressive fatal encephalopathy, severe infantile macrocystic leukodystrophy with micropolygyria
ERP4	1.0594	0.864	0.816	5/6	-0.196	1.3E-03	Yes	Member of the p24 family involved in ER to Golgi transport; similar to Emp24p and Erv25p; ERP4 has a paralog, ERP2, that arose from the whole genome duplication
RIM8	0.8681	0.673	0.777	6/6	-0.19	2.0E-04	Yes	Protein involved in proteolytic activation of Rim101p; part of response

					5			to alkaline pH; interacts with ESCRT-1 subunits Stp22p and Vps28p; essential for anaerobic growth; member of the arrestin-related trafficking adaptor family
AIM22	1.0110	0.822	0.813	6/6	-0.189	2.1E-04	Yes	Putative lipoate-protein ligase; required along with Lip2 and Lip5 for lipoylation of Lat1p and Kgd2p; similar to E. coli LplA; null mutant displays reduced frequency of mitochondrial genome loss
SSE1	0.8700	0.683	0.786	5/6	-0.187	1.0E-02	Yes	ATPase component of heat shock protein Hsp90 chaperone complex; serves as nucleotide exchange factor to load ATP onto the SSA class of cytosolic Hsp70s; plays a role in prion propagation and determining prion variants; binds unfolded proteins; member of Hsp110 subclass of HSP70 proteins; deletion results in spindle elongation in S phase; SSE1 has a paralog, SSE2, that arose from the whole genome duplication
CMK2	1.1180	0.932	0.835	5/6	-0.186	5.4E-03	Yes	Calmodulin-dependent protein kinase; may play a role in stress response, many CA++/calmodulan dependent phosphorylation substrates demonstrated in vitro, amino acid sequence similar to mammalian Cam Kinase II; CMK2 has a paralog, CMK1, that arose from the whole genome duplication
NRT1	1.1053	0.920	0.832	5/6	-0.185	1.6E-03	Yes	High-affinity nicotinamide riboside transporter; also transports thiamine with low affinity; major transporter for 5-aminoimidazole-4-carboxamide-1-beta-D-ribofuranoside (acadesine) uptake; shares sequence similarity with Thi7p and Thi72p; proposed to be involved in 5-fluorocytosine sensitivity
YOR072W	1.0890	0.907	0.832	6/6	-0.183	2.0E-03	Yes	Dubious open reading frame; unlikely to encode a functional protein, based on available experimental and comparative sequence data; partially overlaps the dubious gene YOR072W-A; diploid deletion strains are methotrexate, paraquat and wortmannin sensitive
LSM6	0.9271	0.746	0.806	5/6	-0.181	1.1E-02	Yes	Lsm (Like Sm) protein; part of heteroheptameric complexes (Lsm2p-7p and either Lsm1p or 8p): cytoplasmic Lsm1p complex involved in mRNA decay; nuclear Lsm8p complex part of U6 snRNP and possibly involved in processing tRNA, snoRNA, and rRNA
GSH1	0.3554	0.177	0.502	6/6	-0.178	1.1E-04	Yes	Gamma glutamylcysteine synthetase; catalyzes the first step in glutathione (GSH) biosynthesis; expression induced by oxidants, cadmium, and mercury; protein abundance increases in response to DNA replication stress
KTR7	1.1905	1.012	0.852	5/6	-0.178	1.4E-03	Yes	Putative mannosyltransferase involved in protein glycosylation; member of the KRE2/MNT1 mannosyltransferase family; KTR7 has a paralog, KTR5, that arose from the whole genome duplication
RSM22	0.6130	0.440	0.735	5/6	-0.173	2.4E-02	Yes	Mitochondrial ribosomal protein of the small subunit; also predicted to be an S-adenosylmethionine-dependent RNA methyltransferase

OCA2	1.1671	0.998	0.857	5/6	-0.170	4.6E-03	Yes	Protein of unknown function; similar to predicted tyrosine phosphatases Oca1p and Siw14p; green fluorescent protein (GFP)-fusion protein localizes to the cytoplasm; YNL056W is not an essential gene
PHB2	1.0584	0.889	0.844	5/6	-0.169	1.0E-02	Yes	Subunit of the prohibitin complex (Phb1p-Phb2p); prohibitin is a 1.2 MDa ring-shaped inner mitochondrial membrane chaperone that stabilizes newly synthesized proteins; determinant of replicative life span; involved in mitochondrial segregation; prohibitin deficiency induces a mitochondrial unfolded protein response (mtUPR)
MSW1	1.0021	0.833	0.832	5/6	-0.169	9.2E-04	Yes	Mitochondrial tryptophanyl-tRNA synthetase
VPS21	1.0228	0.856	0.840	5/6	-0.167	3.4E-03	Yes	Endosomal Rab family GTPase; required for endocytic transport and sorting of vacuolar hydrolases; required for endosomal localization of the CORVET complex; required with YPT52 for MVB biogenesis and sorting; involved in autophagy and ionic stress tolerance; geranylgeranylation required for membrane association; protein abundance increases in response to DNA replication stress; mammalian Rab5 homolog; VPS21 has a paralog, YPT53, that arose from the whole genome duplication
CIK1	0.9727	0.806	0.831	5/6	-0.166	8.5E-03	Yes	Kinesin-associated protein; required for both karyogamy and mitotic spindle organization, interacts stably and specifically with Kar3p and may function to target this kinesin to a specific cellular role; locus encodes a long and short transcript with differing functions; CIK1 has a paralog, VIK1, that arose from the whole genome duplication
SNF8	0.2734	0.107	0.409	5/5	-0.166	6.1E-03	Yes	Component of the ESCRT-II complex; ESCRT-II is involved in ubiquitin-dependent sorting of proteins into the endosome; appears to be functionally related to SNF7; involved in glucose derepression
LSM7	1.1094	0.948	0.857	5/6	-0.161	1.1E-02	Yes	Lsm (Like Sm) protein; part of heteroheptameric complexes (Lsm2p-7p and either Lsm1p or 8p): cytoplasmic Lsm1p complex involved in mRNA decay; nuclear Lsm8p complex part of U6 snRNP and possibly involved in processing tRNA, snoRNA, and rRNA; protein abundance increases and forms cytoplasmic foci in response to DNA replication stress
AIM10	0.3001	0.141	0.482	6/6	-0.159	1.1E-03	Yes	Protein with similarity to tRNA synthetases; non-tagged protein is detected in purified mitochondria; null mutant is viable and displays elevated frequency of mitochondrial genome loss
GLN3	0.5562	0.397	0.716	6/6	-0.159	1.9E-03	Yes	Transcriptional activator of genes regulated by nitrogen catabolite repression; localization and activity regulated by quality of nitrogen source and Ure2p

GLC8	0.9775	0.819	0.840	6/6	-0.158	5.2E-04	Yes	Regulatory subunit of protein phosphatase 1 (Glc7p); involved in glycogen metabolism and chromosome segregation; proposed to regulate Glc7p activity via conformational alteration; ortholog of the mammalian protein phosphatase inhibitor 2; protein abundance increases in response to DNA replication stress
SPE2	0.2830	0.125	0.454	5/5	-0.158	4.4E-03	Yes	S-adenosylmethionine decarboxylase; required for the biosynthesis of spermidine and spermine; cells lacking Spe2p require spermine or spermidine for growth in the presence of oxygen but not when grown anaerobically
ATG17	1.0098	0.853	0.846	5/6	-0.157	4.7E-03	Yes	Scaffold protein responsible for phagophore assembly site organization; regulatory subunit of an autophagy-specific complex that includes Atg1p and Atg13p; stimulates Atg1p kinase activity; human ortholog RB1CC1/FIP200 interacts with p53, which inhibits autophagy in human cells
ESC1	1.0439	0.887	0.851	5/6	-0.157	3.7E-03	Yes	Protein involved in telomeric silencing; required for quiescent cell telomere hypercluster localization at nuclear membrane vicinity; interacts with PAD4-domain of Sir4p
UBP6	1.1328	0.976	0.864	5/6	-0.157	8.6E-03	Yes	Ubiquitin-specific protease; situated in the base subcomplex of the 26S proteasome, releases free ubiquitin from branched polyubiquitin chains en bloc, rather than from the distal tip of the chain; negatively regulates degradation of ubiquitinated proteins by the proteasome; works in opposition to Hul5p polyubiquitin elongation activity; mutant has aneuploidy tolerance; human homolog UBP14 complements yeast null mutant
ATX2	0.9952	0.839	0.842	5/6	-0.157	1.0E-02	Yes	Golgi membrane protein involved in manganese homeostasis; overproduction suppresses the sod1 (copper, zinc superoxide dismutase) null mutation
IAI11	1.0962	0.940	0.857	5/6	-0.156	5.0E-04	Yes	Putative protein of unknown function; the authentic, non-tagged protein is detected in highly purified mitochondria in high-throughput studies; YBL059W has a paralog, YER093C-A, that arose from the whole genome duplication
RIM9	0.8147	0.659	0.809	5/6	-0.156	2.2E-03	Yes	Plasma membrane protein of unknown function; involved in the proteolytic activation of Rim101p in response to alkaline pH; interacts with Rim21p and Dfg16p to form a pH-sensing complex in the Rim101 pathway and is required to maintain Rim21p levels; has similarity to A. nidulans PalI;
PRM4	1.0618	0.906	0.855	5/6	-0.156	1.4E-02	Yes	Pheromone-regulated protein proposed to be involved in mating; predicted to have 1 transmembrane segment; transcriptionally regulated by Ste12p during mating and by Cat8p during the diauxic shift
POG1	1.2959	1.141	0.882	5/6	-0.155	8.8E-03	Yes	Nuclear chromatin-associated protein of unknown function; may have a role in cell cycle regulation; overexpression promotes recovery from pheromone induced arrest and suppresses the stress

								sensitivity caused by a mutation in the E3 ubiquitin ligase Rsp5p; binds upstream of BAR1 and cell cycle-related genes; phsosphoylated form may be ubiquitinated by Dma2p; potential Cdc28p substrate; SBF regulated
BUD21	0.5866	0.432	0.738	5/6	-0.154	3.8E-02	Yes	Component of small ribosomal subunit (SSU) processosome; this complex contains U3 snoRNA; required at post-transcriptional step for efficient retrotransposition; absence results in decreased Ty1 Gag:GFP protein levels; originally isolated as bud-site selection mutant that displays a random budding pattern
NGL1	1.0113	0.857	0.849	5/6	-0.154	2.7E-03	Yes	Putative endonuclease; has a domain similar to a magnesium-dependent endonuclease motif in mRNA deadenylase Ccr4p; the authentic, non-tagged protein is detected in highly purified mitochondria in high-throughput studies
DNM1	1.0257	0.872	0.854	5/6	-0.154	5.0E-03	Yes	Dynamin-related GTPase involved in mitochondrial organization; required for mitochondrial fission and inheritance; self assembles on the cytoplasmic face of mitochondrial tubules at sites where division will occur; participates in endocytosis and regulates peroxisome fission along with Vps1p; mutants in the human ortholog DNM1L, which mediates mitochondrial fission, peroxisomal division, autophagy, and mitophagy, are associated with slowly progressive infantile encephalopathy
SEC28	0.3474	0.194	0.579	6/6	-0.154	5.1E-03	Yes	Epsilon-COP subunit of the coatomer; regulates retrograde Golgi-to-ER protein traffic; stabilizes Cop1p, the alpha-COP and the coatomer complex; non-essential for cell growth; protein abundance increases in response to DNA replication stress
RMD9	0.7124	0.563	0.801	5/6	-0.149	3.4E-02	Yes	Mitochondrial protein required for respiratory growth; mutant phenotype and genetic interactions suggest a role in delivering mt mRNAs to ribosomes; located on matrix face of the inner membrane and loosely associated with mitoribosomes; RMD9 has a paralog, YBR238C, that arose from the whole genome duplication
SSZ1	0.4767	0.329	0.694	5/6	-0.148	2.3E-02	Yes	Hsp70 protein that interacts with Zuo1p (a DnaJ homolog); interacts with Zuo1p to form a ribosome-associated complex that binds the ribosome via the Zuo1p subunit; also involved in pleiotropic drug resistance via sequential activation of PDR1 and PDR5; binds ATP
SLZ1	1.1846	1.037	0.876	5/6	-0.148	7.5E-04	Yes	Sporulation-specific protein with a leucine zipper motif; subunit of the MIS complex which controls mRNA methylation during during the induction of sporulation
HAC1	1.0212	0.874	0.857	5/6	-0.147	5.4E-03	Yes	Basic leucine zipper (bZIP) transcription factor (ATF/CREB1 homolog); regulates the unfolded protein response, via UPRE binding, and membrane biogenesis; ER stress-induced splicing pathway facilitates

								efficient Hac1p synthesis; two functional forms of Hac1p are produced; translation initiation is repressed under non-stress conditions; protein abundance increases in response to DNA replication stress
RUD3	0.9087	0.763	0.840	5/6	-0.146	4.5E-04	Yes	Golgi matrix protein; involved in the structural organization of the cis-Golgi; interacts genetically with COG3 and USO1
POM33	1.0146	0.871	0.860	5/6	-0.144	1.5E-03	Yes	Transmembrane nucleoporin; involved in nuclear pore complex (NPC) distribution, assembly or stabilization; highly conserved across species, orthologous to human TMEM33 and paralogous to Per33p; protein abundance increases in response to DNA replication stress
HOM6	0.8461	0.702	0.832	5/6	-0.144	5.4E-03	Yes	Homoserine dehydrogenase (L-homoserine:NADP oxidoreductase); dimeric enzyme that catalyzes the third step in the common pathway for methionine and threonine biosynthesis; enzyme has nucleotide-binding, dimerization and catalytic regions
TDA3	1.1407	1.000	0.877	5/6	-0.141	6.9E-04	Yes	Putative oxidoreductase involved in late endosome to Golgi transport; physical and genetical interactions with Btn2p; null mutant is viable, has extended S phase, and sensitive to expression of top1-T722A allele; similar to human FOXRED1
PEX15	0.9351	0.795	0.852	5/6	-0.140	4.4E-03	Yes	Tail-anchored type II integral peroxisomal membrane protein; required for peroxisome biogenesis; cells lacking Pex15p mislocalize peroxisomal matrix proteins to cytosol; overexpression results in impaired peroxisome assembly
HIS3	1.0029	0.865	0.864	5/6	-0.138	2.3E-03	Yes	Imidazoleglycerol-phosphate dehydratase; catalyzes the sixth step in histidine biosynthesis; mutations cause histidine auxotrophy and sensitivity to Cu, Co, and Ni salts; transcription is regulated by general amino acid control via Gcn4p
RPL31A	0.5801	0.443	0.766	6/6	-0.137	4.6E-03	Yes	Ribosomal 60S subunit protein L31A; associates with karyopherin Sxm1p; loss of both Rpl31p and Rpl39p confers lethality; homologous to mammalian ribosomal protein L31, no bacterial homolog; RPL31A has a paralog, RPL31B, that arose from the whole genome duplication
AIM20	1.2117	1.075	0.889	5/6	-0.137	6.7E-03	Yes	Protein of unknown function; overexpression causes cell cycle delay or arrest; green fluorescent protein (GFP)-fusion protein localizes to vacuole; null mutant displays elevated frequency of mitochondrial genome loss; relocalizes from nucleus to cytoplasm upon DNA replication stress; AIM20 has a paralog, SKG1, that arose from the whole genome duplication
BEM3	1.1142	0.979	0.881	5/6	-0.135	4.0E-03	Yes	Rho GTPase activating protein (RhoGAP); involved in control of the cytoskeleton organization; targets the essential Rho-GTPase Cdc42p, which controls establishment and maintenance

								of cell polarity, including bud-site assembly
TIF4631	0.9033	0.772	0.856	5/6	-0.131	8.9E-04	Yes	Translation initiation factor eIF4G; subunit of the mRNA cap-binding protein complex (eIF4F) that also contains eIF4E (Cdc33p); interacts with Pab1p and with eIF4A (Tif1p); also has a role in biogenesis of the large ribosomal subunit; TIF4631 has a paralog, TIF4632, that arose from the whole genome duplication
HOM2	1.0217	0.892	0.874	5/6	-0.130	3.9E-04	Yes	Aspartic beta semi-aldehyde dehydrogenase; catalyzes the second step in the common pathway for methionine and threonine biosynthesis; expression regulated by Gcn4p and the general control of amino acid synthesis
MRPL38	0.6645	0.537	0.810	6/6	-0.127	2.0E-03	Yes	Mitochondrial ribosomal protein of the large subunit; appears as two protein spots (YmL34 and YmL38) on two-dimensional SDS gels; protein abundance increases in response to DNA replication stress
YGR122W	0.8030	0.677	0.845	5/6	-0.126	1.2E-02	Yes	Protein that may be involved in pH regulation; probable ortholog of A. nidulans PalC, which is involved in pH regulation and binds to the ESCRT-III complex; null mutant does not properly process Rim101p and has decreased resistance to rapamycin; GFP-fusion protein is cytoplasmic; relative distribution to cytoplasm increases upon DNA replication stress
AVT1	1.0682	0.943	0.883	5/6	-0.126	1.4E-03	Yes	Vacuolar transporter; imports large neutral amino acids into the vacuole; member of a family of seven S. cerevisiae genes (AVT1-7) related to vesicular GABA-glycine transporters
MRPL23	0.7791	0.655	0.842	5/6	-0.125	2.8E-03	Yes	Mitochondrial ribosomal protein of the large subunit; localizes to vacuole in response to H2O2
PET123	0.9432	0.819	0.871	5/6	-0.124	7.8E-03	Yes	Mitochondrial ribosomal protein of the small subunit; PET123 exhibits genetic interactions with PET122, which encodes a COX3 mRNA-specific translational activator
SWC7	1.0570	0.935	0.886	5/6	-0.122	6.1E-03	Yes	Protein of unknown function; component of the Swr1p complex that incorporates Htz1p into chromatin
RNR4	0.2887	0.167	0.584	6/6	-0.122	1.1E-03	Yes	Ribonucleotide-diphosphate reductase (RNR) small subunit; the RNR complex catalyzes the rate-limiting step in dNTP synthesis and is regulated by DNA replication and DNA damage checkpoint pathways via localization of the small subunits; relocalizes from nucleus to cytoplasm upon DNA replication stress; RNR4 has a paralog, RNR2, that arose from the whole genome duplication
HAT1	1.0995	0.978	0.890	5/6	-0.122	1.2E-03	Yes	Catalytic subunit of the Hat1p-Hat2p histone acetyltransferase complex; uses the cofactor acetyl coenzyme A to acetylate free nuclear and cytoplasmic histone H4; involved in telomeric silencing and DNA double-strand break repair

INO4	0.5343	0.415	0.784	6/6	-0.119	5.1E-03	Yes	Transcription factor involved in phospholipid synthesis; required for derepression of inositol-choline-regulated genes involved in phospholipid synthesis; forms a complex, with Ino2p, that binds the inositol-choline-responsive element through a basic helix-loop-helix domain
ATP12	0.5745	0.455	0.801	5/6	-0.119	1.7E-02	Yes	Assembly factor for F1 sector of mitochondrial F1F0 ATP synthase; conserved protein; required for assembly of alpha and beta subunits into F1 sector of mitochondrial F1F0 ATP synthase; human homolog ATPAF2 can complement yeast atp12 mutant; mutation of human homolog reduces active ATP synthase levels and is associated with the disorder ATPAF2 deficiency
MMS22	0.6060	0.487	0.805	5/6	-0.119	1.8E-03	Yes	Subunit of E3 ubiquitin ligase complex involved in replication repair; stabilizes protein components of the replication fork, such as the fork-pausing complex and leading strand polymerase, preventing fork collapse and promoting efficient recovery during replication stress; required for accurate meiotic chromosome segregation
MRPS5	0.7351	0.619	0.843	5/6	-0.116	9.4E-04	Yes	Mitochondrial ribosomal protein of the small subunit
MDJ1	0.4736	0.358	0.751	6/6	-0.116	3.8E-03	Yes	Co-chaperone that stimulates HSP70 protein Ssc1p ATPase activity; involved in protein folding/refolding in the mitochodrial matrix; required for proteolysis of misfolded proteins; member of the HSP40 (DnaJ) family of chaperones
MGM101	0.6571	0.543	0.830	5/6	-0.114	5.1E-03	Yes	Protein with a role in mitochondrial DNA recombinational repair; also involved in interstrand cross-link repair; binds to and catalyzes the annealing of single-stranded mtDNA; oligomerizes to form rings and filaments; related to Rad52-type recombination proteins, with limited overall similarity but sharing conserved functionally important residues; component of the mitochondrial nucleoid, required for the repair of oxidative mtDNA damage and mitochondrial genome maintenance
MRS1	0.9210	0.807	0.877	5/6	-0.114	4.6E-03	Yes	Splicing protein; required for splicing of two mitochondrial group I introns (BI3 in COB and AI5beta in COX1); forms a splicing complex, containing four subunits of Mrs1p and two subunits of the BI3-encoded maturase, that binds to the BI3 RNA; MRS1 has a paralog, CCE1, that arose from the whole genome duplication
SEA4	1.0058	0.899	0.894	5/6	-0.107	2.1E-04	Yes	Subunit of SEACAT, a subcomplex of the SEA complex; Sea4p, along with Rtc1p and Mtc5p, redundantly inhibit the TORC1 inhibitory role of the Iml1p/ SEACIT (Iml1p-Npr2p-Npr3p) subcomplex, a GAP for GTPase Gtr1p (EGOC subunit) in response to amino acid limitation, thereby resulting in activation of TORC1 signaling; SEA is

								a coatomer-related complex that associates dynamically with the vacuole; contains an N-terminal beta-propeller fold and a C-terminal RING motif
YGR219W	0.7008	0.594	0.849	5/6	-0.107	4.6E-04	Yes	Dubious open reading frame; unlikely to encode a functional protein, based on available experimental and comparative sequence data; partially overlaps the verified ORF MRPL9/YGR220C
ATP11	0.7607	0.654	0.861	5/6	-0.106	2.2E-03	Yes	Molecular chaperone; required for the assembly of alpha and beta subunits into the F1 sector of mitochondrial F1F0 ATP synthase; N-terminally propionylated in vivo
FYV7	0.5717	0.467	0.822	5/6	-0.105	1.1E-02	Yes	Essential protein required for maturation of 18S rRNA; required for survival upon exposure to K1 killer toxin
RNR1	0.7466	0.646	0.866	6/6	-0.101	2.3E-05	Yes	Major isoform of large subunit of ribonucleotide-diphosphate reductase; the RNR complex catalyzes rate-limiting step in dNTP synthesis, regulated by DNA replication and DNA damage checkpoint pathways via localization of small subunits; relative distribution to the nucleus increases upon DNA replication stress; RNR1 has a paralog, RNR3, that arose from the whole genome duplication
MSN5	0.9134	0.815	0.895	5/6	-0.098	1.4E-02	Yes	Karyopherin; involved in nuclear import and export of proteins, including import of replication protein A and export of Far1p and transcription factors Swi5p, Swi6p, Msn2p, and Pho4p; required for re-export of mature tRNAs after their retrograde import from the cytoplasm; exportin-5 homolog
LYS14	0.2846	0.189	0.688	5/5	-0.096	2.7E-02	Yes	Transcriptional activator involved in regulating lysine biosynthesis; involved in the regulation of genes of the lysine biosynthesis pathway; requires 2-aminoadipate semialdehyde as co-inducer
MNN10	0.5353	0.441	0.827	5/6	-0.094	5.1E-03	Yes	Subunit of a Golgi mannosyltransferase complex; complex mediates elongation of the polysaccharide mannan backbone; membrane protein of the mannosyltransferase family; other members of the complex are Anp1p, Mnn9p, Mnn11p, and Hoc1p
CUE3	0.7291	0.636	0.877	5/6	-0.094	4.4E-02	Yes	Protein of unknown function; has a CUE domain that binds ubiquitin, which may facilitate intramolecular monoubiquitination
REG1	0.3813	0.289	0.766	5/6	-0.093	1.2E-02	Yes	Regulatory subunit of type 1 protein phosphatase Glc7p; involved in negative regulation of glucose-repressible genes; involved in regulation of the nucleocytoplasmic shuttling of Hxk2p; REG1 has a paralog, REG2, that arose from the whole genome duplication
PDX3	0.3892	0.324	0.831	5/6	-0.066	1.9E-03	Yes	Pyridoxine (pyridoxamine) phosphate oxidase; has homologs in E. coli and Myxococcus xanthus; transcription is under the general control of nitrogen metabolism